THE UNIVERSITY OF
WARWICK

Library Declaration and Deposit Agreement

1. STUDENT DETAILS

Please complete the following:

Full name: Adam Dickinson

University ID number: 0867190

2. THESIS DEPOSIT

2.1 I understand that under my registration at the University, I am required to deposit my thesis with the University in BOTH hard copy and in digital format. The digital version should normally be saved as a single pdf file.

2.2 The hard copy will be housed in the University Library. The digital version will be deposited in the University's Institutional Repository (WRAP). Unless otherwise indicated (see 2.3 below) this will be made openly accessible on the Internet and will be supplied to the British Library to be made available online via its Electronic Theses Online Service (EThOS) service.
[At present, theses submitted for a Master's degree by Research (MA, MSc, LLM, MS or MMedSci) are not being deposited in WRAP and not being made available via EthOS. This may change in future.]

2.3 In exceptional circumstances, the Chair of the Board of Graduate Studies may grant permission for an embargo to be placed on public access to the hard copy thesis for a limited period. It is also possible to apply separately for an embargo on the digital version. (Further information is available in the *Guide to Examinations for Higher Degrees by Research*.)

2.4 *If you are depositing a thesis for a Master's degree by Research, please complete section (a) below. For all other research degrees, please complete both sections (a) and (b) below:*

(a) Hard Copy

I hereby deposit a hard copy of my thesis in the University Library to be made publicly available to readers (please delete as appropriate) ~~EITHER~~ immediately ~~OR after an embargo period of ..... months/years as agreed by the Chair of the Board of Graduate Studies.~~

I agree that my thesis may be photocopied. (YES) / NO (*Please delete as appropriate*)

(b) Digital Copy

I hereby deposit a digital copy of my thesis to be held in WRAP and made available via EThOS.

Please choose one of the following options:

EITHER My thesis can be made publicly available online. (YES) / NO (*Please delete as appropriate*)

OR My thesis can be made publicly available only after.....[date] (Please give date)
YES / NO (*Please delete as appropriate*)

OR My full thesis cannot be made publicly available online but I am submitting a separately identified additional, abridged version that can be made available online.
YES / NO (*Please delete as appropriate*)

OR My thesis cannot be made publicly available online. YES / NO (*Please delete as appropriate*)

3. GRANTING OF NON-EXCLUSIVE RIGHTS

Whether I deposit my Work personally or through an assistant or other agent, I agree to the following:

Rights granted to the University of Warwick and the British Library and the user of the thesis through this agreement are non-exclusive. I retain all rights in the thesis in its present version or future versions. I agree that the institutional repository administrators and the British Library or their agents may, without changing content, digitise and migrate the thesis to any medium or format for the purpose of future preservation and accessibility.

4. DECLARATIONS

(a) I DECLARE THAT:

- I am the author and owner of the copyright in the thesis and/or I have the authority of the authors and owners of the copyright in the thesis to make this agreement. Reproduction of any part of this thesis for teaching or in academic or other forms of publication is subject to the normal limitations on the use of copyrighted materials and to the proper and full acknowledgement of its source.
- The digital version of the thesis I am supplying is the same version as the final, hard-bound copy submitted in completion of my degree, once any minor corrections have been completed.
- I have exercised reasonable care to ensure that the thesis is original, and does not to the best of my knowledge break any UK law or other Intellectual Property Right, or contain any confidential material.
- I understand that, through the medium of the Internet, files will be available to automated agents, and may be searched and copied by, for example, text mining and plagiarism detection software.

(b) IF I HAVE AGREED (in Section 2 above) TO MAKE MY THESIS PUBLICLY AVAILABLE DIGITALLY, I ALSO DECLARE THAT:

- I grant the University of Warwick and the British Library a licence to make available on the Internet the thesis in digitised format through the Institutional Repository and through the British Library via the EThOS service.
- If my thesis does include any substantial subsidiary material owned by third-party copyright holders, I have sought and obtained permission to include it in any version of my thesis available in digital format and that this permission encompasses the rights that I have granted to the University of Warwick and to the British Library.

5. LEGAL INFRINGEMENTS

I understand that neither the University of Warwick nor the British Library have any obligation to take legal action on behalf of myself, or other rights holders, in the event of infringement of intellectual property rights, breach of contract or of any other right, in the thesis.

Please sign this agreement and return it to the Graduate School Office when you submit your thesis.

Student's signature:  Date: 17/10/13

The Role of Mitochondrial DNA in Tumorigenesis

by

Adam Dickinson

A thesis submitted for the degree of Doctor of Philosophy

University of Warwick, Warwick Medical School,
Department of Metabolic and Vascular Health

October 2013

Table of Contents

List of Figures

List of Tables

Acknowledgments

This thesis represents an eventful journey that took me thousands of miles across the globe from Coventry, to Melbourne before finally returning home to my roots in Liverpool. Throughout this journey I've had the support of many people who I'd now wish to thank.

Firstly I'd like to thank my supervisor, Justin, for his guidance and advice throughout my studies and for the providing me with the opportunity to perform my research at MIMR and gain invaluable experience. I would also like to thank my lab colleagues, Jacqui Johnson, Richard Kelly and Vanessa Yeung for their assistance in the lab, informative discussions, plenty of banter and extortionately priced beers (mainly Richard). A thank you also goes to Matt McKenzie for his input and advice on numerous aspects of my work and Jacqui Donoghue for her assistance with *in vivo* experiments. I'd also like to thank the whole of CRD for their support and for also making me feel welcome in Melbourne. I am also extremely grateful to Jonathan Feuer and the University of Warwick for providing the scholarship that permitted me to complete my studies.

I will be forever indebted to my Mum, Dad, Nan and Grandad for their endless support in all of my undertakings, both big and small and for that I will be forever grateful. A huge thank you to my big sister, Laura, who has provided excellent advice and support over the years and also the rest of my family for their support. Cheers to my best mates Graeme (Gman), Matty (Stick) and Melia (I don't know how to text) who kept in regular contact while I was "Down Under' and kept me updated and entertained with goings on back home and for the sharing of many beers during my trips home.

My last acknowledgment goes to Anneka who accompanied me to Australia and endured countless presentation practices, rants and weekend trips to the lab. A huge amount of thanks and gratitude goes to you for your support over the last three years, which allowed me to not complete this thesis but also have an awesome time along the way. Thanks! I can now finally put your nemesis (my PhD) to rest and subtly quote Gordon Ramsey…DONE!

Declaration

No portion of work referred to in this thesis has been submitted in support of an application for another degree or qualification at the University of Warwick or any other academic institution.

I declare that the work contained in this thesis is my own work with the exception the tumor formation and immunohistochemical assays, which were kindly performed by Dr Jacqueline Donoghue and this is stated in the appropriate sections of the *General Materials and Methods*.

List of Communications

Manuscripts

Dickinson A, Yeung KY, Donoghue J, Baker MJ, Kelly RD, McKenzie M, Johns TG, St John JC. The regulation of mitochondrial DNA copy number in glioblastoma cells. *Cell Death & Differentiation*. 2013 Aug 30

Book chapters

Yeung KY, **Dickinson A**, St John JC. Mitochondrial DNA in Cancer Cells. *Mitochondrial DNA, disease and stem cells. Springer (St. John J.C., ed.) Springer Verlag. 2012.*

Poster presentations

Dickinson A, Yeung KY and St John JC. Abnormal regulation of mitochondrial DNA copy number in glioblastoma multiforme cancer stem cells. 45th Annual Meeting of The Society for the Study of Reproduction (SSR), Pennsylvania State University, USA, August 12th-15th 2012.

Yeung KY**, Dickinson A** and St John JC. Identification of mitochondrial DNA variants in cancer stem cells using next generation sequencing. 45th Annual Meeting of The Society for the Study of Reproduction (SSR), Pennsylvania State University, USA, August 12th-15th 2012

Dickinson A, Donoghue J, Johns TG, St John JC. Mitochondrial DNA is required for the maintenance of glioblastoma multiforme tumorigenicity. AussieMit 2012. Melbourne, Australia, December 10-12th 2012.

Abstract

Mitochondria are cytoplasmic organelles that are found in almost all mammalian cells. Mitochondria contain their own genome, mitochondrial DNA (mtDNA) that encodes 13 subunits of the electron transfer chain, which is the primary generator of cellular energy. Precise regulation of mtDNA copy number is essential for normal cell function and also the differentiation of stem cells into specialized cell types. Abnormal regulation of mtDNA copy number is associated with cellular dysfunction, mitochondrial disease and more recently cancer. Glioblastoma multiforme (GBM) is a highly malignant subgroup of brain tumors that exhibit similar characteristics to human neural stem cells (hNSCs) including multipotency and the expression of the stem cell factors. It is unknown how GBM cells regulate their mtDNA copy number during differentiation and whether this differs to hNSCs. Furthermore, it is unknown what role mtDNA plays in the gene expression profiles and the tumorigenicity of GBM.

To address these issues, GBM cells and hNSCs were differentiated for 28 days and their mtDNA copy number and gene expression were analyzed. In addition, GBM cells were progressively depleted of their mtDNA using the depletion agent, 2'-3'-dideoxycytidine, and their *in vivo* tumorigenicity assessed.

hNSCs and GBM cell lines regulated their copy number in a differential manner during differentiation. hNSCs progressively expanded their mtDNA copy number and adopted a differentiated phenotype whilst GBM cells failed to mimic these processes and their differentiation was incomplete. In addition, progressive depletion of mtDNA copy number in GBM cells resulted in reduced proliferation rates and the down regulation of stem cell factors. *In vivo*, mtDNA depleted GBM cells formed tumors at a reduced rate and frequency relative to non-depleted cells.

These outcomes demonstrate that mtDNA copy number is abnormally regulated in GBM cells and hinders their ability to complete differentiation. The failure of mtDNA-depleted GBM cells to consistently generate tumors strongly suggests that maintenance of mtDNA copy number is essential for GBM cells to be tumorigenic.

Abbreviations

ACHE	acetylcholinesterase
ADP	adenosine diphosphate
AIM	astrocyte induction media
AKT	protein kinase B
ALK	anaplastic lymphoma kinase
APOE	apolipoprotein E
ASCL1	achaete-scute homolog 1
ATP	adenosine triphosphate
BDNF	brain derived neurothrophic factor
bFGF	basic fibroblast growth factor
bp	base pairs
BrdU	bromodeoxyuridine
BSA	bovine serum albumin
CD	cluster of differentiation
CD133	cluster of differentiation 133
cDNA	complementary deoxyribonucleic acid
cm^2	centimeter squared
CO_2	carbon dioxide
CoA	coenzyme A
CoQ	coenzyme Q
COX	cytochrome c oxidase
CSC	cancer stem cell
CSM	cybrid selection media
Ct	cycle threshold
Cyt C	cytochrome complex
DAPI	4',6-diamidino-2-phenylindole
ddC	2'-3'-dideoxycytidine
dFBS	dialyzed fetal bovine serum
dH_2O	deionized water
DLL1	delta-like protein
DMEM	dulbecco’s modified eagle's medium
DMSO	dimethyl sulfoxide

DNA	deoxyribonucleic acid
dNTP	denucleoside triphosphate
DRD2	dopamine receptor D2
EDTA	ethylenediaminetetraacetic acid
EGF	epidermal growth factor
ESC	embryonic stem cell
ETC	electron transfer chain
F6P	fructose 6 phosphate
FAD	flavin adenine dinucleotide
$FADH_2$	flavin adenine dinucleotide (reduced)
FBS	fetal bovine serum
FCCP	carbonyl cyanide-4-trifluoromethoxy-phenylhydrazone
FGF	fibroblast growth factor
FGF13	fibroblast growth factor 13
FH	fumarate hydratase
FITC	fluorescein isothiocynante
GAPDH	glyceraldehyde 3-phosphate dehydrogenase
GBM	glioblastoma multiforme
GDNF	glial-cell derived neurothrophic factor
GFAP	glial fibrillary acidic protein
GTP	guanosine triphosphate
GUSB	beta-glucuronidase
H	hydrogen
H+	proton
H_2O	water
HAT	hypoxanthine-aminopterin-thymidine
HEY1	hairy/enhancer-of-split related with YRPW motif protein 1
HIF	hypoxia inducible factor
HIF1α	hypoxia inducible factor 1 alpha
HIV	human immunodeficiency virus
HMG	high mobility group
hNSC	human neural stem cell
HPRT1	hypoxanthine guanine phosphoribosyltransferase
HRM	high resolution melting curve

HSC	hematopoietic stem cell
HSP1	heavy strand promoter 1
HSP2	heavy strand promoter 2
HSP90AB1	heat shock protein HSP 90-beta
hTERT	telomerase reverse transcriptase (human)
IDH1	isocitrate dehydrogenase 1
IDH2	isocitrate dehydrogenase 2
iPS	induce pluripotent stem cell
LDH	lactate dehydrogenase
LOHN	leber's hereditary optic neuropathy
LN_2	liquid nitrogen
LSP	light strand promoter
MAG	myelin associated glycoprotein
MAP2	microtubule associated protein 2
MBP	myelin basic protein
MEF	mouse embryonic fibroblast
MELAS	mitochondrial encephalomyopathy, lactic acidosis and stroke-like episodes
MERRF	myoclonic epilepsy with ragged red fibers
mg	milligram
ml	millilitre
mM	millimolar
mm^3	millimeter cubed
Mol	mole
mtDNA	mitochondrial DNA
mtRNApol	mitochondrial specific-RNA polymerase
mtRNA	mitochondrial RNA
mtSSB	mitochondrial single stranded binding protein
NAD	nicotinamide adenine dinucleotide
NADH	nicotinamide adenine dinucleotide (reduced)
NADP	nicotinamide adenine dinucleotide phosphate
NAPDH	nicotinamide adenine dinucleotide phosphate (reduced)
NARP	neuropathy, ataxia, and retinitis pigmentos
NFkB	nuclear factor kappa

ng	nanogram
NH_4	ammonium
nm	nanometer
nM	nanomolar
NPTX	human neuronal pentraxin-1
NRF1	nuclear respiratory factor 1
NRF2	nuclear respiratory factor 2
NSC	neural stem cell
O_2	oxygen
O4	oligodendrocyte marker 4
OAA	oxaloacetic acid
O_H	the origin of replication of the heavy strand
O_L	the origin of replication of the light strand
OXPHOS	oxidative phosphorylation
PA	pyruvate acid
PBS	phosphate buffered saline
PCNA	proliferating cell nuclear antigen
PCR	polymerase chain reaction
PDH	pyruvate dehydrogenase
PFA	paraformaldehyde
PGC1α	peroxisome proliferator-activated receptor gamma co-activator 1-alpha
PGC1β	peroxisome proliferator-activated receptor gamma co-activator 1-beta
POLG	polymerase gamma
POLGA	polymerase gamma A
POLGB	polymerase gamma B
PPP	pentose phosphate pathway
PTEN	phosphate and tensin homolog
R6G	rhomadine 6G
RNA	ribonucleic acid
ROS	reactive oxygen species
rpm	revolutions per minute
rRNA	ribosomal RNA

RT-PCR	reverse transcription PCR
SCID	severe combined immunodeficiency
SD-DMEM	standard DMEM
SDH	succinate dehydrogenase
SEM	standard error of the mean
SEMA4D	semaphorin-4D
SHH	sonic hedgehog
T_a	annealing temperature
TAE	tris base, acetic acid and ethylenediaminetetraacetic acid
TCA	tricarboxylic acid cycle
TFAM	mitochondrial-specific transcription factor A
TFB1M	mitochondrial transcription factor B1
TFB2M	mitochondrial transcription factor B2
TIC	tumor initiating cell
TK	thymidine kinase
TK-	thymidine kinase negative
TK+	thymidine kinase positive
T_m	melting temperature
TRITC	tetramethyl rhodamine isothiocyanate
tRNA	transfer RNA
UV	ultra violet
v/v	volume to volume
VEGFA	vascular endothelial factor A
w/v	weight to volume
α	alpha
α-KG	alpha ketoglutarate
β	beta
β-ACTIN	beta actin
Δ	delta
μg	microgram
μl	microliter
μM	micromolar
ρ0	rho zero

^{o}C	celsius
%	percent

Chapter 1:General Introduction

1.1 Mitochondria

Mitochondria are cytoplasmic organelles that are found in almost every cell type of the mammalian body. The primary function of mitochondria is to generate cellular energy, or adenosine triphosphate (ATP), via oxidative phosphorylation (OXPHOS) and the electron transfer chain (ETC) (Pfeiffer et al., 2001). In addition, mitochondria also play essential roles in fatty acid oxidation (Hirschey et al., 2010), regulation of apoptosis (Joza et al., 2001), calcium homeostasis (Brini, 2003) and steroidogenesis (Bose et al., 2002), amongst others.

It is largely accepted that mitochondria are derived from an endo-symbiotic interaction between primitive anaerobic eukaryotes and α-protobacterium (Kurland and Andersson, 2000). The relationship, which developed over millions of years, granted eukaryotes access to the bacterium's enzymatic machinery to perform oxidative respiration. In support of this symbiotic relationship, mitochondria share a similar membrane structure to gram-negative bacteria (Kurland and Andersson, 2000). Mitochondria contain a double membrane, consisting of an outer membrane that is freely permeable to small molecules and ions and a folded inner-membrane that is largely impermeable (Smoly et al., 1970). Transfer of molecules such as protons (H+) across the inner membrane occurs via inner-membrane bound transporters (Nicholls and Ferguson 2002). The membrane bound transporters consist of five super complexes that form the ETC. The inner-mitochondrial membrane encloses the viscous region called the mitochondrial matrix (Frey and Mannella, 2000), which

harbors all the enzymatic components involved in the tricarboxylic acid cycle (TCA cycle), β-oxidation and amino acid oxidation (Baltzer et al., 2010). All of the processes that drive ATP production through oxidative pathways are found within the mitochondrion. Glycolysis, which can be performed under aerobic and anaerobic conditions, takes place in the cytosol (Meyerhof, 1951).

1.1.1 Glycolysis

Glycolysis is an energetic pathway that involves the conversion of one molecule of glucose to two molecules of pyruvate via a series of enzymatic reactions (Meyerhof, 1951). Energy is conserved during these reactions in the form of ATP and nicotinamide adenine dinucleatide (NADH) (Meyerhof, 1951). Glycolysis is composed of ten steps, which can be divided into two 5-step phases, the *preparatory phase* and the *payoff phase*. During the *preparatory phase,* glucose is converted to glyceraldehyde-3-phosphate and dihydroxacetone phosphate in a series of reactions that requires two molecules of ATP to be donated (Nelson and Cox 2008). The *payoff phase* recovers the invested ATP molecules by converting glyceraldehyde-3-phosphate to pyruvate, which in total yields 4 molecules of ATP with a net gain of 2 molecules of ATP and 2 molecules of NADH (Nelson and Cox 2008). Under aerobic conditions, eukaryotes are able to further metabolize glycolysis-derived pyruvate via the TCA cycle (Section 1.1.2) (Krebs and Johnson, 1937). The substrates and electron donors that are generated through the TCA cycle are subsequently utilized by the ETC to generate ATP (Krebs and Johnson, 1937; Mitchell, 1961). Under anaerobic conditions the oxidization of pyruvate occurs at a reduced rate and a large proportion of pyruvate is converted to lactate by lactate

dehydrogenase (LDH) (Nelson and Cox 2008) in a process known as anaerobic respiration or fermentation.

1.1.2 The TCA cycle

Prior to entry into the TCA cycle, glycolysis-derived pyruvate is converted into acetyl-CoA by pyruvate dehydrogenase (PDH) (Figure 1.1) (Krebs and Johnson, 1937). Alternate sources of acetyl-CoA are also derived from β-oxidation and amino acid oxidation processes (Baltzer et al., 2010) and the reactions of the TCA cycle are illustrated in Figure 1.1. With each TCA cycle, 3 molecules of NADH, 1 molecule of flavin adenine dinucleotide ($FADH_2$), 1 molecule of guanosine triphosphate (GTP) (or ATP) are generated and 2 molecules of CO_2 are released (Figure 1.1) (Krebs and Johnson, 1937)Nelson and Cox 2008). The NADH and $FADH_2$ that are generated from glycolysis and the TCA cycle are subsequently utilized by the ETC where they function as electron donors (Mitchell, 1961).

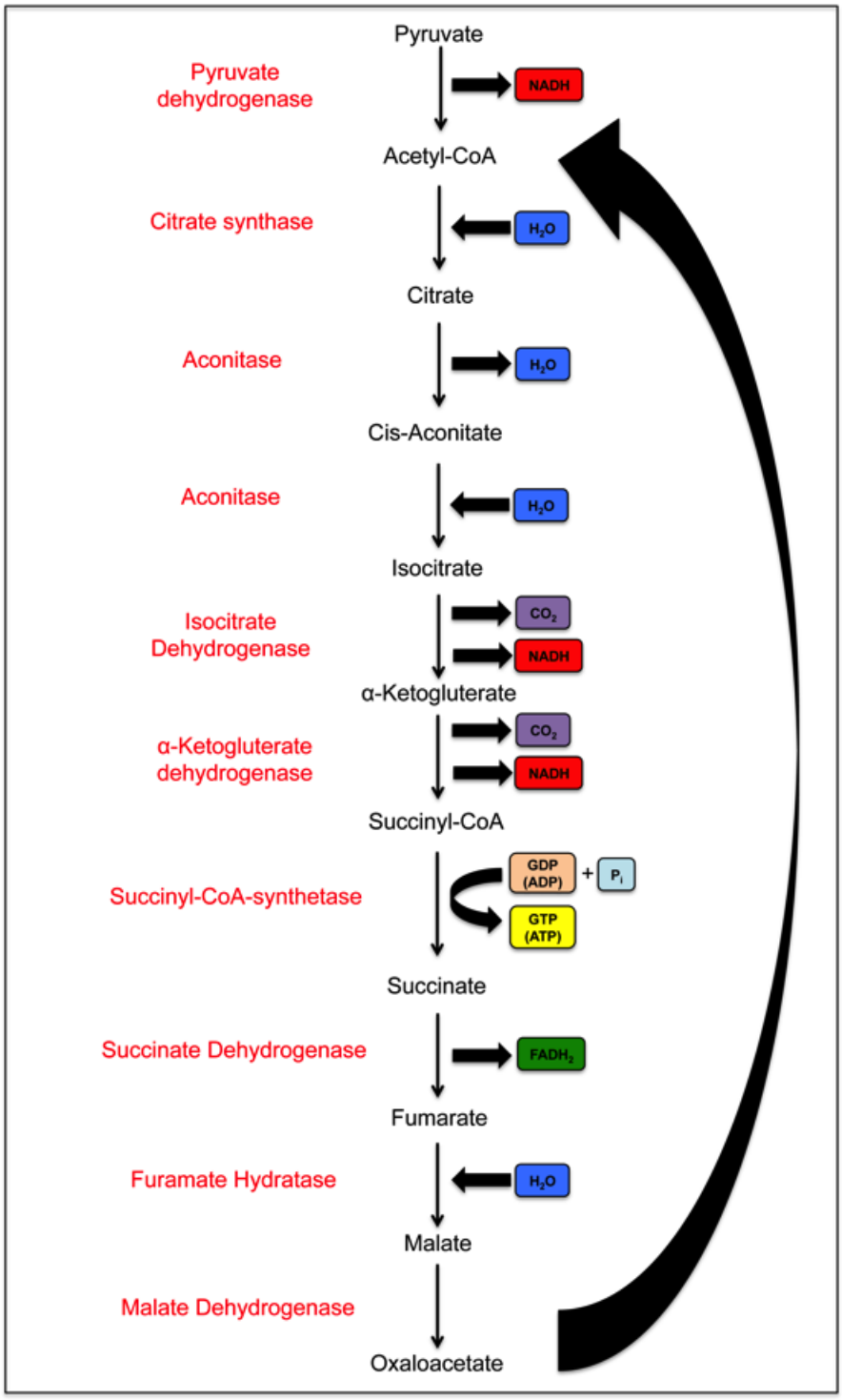

Figure 1.1. Schematic representation of the tricarboxylic cycle. The enzymes of the cycle are highlighted in red text. The short black arrows indicate the substrates that are consumed and generated by the cycle. The long black arrow represents the continuation of the cycle.

1.1.3 The ETC and OXPHOS

The ETC is composed of five membrane bound protein super-complexes, Complex I (NADH dehydrogenase), Complex II (Succinate Dehydrogenase), Complex III (Cytochrome C Reductase), Complex IV (Cytochrome C Oxidase) and Complex V (ATP Synthase) (Adam-Vizi and Chinopoulos, 2006; Mitchell, 1961). Each of ETC complexes consists of multiple subunits that are assembled in the mitochondria with Complexes I-V containing 45, 4, 11, 13 and 16 subunits, respectively (Griguer and Oliva, 2011). Electrons from NADH and $FADH_2$ are donated to complexes I and II respectively, and each complex is able to initiate OXPHOS (Figure 1.2) (Adam-Vizi and Chinopoulos, 2006; Mitchell, 1961). Electrons are subsequently shuttled to Coenzyme Q and Complex III. From Complex III electrons are accepted by Cytochrome C, which in turn donates electrons to Complex IV. In the final electron transfer step, O_2 accepts two electrons, which leads to the generation of H_2O. The flow of electrons through Complexes I, III and IV are accompanied by the transport of protons (H+) across the inner-membrane into the inter-membrane space (Figure 1.2) (Adam-Vizi and Chinopoulos, 2006; Mitchell, 1961). The transport of protons creates an electrochemical gradient in which the inter-membrane space and mitochondrial matrix become positively and negatively charged, respectively (Adam-Vizi and Chinopoulos, 2006; Mitchell, 1961). The electrochemical gradient is utilized by Complex V, which transports protons back across the inner-membrane into the mitochondrial matrix whilst regenerating ATP from ADP and inorganic phosphate (Figure 1.2) (Adam-Vizi and Chinopoulos, 2006; Mitchell, 1961).

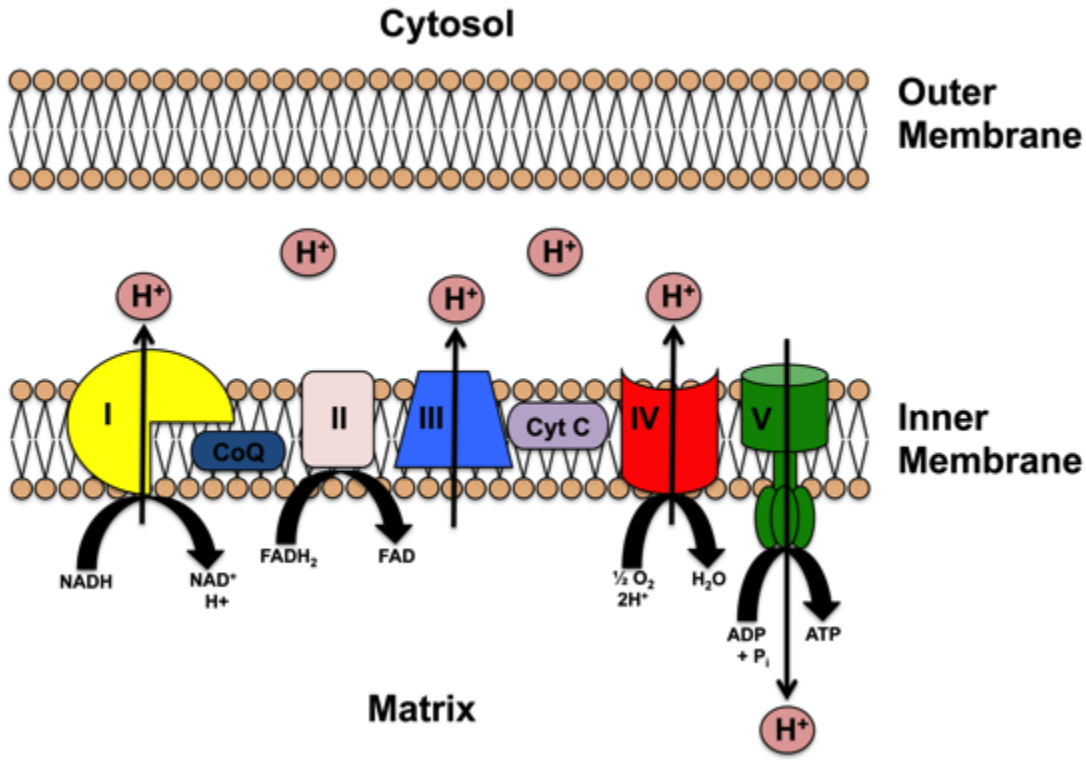

Figure 1.2. Schematic representation of the electron transfer chain. Electrons are donated to Complexes I and II and are subsequently passed along the chain through each of the complexes. The transfer of electrons is accompanied by a shuttling of protons (H+) across the inner mitochondrial membrane by Complexes I, II and IV, which creates an electrochemical gradient. Protons re-enter the mitochondrial matrix via Complex V, which regenerates ATP from ADP and inorganic phosphate.

Abbreviations: I (Complex I), II (Complex II), III (Complex III), IV (Complex IV), V (Complex V), H+ (Protons), ADP (Adenosine di-phosphate), ATP (Adenosine tri-phosphate), Cyt C (Cytochrome C), CoQ (Coenzyme Q), FAD (flavin adenine dinucleotide), $FADH_2$ (flavin adenine dinucleotide reduced), H (Hydrogen), H_2O (Water), NAD (nicotinamide adenine dinucleotide), NADH (nicotinamide adenine dinucleotide reduced), P_i (inorganic phosphate), O_2 (Oxygen).

The net combined yield of ATP from glycolysis and OXPHOS ranges between 30-36 molecules of ATP (2 from glycolysis and 28-34 from OXPHOS) per glucose molecule (See Table 1.I) (Brown, 1992; Pfeiffer et al., 2001). In comparison to OXPHOS, glycolysis is a relatively inefficient source of ATP production and thus, most eukaryotic cells utilize OXPHOS extensively under aerobic conditions (Brown, 1992; Pfeiffer et al., 2001). Table 1.I below summarizes the combined ATP yield of glycolysis, TCA cycle and the ETC.

Enzymatic Reaction	Reaction Yield	ATP Yield
1x Glucose → Glucose-6-phosphate	-1 ATP	-1
1x Frutose-6-phosphate → Fructose 1,6-bisphosphte	-1 ATP	-1
2x Glyceraldehyde-3-phosphate → 2x 1,3-Bisphosphoglycerate	2x NADH	3-5
1x 1,3-Bisphosphoglycerate → 2x 3-Phosphoglycerate	2x ATP	2
2x Phosphoenolpyruvate → 2x Pyruvate	2x ATP	2
2x Pyruvate → 2x Acetyl-CoA	2x NADH	5
2x Isocitrate → 2x α-ketoglutarate	2x NADH	5
2x α-ketoglutarate → 2x Succinyl-CoA	2x NADH	5
2x Succinyl-CoA → 2x Succinate	2x GTP/ATP	2
2x Succinate → 2x Fumarate	2x $FADH_2$	5
2x Malate → 2x Oxaloacetate	2x NADH	5

Table 1.I Summary of Glycolysis and TCA cycle reactions that subsequently consume or generate ATP through OXPHOS**.** Table modified from Nelson and Cox 2008.

1.1.4 Mitochondrial DNA

The ETC super-complexes consist of multiple protein subunits that are encoded by both the nuclear and mitochondrial genomes (mtDNA). The exception is Complex II, which is entirely encoded by nuclear factors (Clayton, 1998). MtDNA is a maternally inherited double-stranded genome consisting of a heavy (H) and a light (L) strand (Attardi and Schatz, 1988). In humans, mtDNA is 16,569kb in length and encodes 13 subunits of the ETC (7 of Complex I, 1 of Complex III, 3 of Complex IV and 2 of Complex V) and 22 transfer RNAs (tRNAs) and 2 ribosomal RNAs (rRNAs), which are essential for the decoding and subsequent translation of mtRNA into mitochondrial proteins (Anderson et al., 1981) (Figure 1.3). The remaining nuclear encoded subunits of the ETC are synthesized by cytosolic ribosomes and imported into the mitochondria prior to assembly into ETC complexes (Hildenbeutel et al., 2008; Kurland and Andersson, 2000).

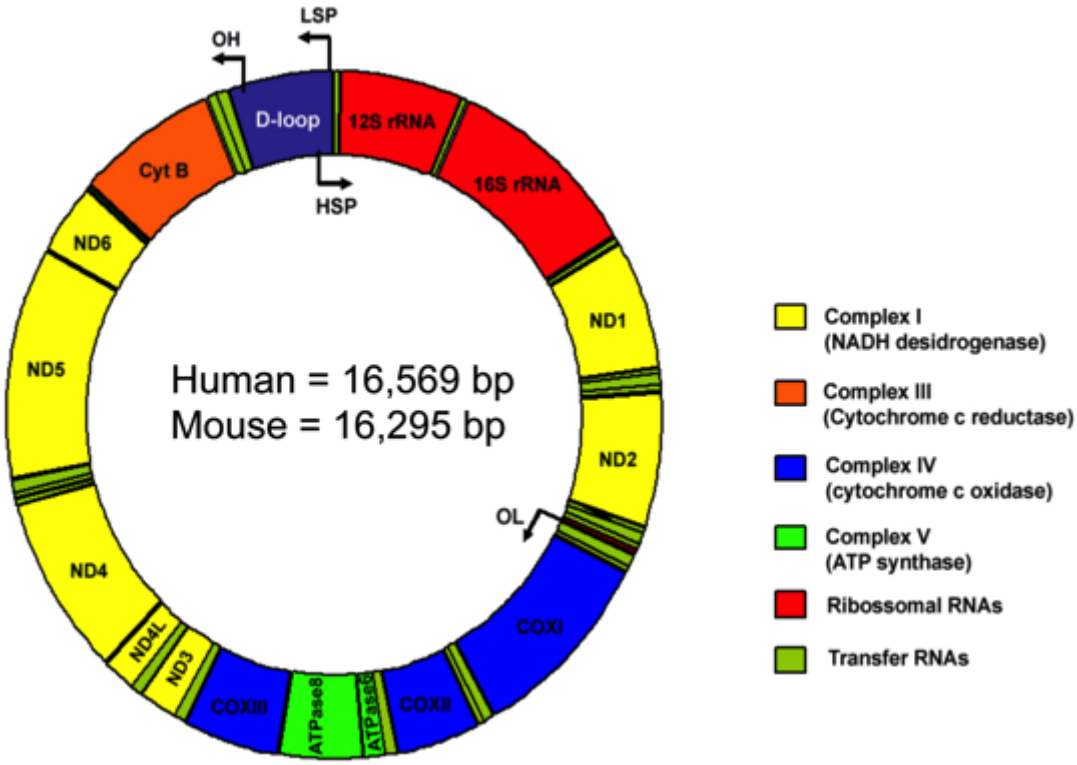

Figure 1.3. Diagrammatic representation of the mitochondrial genome (mtDNA). MtDNA is a circular genome that encodes 13 subunits of the electron transfer chain, 22 tRNAs and 2 rRNAs. The colours of the genes correspond to the complexes shown in the key.

Each mitochondrion contains multiple copies of mtDNA (1-15 copies) (Legros et al., 2004; Satoh and Kuroiwa, 1991). When each copy of mtDNA is identical this state is referred to as homoplasmy. Mutations in mtDNA can occur through point mutations, insertions and deletions and this can lead to the coexistence of mutant and wild type copies of mtDNA within single or multiple mitochondria, which generates a state referred to as heteroplasmy. The level of heteroplasmy can vary greatly from 1-100% (Carling et al., 2011) within individual mitochondria and can also vary greatly between mitochondria of different tissue types (Schwartz and Vissing, 2002). The manifestation of a pathological state

generally does not occur until the percentage, or mutant load, of mtDNA reaches a threshold level, which can range from 60-90% (Chinnery et al., 1997). Once this threshold has been reached, bioenergetic defects begin to arise at a cellular level due to reduced ETC function, which is instigated by mutant mtDNA encoded subunits contributing to the formation of abnormal ETC Complexes.

Severe bioenergetic defects can elicit deleterious effects at cellular and tissue levels (Wallace, 1999; Wallace, 2005). Since mtDNA is essential for ETC function and OXPHOS, mtDNA mutations severely affect high-energy requiring tissue types, such as skeletal muscle and neural tissue (Wallace, 1999; Wallace, 2005). This is evidenced by the mitochondrial DNA diseases that primarily effect neural and skeletal tissue and include Leber's hereditary optic neuropathy (LHON) (Holt et al., 1989), Mitochondrial encephalomyopathy, lactic acidosis, and stroke-like episodes (MELAS) (Schon et al., 1992) and Neuropathy, ataxia, and retinitis pigmentosa (NARP) (Holt et al., 1990). In addition, mutations in mtDNA have also been associated with other neurological disorders, such as Parkinson's disease and also diabetes (Wallace, 1999; Wallace, 2005).

1.1.5 MtDNA transcription and replication

MtDNA contains no introns, however, there are two non-coding regions (Anderson et al., 1981). The displacement loop (D-Loop) is the largest non-coding region, spanning ~1200 base pairs (bp) and encompasses the origin of replication for the H-strand (O_H) and the promoters of L-strand transcription (HSP1, HSP2 and LSP) of mtDNA (Anderson et al., 1981). The second non-

coding region is a short 30 bp sequence that contains the origin of replication of the L-strand (O_L) (Anderson et al., 1981), which is located two-thirds around the mitochondrial genome from the D-loop region.

Mitochondria do not possess the biological machinery required to replicate their own genome and, in order to mediate this process, they rely exclusively on nuclear encoded factors that are translocated and imported into the mitochondrial matrix (Falkenberg et al., 2007). Peroxisome proliferator-activated receptor gamma coactivator 1-alpha (PGC1α) is a protein that plays a key role in energy metabolism and is a master regulator of mitochondrial biogenesis (Wu et al., 1999). In response to external physiological stimuli (Puigserver et al., 1998; Zhu et al., 2010), PGC1α interacts with multiple transcription factors including the nuclear respiratory factors (NRF1 and NRF2) (Wu et al., 1999). The NRFs bind to the promoter region of the high mobility group (HMG) protein, mitochondrial transcription factor A (TFAM) (Wu et al., 1999). TFAM interacts with mtDNA via the D-loop region, which is the primary site of interaction between the nuclear-encoded transcription and replication factors and mtDNA (Anderson et al., 1981). TFAM binds to the enhancer regions of the LSP and HSP and induces structural changes to mtDNA and exposes the promoter region (Falkenberg et al., 2007). The mitochondrial specific-RNA polymerase (mtRNApol) and mitochondrial transcription factor B1 (TFB1M) and B2 (TFB2M) are recruited and assist in the initiation of mtDNA transcription and subsequently generate a RNA-DNA hybrid primer (Fernandez-Silva et al., 2003; Gleyzer et al., 2005). The hybrid primer is utilized by the mitochondrial specific polymerase, Polymerase Gamma (POLG) to initiate mtDNA replication (Ropp

and Copeland, 1996). POLG is a heterotrimer enzyme consisting of a catalytic subunit, POLGA, and two accessory subunits, POLGB. POLGA is responsible for the replication of mtDNA whilst POLGB is essential for recognition of the hybrid primer and for high fidelity binding to POLGA (Carrodeguas et al., 2001; Ropp and Copeland, 1996). Other factors that assist in the process of mtDNA replication include the mtDNA helicase, TWINKLE (Li et al., 1999), and mitochondrial single stranded binding protein, MTSSB (Takamatsu et al., 2002). Since mtDNA transcription and replication is reliant on multiple factors, the precise orchestration of these factors is essential for efficient transcription and replication to occur and to maintain normal cell function (Clayton, 1998).

Currently, there are two proposed models of mtDNA replication, the asymmetric model and the coupled strand synthesis model. The asymmetric model was first proposed in 1972 and suggests that replication of mtDNA occurs at the HSP and proceeds two-thirds around the genome to the LSP (Shadel and Clayton, 1997). From the LSP, replication occurs in the opposite direction and completes the process of replication. The long-standing asymmetric model has since been challenged, which led to the development of the coupled strand synthesis model (Yasukawa et al., 2006). This model suggests that mtDNA replication occurs in a similar manner to nuclear DNA replication in which replication occurs bi-directionally from the HSP and H and L strands, simultaneously. It is likely that both models of replication occur simultaneously, however, this topic remains highly disputed (Bogenhagen and Clayton, 2003; Holt and Jacobs, 2003)

1.2 Mitochondrial DNA Copy Number

1.2.1 MtDNA copy number regulation during (in vitro) development

In order to analyze how mtDNA copy number is regulated during development reliable *in vitro* models are required. Stem cells are specialized populations of cells that are able to self-renew, which generates two identical daughter cells, or they differentiate into specialized cell types. The differentiation of stem cells often mimics *in vivo* development. Advances in cell biology techniques over the past two decades have resulted in the establishment stem cell lines *in vitro* from both embryonic and adult origins and are now a powerful research tools. Stem cell models of development allow scientists to consistently mimic *in vivo* developmental processes (Kehat et al., 2001; Lumelsky et al., 2001; Wichterle et al., 2002) *in vitro* and they also provide an excellent opportunity to investigate how mtDNA copy number is regulated during development.

Embryonic stem cells (ESCs) are one of the most intensely researched stem cell types and have contributed greatly to our understanding of the regulation of mtDNA copy number and its impact on energy metabolism (Cho et al., 2006; Facucho-Oliveira et al., 2007; Prigione et al., 2010; St John et al., 2005; Varum et al., 2011). ESCs are derived from the inner cell mass of a blastocyst (Evans and Kaufman, 1981; Thomson et al., 1998) and were first derived from mice in the 1980's (Evans and Kaufman, 1981; Thomson et al., 1998). ESCs are pluripotent, which is demonstrated by their ability to generate cell types of the three primary germ layers, the ectoderm, mesoderm and endoderm as well as germ cells (Bradley et al., 1984; Hubner et al., 2003). ESCs are also characterized by their self-renewal and proliferative properties. ESCs express a

core set of transcription factors, OCT4, NANOG and SOX2 and these that are essential for the maintenance of pluripotency (Ginis et al., 2004). Down regulation of these factors is associated with the onset of differentiation (Cai et al., 2006; Zaehres et al., 2005).

Undifferentiated ESCs are associated with low mtDNA copy number, defined as the mtDNA set point (Facucho-Oliveira et al., 2007), and express the nuclear encoded mtDNA transcription and replication factors, POLGA, POLGB and TFAM, at low levels (Facucho-Oliveira et al., 2007; St John et al., 2005). The mitochondrial biogenesis factors, PGC1α, PGC1β and NRF1 are also expressed at low levels (Prigione et al., 2010). Low mtDNA copy number in ESCs is accompanied by the presence of immature mitochondria that are spherical in morphology; contain poorly organized cristae and a matrix with low electron density (Cho et al., 2006; St John et al., 2005). The combination of low mtDNA copy number and immature mitochondria results in ESCs possessing low oxidative capacity (Varum et al., 2011). In agreement, ESCs express low levels of the ETC subunits and TCA enzymes and generate low levels of ATP (Cho et al., 2006; Facucho-Oliveira et al., 2007; Prigione et al., 2010; St John et al., 2005; Varum et al., 2011) relative to mature cells types. ESCs are thus heavily reliant on glycolysis as a means of metabolic support and express increased levels of glycolytic enzymes, exhibit a high rate of glycolytic flux and secrete elevated levels of lactate relative to mature or differentiated cell types (Prigione et al., 2010; Varum et al., 2011).

Differentiated/mature cell types, such are neurons and myocytes, require large amounts of ATP to perform their specific cellular functions (Moyes et al., 1998). In order to meet this energetic demand, these cell types rely extensively on OXPHOS for the generation of ATP (Chung et al., 2007). High-energy cell types also possess high mtDNA copy number and mature mitochondrial networks, which are consistent with an increase in OXPHOS utilization (Cho et al., 2006; Miller et al., 2003). It is therefore likely that the transition from stem cell to mature cell type requires a shift from glycolytic to oxidative metabolism that is accomplished by an increase in mtDNA copy number and expression of the nuclear and mtDNA encoded subunits and assembly factors of the ETC.

Evidence of this transition has been observed in multiple studies. Differentiation of murine ESCs was associated with an expansion of mtDNA copy number; increased expression of mtDNA transcription and replication factors and ETC associated genes (Facucho-Oliveira et al., 2007). These changes did not occur at the onset of differentiation (Day 0) and are observed on Day 6 of differentiation. In a study of murine neural stem cells (NSCs), a multipotent stem cell population found within the brain (Wang et al., 2011; Wang et al., 2010), mtDNA copy number was immediately and progressively increased following the onset of differentiation. NSCs are multipotent and give rise to only neural cell types. It is plausible that expansion of mtDNA copy number occurs at the time of lineage specification, which may occur earlier in NSCs due to their restricted potency.

Differentiated cell types have been shown to express higher levels of ETC and TCA cycle enzymes, consume greater concentrations of O_2, generate higher levels of ATP and secrete less lactate than ESCs (Chung et al., 2007; Prigione et al., 2010; Varum et al., 2011). Changes in gross mitochondrial morphology also occur during differentiation, with mitochondria becoming more elongated with complex cristae and dense matrices (Cho et al., 2006; Varum et al., 2011). Furthermore, mitochondrial membrane potential increases and is consistent with increased proton flow across the mitochondrial membrane and increased utilization of the ETC (Cho et al., 2006; Facucho-Oliveira et al., 2007; Prigione et al., 2010; St John et al., 2005; Varum et al., 2011).

In summary, the journey of an undifferentiated stem cell to a fully differentiated cell type requires dynamic changes in mtDNA copy number and mitochondrial function. Acquisition of mtDNA copy number occurs during differentiation and lineage specification and reflects the future metabolic requirements of the terminally differentiated cell type. Changes in mtDNA copy number and maintenance of copy number are regulated entirely by nuclear encoded factors and their precise interaction with the mitochondrial genome is essential to maintain normal cellular function. The loss of a cell's ability to regulate/maintain mtDNA copy number is associated with mitochondrial diseases (Wallace, 1999; Wallace, 2005) and more recently cancer.

1.2.2 Tumorigenesis and the association with mtDNA copy number

Tumorigenesis is the formation or development of cancer. It is a complex process that can be summarized by the "transformation" of a normal cell into a

cancer/tumor cell that subsequently undergoes uncontrolled cell division and develops into a tumor mass (Evan and Vousden, 2001; Reya et al., 2001). It is well established that tumorigenesis is associated with abnormal regulation of chromosomal genes that regulate cell proliferation (oncogenes & tumor suppressors) and apoptosis (Evan and Vousden, 2001; Reya et al., 2001). However, the role that mtDNA plays in tumorigenesis is less clear. As discussed earlier in this chapter, the regulation of mtDNA copy number is essential to support normal cellular function and deviations or changes in mtDNA copy number are associated with cellular dysfunction and disease. It is, therefore, likely that abnormal regulation of mtDNA copy number plays a role in tumorigenesis. In support of this hypothesis, changes in mtDNA copy number in tumors, relative to the neighboring healthy tissue, are now well documented and are summarized in Table 1.II. The possible mechanisms for changes in mtDNA copy number in tumors are discussed in more detail below.

Tumor origin	MtDNA copy number	Reference
Breast	Decreased	(Fan et al., 2009; Mambo et al., 2005; Tseng et al., 2006; Yu et al., 2007)
Gastric	Decreased	(Wu et al., 2005)
Colon	Decreased	(Chen et al., 2011)
Liver	Decreased	(Lee et al., 2004; Vivekanandan et al., 2010; Yamada et al., 2006; Yin et al., 2004)
Brain	Increased	(Liang and Hays, 1996)
Head & Neck	Increased	(Jiang et al., 2005; Kim et al., 2004; Shieh et al., 2004)
Lung	Decreased	(Lin et al., 2008)
Prostrate	Increased	(Mizumachi et al., 2008)
Acute lymphoblastic leukemia	Increased	(Egan et al., 2010)
Endometrial	Increased	(Wang et al., 2005)
Esophageal	Increased	(Tan et al., 2006)
Non-Hodgkin lymphoma	Increased	(Kusao et al., 2008)
Ovarian	Increased	(Wang et al., 2006)
Thyroid	Increased	(Mambo et al., 2005)
Ewings sarcoma	Decreased	(Yu et al., 2010)
Fibrolamellar	Decreased	(Vivekanandan et al., 2010)
Renal cell	Decreased	(Heddi et al., 1996; Meierhofer et al., 2004; Selvanayagam and Rajaraman, 1996; Xing et al., 2008)

Table 1.II. Summary of the changes in mtDNA copy number in tumors.

1.2.3 Mechanisms for increased mtDNA copy number in tumor cells

Some tumor types consistently show increases in mtDNA copy number relative to healthy neighboring tissues (See Table 1.II). Increases in mtDNA copy number are associated with the ageing process (Lee et al., 1998) and the probability of the development of cancer also increases during ageing, although cancer can also affect the young (Finkel et al., 2007). There is also evidence to suggest that mtDNA mutations/deletions accumulate during ageing (Lee et al., 1998; Richter et al., 1995; Wei, 1998) and it is hypothesized that the increases

in mtDNA act as a compensatory mechanism for OXPHOS defects that are a consequence of accrued mtDNA rearrangements and exposure to oxidative stress over time (Lee et al., 2000).

Experimentally, increases in mtDNA copy number in response to oxidative stress have been demonstrated by Lee et al., who observed increases in mtDNA copy number in primary lung cells following hydrogen peroxide exposure (Lee et al., 2000). The authors concluded that changes in mtDNA copy number are early molecular events to support adaption to exogenous and endogenous oxidative stress (Lee et al., 2000). In support of the association of increased mtDNA copy number and ageing, the analysis of brain tissues from aged rhesus monkeys and murine NSCs revealed elevated mtDNA copy number relative to non-aged controls (Mao et al., 2012; Stoll et al., 2011). The aged NSCs exhibited a reduced OXPHOS profile and increased glycolytic activity despite the increases in mtDNA content. These outcomes suggest that OXPHOS becomes increasingly defective during ageing. The development of OXPHOS defects is likely to be multifactorial, however, there is now evidence to suggest that mtDNA mutations play a key role in this process since mtDNA mutations occurred at an increased frequency in aged rhesus monkey neural tissue relative to non-aged controls (Mao et al., 2012).

MtDNA copy number is cell specific and is related to the specialized function of individual or groups of cells (Kelly et al., 2013). Interestingly, changes to mtDNA copy number during ageing also appear to occur in a cell/tissue specific manner. Whilst increases in mtDNA copy number have been observed in

stressed lung cells and aged neural tissue (Lee et al., 2000; Mao et al., 2012), mtDNA copy number was reduced in aged liver tissue and unchanged in aged cardiomyocytes, relative to non-aged controls (Barazzoni et al., 2000). Similar to aged tissues, alterations in mtDNA copy number in tumor cells appear to be tumor specific (see Table 1.II). Nevertheless, a correlation exists between ageing, the accumulation of mtDNA rearrangements and OXPHOS defects.

1.2.4 Mechanisms for decreased mtDNA copy number in tumors

There are 16 known DNA polymerases that function in eukaryotic cells. POLGA is the only DNA polymerase that is currently known to replicate mtDNA and is, therefore, vital to mitochondrial function (Hance et al., 2005). Loss of POLGA function in tumor cells has been shown to cause reductions in mtDNA copy number (mtDNA depletion), increased production of mitochondrial reactive oxygen species (ROS) and an overall decrease in mitochondrial function (Chan and Copeland, 2009; Chandra and Singh, 2011). A study by Singh et al. outlined a possible mechanism by which POLGA mutations could promote tumorigenesis (Singh et al., 2009), by ectopically expressing a proofreading deficient POLGA into a breast cancer cell line. The proofreading deficient POLGA induced mtDNA depletion in the transformed cells compared to controls. In addition, the transformed cells showed enhanced tumorigenic potential in *in vitro* based assays (Singh et al., 2009). This study highlighted that defects in POLGA can potentially play a role in mtDNA depletion syndromes and enhanced tumorigenicity of tumor cells.

Loss of TFAM function is associated with respiratory chain defects and has recently been linked with cancer (Hansson et al., 2004). TFAM is an essential transcription factor involved in mtDNA transcription and replication and there is evidence to suggest precise regulation of TFAM protein levels are required to maintain mtDNA copy number (Litonin et al., 2010). A recent study by Guo et al. comprehensively described the potential role that TFAM mutations may play in tumorigenesis and to date is the only study highlighting this association. In this study, truncating mutations in TFAM were associated with 74% of colorectal tumors that exhibited microsatellite instability, whilst no mutations were observed in tumors with microsatellite stability (Guo et al., 2011). *In vitro*, cells with truncating mutations exhibited reduced TFAM protein levels, mtDNA depletion and reduced mtDNA gene expression relative to cells with wild type TFAM. Cells expressing mutant TFAM also generated tumors in immunocompromised mice at an accelerated rate relative to controls and suggests that mutant TFAM elicits a growth advantage. Finally, cells harboring the TFAM mutant exhibited enhanced resistance to the chemo-agent, cisplatin, compared to wild type controls. Since TFAM interacts directly with the mtDNA HSP within the D-loop (Ekstrand et al., 2004), it is likely that mutations in TFAM compromise interactions with the D-loop. In support of this hypothesis, mutant TFAM was shown to bind to the D-loop region at a reduced affinity in comparison to wild type TFAM (Guo et al., 2011). Collectively, this seminal study demonstrated that TFAM mutations contribute to mtDNA depletion and promotes proliferation and chemo-resistance (Guo et al., 2011). Given the importance of POLG and TFAM to mtDNA transcription and replication, it is important to consider whether factors upstream of these factors, such as

PGC1α and the NRFs, may also be exerting strong effects on mtDNA copy number in tumor cells. However, at present very little research has been preformed on their respective roles in the regulation of mtDNA copy number in tumor cells.

The D-loop is a ~1200bp non-coding region of mtDNA that contains three regulatory sites for mtDNA transcription and replication (Anderson et al., 1981). Mutations within the D-loop have been frequently reported in various tumor types (Lee et al., 2004; Yu et al., 2010; Yu et al., 2007). Given the importance of the D-loop region, it is likely that mutations within the D-loop region also disrupt the binding affinity of TFAM and the initiation of mtDNA transcription and replication. This could lead to reduced mtDNA turn over and depletion over time. Experimental evidence supports this hypothesis with an association of D-loop mutations with mtDNA depletion in hepatocellular carcinoma (Lee et al., 2004), breast cancer (Yu et al., 2007), and Ewings sarcoma (Yu et al., 2010). In addition, mtDNA depletion has also been associated with increased tumorigenicity and resistance to chemo-agents in tumors (Guo et al., 2011; Singh et al., 2009). It is, therefore, likely that mutations within the D-loop region may play a role in the initiation and or maintenance of tumorigenesis.

p53 is a tumor suppressor gene that is implicated in DNA repair, cell cycle control and apoptosis (Achanta et al., 2005). In addition, p53 interacts directly with POLGA and functions to maintain mtDNA integrity in response to insults such as mitochondrial ROS, which are generated by the ETC and are potentially harmful to mtDNA due to their close proximity to each other (Achanta

et al., 2005). Achanta et al. demonstrated that p53 enhances the DNA replication and proofreading properties of POLGA (Achanta et al., 2005). The knockdown of p53 was shown to have the reverse effect and increased the frequency of mtDNA damage and increased the frequency of *in vivo* mutations (Achanta et al., 2005). p53 also functions as a checkpoint protein during mitochondrial biogenesis and acts as an external repair protein. In addition, the loss of p53 expression was associated with mtDNA depletion (Kulawiec et al., 2009a). Loss of p53 function occurs at a high frequency in cancer and is observed in ~50% of tumors (Vogelstein et al., 2000). Given the association of p53 with mtDNA, it is likely that the loss of p53 function will induce deleterious effects on mtDNA that include the loss of mtDNA integrity and also increases the likelihood of abnormal mtDNA replication through reduced POLG function (Achanta et al., 2005). Consequently, loss of p53 function may play an indirect role in mtDNA depletion, establishment of multiple mtDNA variants and large-scale deletions, which are often observed in tumors (Chen et al., 2011; Lee et al., 2004; Shieh et al., 2004; Yu et al., 2010; Yu et al., 2007).

1.2.5 MtDNA-less tumor cells

The observed alterations in mtDNA copy number in tumors strongly suggest that mtDNA plays either a direct or indirect role in tumorigenesis. In an attempt to further elucidate this role, multiple laboratories have completely removed mtDNA from tumor cells. The removal of mtDNA is a powerful technique that allows scientists to determine how mtDNA alters cellular function. *In vitro*, tumor cells can be progressively depleted of mtDNA by long-term exposure to ethidium bromide (King and Attardi, 1989). Low concentrations of ethidium

bromide intercalate into mtDNA and inhibit the activity of POLGA, which results in stalled mtDNA replication and transcription (King and Attardi, 1989). As the cell continues to divide, mtDNA is sequentially diluted until a surviving population of cells remains that are devoid of mtDNA and are referred to as ρ0 cells. To this end, ρ0 cells have been derived from multiple tumor cell types that include lung (A549) (Amuthan et al., 2002), bone (143BTK-) (Singh et al., 2005) and cervical (HeLa) cancer cells (Shidara et al., 2005), amongst others. Due to the loss of mtDNA, ρ0 cells possess OXPHOS defects and rely extensively on glycolysis for the generation of ATP (King and Attardi, 1989). Consequently, the study of ρ0 tumor cells provides the opportunity to investigate how the loss of mtDNA impacts upon the functions of tumor cells, particular their tumorigenic properties.

The effects of mtDNA depletion using ethidium bromide in tumor cells vary considerably in the literature. Loss of mtDNA resulted in enhanced tumorigenicity in breast (Kulawiec et al., 2009b), lung (Amuthan et al., 2002), osteosarcoma (Singh et al., 2005), melanoma (Ballot et al., 2010) and prostrate tumor cells. However, other studies have reported reduced tumorigenicity in tumor cells derived from the same tumor types listed above (Cavalli et al., 1997; Magda et al., 2008; Yen et al., 2005). There is some evidence to suggest that mtDNA depletion not only alters cell metabolism but can also induce changes in nuclear gene expression and induce epigenetic modification (Singh et al., 2005; Smiraglia et al., 2008). Interestingly, gene expression and epigenetic changes were reversible in ρ0 cells following the re-population of tumor cells with donor mtDNA (Singh et al., 2005; Smiraglia et al., 2008). These reports provide strong

evidence that mtDNA interacts with nuclear DNA (nuclear-mtDNA cross talk) and suggests that mtDNA may play a direct role in tumorigenic transformation.

1.3 New approaches for investigating the role of mtDNA in tumor cells: Multipotent tumor cells

It remains to be fully determined how tumor cells regulate their mtDNA copy number relative to normal cells. The studies cited in Table 1.II directly compared the mtDNA copy number of tumor tissue to neighboring healthy tissue. These studies have provided invaluable insight into how copy number in tumor cells differs to that of normal cells, however, they do not show how mtDNA copy number is regulated over time. Over the last decade, a number of studies have identified subpopulations of cells within tumors that exhibit stem cell-like properties. It has been speculated that the self-renewal and differentiation these stem cell-like cells may underpin tumor heterogeneity. The study of these cell types would provide valuable insight into how mtDNA copy number is regulated in tumor cells and also during tumorigenesis. Tumor cells exhibiting stem cell-like properties are commonly refereed to as cancer stem cells (CSCs) or tumor initiating cells (TICs) (Clarke et al., 2006). Although the existence of CSCs remains a controversial topic, self-renewing tumor cells have been identified in blood (Lapidot et al., 1994), brain (Singh et al., 2003), breast (Al-Hajj et al., 2003), prostrate (Collins et al., 2005) and colon cancers (Ricci-Vitiani et al., 2007).

The drive behind the identification of CSCs originates from hematological research (Lapidot et al., 1994; Spangrude et al., 1988). Hematopoietic stem

cells (HSCs) are characterized by a battery of surface antigens and/or clusters of differentiation (CD) markers (Spangrude et al., 1988). The application of these criteria led to the identification of a subpopulation of tumorigenic self-renewing leukemic cells (Lapidot et al., 1994). Subsequently, probing for stem cell characteristics in solid tumors led to the identification of self-renewing tumor cell types (Al-Hajj et al., 2003; Collins et al., 2005; Ricci-Vitiani et al., 2007; Singh et al., 2003). One tumor subtype that exhibits striking stem cell-like characteristics are glioblastoma multiforme (GBM).

GBM is the most common and malignant primary brain tumor and accounts for more than 70% of all central nervous system malignancies (Buckner et al., 2007). GBM is renowned for its resistance to current therapeutic strategies and the median prognosis for GBM patients currently remains at 12 to 15 months despite recent advances in medical therapeutics (Buckner et al., 2007; Hess et al., 2004). GBM is characterized by its cellular heterogeneity, proliferative nature, chromosomal instability, angiogenic and infiltrative properties and resistance to multimodal therapies (Furnari et al., 2007; Park and Rich, 2009). It has been speculated that the cellular heterogeneity and therapeutic resistance of GBM is due to the presence of CSCs (Figure 1.4) that share multiple characteristics with neural stem cells (NSCs).

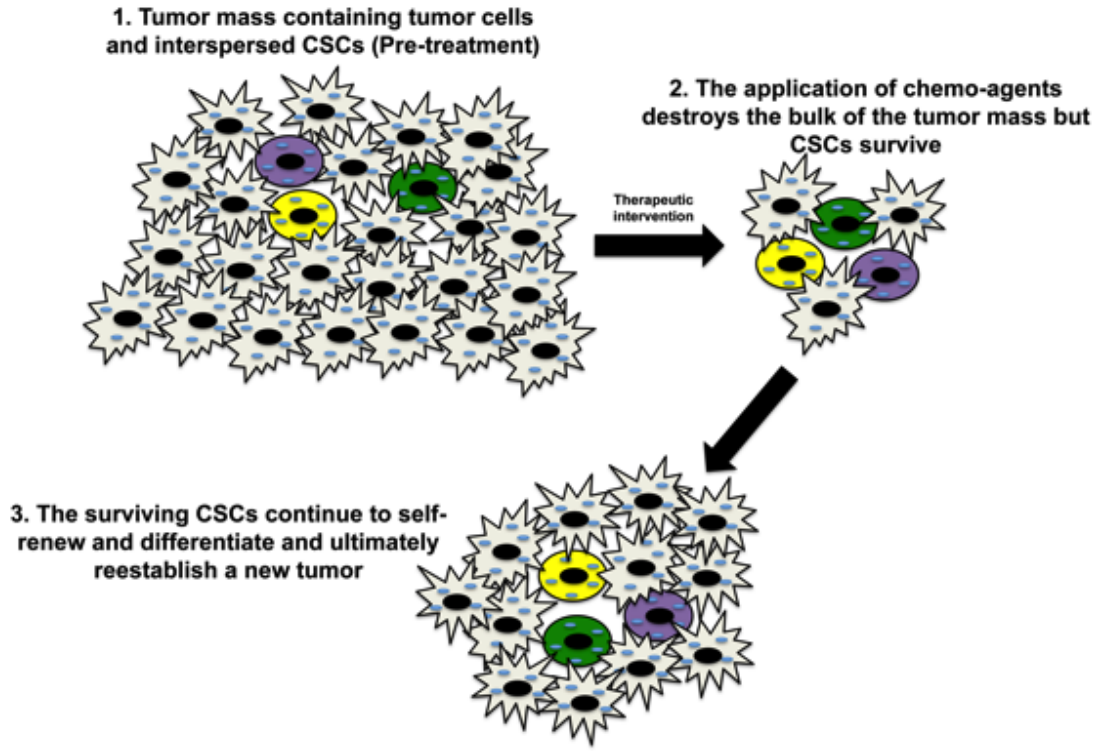

Figure 1.4. Diagrammatic representation of cancer stem cell mediated therapeutic resistance. 1. The tumor mass contains a heterogeneous population of cells with interspersed CSCs (brightly coloured cells). 2. Following aggressive chemotherapy, the bulk of the tumor is destroyed, however, CSCs are able to survive. 3. Overtime, the CSCs self-renew and give rise to differentiated progeny and a secondary tumor is established.

1.3.1 GBM and NSCs

In vivo, NSCs reside within the subventricular zone and dentate gyrus of the brain (Gage, 2000; McKay, 1997). *In vitro*, NSCs have been derived from differentiating ESCs by defined culture conditions (Ying et al., 2003). A key characteristic of NSCs is their ability to form and propagate as floating aggregates of cells called neurospheres (Svendsen et al., 1998; Ying et al., 2003). *In vitro*, NSCs are cultured in media containing the growth factors epidermal growth factor (EGF) and fibroblast growth factor (FGF), which promote proliferation and self-renewal (Ying et al., 2003). NSCs express a core

set of markers that include NESTIN, MUSASHI1 and SOX2 (Kaneko et al., 2000; Lendahl et al., 1990; Li et al., 1998).

GBM cells with NSC-like properties were first isolated from tumors by Singh et al in 2003 (Galli et al., 2004; Singh et al., 2003). Putative GBM CSCs were responsive to media containing EGF an FGF and propagated as non-adherent neurospheres. In addition, the culture of GBM CSCs under NSC conditions was shown to maintain the genetic phenotype of the parental tumor from which the CSCs were established, whereas culture in media containing serum resulted in changes in both their genetic and epigenetic status and tumorigenicity (Lee et al., 2006). GBM CSCs express a number of NSC factors that include but are not limited to NESTIN, SOX2, MUSASHI1 and CD133 (Ma et al., 2008). The intensity of expression of these factors in GBM tumors has been shown to closely correlate with patient prognosis, with high levels of expression indicating a poor clinical outcome (Ma et al., 2008). Coupled to the expression of stem cell factors, GBM CSCs have also been shown to overexpress DNA repair proteins (Bao et al., 2006a) and drug transporters (Frosina, 2009) that collectively provide anti-apoptotic characteristics.

1.3.2 Markers of GBM CSCs

The direct comparison of GBM CSCs and NSCs has led to the identification of a number of factors that are associated with GBM CSC populations, which appear to play a similar role in both GBM CSCs and NSCs. CD133 (Prominin-1) is a cell surface glycoprotein that is expressed in multiple adult stem cell populations (Uchida et al., 2000; Yin et al., 1997). CD133 has received much attention as a

defined GBM CSC marker over recent years with reports that CD133+ cells were a therapeutically resistant population of GBM CSCs with elevated DNA repair mechanisms and expression of drug transporters (Bao et al., 2006a). Other laboratories suggested that only CD133+ GBM CSCs could give rise to tumors in severe combined immunodeficiency (SCID) mice, whilst CD133- cells were not tumorigenic (Beier et al., 2007). However, recent studies by Wang et al and others demonstrated that CD133- cells were in fact tumorigenic and capable of self-renewal, differentiation and could give rise to both CD133- and CD133+ cells (Chen et al., 2010; Ogden et al., 2008; Wang et al., 2008a). These studies provided strong evidence that CD133 was not a unique marker of GBM CSCs.

Other factors identified as a potential GBM CSC markers include the core NSC factors, namely NESTIN, MUSASHI1 and SOX2 (Galli et al., 2004; Singh et al., 2003). NESTIN is a type IV intermediate filament protein that is expressed in NSCs and embryonic tissue (Zimmerman et al., 1994). Its expression is elevated in GBM CSCs and has been associated with the de-differentiation status of GBM, cell motility and invasiveness (Dell'Albani, 2008). MUSASHI1 is a transcription factor that is essential for the maintenance of stemness in NSCs and is often overexpressed in GBM CSCs (Ma et al., 2008). The abolition of MUSASHI1 expression has been shown to reduce GBM tumor growth (Sureban et al., 2008) and provides evidence to suggest that MUSASHI1 performs a similar role in GBM and NSCs. SOX2 is from the family of high mobility group (HMG) proteins and is an essential transcription factor that plays a key role in maintenance of stemness in NSCs and also ESCs (Fong et al., 2008; Kim et al.,

2008; Suh et al., 2007). SOX2 plays key role in the maintenance of stemness and tumorigenicity of GBM CSCs as silencing of SOX2 resulted in decreased cell proliferation, cell cycle entry and tumorigenicity *in vivo* (Gangemi et al., 2009). Furthermore, the silencing of SOX2 was accompanied by reduced NESTIN and OCT4 expression (Oppel et al., 2011) and strongly suggests that embryonic signaling networks are active in GBM. OCT4, along with NANOG and SOX2, form a core set of pluripotent stem cell factors (Kim et al., 2008). Although GBM cells are not pluripotent, the expression of these factors has been associated with GBM tumorigenicity (Clement et al., 2007; Ma et al., 2008; Zbinden et al., 2010). Indeed, the expression of OCT4 has been linked to increased GBM motility and invasiveness (Kobayashi et al., 2012). A recent study by Zbinden et al reported the expression of NANOG in GBM samples and also observed that NANOG, OCT4 and NESTIN expression were enriched in CD133+ cells (Zbinden et al., 2010). The knockdown of NANOG in GBM cells resulted in reduced clonogenicity, cell proliferation and *in vivo* tumorigenicity. The knockdown of NANOG was also associated with the down regulation of OCT4 and NESTIN (Zbinden et al., 2010) and provides further evidence of active embryonic signaling in GBM CSCs.

The above studies strongly suggest that GBM CSCs are characterized by a number of cellular markers despite the optimism that a single marker could identify GBM CSCs and provide a potential therapeutic target. Nevertheless, recent studies point towards the activation of embryonic signaling pathways in the establishment of a stem cell-like phenotype in GBM cells. Indeed, GBM CSCs appear to have undergone a form of cellular reprogramming that is not

too dissimilar to induced pluripotent stem (iPS) cells. iPS cells are derived from somatic cells that are induced to express pluripotent factors (Takahashi et al., 2007; Takahashi and Yamanaka, 2006). Indeed, GBM CSCs have been shown to express some of the factors used to generate iPS cells, OCT4, SOX2 and the proto-oncogene c-MYC (Kobayashi et al., 2012; Oppel et al., 2011; Wang et al., 2008b). Since GBM CSCS often express multipotent and pluripotent factors it is likely that the abnormal regulation of these factors is a major driving force behind the malignancy of GBM, through the promotion of proliferative and anti-apoptotic properties. It is, therefore, likely that targeting these pathways may prove effective at enriching for GBM CSC populations and also provide novel therapeutic targets.

1.3.3 NSC and GBM CSC multipotency and the implications for mtDNA copy number

Another property that GBM CSCs share with NSCs is multipotency. NSCs have been successfully differentiated into neuronal and glial (astrocytes and oligodendrocyte) cell types using defined culture conditions (Brustle et al., 1999; Fraichard et al., 1995; Li et al., 2005; Nat et al., 2007; van Inzen et al., 1996). Likewise, GBM CSCs have been differentiated into neuronal and glial-like cell types (Galli et al., 2004; Singh et al., 2003) (Figure 1.5). Therefore, NSCs and multipotent GBM CSCs are powerful research tools. NSCs can be utilized to enhance our understanding of neural development whilst GBM CSCs can provide valuable insight into abnormal development and tumorigenesis. Furthermore, these cell types also provide excellent models to enhance our understanding of the role of mtDNA copy number in stem cell differentiation and

tumorigenesis. Due to the similarity of GBM CSCs with NSCs, it is essential to determine whether GBM CSCs regulate their mtDNA copy number in a similar manner to NSCs as they undergo differentiation. Currently no data exist for the regulation of mtDNA copy number in CSCs and the analysis of differentiating GBM CSCs would, therefore, be a novel approach and provide essential insight into the role of mtDNA in GBM and also CSCs.

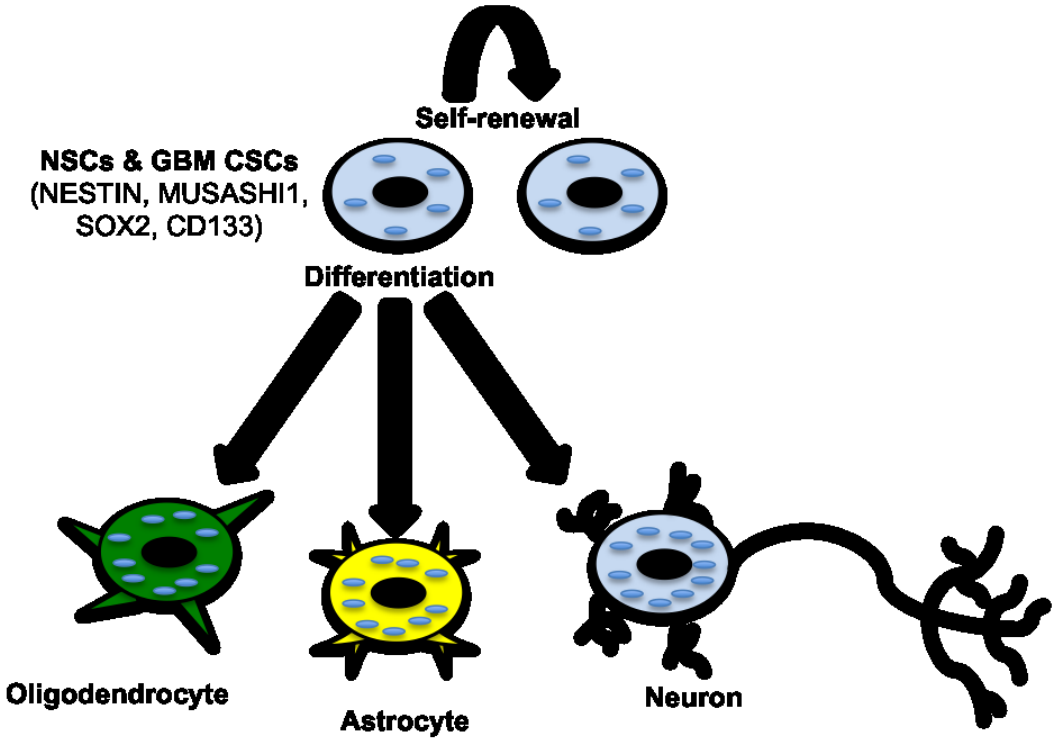

Figure 1.5. Diagrammatic representation of NSC and GBM CSCs and their differentiated progeny. In the undifferentiated state, NSCs and GBM CSCs have been shown express the stem cell factors NESTIN, MUSASHI1, SOX2 and CD133. Following the onset of differentiation, NSCs give rise to neuronal and glial cell types. In addition, GBM CSCs give rise to differentiated progeny that express markers of neuronal and glial cell types. Both NSCs and GBM CSCs provided excellent experimental models to investigate how mtDNA copy number is regulated in normal and abnormal development.

1.4 Conclusion

Stem cells are associated with low mtDNA copy number, immature mitochondria and possess low OXPHOS capacity. The onset of differentiation involves the maturation of mitochondria and a concurrent increase in mtDNA copy number and the expression of differentiation markers in order to allow fully differentiated cell types to generate sufficient quantities of ATP via OXPHOS. GBM CSCs share remarkable similarities with hNSCs, which include self-renewal, multipotency and gene expression profiles. However, it remains to be determined whether differentiating GBM CSCs and hNSCs regulate mtDNA in a similar manner. To date, data for mtDNA copy number only exists from established tumors and does not discriminate between CSCs and their differentiated progeny. Thus, GBM CSCs provide the opportunity to enhance our understanding of the regulation of mtDNA copy number in tumorigenesis. In addition, tumors often express altered mtDNA copy number relative to healthy tissue and there is evidence to suggest that these changes promote a tumorigenic phenotype. It is, therefore, essential to fully determine how changes in mtDNA content affect tumor cell function and tumorigenicity in order to enhance our understanding of tumor cell biology and to develop novel therapeutic approaches.

1.5 Hypothesis

I hypothesize that GBM CSCs will show differential regulation of mtDNA copy number relative to hNSCs in a process that is underpinned by the abnormal expression of nuclear-encoded factors. Since mtDNA copy number is essential for normal cell function, I hypothesize that depleting GBM CSCs of mtDNA will

alter their gene expression patterns and tumorigenicity. Finally, mtDNA mutations have been shown to induce cellular dysfunction and I therefore hypothesize that altering the mtDNA genotype of tumor cells will alter their mtDNA copy number and differentiation potential.

1.6 Aims

The primary aims of each of the experimental chapters described in this thesis are to:

1. Determine how mtDNA copy number is regulated in differentiating hNSCs and GBM cell lines, *in vitro*, and the role this plays in the use of OXPHOS (Chapter 3)
2. Determine the effects of mtDNA depletion on the gene expression profiles and proliferation rates of HSR-GBM1 cells *in vitro* (Chapter 4)
3. Determine the effects of varying degrees of mtDNA depletion on the tumorigenicity of HSR-GBM1 cells *in vivo* (Chapter 5)
4. Determine how changes in mtDNA genotype impact upon the regulation of mtDNA copy number, gene expression and differentiation of tumor cells *in vitro* (Chapter 6)

Chapter 2: General Materials and Methods

2.1 Preparation of cell culture growth factors and solutions

2.1.1 Preparation of poly-L-ornithine

50 mg of poly-L-ornithine (Sigma, St. Louis, MO, USA) was dissolved in 5 ml of deionized H_2O (dH_2O) to generate a stock solution of 10 mg/ml. The solution was filter sterilized and 50 μl aliquots were transferred into 600 μl tubes (Axygen, Union City, CA, USA) and stored at -20°C until use.

2.1.2 Preparation of laminin

Laminin stock solution (1 mg/ml; Sigma) was diluted 1:50 to a working concentration of 20 μg/ml in sterile dH_2O. 10 ml aliquots were transferred into 15ml tubes (BD Biosciences, Franklin Lakes, NJ, USA) and stored at -20°C until use.

2.1.3 Preparation of epidermal growth factor (EGF)

100 μg of lyophilized EGF (Millipore, Bellerica, MA) was reconstituted in 5 ml of sterile 0.1% (w/v) bovine serum albumen (BSA; Sigma) in phosphate buffered saline (PBS) (Invitrogen, Carlsbad, CA, USA) to generate a 20 μg/ml stock solution. 250 μl aliquots were transferred into 1.7 ml tubes (Axygen, Union City, CA, USA) and stored at -20°C until use.

2.1.4 Preparation of basic fibroblast growth factor (bFGF)

50 μg of lyophilized bFGF (Millipore) was reconstituted in 5 ml of sterile 0.1% (w/v) BSA in PBS to generate a 10 μg/ml stock solution. 250 μl aliquots were transferred into 1.7 ml tubes and stored at -20^{o}C until use.

2.1.5 Preparation of uridine

250 mg of uridine (Sigma) was dissolved in 5 ml of dH_2O to generate a 50 mg/ml stock solution. The solution was filter sterilized and 250 μl aliquots were transferred into 1.7 ml tubes and stored at -20^{o}C until use.

2.1.6 Preparation of bromo-deoxyuridine (BrdU)

50 mg of BrdU (Sigma) was dissolved in 5 ml of 5% (v/v) ethanol to generate a 10 mg/ml stock solution. The solution was filter sterilised and 500 μl aliquots were transferred into 1.7 ml tubes and stored at -20^{o}C until use.

2.1.7 Preparation of 2'-3'-dideoxycytidine (ddC)

21.1 mg of ddC (Sigma) was dissolved in 10 ml of dH_2O to generate a stock solution of 10 μM. The solution was filter sterilized and 250 μl aliquots were transferred into 1.7 ml tubes and stored at -20^{o}C until use.

2.1.8 Preparation of dialyzed fetal bovine serum (dFBS)

40 ml of fetal bovine serum (FBS) (Invitrogen) was dispensed into 25 cm of dialysis tubing (Fisher Scientific, Waltham, MA, USA) and sealed by a double knot in the dialysis tubing. The tubing was transferred to a 5-litre beaker,

secured, and suspended vertically in 5 litres of PBS. PBS was continuously stirred at 4°C for 24 hours with a PBS change after 12 hours. dFBS was removed from the dialysis tubing and transferred to a 50 ml tube (BD Biosciences, Franklin Lakes, NJ, USA) and filter sterilized. 10 ml of dFBS was aliquoted into 15 ml tubes and stored at -20°C until use.

2.1.9 Preparation of cytochalasin B

10 mg of cytochalasin B (Sigma) was dissolved in 5 ml of dimethyl sulfoxide (DMSO; Sigma) to generate a working concentration of 2 mg/ml. 200 μl aliquots were transferred into 1.7 ml tubes and stored at -20°C until use.

2.2 Cell culture

2.2.1 Fibronectin treatment of culture plates

Cell culture dishes (BD Biosciences, Franklin Lakes, NJ, USA) were pre-treated with fibronectin prior to cell seeding to promote cell attachment. A stock solution of fibronectin (1 mg/ml; Millipore) was diluted 1:50 in sterile PBS to a working concentration of 20 μg/ml. Culture vessels were coated with 1.5 ml/10 cm^2 of the fibronectin solution and incubated at 37°C for 1 hour or overnight at 4°C. For short-term storage (2-4 weeks), culture vessels coated with fibronectin, wrapped in parafilm and stored at 4°C until use. Prior to use, the fibronectin solution was removed and culture vessels were used immediately for cell plating.

2.2.2 Poly-L-Ornithine and laminin treatment of culture plates

Culture dishes were pre-treated with poly-L-ornithine and laminin prior to cell seeding to promote cell attachment. A stock solution (10 mg/ml) of poly-L-ornithine was diluted 1:500 in sterile dH_2O to a working concentration of 20 μg/ml. Culture vessel surfaces were coated with 1.5 ml/10 cm^2 of the poly-L-ornithine solution and incubated at 37°C for 1 hour. Following incubation, poly-L-ornithine was removed and culture vessels were washed twice with sterile H_2O. Culture vessel surfaces were immediately coated with laminin (20 μg/ml; 1.5 ml/10 cm^2) and incubated at 37°C for 2 hours. Following incubation, laminin was removed and culture vessels were washed with sterile PBS. Prior to use, PBS was removed and the culture vessels were used immediately for cell plating. For short-term storage (1-2 weeks), culture plates treated with poly-L-ornithine/laminin, wrapped in parafilm and stored at 4°C until use.

2.2.3 Culture of human neural stem cells

Human neural stem cells (hNSCs) derived from the NIH-approved H9 (WA09) human embryonic stem cell line were purchased from Invitrogen (Invitrogen). For routine culture, hNSCs were cultured as a monolayer at a density of 5 x 10^4 cells/cm^2 on fibronectin coated culture plates in StemPro Complete Medium. StemPro Complete Medium consisted of Dulbecco's Modified Essential Medium (DMEM)/F12 (1:1), 2% (v/v) StemPro Neural Supplement, 2 mM Glutamax (both from Gibco, Carlsbad, CA, USA), bFGF (20 ng/ml) and EGF (20 ng/ml) at 37°C with 5% CO_2/95% humidity. Culture media was replenished every two days.

hNSCs were enzymatically passaged at 70-80% confluence. Culture media was removed and hNSCs were washed twice in sterile PBS and 150 μl/10 cm^2 of Accutase (Sigma) was added and incubated at 37^oC for 2-3 minutes and cell detachment monitored. Following incubation, cells were gently agitated to promote detachment and four volumes of StemPro Complete Medium was added to neutralize the Accutase enzymatic activity and cells were gently triturated to generate a single cell suspension. The cell suspension was transferred to a 15 ml tube (BD Biosciences) and centrifuged at 1800 rpm for 3 minutes to obtain a cell pellet. The supernatant was removed and cells were resuspended in 2-5 ml of fresh StemPro Complete Medium and cell counts performed, as described in *Cell counting* (Section 2.2.6). hNSCs were re-plated on to fibronectin coated culture plates at a density of 5 x 10^4 cells/cm^2.

2.2.4 Culture of GBM CSCs

The human Glioblastoma Multiforme (GBM) CSC line, HSR-GBM1 (Galli *et al*. 2004), was kindly donated by Professor Neil Watkins ((Centre for Cancer Research (CCR) Monash Institute of Medical Research (MIMR) Australia)). The GBM CSC lines, GBM-L1 and GBM-L2, were kindly donated by Associate Professor Terrance Johns (CCR, MIMR, Australia). GBM CSCs were routinely cultured as floating neurospheres in 6-well ultra low attachment plates (Sigma) at a density of 192,000 cells/ml in StemPro Complete Medium at 37^oC with 5% CO_2/95% humidity. Culture media was replenished ever 2 days. GBM CSCS were passaged every 5-7 days.

GBM CSCs were passaged by transferring the neurospheres to 15 ml tubes and centrifuging at 1800 rpm for 3 minutes to obtain cell pellets. The supernatant was removed and 100-200 μl Accutase added. Using a 200 μl pipette set at a 180 μl range, the pelleted cells were gently triturated and then incubated at 37^{o}C for 2-3 minutes. After incubation, 1 ml of StemPro Complete Medium was added and GBM CSCs were dissociated into a single cell suspension and centrifuged at 1800 rpm for 3 minutes. The supernatant was removed and GBM CSCs were resuspended in 2-5ml of fresh StemPro Complete Medium and a cell count was performed, as described in *Cell counting* (Section 2.2.6). GBM cells were resuspended at a density of 192,000 cells/ml of StemPro Complete Medium and transferred into culture vessels.

2.2.5 Culture of osteosarcoma (143BTK-) cell lines

Human osteosarcoma cell lines (143B) deficient in thymidine kinase activity (TK-) (143BTK-) were kindly donated my Dr. Matthew McKenzie ((Centre for Reproduction and Development (CRD) MIMR, Australia)). 143BTK- cells have previously been utilized to derive cells devoid of mtDNA through the long-term exposure to ethidium bromide and are termed rho zero (ρ0) (King and Attardi, 1989). These studies have allowed scientists to analyze how the loss of mtDNA affects cellular function. ρ0 cells can also be repopulated with donor mtDNA through the fusion of ρ0 cells with cytoplasts from various cell sources. The subsequent hybrid cells are referred to as trans-mitochondrial cybrids. Trans-mitochondrial cybrid technology allows for the repopulation of ρ0 cells with mtDNA that contain specific mutations and allows for the investigation of how mtDNA mutations impact upon cellular function. All the 143BTK- cell lines that

were donated and also the trans-mitochondrial cybrids that were derived through cell fusion experiments are listed in the table below.

Cell Line	MtDNA status	MtDNA Mutation	Associated mtDNA Disease
143BTK-$^{\rho+}$	143BTK- mtDNA	Multiple variants	N/A
143BTK-$^{\rho0}$	No mtDNA	N/A	N/A
143BTK-^{3243}	A3243G mutation	$tRNA^{Leu(UUR)}$	MELAS
143BTK-^{8993}	T8993G mutation	ATPase6	NARP
143BTK-^{11778}	G11778A mutation	ND4	LOHN
143BTK-^{NSC}	hNSC mtDNA	Wild type	None
143BTK-^{GBM}	HSR-GBM1 mtDNA	Multiple variants	N/A
143BTK-^{GBML1}	GBM-L1 mtDNA	Multiple variants	N/A
143BTK-^{GBML2}	GBM-L2 mtDNA	Multiple variants	N/A

Table 2 I. Summary of 143BTK- cell lines and trans-mitochondrial cybrids.

143BTK- cells were routinely cultured in standard DMEM (SD-DMEM) consisting of DMEM, 2 mM Glutamax, 10 mM Sodium Pyruvate, 10% (v/v) FBS, 1% (v/v) penicillin/streptomycin (all from Gibco) and uridine (50 mg/ml; Sigma). Uridine provides the necessary pyrimidines required for DNA synthesis. Uridine synthesis is dependent on the presence of a functional respiratory chain. Since 143BTK-$^{\rho0}$ cells are devoid of mtDNA and contain a compromised respiratory chain, uridine supplementation is required to allow efficient DNA synthesis to occur. The remaining 143BTK- cell lines that contained single mtDNA point mutations, which have deleterious effects on respiratory chain function, were also supplemented with uridine to support DNA synthesis. 143BTK- cells were incubated at 37^{o}C with 5% CO_2/95% and media was replenished every 2 days.

143BTK- cells were passaged at 70-80% confluence. Culture media was removed and cells were washed twice in sterile PBS and incubated with Accutase (150 μl/10 cm^2) at 37°C for 2-3 minutes and cell detachment monitored. Following incubation, cells were gently agitated to promote detachment and four volumes of SD-DMEM were added and the cells were gently triturated to generate a single cell suspension. The cell suspension was transferred to a 15 ml tube and centrifuged at 1800 rpm for 3 minutes. 143BTK- cells were suspended in SD-DMEM and re-plated at a ratio of 1:4 in culture vessels and the total media volume increased to 3 ml/10 cm^2.

2.2.6 Cell counting

Cell counts were performed using a haemocytometer (BRAND GMBH, Wertheim, Germany). 15 µl of cell suspension were added to 15 µl of trypan blue (Sigma), resulting in a dilution factor of 2. Trypan blue (Sigma) is unable to penetrate live cells with intact cell membranes and allows the determination between live (white) and dead (blue) cells during counting. 10 µl of cell/trypan suspension was applied to each chamber (x2) of the haemocytometer. The number of non-trypan blue stained cells in 4 quadrants of the haemocytometer grid was counted per chamber, resulting in a total of 8 quadrants being counted. The total number of cells was divided by 8 to generate a mean cell count per quadrant. The mean cell count number was then subjected to the following calculation:

$$Cells/ml = (Mean\ cell\ count \times dilution\ factor) \times 10^4$$

2.2.7 Cryopreservation of cell line stocks

Low passage stocks of cell lines were maintained where possible using cryopreservation. Cell lines were frozen at the time of passaging using the protocols outlined in *Cell culture* (Sections 2.2.3-2.2.5). Cells were harvested, resuspended in their respective media and cell counts performed, as described in *Cell counting* (Section 2.2.6). Cells were centrifuged to obtain cell pellets and were resuspended at a density of 1-2 x 10^6 cells/ml in respective media with 10% (v/v) DMSO and transferred to 2 ml cryovials (Nunc, Rochester, NY, USA). The cryovials were transferred to a Mr Frosty (Nalgene, Waltham, MA, USA) container containing 200 ml isopropanol (Merck, Darmstadt, Germany) and stored at -80^{o}C for 24 hours. The combination of the Mr Frosty container and isopropanol provides a freezing rate of 1ºC/min, which reduces the loss of cell viability during freezing. After 24 hours, cryovials were transferred to designated storage boxes and immersed in LN_2 for long-term storage.

2.3 Differentiation Experiments

2.3.1 Differentiation of hNSCs

hNSCs were cultured and passaged, as described above *Culture of human neural stem cells* (Section 2.2.3), until sufficient cells were available for experiments. hNSCs were harvested using Accutase, as described in *Culture of human neural stem cells* (Section 2.2.3), and resuspended in 2-5 ml of StemPro Complete Medium and cell counts were performed, as described in *Cell counting* (Section 2.2.6).

For astrocyte differentiation, undifferentiated (Day 0) hNSCs were seeded onto fibronectin coated culture plates at a density of 5 x 10^4 cells/cm^2 and cultured in Astrocyte Induction Medium (AIM) consisting of DMEM, 2 mM Glutamax, 10 mM Sodium Pyruvate, 1% (v/v) N2 supplement, 2% (v/v) FBS and 0.1 mM β-mercaptoethanol (all from Gibco). Cells were incubated at 37^oC with 5% CO_2/95% humidity for up to 28 days with media changes every 3 days.

Samples were harvested at selected time points for DNA/RNA analysis. For immunocytochemical analysis, hNSCs were seeded at the densities, described above, into the wells of 8-well chamber slides (Ibidi, München, Germany) and cultured in AIM for up to 28 days.

2.3.2 Differentiation of GBM cell lines

GBM cell lines were cultured and passaged, as described in *Culture of GBM cell lines* (Section 2.2.4), until sufficient cell numbers were available for experiments. GBM cells were removed from culture dishes and transferred to a 15 ml tube and centrifuged at 1800 rpm for 3 minutes to obtain a cell pellet. GBM cells were dissociated into single cells using Accutase and a cell count performed, as described in *Culture of GBM cell lines* (Section 2.2.4) and *Cell counting* (Section 2.2.6).

For astrocyte differentiation, undifferentiated GBM cells (Day 0) were seeded at a density of 2.5 x 10^4 cells/cm^2 onto fibronectin treated culture plates in AIM, as

described above. Cells were incubated at 37^{o}C with 5% CO_2/95% humidity for up to 28 days with media changes every 3 days.

Samples were harvested at selected time points for DNA/RNA analysis. For immunocytochemical analysis, GBM cells were seeded at the densities, described above, into the wells of 8-well chamber slides and cultured in AIM for up to 28 days.

2.3.3 Mitochondrial DNA depletion of HSR-GBM1 cells

HSR-GBM1 cells were cultured, as described in *Culture of GBM cell lines* (Section 2.2.4), with the exception that ddC (10 μm) and uridine (50 mg/ml) were added to the culture medium. Culture media was replenished daily through half volume changes of media for up to 50 days. Cell samples were collected every 7 days. MtDNA depleted HSR-GBM1 cells were differentiated after 7, 14 and 21 days of depletion, as described in *Differentiation of GBM cell lines* (Section 2.3.2), or cultured as neurospheres in StemPro Complete Medium with uridine for 14 days to asses mtDNA copy number recovery.

2.4 Extraction of nucleic acids

2.4.1 RNA extraction from intact cells with DNase treatment

Prior to RNA extraction, cells were collected, transferred to 1.7 ml tubes and pelleted by centrifugation. Total RNA was extracted from cells using the RNeasy Mini Kit (Qiagen, Valencia, CA, USA), according to the manufacturer's protocol.

Qiagen supplied all the reagents provided within the RNeasy Mini kit and the 70% (v/v) ethanol was purchased from Merck.

Cell samples (<5 x 10^6 cells) were lysed with 350 μl of Buffer RLT. For low cell number samples, culture media was removed from culture flasks and cells washed twice with PBS and 350 μl of lysis Buffer RLT added directly to the cells and gently agitated for up to 5 minutes to promote cell lysis before transfer to 1.7 ml tubes. Samples were lysed thoroughly by pulse vortexing and pipetting to produce a lysate. The lysate was homogenized using a QIAshredder spin column (Qiagen). The lysate was transferred into a QIAshredder spin column assembled in a 2 ml collection tube, centrifuged at 13,000 rpm for 2 minutes and the flow-through retained. 350 μl of 70% (v/v) ethanol was added and mixed gently by pipetting and inverting the tubes. The lysate/ethanol solution was applied to an RNeasy spin column assembled in a 2 ml collection tube and centrifuged at 13,000 rpm for 1 minute. The flow-through was discarded and the collection tube reused in subsequent steps. 350 μl of Buffer RW1 was added to the spin column and centrifuged at 13,000 rpm for 1 minute and the flow-through discarded.

To remove any contaminating genomic DNA, samples were treated with DNase I. 80 μl of DNase I (30 Units; Qiagen) in Buffer RDD was applied to the spin column and incubated at room temperature for 30 minutes. Following incubation, 350 μl of Buffer RW1 was added to the spin column and centrifuged at 13,000 rpm for 1 minute and the flow-through discarded. 500 μl of Buffer RPE was applied to the spin column and centrifuged at 13,000 rpm for 1 minute and the

flow-through discarded. A second application of 500 μl of Buffer RPE was added to each spin column and centrifuged at 13,000 rpm for 2 minutes and the flow-through discarded. The spin column was transferred to a clean 2 ml collection tube and centrifuged for an additional minute at 13,000 rpm to ensure all residual wash solutions had been removed. The spin column was placed into a clean 1.7 ml tube and RNA recovered by elution with the addition of 50 μl of RNase-free water directly to the spin column membrane and centrifuged at 13,000 rpm for 1 minute. Total RNA was stored at -80^{o}C until required.

2.4.2 RNA extraction from tumor samples

Up to 30 μg of tumor tissue was isolated using a clean scalpel blade and transferred to a clean 5 ml tube. 700 μl of lysis Buffer RTL was applied and tumor samples were disrupted using a Pro 200 tissue homogenizer (Pro Scientific, Oxford, USA). 700 μl of 70% (v/v) ethanol was added to the sample and mixed by pulse vortexing. Up to 700 μl solution was applied to an RNeasy spin column assembled in a 2 ml collection tube and centrifuged at 13,000 rpm for 1 minute. This step was repeated until all of the solution had been applied to the RNeasy spin column. Total RNA was extracted from samples and DNase treated by following the protocol, as described in *RNA extraction from intact cells with DNase treatment* (Section 2.4.1). Total RNA was stored at -80^{o}C until required.

2.4.3 DNA extraction from intact cells

Total DNA was extracted using the DNeasy Blood and Tissue Kit (Qiagen), according the manufacturer's protocols. Pelleted cell samples were resuspended in 200 μl PBS and 20 μl of Proteinase K (20 mg/ml; Qiagen) and 4 μl RNase A (100 mg/ml; Qiagen) was added to remove any contaminating protein and RNA. 200 μl of Lysis Buffer AL was added to each sample and mixed by pulse vortexing and incubated at 56^{o}C for 15 minutes.

For direct cell lysis from culture plates, culture media was moved and cells washed twice with PBS. PBS was removed and the lysis solution of PBS, Proteinase K, RNase A and Buffer AL (total 424 μl) were added directly to the cells and incubated at room temperature for 5 minutes. After incubation the lysis solution was gently triturated and transferred to a clean 1.7 ml tube. The samples were pulse vortexed for 15 seconds and incubated at 56^{o}C for 15 minutes.

Following incubation, 200 μl of 96-100% (v/v) ethanol was added to each sample and mixed thoroughly by pulse vortexing. The lysate/ethanol solution was transferred to a DNeasy Mini spin column assembled in a 2 ml collection tube and centrifuged at 13000 rpm for 1 minute, the flow-through was discarded and the spin column transferred to a new collection tube. 500 μl of Buffer AW1 was applied to the spin column and centrifuged at 13000 rpm for 1 minute and the flow-through discarded and the spin column transferred to a clean collection tube. 500 μl of Buffer AW2 was applied to the spin column and centrifuged at 13,000 rpm for 3 minutes to dry the spin column filter. The flowthrough was

discarded and the spin column was transferred to a clean collection tube and centrifuged at 13,000 rpm for 1 minute to remove any residual wash solutions. The spin column was placed into a clean microcentrifuge tube and 100-200 μl of Elution Buffer AE applied. Spin columns were incubated at room temperature for 1 minute and centrifuged at 13000 rpm for 1 minute to recover DNA. DNA was stored at -20^{o}C until required.

2.4.4 DNA extraction from tumor samples

Up to 30 μg of tumor tissue was isolated using a clean scalpel blade and transferred to a clean 5 ml container. 180 μl of Tissue Lysis Buffer ATL, 20 μl Proteinase K (20 mg/ml) (Qiagen) and 4 μl RNase A (100 mg/ml) was applied to the tissue sample. Tissue samples were disrupted using a tissue homogenizer and incubated overnight at 56^{o}C. Following incubation, the solution was centrifuged at 13,000 rpm for 2 minutes and the supernatant carefully transferred to a clean 1.7 ml tube. 200 μl of Buffer AL was applied to the solution, mixed by pulse vortexing and incubated for a further 10 minutes at 56^{o}C. After incubation 200 μl of 100% (v/v) ethanol was added to the solution and mixed by pulse vortexing. The solution was applied to a DNeasy Mini spin column assembled in a 2 ml collection tube and samples were further processed, as described in *DNA extraction from intact cells* (Section 2.4.3). DNA was stored at -20^{o}C until required.

2.4.5 Quantification of nucleic acids

Extracted RNA and DNA was quantified and assessed for purity using the NanoDrop ND-1000 UV-Vis Spectrometer. The NanoDrop loading surface was cleaned and 1.5 μl of dH_2O applied to initialize the ND-1000 Software Version 3.2.0 (NanoDrop Technologies, Wilmington, USA). A second application of 1.5 μl dH_2O was used to blank the ND-1000 software to register a zero value. 1.5 μl of RNA/DNA was applied to the NanoDrop and absorbance was measured at 220-350 nm. Ratios of absorbance at 260/280 nm and 260/230 nm were calculated by the ND-1000 Software. Ratios of 1.7-2.1 indicated good quality and a high level of purity of RNA/DNA.

2.5 Polymerase Chain Reaction (PCR)

2.5.1 Reverse transcription

Complementary DNA (cDNA) was synthesised from Total RNA by reverse transcription using the Bioline System (Bioline, London, UK). Up to 1 μg of RNA was transferred to clean 200 μl PCR tubes and reverse transcribed in reactions consisting of 2.5 mM $Oligo(dt)^{18}$ (Bioline) and dH_2O to a final volume of 20 μl. The mixture was heated to 70^{o}C for 5 minutes using an RT-200 thermal-cycler and immediately cooled on ice. To the mixture, 1x Reaction Buffer, 0.3 mM dNTPs 40U Ribosafe RNase inhibitor, 200U BioScript enzyme (all from Bioline) and dH_2O to a volume of 10 μl were added and gently mixed. The reaction mixture was heated to 42^{o}C for 60 minutes, 72^{o}C for 10 minutes and immediately cooled on ice. cDNA was stored at -20^{o}C until required.

2.5.2 Primer design

Primer pairs for genes of interests were designed using the Primer-Blast Designing Tool (National Centre for Biotechnology Information, NCBI, Bethesda, MD, USA) using complete sequences that were available online (NCBI; http://www.ncbi.nlm.nih.gov/gene). Where possible, primer pairs were designed included similar G/C content and similar length in order that the primers would possess similar annealing temperatures. Furthermore, where possible, primer pairs were designed to span introns or exon-exon junctions so that presence of genomic DNA contamination could be identified by gel electrophoresis. Primer annealing temperatures were estimated using the following equation (Sambrook et al. 1989):

$$T_a = \%C/G \times 0.41 + 64.9 - 600/n$$

where T_m corresponds to the melting temperature, %G/C corresponds to the percentage of guanosine (G) and cytosine (C) nucleotides in the primer and n corresponds to the total number of base pairs in the primer.

Primer pairs were designed to have annealing temperatures between 52-60^{o}C and generate PCR products of 150-300 bp in length. Furthermore, primer pairs were assessed for specificity using the human BLAST sequence program (NCBI) prior to fabrication using the Custom Oligos Design Package (Sigma). Primer pairs were tested upon delivery by performing PCR reactions using annealing temperatures set at T_a, T_a+1^{o}C and T_a-1^{o}C to determine the optimal annealing temperature.

2.5.3 PCR

Genes of interest were amplified using conventional PCR (using DNA templates) and reverse transcription PCR (RT-PCR) (using cDNA templates). PCR and RT-PCR reactions were performed in clean 200 µl PCR reaction tubes (Axygen). Reaction volumes of 50 µl consisted of 200 ng DNA or cDNA, 1x NH_4 PCR Buffer, 1mM $MgCl_2$, 0.5 nM dNTPs, 5U BioTaq DNA Polymerase (all from Bioline), 1 µM forward and reverse primers (see individual experimental chapters) and dH_2O to a volume of 50 µl. PCR reactions were performed using a RT-200 thermal-cycler (MJ Research, Waltham, MA, USA) and consisted of an initial denaturation step at 95^{o}C for 5 minutes and 35 cycles of denaturation at 94^{o}C for 30 seconds, annealing for 30 seconds at primer specific temperatures (see individual experimental chapters), extension at 72^{o}C for 45 seconds and a final extension step at 72^{o}C for 5 minutes.

2.5.4 Gel electrophoresis

PCR products were resolved using gel electrophoresis. 20 µl of PCR product was mixed with 5 µl of 5x loading buffer (Bioline) and loaded into the wells of a 2% (w/v) agarose gel in 1 x tris-acetic-ethylenediaminetetraacetic acid (EDTA) (TAE) buffer (Merck). DNA products were electrophoretically separated at 90mV for 1 hour. PCR products were fluorescently labeled with 1x SyberSafe (Invitrogen) for visualization under ultra violet (UV) light. PCR product size was determined by comparison to a DNA ladder (Hyperladder IV; Bioline) containing DNA fragments of known length (100-1000 bp).

2.5.5 PCR product purification

PCR products were visualised under UV light and manually excised using a clean scalpel blade and transferred to a clean 1.7 ml tube. DNA was extracted from the agarose gel slices using the QIAquick Gel Extraction Kit (Qiagen), according to the manufacturer's protocols. The weight of gel slices was determined by weighing each eppendorf tube prior and after the addition of gel slices. Three volumes of Buffer QG were added to 1 volume of gel slice (300 μl per 100 mg of gel) and incubated at 50^{o}C for 10 minutes (or until gel slice is dissolved) with gentle agitation by brief pulse vortexing every 2 to 3 minutes. One gel volume (100 μl per 100 mg) of isopropanol (Merck) was added to the sample and mixed gently by inverting the microcentrifuge tubes. The sample mixture was applied to a QIAquick spin column assembled in a 2 ml collection tube and centrifuged at 13,000 rpm for 1 minute. The flow-through was discarded and a collection tube reused for subsequent wash steps. 500 μl of Buffer QG was applied to the spin column and centrifuged at 13,000 rpm for 1 minute and the flow though was discarded. 750 μl of Buffer PE was applied to the spin column and centrifuged at 13,000 rpm for 1 minute and the flowthrough was discarded. The spin column was centrifuged at 13,000 rpm for an additional minute to remove any residual wash solutions. The flowthrough was discarded and the spin column transferred to a clean 1.7 ml tube. DNA was recovered by elution with 30-50 μl of Buffer EB followed by centrifugation at 13,000 rpm for 1 minute. Purified DNA was stored at -20^{o}C until required.

2.5.6 DNA sequencing

To confirm that the PCR products generated through RT-PCR contained the sequences of the gene target, DNA products excised from agarose gels were purified using the QIAquick gel extraction kit, as described in *PCR product purification* (Section 2.5.5). DNA was sequenced using the automated direct sequencer an Applied Biosystems 3130xl Genetic Analyzer and the Applied Biosystems BigDye Terminator 3.1 reaction kit (both from Applied Biosystems, Carlsbad, CA, USA). Reaction mixtures consisted of 50-200 ng (1-6 μl) of DNA, 312 nM of primer (see individual experimental chapters) and dH_2O to a volume of 16 μl. DNA samples were sequenced through the Monash Health Translational Precinct (MHTP) Medical Genomics Facility (Monash Institute of Medical Research, Clayton, VIC, Australia). Sequence files were analyzed for sequence read quality using the sequence viewer software, 4 Peaks (v1.7.1) (mekentosj.com). DNA sequences were analyzed using the Basic Local Alignment Tool (BLAST; NCBI; http://blast.ncbi.nlm.nih.gov) to confirm that correct DNA regions had been amplified.

2.6 Real-Time PCR

2.6.1 Preparation of PCR standards

For the preparation of PCR standards, PCR products were generated through the amplification of DNA (mtDNA & β-Globin for absolute quantification of mtDNA copy number) or cDNA (genes of interest for relative quantification) using conventional PCR or RT-PCR, respectively (see individual experimental chapters). PCR products were resolved using 2% agarose gels, purified and

quantified, as described in *Gel electrophoresis* (Section 2.5.4*), PCR product purification* (Section 2.5.5*)* and *Quantification of nucleic acids* (Section 2.4.5*)*. PCR products were diluted in sterile dH_2O to generate a series of 10-fold dilutions ranging from 1 x 10^{-2} ng/μl - 1 x 10^{-8} ng/μl. PCR products were stored at 4^{o}C and -20^{o}C for short and long-term storage, respectively.

2.6.2 Real-time PCR

Real-time PCR reactions were performed using a 72-well Rotorgene-3000 Real-time PCR machine (Corbett Research, Cambridge, UK). 20 μl reaction mixtures contained 10 μl of 2x SensiMix (Bioline), 6 μl dH_2O, 1 μl (0.25 μM) of each forward and reverse primer (see individual experimental chapters) and 2 μl (20 ng) of template (DNA or cDNA).

Reaction conditions consisted of initial denaturation at 95^{o}C for 15 minutes followed by 40 cycles of denaturation at 95^{o}C for 15 seconds, annealing at primer specific temperatures for 15 seconds (see individual experimental chapters) and extension at 72^{o}C for 15 seconds. Data were acquired from the FAM/Sybr channel during the extension phase (excitation at 470 nm and detection at 510 nm). To eliminate fluorescent signals generated by potential primer dimers in the PCR reaction, a secondary acquisition phase of 15 seconds was applied to each of the 40 cycles of PCR (see individual experimental chapters). Secondary acquisition temperatures were specific to primer pairs (see individual experimental chapters) and were set at just below the melting temperature of the amplicon of interest.

Melt curve analysis was performed in a subsequent cycle by ramping the temperature from 47°C to 98°C at 1°C intervals and data were acquired from the FAM/Sybr channel. Standards were run in duplicate whilst DNA and cDNA samples were run in triplicate and each reaction was performed twice, generating 6 values per DNA/cDNA sample. The closest values were expressed as mean ± SEM (Bustin, 2000).

2.6.3 Gene expression analysis

Relative expression of gene targets was determined by real-time PCR using reaction conditions described in the individual experimental chapters. Relative expression was calculated using the Pfaffl method (Pfaffl, 2001). The Pfaffl method allows the expression of a gene of interest to be compared across multiple samples i.e. control and test samples. In order to normalize against the unknown amount of cells present in the RNA extraction process and also the extraction efficiency, the expression of a gene of interest is expressed relative to the housekeeping gene or genes. Housekeeping genes selected upon their consistent levels of expression across cell lineages and all stages of differentiation. Relative gene expression was calculated using the following formula:

$$Ratio = \frac{(E_{Target})^{\Delta Target\ Ct\ (Ct\ control\ -\ Ct\ sample)}}{(E_{Housekeeping})^{\Delta\ Housekeeping\ Ct\ (Ct\ control\ -\ Ct\ sample)}}$$

Where the E_{Target} and $E_{Housekeeping}$ are the PCR amplification efficiencies (calculated from the standard curve) of the real-time PCR reactions for the gene of interest and housekeeping gene, respectively. *Δ Target Ct (Ct control – Ct*

sample) is the difference in Ct value of the gene target between the control and test samples. *Δ Housekeeping Ct (Ct control – Ct sample)* is the difference in Ct of the housekeeping gene between the control and test samples. This equation presents the expression of the gene of interest in the test sample relative to the control sample.

2.6.4 MtDNA copy number analysis

MtDNA copy number was quantified by real-time PCR using reaction conditions described in the individual experimental chapters. In order to quantify mtDNA copy number in an unknown number of cells, DNA concentration, per ng, was extrapolated from standard curves generated for known concentrations of purified mtDNA and β-Globin PCR product. Sample DNA concentrations were converted to copies per gene, per reaction, using the following equation:

$$N = (ng\ of\ DNA \times 6.023 \times 10^{14}) / (N_{bp} \times 660)$$

where N is the number of molecules per reaction. 6.023×10^{14} is a conversion of 1 mol to 1 nmol using Avogadro's constant, which states 1 mol contains 6.023×10^{23}. N_{bp} is the number of base pairs of the amplicons of interest and 660 is the mean molecular weight of a nucleic acid base paring in Daltons (Da). The closest 4 values generated per sample for mtDNA and β-Globin were then subjected to the following equation:

$$\text{No. of mtDNA copies/cell} = \frac{\text{No. of copies of mtDNA}}{\text{(No. of copies of } \beta\text{-Globin/2)}}$$

The calculated number of β-Globin copies was divided by 2 since each cell contains two copies, or alleles of the β-Globin gene. This value permits the calculation of mtDNA copy number cell and also represents the number of cells from which DNA has been extracted in a given reaction. Calculated values were subsequently expressed as mean ± SEM (Bustin, 2000).

2.6.5 SABiosciences real-time PCR gene expression array (RT^2 Profiler)

Total RNA was extracted from cells using the RNeasy Mini Kit with the on-column DNase treatment step, as described in *RNA extraction from intact cells* (Section 2.4.1). An additional genomic DNA elimination step was performed by adding 2 μl of 5x genomic DNA Elimination Buffer (SABiosciences, Valencia, CA, USA) to 1-8 μl (400 ng) of total RNA and incubated at 42°C for 10 minutes.

cDNA was synthesized using the RT^2 First Strand Kit (SABiosciences) according to the manufacturers protocol. Each 20 μl reaction contained 400 ng of DNA-free RNA (10 μl), 4 μl 5x RT Buffer, 1 μl Primer and External Control Mix, 2 μl RT Enzyme Mix (all from SABiosciences) and 3 μl dH_2O. The reactions were performed on a RT-200 thermal-cycler at 42°C for 15 minutes and stopped by incubating at 95°C for 5 minutes. Prior to PCR Array analysis, 91 μl of RNase/DNase free H_2O was added to the cDNA and gently mixed.

Real-time reactions were performed in 384-well optical reaction plates (Applied Biosciences). A master mix consisting of 550 μl RT^2 SYBR Green/ROX (SABiosciences), 448 μl sterile dH_2O and 102 μl cDNA was prepared for each replicate of the array (4 replicates per plate). Final reaction volumes were 10 μl and were prepared using a CAS-1200 Robotic Liquid Handling System (Corbett Robotics, Queensland, Australia). Real-time reactions were conducted on an ABI 7900HT Real Time PCR instrument (Applied Biosystems) and consisted of an initial denaturation step at 95°C for 5 minutes followed by 40 cycles of denaturation at 95°C and annealing/extension at 60°C for 1 minute.

PCR reactions were performed in triplicate for each target gene and data were generated in the form of cycle threshold (Ct) values. This value represents the point at which fluorescence intensity generated in the PCR reaction reaches a set threshold above the background signal. Relative gene expression was calculated by the ΔΔCt method (Livak and Schmittgen, 2001) and normalized against the average Ct values of 5 housekeeping genes (*GUSB, HPRT1, HSP90AB1, GAPDH* and *β-ACTIN*).

2.6.6 High resolution melting (HRM) curve analysis

Detection of mtDNA variants was confirmed using HRM curve analysis. HRM utilizes fluorescent dyes that intercalate into double stranded DNA molecules, which are generated through the PCR reaction. HRM analysis allows for the monitoring of the fluorescent signals present in PCR products in real-time. The melting temperatures of PCR products are determined by the G/C nucleotide content, therefore, single or multiple base changes result in a shift in the melting

temperature of a PCR product. The shifts in melting temperature are detected in real-time as a rate of change in fluorescent signal during the melting of PCR products as the products are subjected to a progressive ramping in temperature. The changes in melting temperature are subsequently extrapolated as melting curve profiles. Shifts in these profiles compared to wild-type/control samples are indicative of DNA mutations or variants.

DNA samples were initially subjected to HRM-PCR. Reaction mixtures contained 10 ng/µl genomic DNA, 1x HRM master mix with LCGreen® Plus+ (TrendBio, Melbourne, Victoria, Australia), 2.5 µM forward and reverse primers (see individual experimental chapters), sterile dH_2O to a volume of 10 µl and 20 µl of mineral oil (Sigma). HRM reactions were performed on a MultiGene™ Gradient Thermal Cycler (Labnet International, Edison, NJ, USA) with the following conditions: An initial denaturation step at 95°C for 2 minutes followed by 45 cycles of denaturation at 94°C for 30 seconds and annealing for 30 seconds at primer specific temperatures (see Experimental Chapters). A final step of 95°C for 30 seconds was performed to allow hetroduplex formation and samples were held at 4°C prior to further processing. Amplified products were analysed using the LightScanner (Idaho Technologies, Salt Lake City, Utah, USA) by progressively ramping from 70-90°C and data analysis was performed using the LightCycler-480 software package (Roche Diagnostics, Castle Hill, NSW, Australia). Melting curves were normalized by the omission of melt profiles generated from non-template controls (H_2O). Samples were referenced against a baseline/control melting profile, which was derived from hNSCs that contained wild type mtDNA.

2.7 Cellular respiration

The oxygen (O_2) consumption rates of intact cells were determined by high-resolution respirometry (Oroboros Oxygraph-2K, Innsbruck, Austria). The Oxygraph-2k system was calibrated by determining the zero and maximum O_2 values within each measurement chamber. 2.2 ml of sodium dithionite (5 mg/ml; Sigma) was dissolved in Hanks balances salt solution (HBSS; Gibco) and added to each measurement chamber; which were subsequently sealed, maintained at 37^{o}C and continuously stirred at 750 rpm. The sodium dithionite solution removed >99% of the O_2 present in the measurement chambers and these values were used to set zero O_2, or baseline, for subsequent measurements. For maximal O_2 calibration, the measurement chamber contents were aspirated and thoroughly washed 5 times with dH_2O. 2.2 ml of fresh HBSS was added to the measurement chambers and sealed. Maximal O_2 concentration was recorded following equilibration of the O_2 flux (rate of change in O_2 concentration) in each measurement chamber. Following the calibration process, analysis of O_2 consumption of intact cells commenced.

For analysis, cells were dissociated using Accutase and cell numbers determined, as described in *Cell culture* and *Cell counting* (Sections 2.2-2.2.6). 1-2 x 10^6 cells were resuspended in 50 μl HBSS and transferred into each measurement chamber using a syringe (Oroboros). O_2 consumption was measured using the integrated software package Datlab (Version 3.1; Oroboros), which presented cellular respiration as O_2 flux (i.e. pmol O_2 per 10^6 cells per second). Following the addition of intact cells and stabilization of O_2 flux, basal/resting O_2 consumption rates were recorded for 5 minutes.

Subsequently, a series of respiratory chain inhibitors were added at 5-minute intervals to manipulate cellular respiration. 4 mg/ml of the ATP synthase (Complex V) inhibitor Oligomycin (Sigma) was added to determine the amount of proton leakage (Leak) across the mitochondrial inner membrane via non-phosphorylating respiration (Non-Phos). The ETC was uncoupled by a titration (50-200 nM) of carbonyl cyanide p-trifluoromethoxy-phenylhydrazone; (FCCP; Sigma) to obtain the maximal respiratory capacity of the ETC. Finally, 5 mM of the complex III inhibitor, Antimycin A (Sigma), was added to determine the background respiration levels occurs outside the respiratory chain and this measurement was subtracted from all calculated values to normalize the data.

2.8 Luciferase and fluorometric based assays

2.8.1 Measurement of total cellular ATP content

Total cellular ATP content was determined using the ATPlite Luminescence ATP Detection Assay (PerkinElmer Life Sciences, Zaventem, Belgium), according the manufacturer's instructions. PerkinElmer Life Sciences provided all reagents in the assay kit. Cells were harvested using Accutase and cell counts performed, as described in *Cell culture* and *Cell counting* (Sections 2.2-2.2.6). 100,000 cells per replicate were resuspended in 100 μl DMEM and transferred to wells of a white 96-well micro-plate (Nunc). To each well, 50 μl of cell lysis buffer was added and the micro-plate was gently agitated using an orbital shaker for 5 minutes. 50 μl of substrate solution was added to each well and the micro-plate was agitated using an orbital shaker for 5 minutes and immediately incubated in the dark for 10 minutes. For each experiment, a

standard curve was prepared using an ATP standard solution, which contained a known quantity of ATP. ATP standards containing 10 µl standard in dH_2O, 90 µl DMEM, 50 µl cell lysis buffer and 50 µl substrate solution were generated using a series of five-fold dilutions from 1 x 10^{-4} M to blank.

Each experimental sample was measured in triplicate and the experiment repeated three times. Luminescence was measured using an optical plate reader (BMG Labtech, Allmendgrün, Ortenberg). A standard curve was generated and analyzed for efficiency using the MARS data analysis package (BMG Labtech). Measurements were corrected for background by removing values generated from the blank standard. ATP content present in samples was extrapolated from the standard curve using the MARS software and reported as nM of ATP per cell.

2.8.2 Measurement of cellular lactate production

Cellular lactate production was determined using a Lactate Assay Kit II (Biovision, San Francisco, CA, USA). Biovision provided all reagents within the Lactate Assay Kit. Cells were cultured under routine conditions, as described in *Cell culture* (Section 2.2). Prior to analysis, culture media was completely removed and replaced with fresh media. After 24 hours, a sample of media (50 µl) was removed for analysis and cells were collected and counted, as described in Cell culture and *Cell counting* (Section 2.2-2.2.6). Reactions were performed in clear 96-well plates (Nunc). Sample reaction mixtures contained 1 µl sample media and 49 µl lactate assay buffer. For standard curve preparation, a lactate stock standard solution (100 mM) was diluted in dH_2O to

a concentration of 1 mM. The 1 mM standard solution was used to prepare standards of 10, 8, 6, 4, 2 and 0 nM by adding 10, 8, 6, 4, 2 and 0 μl of 1 mM standard to each well and lactate assay buffer was added to a volume of 50 μl. To each sample and standard reaction, 2 μl lactate enzyme mix, 2μl lactate substrate mix and 46 μl lactate assay buffer were added. Samples were mixed using an orbital shaker for 5 minutes and incubated at room temperature for 30 minutes. Absorbance was measured at 450nm using an optical plate reader (BMG Labtech). A standard curve was generated and analyzed for efficiency using the MARS data analysis package (BMG Labtech). Measurements were corrected for background by removing values generated from the 0 (blank) standard. The lactate content present in the samples was extrapolated from the standard curve using the MARS software package and reported as lactate concentration per 10^5 cells.

2.9 Statistical analysis

Statistical significance for the RT^2 PCR arrays were determined using the Web-Based PCR Array Data Analysis software (SABiosciences), which used a two-tailed Student's t-test. For real-time PCR, O_2 consumption rates, cellular ATP content and lactate production, and tumors growth curves, statistically significant differences were determined using One-way ANOVA followed by Bonferroni post-hoc test using GraphPad v5.0c (GraphPad Software, Inc., San Diego, CA, USA). Statistical significance was expressed as *$p<0.05$, **$p<0.01$ and ***$p<0.001$.

Chapter 3: The abnormal regulation of mitochondrial DNA copy number and gene expression in glioblastoma multiforme stem-like cells

3.1 Introduction

For the last decade tumor metabolism has been chiefly characterized by aerobic glycolysis, which is also known as the Warburg Effect. The Warburg Effect is a phenomenon by which tumor cells exhibit an enhanced glycolytic state and secrete large amounts of lactate under aerobic conditions that are sufficient to support OXPHOS (Warburg, 1956). Even though OXPHOS is a much more energy-rewarding pathway, elevated glycolytic rates have been shown to be beneficial to rapidly proliferating cells by providing sufficient quantities of ATP and also through the maintenance of pools of biosynthetic intermediates (nucleotides, amino acids, fatty acids), which support growth (Christofk et al., 2008; DeBerardinis et al., 2008; Levine and Puzio-Kuter, 2010; Moreno-Sanchez et al., 2007; Vander Heiden et al., 2009). This is achieved through the incomplete catabolism of glucose, which allows the shunting of glycolysis-derived pyruvate towards anabolic processes via the TCA cycle and pentose phosphate pathway (PPP) (Christofk et al., 2008; DeBerardinis et al., 2008; Levine and Puzio-Kuter, 2010; Moreno-Sanchez et al., 2007; Vander Heiden et al., 2009).

Interestingly in 2011, the synonymous relationship between tumor metabolism and the Warburg Effect was challenged. Recent work now suggests that some tumor cells undergo an alternate form of metabolic reprogramming and enhance their OXPHOS capacity rather than become increasingly glycolytic. This phenomenon is referred to as the “Reverse Warburg Effect” (Pavlides et al., 2009). The underlying concept of the Reverse Warburg Effect is that the human body undergoes metabolic decline during ageing and that ageing cells acquire OXPHOS defects and become increasingly glycolytic (Ertel et al., 2012). Subsequently, glycolytic cells secrete energy rich lactate into the extracellular matrix. Tumor cells with enhanced OXPHOS capacity are then able to consume and metabolize the extracellular lactate to support their cellular function and proliferation (Ertel et al., 2012). In an *in vitro* co-culture system, tumor cells have been shown to induce oxidative stress in fibroblasts cells, which also resulted in premature ageing in the same cells (Lisanti et al., 2011a; Lisanti et al., 2011b). The aged fibroblasts secreted lactate into the culture media that was consumed and utilized by the tumor cells and this process was mediated through an enhanced OXPHOS state in the tumor cells (Lisanti et al., 2011a; Lisanti et al., 2011b). In another study, immunohistochemical analysis of primary breast tumor samples revealed enhanced expression of cytochrome-c-oxidase (COX; Complex III) relative to healthy neighboring cells (Whitaker-Menezes et al., 2011). These studies provide strong evidence that OXPHOS may play an important role in tumor cell metabolism and maintenance of their cellular function.

The above studies demonstrate that tumor cell metabolism is more complex than previously thought. GBM CSCs have been shown to exhibit characteristics of the Warburg Effect (DeBerardinis et al., 2008; DeBerardinis et al., 2007; Wolf et al., 2011) however, much less is known regarding the role of OXPHOS in these cell types. Furthermore, very little is known regarding how mtDNA is regulated GBM CSCs and its implications on metabolism and OXPHOS.

GBM CSCs exhibit stem cell-like properties such as self-renewal and multipotency (Galli et al., 2004; Singh et al., 2003); however, it is unknown whether GBM CSCs regulate their mtDNA in a similar manner to normal stem cells. Furthermore, it is unknown whether GBM CSCs are able to undergo the metabolic transition that occurs during the differentiation of normal stem cells. As a stem cell undergoes differentiation, there is a metabolic transition from glycolysis to OXPHOS metabolism that serves to fulfill the future energy requirements of the terminally differentiated cell type (Cho et al., 2006; Facucho-Oliveira et al., 2007; Prigione et al., 2010; Varum et al., 2011). The differentiation of embryonic stem cells (ESCs) is associated with an expansion in mtDNA copy number that enhances OXPHOS potential by increasing the number of mtDNA copies available for translation into functional subunits of the ETC (Facucho-Oliveira et al., 2007; St John et al., 2005). Since the ETC is encoded by both nuclear and mtDNA both genomes must work synergistically in order to generate a functional respiratory chain (Woodson and Chory, 2008). Human neural stem cells (hNSCs) are the closest non-transformed counterpart of GBM CSCs and it is likely that hNSCs undergo a similar mtDNA copy number

expansion and metabolic transition during differentiation that has previously been observed in ESCs, however this requires confirmation.

The direct comparison of undifferentiated and differentiated hNSCs and GBM CSCs provides an excellent opportunity to analyze how mtDNA is regulated in both normal and transformed multipotent cell populations. Furthermore metabolic profiling of undifferentiated and differentiated GBM CSCs will also further explore the role of OXPHOS in GBM CSCs.

3.2 Hypothesis

GBM CSCs and hNSCs share multiple characteristics that include self-renewal, multi-potency and gene expression profiles. Normal stem cell populations have been shown to contain low numbers of mtDNA copies and the onset of differentiation is associated with an expansion of mtDNA copy number and a transition from glycolytic to OXPHOS metabolism. Tumors cells, including GBM CSCs, show abnormal expression of factors that regulate cell metabolism, such as *c-MYC* (Gordan et al., 2007), and it is likely that this will impact upon the ability of GBM CSCs to undergo differentiation and modulate their mtDNA copy number accordingly and will therefore differ to that of normal hNSCs.

3.3 Aims

1. To determine how mtDNA copy number is modulated during the differentiation of hNSCs and GBM CSCs

2. To determine how the expression of NSC and lineage specific markers are regulated during the differentiation of hNSCs and GBM CSCs

3. To characterize the energy metabolism profiles of undifferentiated and differentiated hNSCs and GBM CSCs through functional experiments.

3.4 Materials and Methods

3.4.1 Cell Culture

hNSCs, HSR-GBM1, GBM-L1 and GBM-L2 cell lines were routinely cultured, as described in *Culture of human neural stem cells* (Section 2.2.3) and *Culture of GBM cell lines* (Section 2.2.4), until sufficient cell numbers were available for experiments. hNSCs and GBM cell lines were differentiated for up to 28 days, as described in *Differentiation of hNSCs* (Section 2.3.1) and *Differentiation of GBM cell lines* (Section 2.3.2).

`

3.4.2 MtDNA copy number analysis

MtDNA copy number was quantified in undifferentiated and differentiated hNSC and GBM CSCs using real-time PCR, as described in *Real-time PCR* (Section 2.6) and *MtDNA copy number analysis* (Section 2.6.4), using primer pairs specific to mtDNA and β-Globin. Primer sequences and annealing and secondary acquisition temperatures are listed in Table 3.I.

3.4.3 Gene expression analysis

The expression of the NSC and lineage specific markers, *NESTIN, MUSASHI1, CD133* and *GFAP* were analyzed by real-time PCR and the Pfaffl method (Pfaffl, 2001), as described in *Real-time PCR* (Section 2.6) and *Gene expression analysis* (Section 2.6.3). *β-ACTIN* was selected as the housekeeping gene. Primer sequences and annealing and secondary acquisition temperatures are listed in Table 3.I.

Gene	Forward Primer	Reverse Primer	Product Length (bp)	Annealing Temperature (°C)	Secondary Acquisition Temperature (°C)
β-ACTIN	CAAAACCTAACTTGCGCAGA	TTTTAGGATGGCAAGGGACT	261	56	80
β-GLOBIN	CAACTTCATCCACGTTCACC	GAAGAGCCAAGGACAGGTAC	268	56	80
CD133	GCATTGGCATCTTCTATGGTT	CGCCTTGTCCTTGGTAGTGT	190	55	78
GFAP	GAAGCTCCAGGATGAAACCA	ACCTCCTCCTCGTGGATCTT	165	55	80
MtDNA	CGAAAGGACAAGAGAAATAAGG	CTGTAAAGTTTTAAGTTTTATGCG	152	53	76
MUSASHI1	AGAAAGCTCAGCCAAAGGAG	GAATTCGGGGAACTGGTAGG	194	55	84
NESTIN	AAACCAGAGCCATGAGACAC	TGGCCTACAGCCTCTTTTTC	156	55	76

Table 3.I. Primer sequences, product sizes and annealing temperatures for conventional PCR, RT-PCR and real-time PCR. Secondary acquisition temperatures are also listed for real-time PCR reactions.

3.4.4 Total ATP content and Lactate production

Total ATP content and lactate production in undifferentiated and differentiated hNSCs and HSR-GBM1 cells was determined using luminescence and fluorescence bases assays, as described in *Measurement of total cellular ATP content* and *Measurement of cellular lactate production* (Section 2.8)**.**

3.4.5 Cellular respiration

Cellular respiration analyses of undifferentiated and differentiated hNSCs and HSR-GBM1 cells were performed using the Oxygraph 2K system, as described in *Cellular respiration,* in the *General Materials and Methods* (Section 2.7.1).

3.4.6 Statistical analysis

Statistical analysis was performed, as described in *Statistical analysis*, in the *General Materials and Methods* (Section 2.11).

3.5 Preliminary Experiments

3.5.1 Analysis of neural stem cell and lineage specific marker expression in GBM CSCs

Three GBM CSC lines were selected for analysis, HSR-GBM1, GBM-L1 and GBM-L2. These cell lines are derived from patient (primary) tumor samples and have not been transformed or immortalized *in vitro*. These cell lines, therefore, provide the closest representation of true malignant cells, *in vitro*.

In the literature, GBM CSCs are reported to express multiple NSC markers (Galli et al., 2004; Ma et al., 2008; Singh et al., 2003) and thus, I sought to confirm the expression of these factors in the three selected GBM CSC lines. Each of the GBM CSC cell lines were propagated as neurospheres and routinely cultured, as described in *Culture of GBM cell lines* (Section 2.2.4). HSR-GBM1 cells were used at high passage (>p60) whilst GBM-L1 and GBM-L2 were used at low passage (<p20). The expression of the NSC markers, *NESTIN*, *MUSASHI1* and *CD133* were determined by RT-PCR and gel electrophoresis, as described in Sections 2.5 and 2.5.4. *β-ACTIN* was selected as a housekeeping gene and primer sequences are listed in Table 3.I. Each of the GBM CSC lines expressed *NESTIN*, which was demonstrated by the generation of PCR products of appropriate size (Figure 3.1). *MUSASHI1* was abundantly expressed in each of the GBM CSC lines as demonstrated by a high fluorescent intensity of the PCR product (Figure 3.1). *CD133* was expressed at low levels in HSR-GBM1 cells and highly expressed in GBM-L1 cells. However, no expression of *CD133* was detectable in GBM-L2 cells

(Figure 3.1). Despite differences in passage number, each of the GBM CSC lines expressed at least 2 out of 3 NSC markers. I therefore reasoned that these cell lines were suitable for the comparison of GBM CSCs with their closest non-transformed counterpart, hNSCs. Furthermore, the gene expression analysis of three GBM CSC lines allows for greater characterization of this tumor cell type.

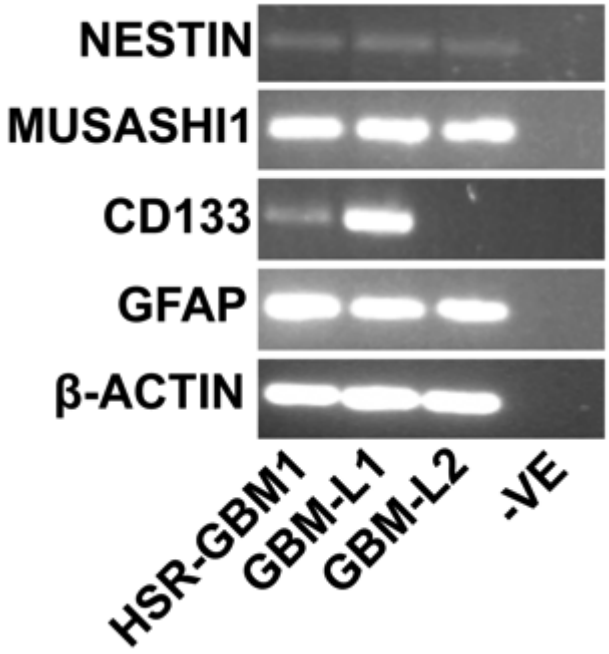

Figure 3.1. RT-PCR analysis of the NSC and lineage specific markers *NESTIN, MUSASHI1, CD133* and *GFAP* in GBM CSCs. *β-ACTIN* was selected as a housekeeping gene.

Reports from the literature suggest that GBM may be derived from transformed glial cells (Buckner et al., 2007). GFAP is an intermediate filament protein that is expressed by glial cells and is also a marker of astrocyte differentiation. I therefore sought to analyze the expression of GFAP in each of the GBM cell lines. I observed that *GFAP* was abundantly expressed in each of the GBM cell lines (Figure 3.1) and likely suggest that the GBM cell lines are of glial origin. In order to determine how the expression of *GFAP* and also *NESTIN, MUSASHI1*

and *CD133* are regulated during differentiation the expression of these genes required a quantitative approach, using real-time PCR (Section 2.6.3).

3.5.2 Optimization of real-time PCR for gene expression analysis

Real-time PCR reactions for *NESTIN, MUSASHI1, CD133, GFAP* and *β-ACTIN* were optimized prior to hNSC and GBM differentiation assays. PCR products for each of the genes of interest were generated using HSR-GBM1 cells and were excised from agarose gels and purified, as described in *PCR product purification* (Section 2.5.5). From each of the purified PCR products, a set of standards ranging from 1×10^{-2} - 1×10^{-6} ng were prepared and used as templates for the real-time PCR reactions. Real-time PCR reactions were performed, as described in *Real-time PCR* (Section 2.6.1 & 2.6.3), using the primer sequences listed in Table 3.I.

For each gene of interest, PCR standards, PCR reaction efficiencies and melting curve analysis are illustrated in Figure 3.2. Reaction efficiencies were subsequently used for the analysis of relative gene expression using the Pfaffl method, as described in *Gene expression analysis* (Section 2.6.3). Melt curve analysis was performed to confirm the generation of a single amplicon of interest. Melting curve analysis was also used to determine the optimal secondary acquisition temperature (Cycling B), to ensure that the data extrapolated from each reaction excluded any PCR artifacts such as primer dimers. Secondary acquisition temperatures for each of the genes of interest are listed in Table 3.I.

A **Nestin Standards**

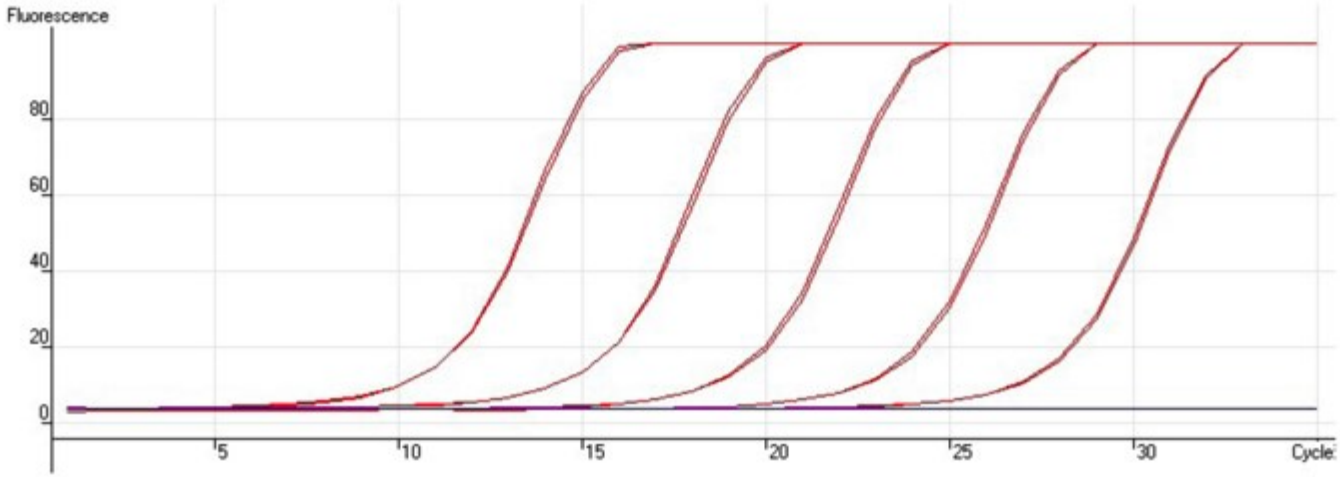

PCR Efficiency

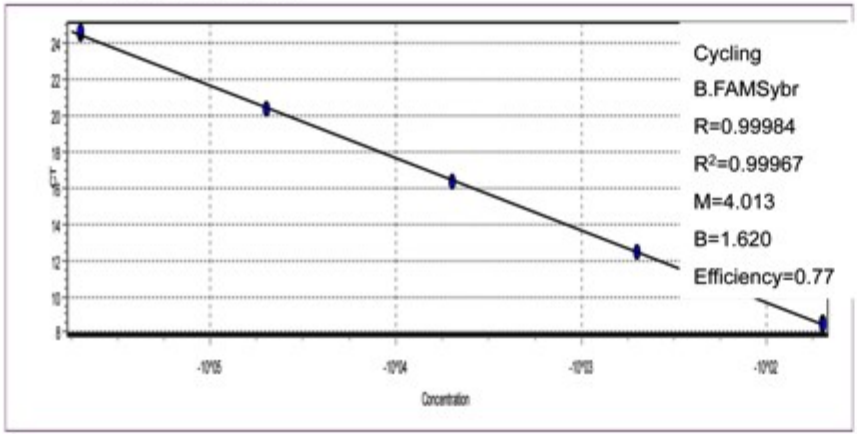

Melt Curve Analysis

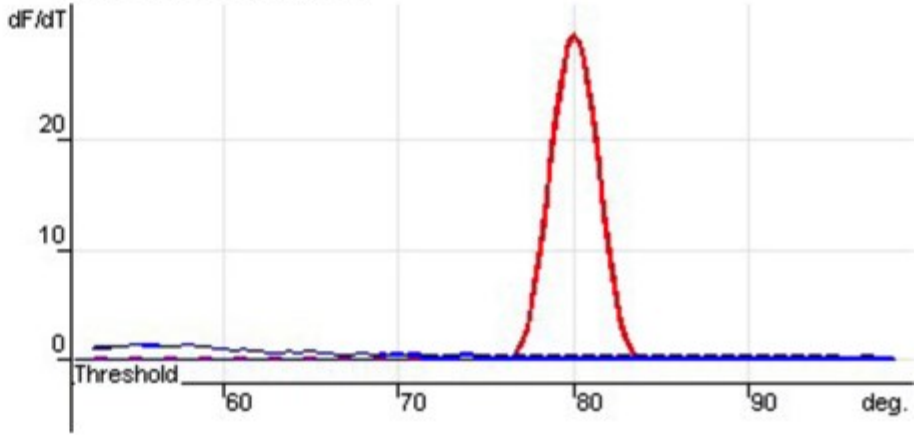

B Musashi1 Standards

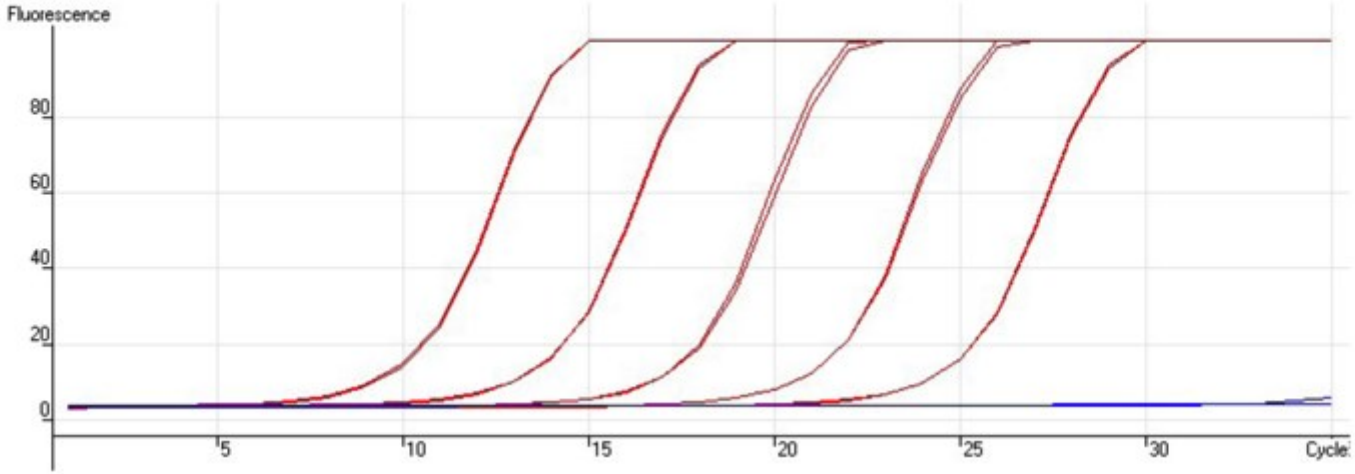

PCR Efficiency

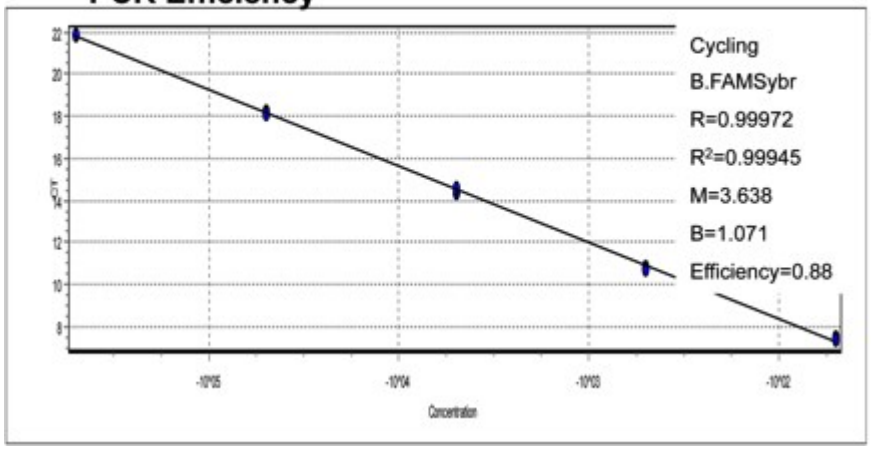

Melt Curve Analysis

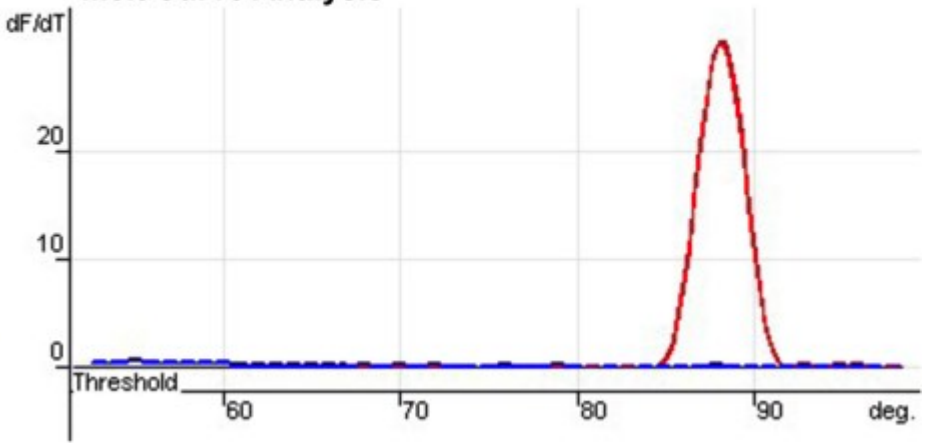

C CD133 Standards

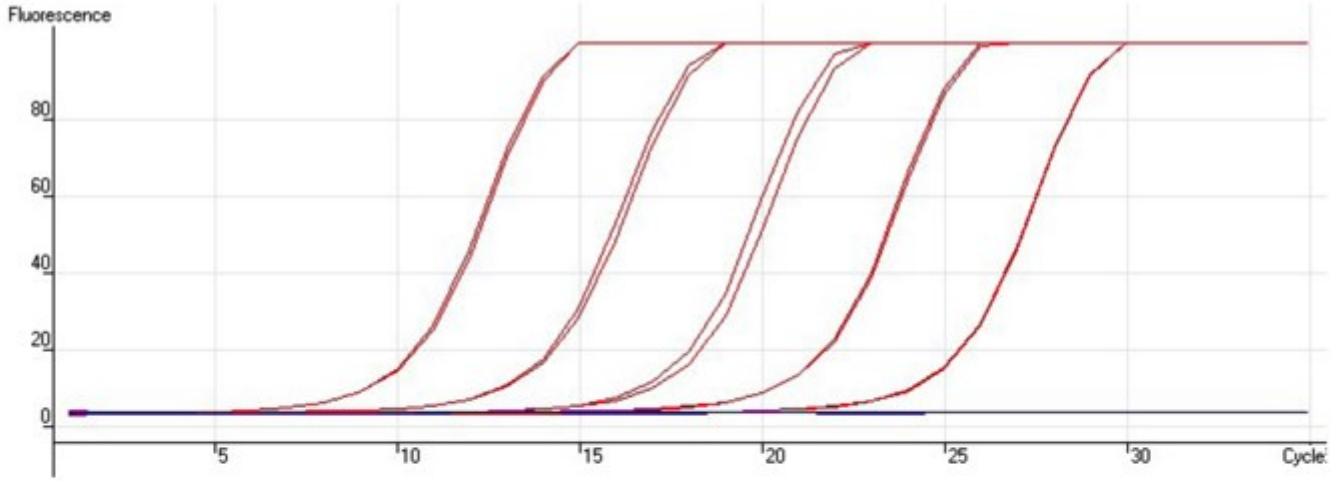

PCR Efficiency

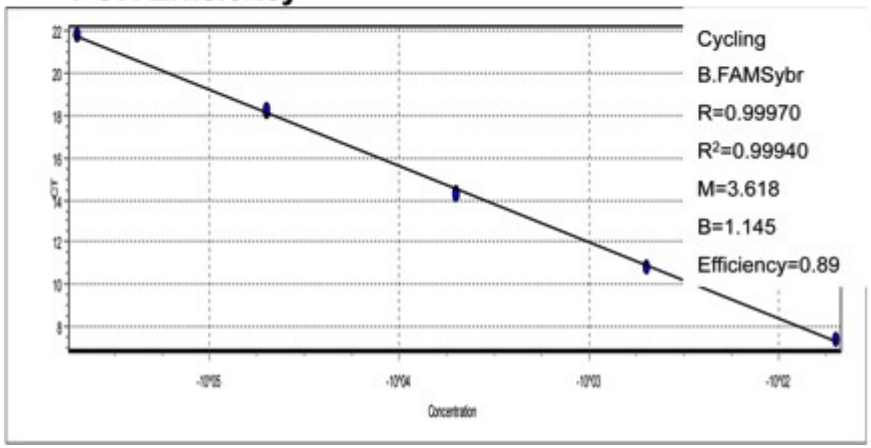

Melt Curve Analysis

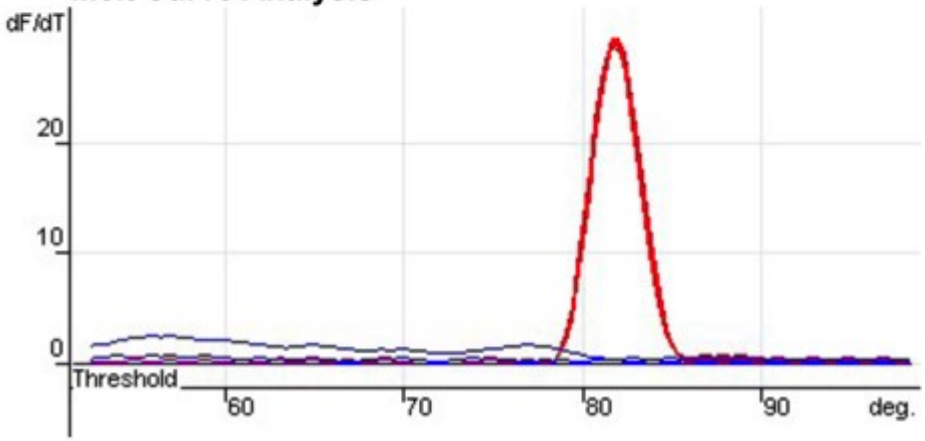

D GFAP Standards

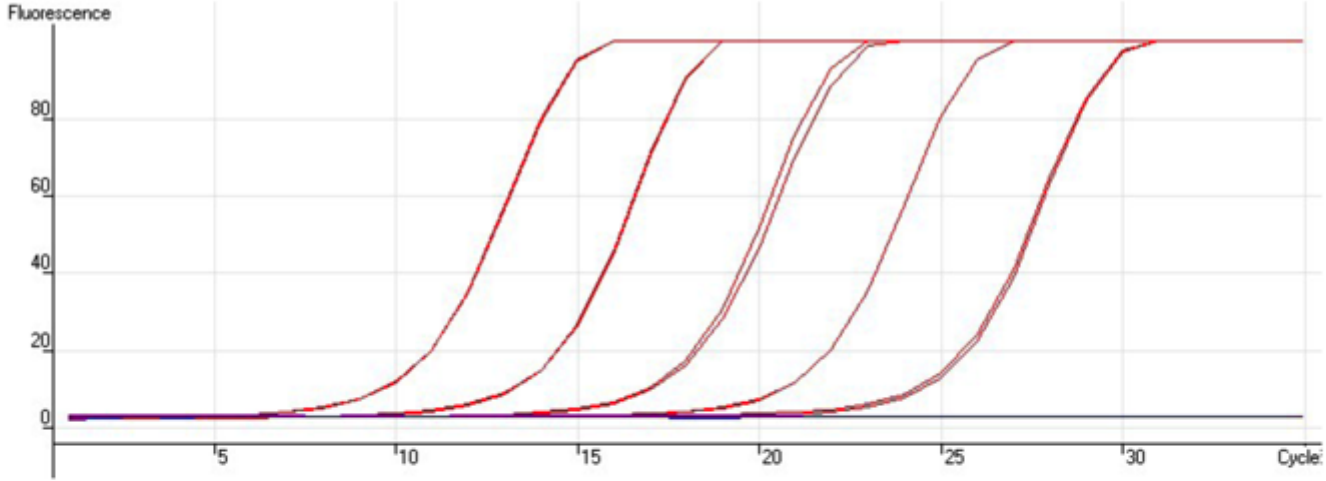

PCR Efficiency

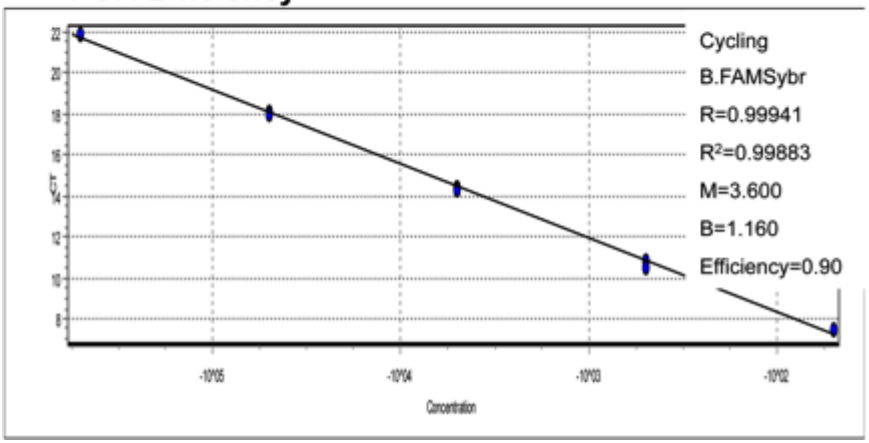

Melt Curve Analysis

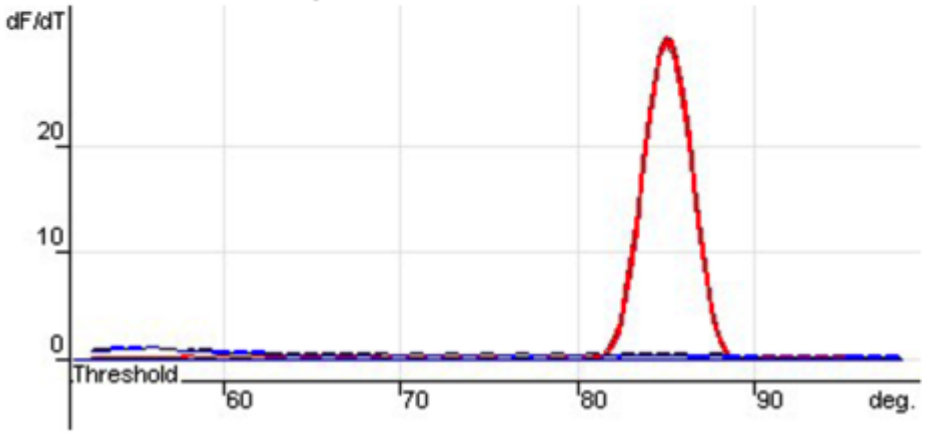

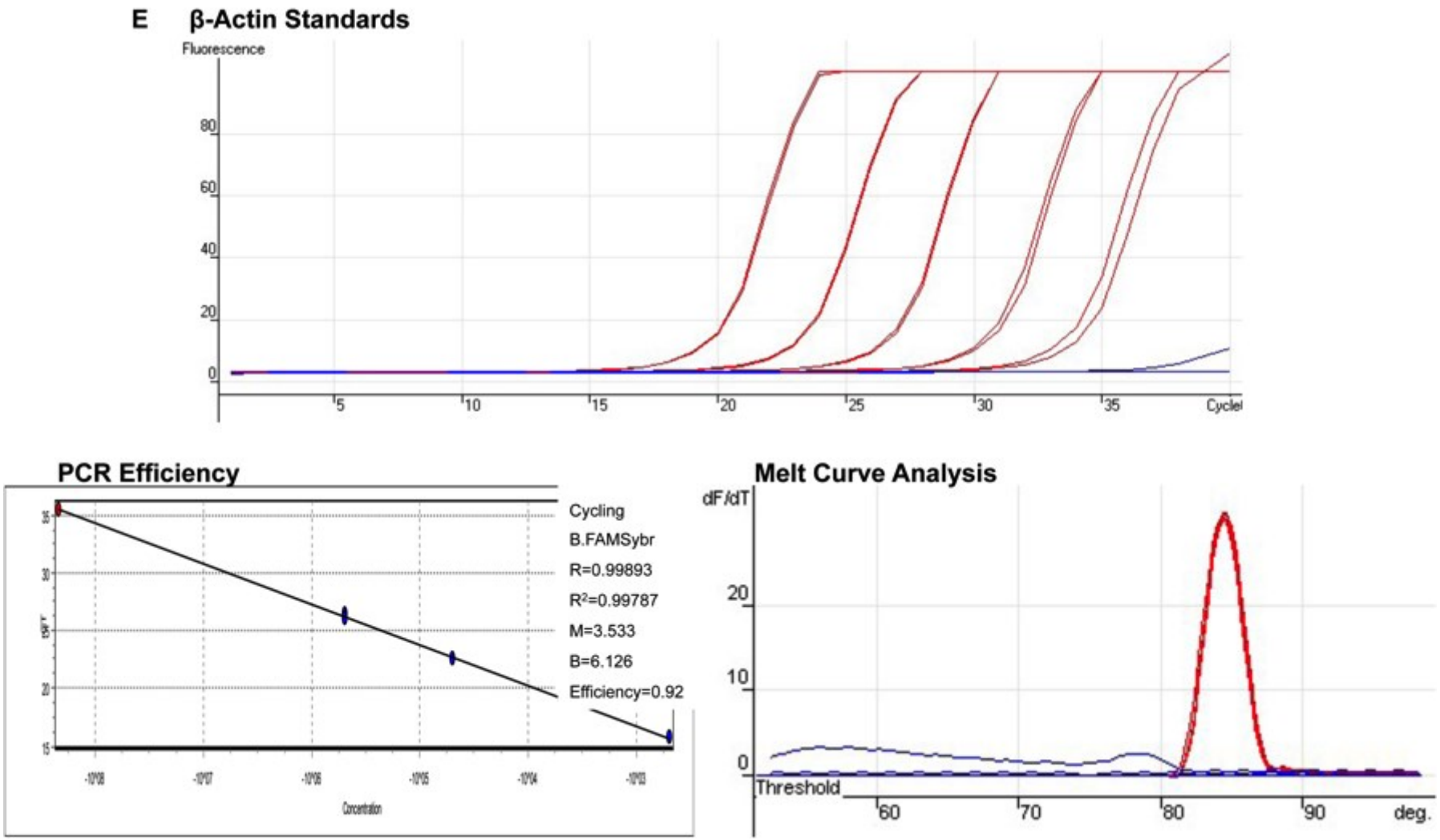

Figure 3.2. Real-time PCR standards, PCR standard curves and melt analyses, as indicated, for *NESTIN* (A)*, MUSASHI1* (B)*, CD133* (C), *GFAP* (D) and *β-ACTIN* (E).

3.5.3 Optimization of real-time PCR for mtDNA copy number analysis

Conventional PCR was performed to obtain the PCR products required to generate DNA standards for mtDNA and β-Globin, respectively (Figure 3.3). PCR reactions were performed, as described in *Polymerase Chain Reaction* (Section 2.5 & 2.5.3), using primer pairs specific for mtDNA and β-Globin (Table 3.I). PCR products were generated from hNSCs and excised from agarose gels and purified, as described in *PCR product purification* (Section 2.5.5). Standards for mtDNA and β-Globin ranging from 1×10^{-2} - 1×10^{-6} ng were prepared and used as templates for real-time PCR reactions. Real-time PCR reactions were performed, as described in *Real-time PCR* (Sections 2.6.2 & 2.6.4). MtDNA and β-Globin standards, PCR reaction efficiencies and melt curve analyses are illustrated in Figure 3.3. Secondary acquisition temperatures for mtDNA and β-Globin are listed in Table 3.I.

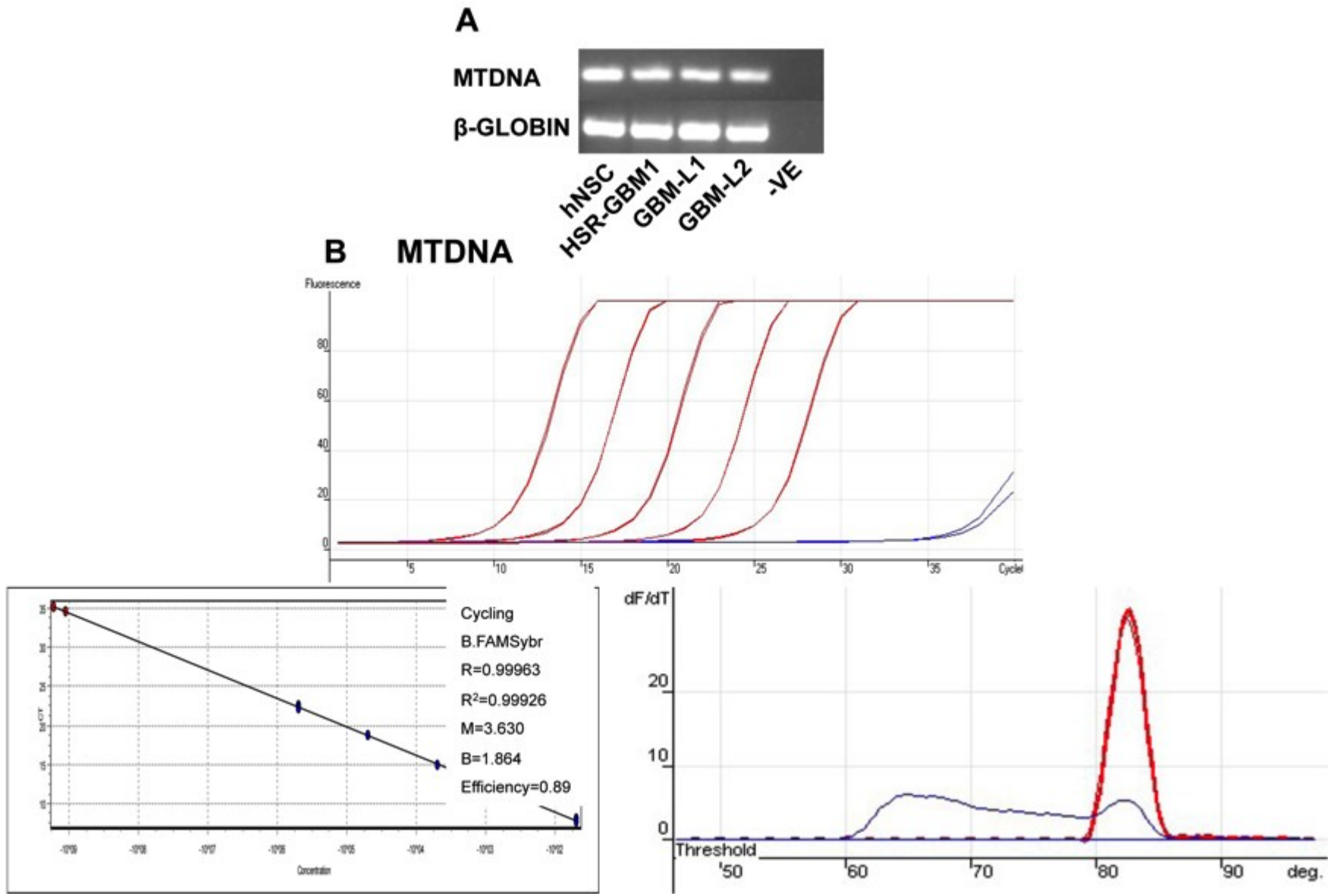
A
MTDNA
β-GLOBIN
hNSC
HSR-GBM1
GBM-L1
GBM-L2
-VE
B
MTDNA
Fluorescence
Cycle
Cycling
B.FAMSybr
R=0.99963
R²=0.99926
M=3.630
B=1.864
Efficiency=0.89
dF/dT
Threshold
deg.

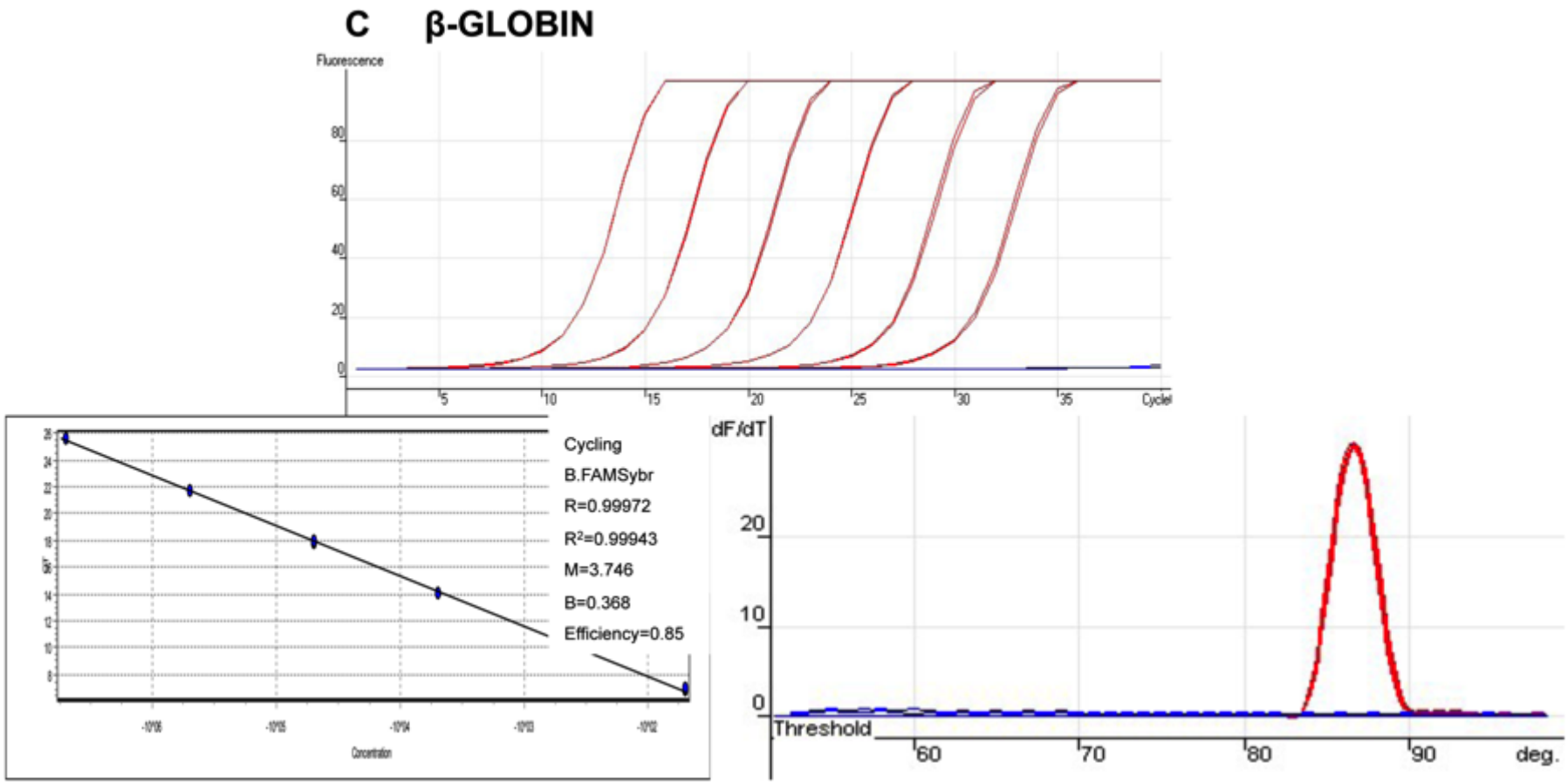

Figure 3.3. Amplification of mtDNA and β-Globin regions by conventional PCR in hNSCs and GBM CSCs (A). Real-time PCR standards, PCR standard curves and melt analyses as indicated, for mtDNA (B) and β-Globin (C).

3.5.4 Optimization and validation of the Oxygraph-2K respiratory system

Prior to O_2 consumption analysis of intact NSC and GBM CSCs using the Oxygraph-2K system, the optimization of respiratory chain inhibitors was required. The Oxygraph-2K system was calibrated and O_2 flux equilibrated prior to analysis, as described in *Cellular respiration* (Section 2.7.1).

Cells were collected and counted, as described in *Cell culture* (Section 2.2) and *Cell counting* (Section 2.2.6) and transferred into the measurement chambers using a syringe. O_2 consumption increased following the addition of cells, as demonstrated by an increase in O_2 flux (red-line) and a reduction in O_2 concentration (blue-line) (Figure 3.4). The subsequent equilibration of O_2 flux was designated as the "Resting" or "Basal" O_2 consumption rate and was recorded (Figure 3.4A). The Complex V (ATP Synthase) inhibitor, Oligomycin, was added to each chamber to determine the rate of non-phosphorylating (Non-Phos) O_2 consumption. A concentration of 4 mg/ml Oligomycin (Pesta and Gnaiger, 2012) was utilized in all experiments and generated stable O_2 consumption rates, as shown in Figure 3.4B.

The ETC uncoupler, FCCP, required titration in order to determine the maximal respiratory capacity of the cells under investigation. The efficacy of FCCP varies depending on cell number, with greater numbers of cells requiring higher concentrations and vice versa. Low concentrations of FCCP resulted in incomplete uncoupling, whilst excess FCCP was inhibitory to O_2 consumption. FCCP was titrated for the analysis of 1-2 $x10^6$ cells. 50 µM of FCCP was added in increments and O_2 consumption was monitored after each addition, as shown

in Figure 3.4C. The addition of FCCP was ceased when O_2 consumption failed to show any further increases (Figure 3.4C). The cumulative concentration of FCCP at which maximal O_2 consumption was observed was regarded as the optimal concentration. For subsequent analyses, one addition of the optimal concentration of FCCP was added to each chamber. This was followed by a second addition of FCCP to confirm that maximal ETC uncoupling had been obtained.

The Complex III (Cytochrome C Reductase) inhibitor, Antimycin A, was used at a concentration of 5 mM (Pesta and Gnaiger, 2012). Antimycin A was the final inhibitor added to each measurement chamber and was used to determine the background O_2 consumption that was occurring independently of the ETC (Figure 3.4D).

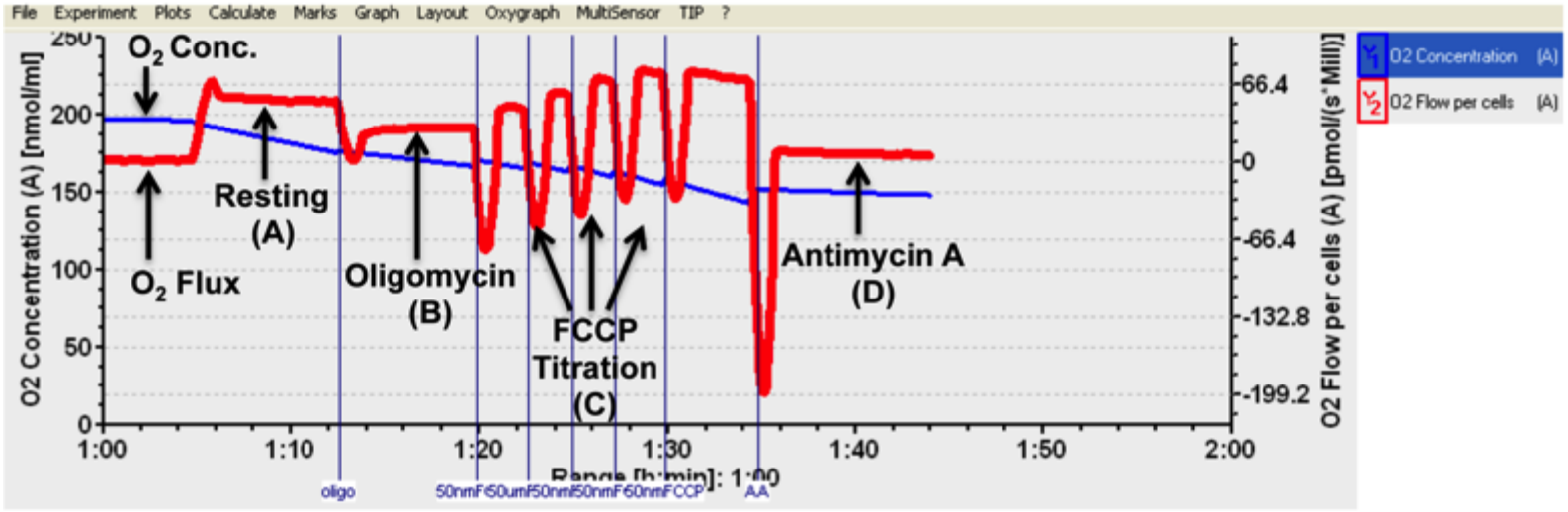

Figure 3.4. Graphical representation of cellular O_2 consumption with the Oxygraph 2K integrated software package, Datlab. The blue line indicates the O_2 concentration and the red line indicates the rate of change in O_2 consumption (O_2 Flux). The O_2 consumption was measured following the addition of cells (A) and manipulation of the ETC following the addition of a series of compounds. The following compounds were added to manipulate the ETC: Oligomycin (B) to inhibit Complex V, FCCP (C) to uncouple the ETC and Antimycin A (D) to inhibit Complex III.

The Oxygraph-2K system is a highly sensitive experimental tool that has been utilized extensively for cellular respiration studies over the past decade with over 950 citations (www.oroboros.at). To confirm the sensitivity and reproducibility of this system I measured the O_2 consumption of six different cell lines. With a defined number of cells ($1x10^6$), the Oxygraph-2K system produced a wide range of O_2 consumption values with small SEMs (Figure 3.5). This was best represented by the differences in O_2 consumption rates between the osteosarcoma lines, 143BTK-$^{\rho+}$ (which contain mtDNA) and the 143BTK-$^{\rho0}$ (devoid of mtDNA and have a limited respiratory capacity). These outcomes demonstrate the sensitivity and reproducibly of the Oxygraph-2K system.

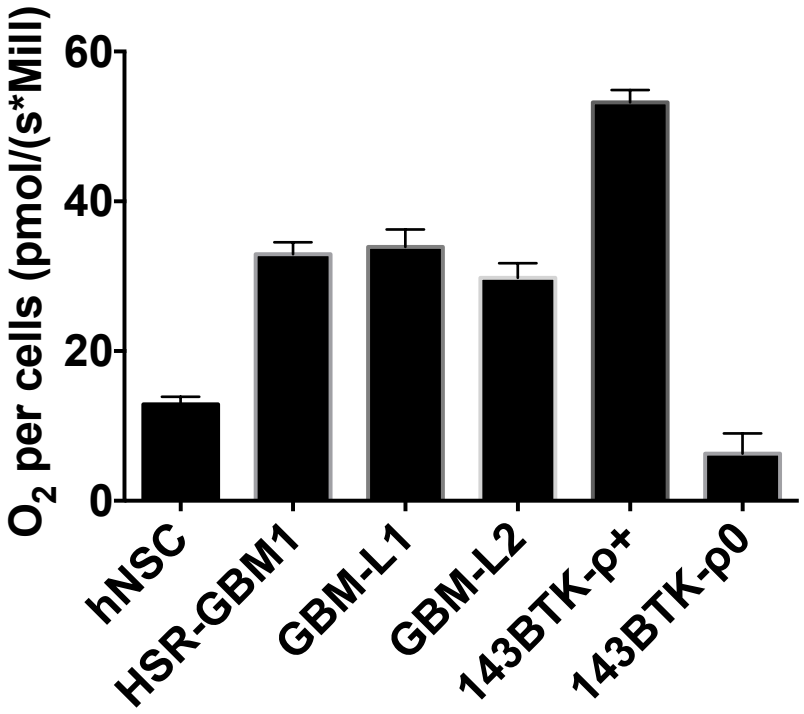

Figure 3.5. Analysis of cellular O_2 consumption in multiple cell lines. The O_2 consumption rates of six different cell line to validate the sensitivity of the Oxygraph-2K system

3.6 Results

3.6.1 MtDNA copy number during differentiation of hNSCs

hNSCs were differentiated in astrocyte induction media for up to 28 days in order to determine how mtDNA copy number was regulated in a non-transformed stem cell population. hNSCs showed a progressive increase in mtDNA copy number during differentiation. MtDNA copy number was increased by 1.78 ($p<0.001$) and 1.92-fold ($p<0.001$) on Day 7 and 14, respectively and cumulated with a 3.20-fold ($p<0.001$) increase by Day 28 (Figure 3.6).

3.6.2 MtDNA copy number during differentiation of GBM CSCs

In order to determine whether multipotent tumor cells are able to regulate mtDNA copy number accordingly during differentiation, I examined mtDNA copy number in three GBM cell lines that share similar characteristics to hNSCs. HSR-GBM1, GBM-L1 and GBM-L2 cells were differentiated under identical conditions to hNSCs, in astrocyte induction media for 28 days and mtDNA copy number was analyzed.

In contrast to hNSCs, HSR-GBM1 cells showed small, but significant increases in mtDNA copy number on Day 7 (1.25-fold; $p<0.001$), Day 14 (1.15-fold; $p<0.01$) and Day 28 of differentiation (1.37-fold; $p<0.001$) (Figure 3.6). However, HSR-GBM1 cells failed to mimic the progressive expansion in mtDNA copy number observed in hNSCs. The GBM-L1 cell line showed an increase in mtDNA copy number on Day 7 (1.98-fold; $p<0.001$; Figure 3.6) and Day 14 (2.48-fold; $p<0.001$). However, on Day 28 the expansion in mtDNA copy

number ceased and was reduced by 1.54-fold compared to Day 14 ($p<0.001$; Figure 3.6). GBM-L2 cells showed a different pattern of mtDNA copy number regulation. No significant increase in copy number was observed on Day 7 of differentiation (Figure 3.6). MtDNA copy number was increased by 1.26-fold ($p<0.01$) on Day 14 and was 1.92-fold ($p<0.001$) greater than Day 0 by Day 28 of differentiation. Although an increase in mtDNA copy number was observed on Day 28 of differentiation, the magnitude of this expansion was not as pronounced as that observed in hNSCs.

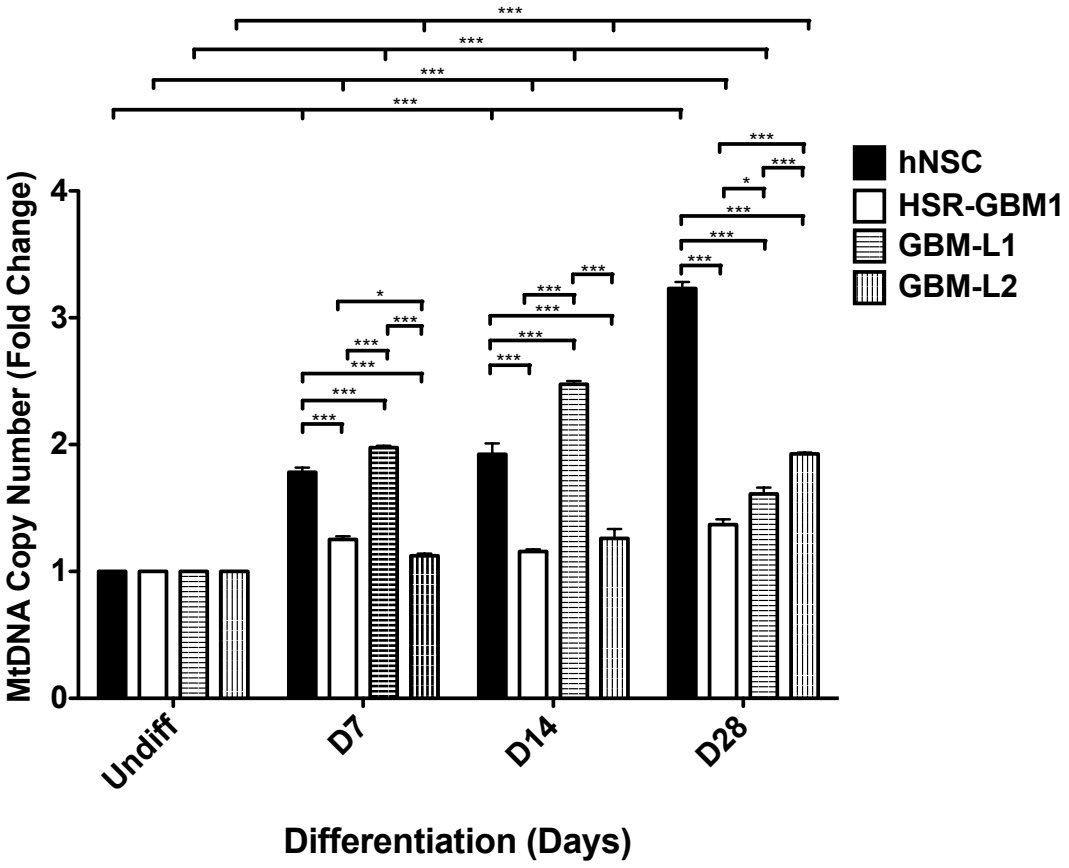

Figure 3.6. Analysis of mtDNA copy number in differentiating hNSCs and GBM CSCs. Fold change in mtDNA copy number relative to Day 0 in hNSCs, HSR-GBM1, GBM-L1 and GBM-L2 cells during 28 days of differentiation. Columns represent mean values ± SEM (n=3). * Indicates $p<0.05$ and *** $p<0.001$.

3.6.3 Neural stem cell and lineage specific marker expression during differentiation

To further characterise the differentiation of hNSCs and HSR-GBM1 cells, the expression of the neural stem cell markers, *NESTIN, MUSASHI1* and *CD133* and the astrocyte-specific marker *GFAP* were analysed. Differing trends were observed for the expression of the neural stem cell markers during the 28-day differentiation period. *NESTIN* expression remained unchanged by Day 28 (Figure 3.7A) in hNSCs and *MUSASHI1* showed significant reductions in expression on Day 14 and 28 ($p<0.001$; Figure 3.7B). In addition, a progressive increase in *CD133* was observed in hNSCs during differentiation ($p<0.001$; Figure 3.7A-C). Despite the varying expression in NSC markers in hNSCs, the astrocyte marker was progressively and significantly increased as differentiation progressed for 28 days ($p<0.001$; Figure 3.7D).

HSR-GBM1 cells showed a significant reduction in the expression of the NSC markers, *NESTIN, MUSASHI1 and CD133* by Day 28 of differentiation ($p<0.001$; Figure 3.7A-C). Interestingly, HSR-GBM1 cells showed an initial surge in *GFAP* expression on Day 7 ($p<0.001$); however, expression was later reduced as differentiation progressed (Figure 3.7D).

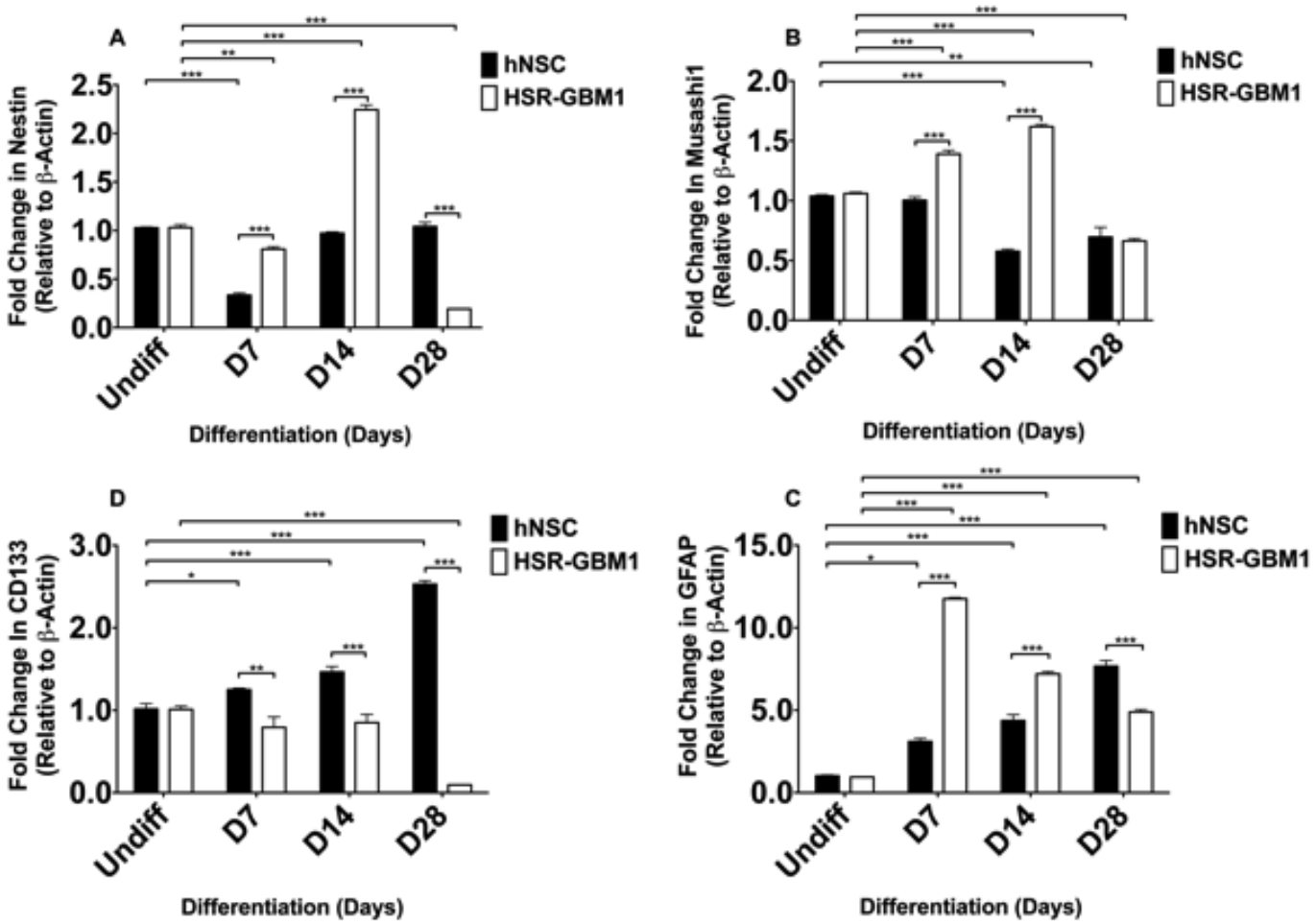

Figure 3.7. Gene expression analysis of hNSCs and HSR-GBM1 cells during differentiation. Fold change in expression relative to Day 0 and weighted against *β-ACTIN* of *NESTIN* (A), *MUSASHI1* (B), *CD133* (C) and *GFAP* (D) in differentiating hNSCs and HSR-GBM1 cells. Columns represent mean values ± SEM (n=3). * Indicates $p<0.05$, ** $p<0.01$ and *** $p<0.001$.

To further investigate whether the regulation of the NSC and lineage specific markers were abnormally regulated in other GBM CSC, gene expression was also analysed in the GBM-L1 and GBM-L2 cell lines. GBM-L1 cells showed significant increases in expression of *NESTIN, MUSASHI1 and CD133* by Day 28 of differentiation ($p<0.001$; Figure 3.8A-C), with the expression of *MUSASHI1* and *CD133* showing progressive increases from Day 14 of differentiation onwards. Furthermore, the expression of *GFAP* was increased significantly from Day 7 of differentiation onwards with an increase of 70-fold by Day 28 ($p<0.001$; Figure 3.8D). GBM-L2 cells exhibited a differing pattern of expression. *NESTIN* expression was elevated on Day 14 ($p<0.001$) of differentiation, however, expression was significantly reduced on Day 28 of differentiation when compared to Day 0 ($p<0.001$; Figure 3.8E). Similarly, an elevation in *MUSASHI1* and *CD133* expression was observed on Day 14 ($p<0.001$; Figure 3.8E-F) of differentiation, which was followed by a reduction in expression by Day 28. *GFAP* expression in GBM-L2 cells showed a similar pattern that of HSR-GBM1 cells, with an initial 54-fold surge in expression on Day 7 ($p<0.001$; Figure 3.8G), which was followed by a reduction in expression through Days 14 and 28 of differentiation.

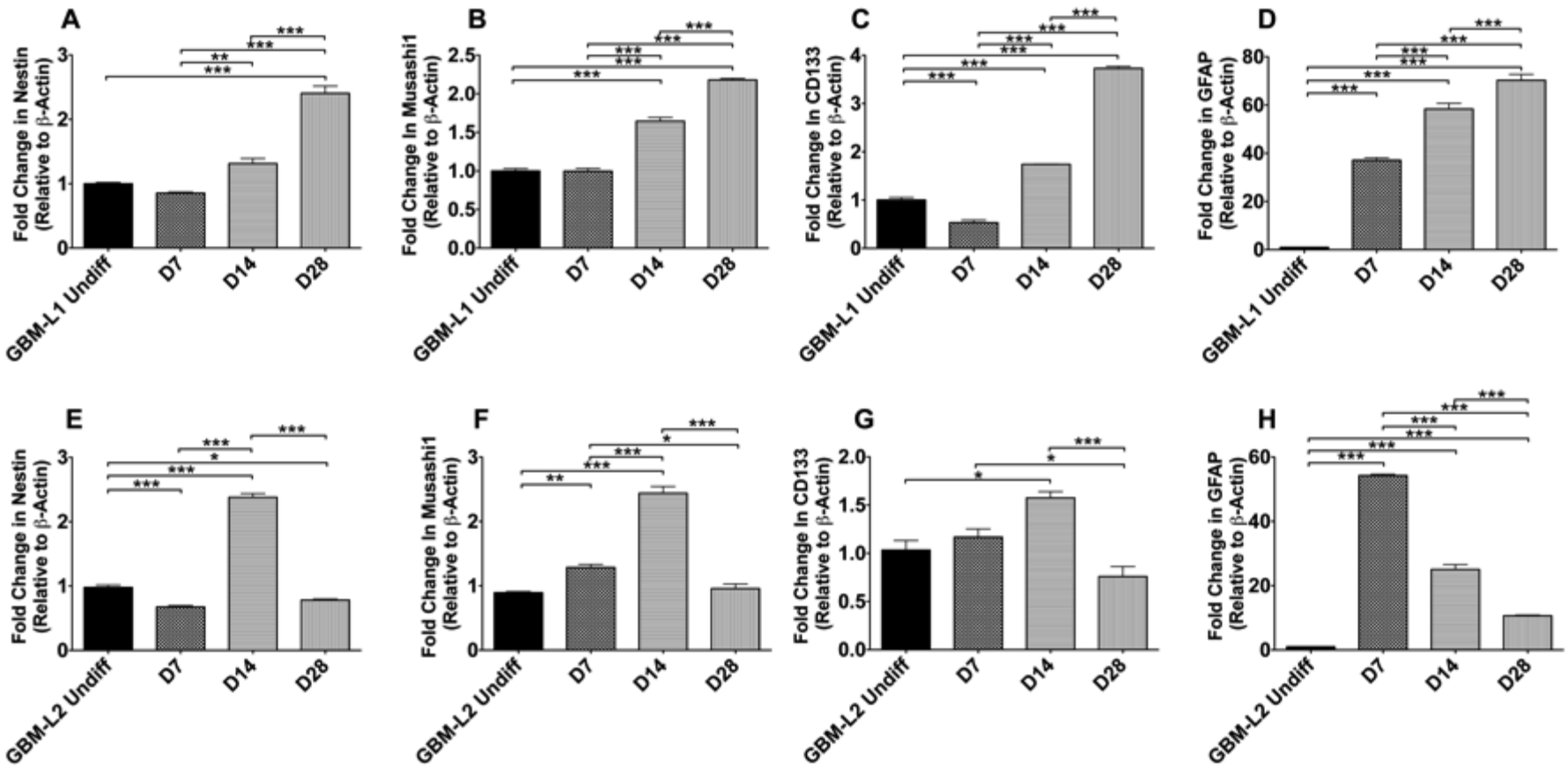

Figure 3.8. Gene expression analysis of GBM-L1 and GBM-L2 cells during differentiation. Fold change in expression relative to Day 0 and weighted against *β-ACTIN* of *NESTIN* (A & E), *MUSASHI1* (B & F), *CD133* (C & G) and *GFAP* (D & H) in differentiating GBM-L1 and GBM-L2 cells. Columns represent mean values ± SEM (n=3). * Indicates $p<0.05$, ** $p<0.01$ and *** $p<0.001$.

The HSR-GBM1 cell line is the most characterized GBM CSC line (Galli et al., 2004). Furthermore, despite their relatively high passage number, HSR-GBM1 cells expressed each of the NSC markers (*NESTIN, MUSASHI1* and *CD133*) abundantly. This demonstrates that this cell line stably exhibits stem cell-like properties over time and thus, the HSR-GBM1 cell line was selected for further comparative analysis with hNSCs.

3.6.4 O_2 consumption analysis

I next determined whether the observed differences between HSR-GBM1 cells and hNSCs in mtDNA copy number regulation also affected the respiratory capacity of these cell types in their undifferentiated and differentiated states. To address these questions the resting O_2 consumption, ETC coupling efficiency, ETC reserve capacity, O_2 consumption, % of ETC devoted to ATP production and the maximal respiratory capacity of HSR-GBM1 cells and hNSCs were analyzed using the Oxygraph-2K respiratory system. In the undifferentiated state, HSR-GBM1 cells showed a 2.32-fold ($p<0.01$) higher rate of resting ('Basal") O_2 consumption than undifferentiated hNSCs (Figure 3.9A). The ETC coupling efficiency, calculated by the ratio of 'Basel'/'Non-Phosphorylating respiration', was not significantly different between the two undifferentiated cell types (Figure 3.9B). Furthermore, the ETC reserve capacity, calculated by the ratio of 'Uncoupled'/'Non-'Non-Phosphorylating respiration', was close to a value of 1 in both undifferentiated cell types, which indicates that the measured resting respiration was at (or near) maximal capacity (Figure 3.9C).

Following 14 days of differentiation, the resting O_2 consumption rate of HSR-GBM1 cells was not significantly different to that of the undifferentiated cells (Figure 3.9A). In addition, ETC coupling was also unchanged (Figure 3.9B), however, ETC reserve capacity was increased by a small but non-significant amount and indicates that a limited amount of ETC capacity was now present (Figure 3.9C). In contrast, hNSCs differentiated for 14 days showed a significant 2.43-fold ($p<0.001$) increase in resting O_2 consumption rate compared to undifferentiated cells (Figure 3.9A). The ETC reserve capacity was also significantly increased ($p<0.001$), to a value of 1.91, indicating that the resting respiration rate was not at maximal capacity (Figure 3.9C). Furthermore, ETC coupling increased in differentiated hNSCs compared to their undifferentiated counterparts ($p<0.05$; Figure 3.9B).

In the undifferentiated state, HSR-GBM1 cells dedicated significantly more O_2 consumption towards the generation of ATP ($p<0.001$; Figure 3.9D), calculated by subtracting the Oligomycin induced O_2 consumption from that of the resting O_2 consumption rates. However, following differentiation, HSR-GBM1 cells did increase the amount of O_2 consumption devoted to ATP generation. In contrast, differentiated hNSCs increased their ATP devoted O_2 consumption by 2.95 fold ($p<0.001$; Figure 3.9D) and were comparable to both undifferentiated and differentiated HSR-GBM1 cells. Interestingly, in the undifferentiated state, both hNSC and HSR-GBM1 cells showed comparable and high % utilization of the ETC for the generation of ATP (Basal – Non-Phos / ETC Reserve x 100) (~50%; Figure 3.9E). Furthermore, the differentiated hNSCs showed a reduction in % utilization of the ETC for ATP generation (~34% $p<0.05$; Figure

3.9E). Even though differentiated hNSCs devoted less ETC capacity to ATP generation, their maximal respiratory capacity was increased by 4.30-fold ($p<0.001$; Figure 3.9F), which overall yielded more ATP dedicated O_2 consumption. Similar to hNSCs, HSR-GBM1 cells also reduced their % utilization of the ETC for the production of ATP. However, HSR-GBM1 cells did not match the increase in maximal respiratory capacity that was observed in hNSCs following differentiation (Figure 3.9F).

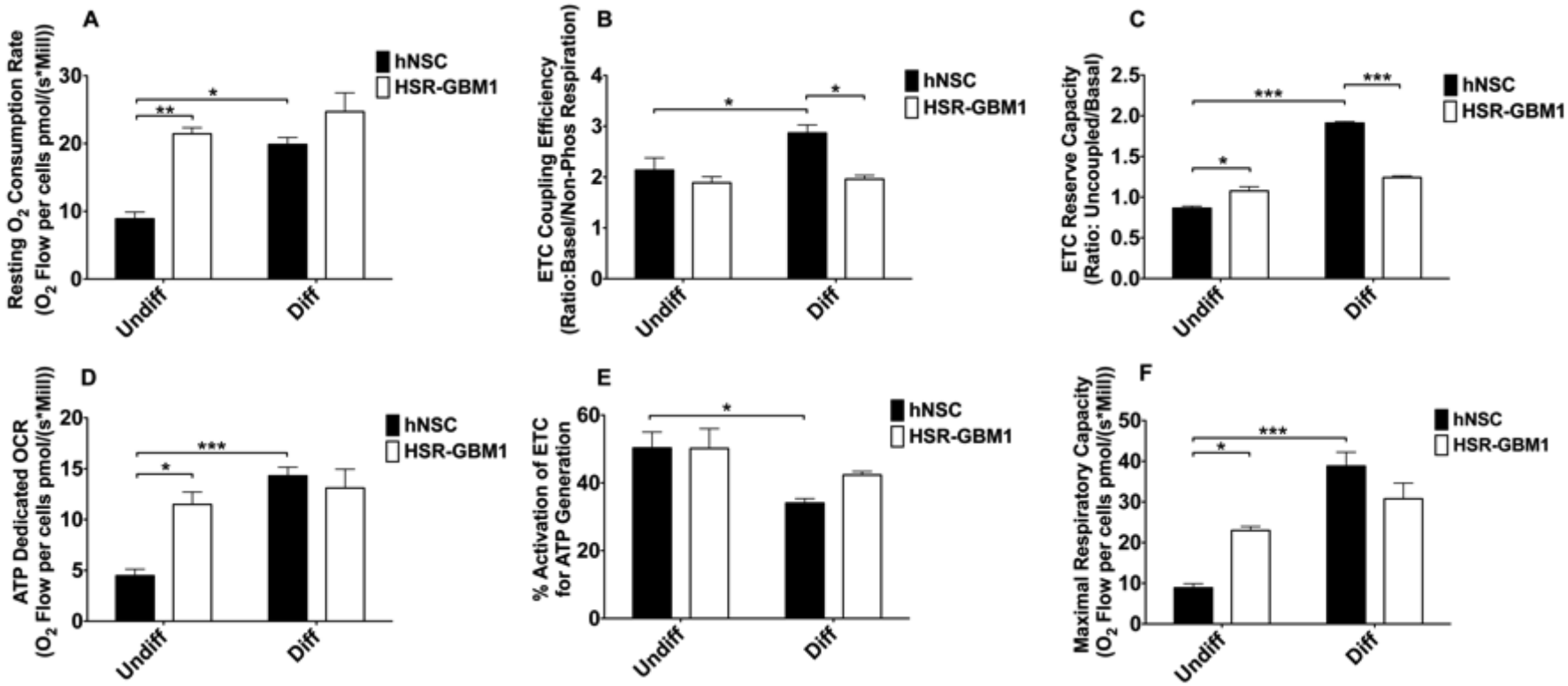

Figure 3.9. Analysis of cellular O_2 consumption of hNSCs and HSR-GBM1 cells. Resting O_2 consumption rates (A), ETC coupling efficiency (B), ETC reserve capacity (C), ATP dedicated O_2 consumption (D), percentage activation of the ETC for ATP production (E) and maximal respiratory capacity (F) of undifferentiated and differentiated hNSCs and HSR-GBM1 cells (n=3). Columns represent mean values. * Indicates $p<0.05$, ** $p<0.01$ and *** $p<0.001$.

3.6.5 Total ATP content and lactate production

To further characterise the metabolic profile of undifferentiated and differentiated HSR-GBM1 cells and hNSCs, I determined the cellular ATP content in each of these cell populations. Undifferentiated HSR-GBM1 cells contained significantly higher total ATP content than undifferentiated hNSCs (1.40-fold; $p<0.001$; Figure 3.10A). HSR-GBM1 cells differentiated for 14 days increased their total ATP content by 1.62-fold ($p<0.001$; Figure 3.10A) compared to their undifferentiated counterparts. However, differentiated hNSCs showed a more profound increase of 4.40-fold ($p<0.001$; Figure 3.10A) in total ATP content compared to undifferentiated hNSCs. Furthermore, differentiated hNSCs showed 2-fold ($p<0.001$) greater total ATP content than differentiated HSR-GBM1 cells (Figure 3.10A).

Lactate production was also measured as an index of glycolytic metabolism. Undifferentiated HSR-GBM1 cells secreted 3.29-fold more lactate than undifferentiated hNSCs ($p<0.001$; Figure 3.10B). After 14 days of differentiation, HSR-GBM1 cells exhibited a reduction in glycolytic metabolism, with lactate production decreasing by 11.52-fold ($p<0.001$). Similarly, hNSCs also showed a reduction in lactate production ($p>0.05$) following differentiation (Figure 3.10B), although this was not statistically significant.

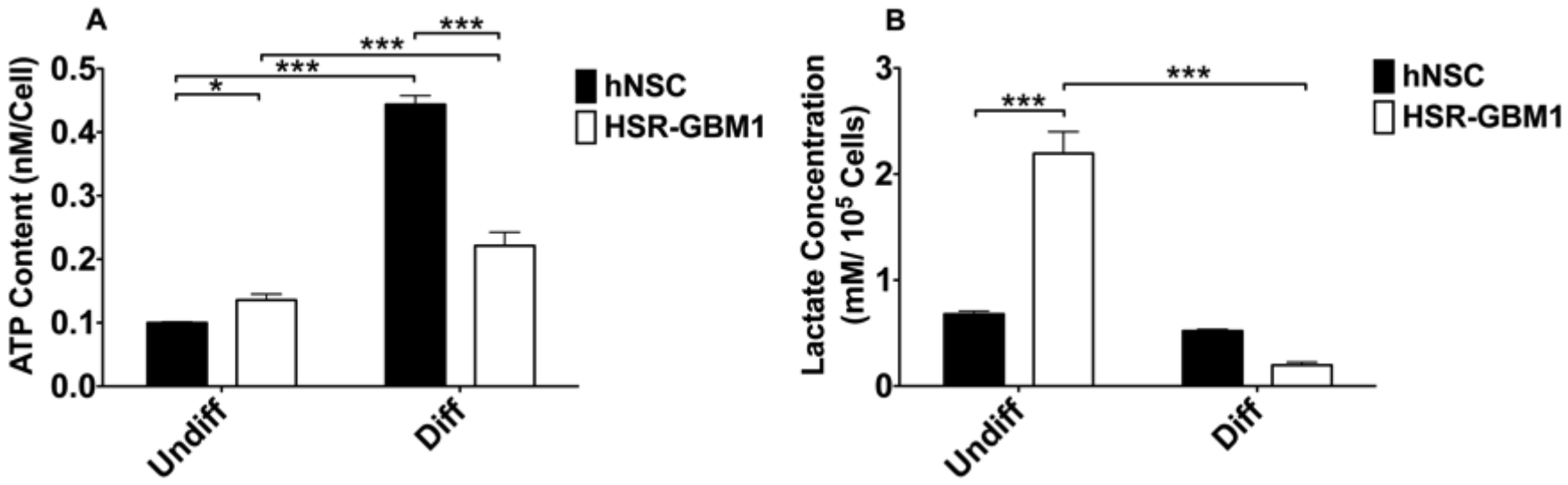

Figure 3.10. Analysis of total ATP content and lactate production of hNSCs and HSR-GBM1 cells. Quantification of total cellular ATP content (A) and lactate production (B) in undifferentiated and differentiated hNSCs and HSR-GBM1 cells. Columns represent mean values ± SEM (n=3). * Indicates $p<0.05$ and *** $p<0.001$.

3.7 Discussion

3.7.1 MtDNA copy number regulation in hNSC and GBM CSCs

NSCs and GBM CSCs share multiple similarities that include self-renewal, multipotency and gene expression profiles (Galli et al., 2004; Ma et al., 2008; Singh et al., 2003). These similarities provided an ideal basis for exploring other areas of cell biology associated with these cell types, such as how differentiation impacts upon mtDNA regulation and energy metabolism. High glycolytic rates are associated with stem cells and tumor cells (Levine and Puzio-Kuter, 2010; Moreno-Sanchez et al., 2007; Vander Heiden et al., 2009), whilst high OXPHOS capacity is associated with differentiated and specialized cell types (Prigione et al., 2010; Varum et al., 2011). It remains to be determined whether multipotent GBM CSCs are capable of undergoing a glycolysis to OXPHOS transition that has been shown to occur in normal multipotent stem cells. Direct comparison of hNSCs and GBM CSCs provided an ideal opportunity to explore the cellular and molecular modifications that occur during differentiation, and identify disparities between normal and transformed cell types that may enhance our understanding of cell biology and potentially aid in the development of novel therapeutic strategies.

In order to address the questions outlined above, hNSCs and three GBM CSC lines (HSR-GBM1, GBM-L1 and GBM-L2) were differentiated for up to 28 days. Throughout differentiation, mtDNA copy number and the expression of neural stem cell and lineage specific markers were evaluated. hNSCs and HSR-GBM1

cells and the energy metabolism profiles of these cells in undifferentiated and differentiated states were assessed.

Differentiating hNSCs showed a gradual increase in mtDNA copy number over a differentiation period of 28 days. In addition, the expansion in mtDNA copy number correlated with continual increases in expression of the astrocyte marker, GFAP. In contrast, HSR-GBM1, GBM-L1 and GBM-L2 cells failed to mimic these outcomes during differentiation and exhibited an asynchronous relationship between mtDNA copy number and *GFAP* expression. HSR-GBM1 cells and GBM-L2 cells failed to match the expansion in mtDNA copy number observed in hNSCs. Furthermore, the expression of *GFAP* peaked early at Day 7 of differentiation and was followed by a gradual decline in expression. GBM-L1 cells showed considerable increases in *GFAP* expression during differentiation but did not show pronounced increases in mtDNA copy number.

These data demonstrate that hNSCs possess a synergistic relationship between the nuclear and mitochondrial genomes that modulates increases in mtDNA copy number and lineage specific gene expression appropriately. Furthermore, these outcomes are in agreement with previous studies using murine stem cell models In the undifferentiated state, ESCs contain few copies of mtDNA (Facucho-Oliveira et al., 2007; Prigione et al., 2010). As differentiation proceeds, there is an acquisition of mtDNA copy number that will reflect the future energy requirements of a specific cell type (Facucho-Oliveira et al., 2007; Prigione et al., 2010). The acquisition of mtDNA copy number is essential to ensure that sufficient quantities of ATP are generated through

OXPHOS to meet the energetic demands of a specialized cell type. In contrast, GBM CSCs show a lack of synchrony between their nuclear and mitochondrial genomes in that an increase in the gene expression of differentiation markers does not occur concurrently with an expansion in mtDNA copy number.

3.7.2 Metabolic profiling of hNSC and HSR-GBM1 cells

In vitro, stem cells exhibit similar metabolic profiles to tumor cells and this is best characterized by a high glycolytic rate. However, it remains to be determined whether multipotent CSCs, such as HSR-GBM1 cells, are capable of mimicking the metabolic shift from glycolysis to OXPHOS that occurs during the differentiation of normal stem cell populations (Cho et al., 2006; Facucho-Oliveira et al., 2007; Prigione et al., 2010; St John et al., 2005; Varum et al., 2011). To address this issue the O_2 consumption, ATP content and lactate production of undifferentiated and differentiated HSR-GBM1 cells and hNSCs were analyzed.

hNSCs and HSR-GBM1 exhibited functional differences in their undifferentiated states. Undifferentiated hNSCs consumed O_2 at lower rate and secreted less lactate than undifferentiated HSR-GBM1 cells. The high levels of lactate production in HSR-GBM1 cells provides evidence that glycolytic activity was high in this cell type. Interestingly, in both cell types, the calculated percentage of ETC utilization of ATP generation was high (~50%). However, the low ATP content in both undifferentiated hNSCs and HSR-GBM1 cells suggests that, although OXPHOS is active, the capacity of this pathway is low in the undifferentiated state.

During differentiation, hNSCs showed considerable increases in both resting and ATP dedicated O_2 consumption, ETC coupling and maximal respiratory capacity that were likely supported by the observed expansion in mtDNA copy number. Furthermore, hNSCs showed profound increases in ATP content during differentiation and a small reduction in lactate production. Collectively, these data indicate that in hNSCs, the expansion of mtDNA copy number correlates with a concurrent increase in OXPHOS capacity and utilization that permits the generation of higher yields of ATP, which are essential for differentiated cell types. In contrast, HSR-GBM1 cells did not increase their resting and ATP dedicated O_2 consumption rates and showed only a small increase in maximal respiratory capacity. It is likely that HSR-GBM1 cells are unable to expand their OXPHOS capacity to a similar extent as hNSCs due to a failed expansion in mtDNA copy number in response to differentiation stimuli. However, HSR-GBM1 cells were able to increase their ATP content and reduce lactate production. These outcomes suggest that HSR-GBM1 may retain a residual potential to utilize OXPHOS during differentiation, however, their OXHPOS capacity is much lower than that of differentiating hNSCs. The stalled expansion in mtDNA copy number in HSR-GBM1 cells likely restricts the availability of the mtDNA-encoded ETC subunits during differentiation and ultimately restricts the ETC capacity of HSR-GBM1 cells and their ability to generate OXPHOS derived ATP.

3.8 Conclusion

In each of the GBM CSC lines analyzed, an expansion in mtDNA copy number did not occur concurrently with an increase in the expression of the lineage specific marker, *GFAP*. These outcomes suggest that an asynchronous relationship between nuclear and mitochondrial genomes exists in the GBM CSC lines examined. I hypothesize that this asynchronous relationship results in incomplete cellular differentiation and is mediated by abnormal nuclear gene expression. Due to this abnormal nuclear expression it is likely that HSR-GBM1 cells are unable to fully establish an increased oxidative capacity that is indicative of differentiated cell types. Despite HSR-GBM1 cells lacking the ability to enhance their OXPHOS capacity, HSR-GBM1 cells were shown to utilize OXPHOS to some degree and it is likely that OXPHOS plays a key role in their normal cellular function. Nevertheless, HSR-GBM1 cells are unable to fully escape an enhanced glycolytic state and display characteristics of the Warburg Effect. In turn this supports rapid cell proliferation, self-renewal and maintains their tumorigenic potential.

Chapter 4: Mitochondrial DNA depletion alters the expression of stem cell associated factors in HSR-GBM1 cells

4.1 Introduction

The maintenance of mtDNA copy number is essential for normal cell function (Wallace, 1999; Wallace, 2005) and there is emerging evidence to support the involvement of altered mtDNA copy number in tumorigenesis, genomic instability and response to chemotherapy (Guo et al., 2011; Singh et al., 2009). Furthermore, mtDNA depletion of tumor cells has provided controversial outcomes; with mtDNA-less tumor cells (ρ0) exhibiting increased and decreased tumorigenicity in conflicting reports (Amuthan et al., 2002; Cavalli et al., 1997; Kulawiec et al., 2009b; Magda et al., 2008).

Although mtDNA encodes only a small proportion of genes compared to the tens of thousands encoded by the nuclear genome, there is evidence to suggest that mtDNA has the power to induce extensive changes in nuclear gene expression. Indeed, ρ0 cell lines showed altered nuclear gene expression and epigenetic modifications (Singh et al., 2005; Smiraglia et al., 2008), which demonstrates that mtDNA status can elicit considerable influence on the nucleus. However, it remains undetermined how changes in mtDNA copy number influence nuclear gene expression and cellular differentiation in GBM cells. To address these issues, HSR-GBM1 cells were depleted of their mtDNA

for up to 50 days using the mtDNA-specific depletion agent, ddC. The gene expression and differentiation potentials of HSR-GBM1 cells were assessed.

4.2 Hypothesis

Depletion of mtDNA from cells allows for the investigation of how mtDNA influences cellular function. I hypothesize that mtDNA depletion induces changes in gene expression in HSR-GBM1 cells by disrupting the synergistic relationship that exists between the nuclear and mitochondrial genomes, which functions to maintain mtDNA copy number and normal cellular function.

4.3 Aims

- To progressively deplete HSR-GBM1 cells of mtDNA using the mtDNA-specific depletion agent, 2'-3'-dideoxycytidine (ddC).
- To determine the effect of mtDNA depletion on gene expression profiles and cell proliferation.
- To investigate whether HSR-GBM1 cells can re-establish their basal mtDNA copy number following varying degrees of mtDNA depletion.
- To determine the effects of mtDNA depletion on HSR-GBM1 differentiation.

4.4 Materials and Methods

4.4.1 MtDNA depletion of HSR-GBM1 cells

HSR-GBM1 cells were cultured, as described in *Culture of GBM cell lines* (Section 2.2.4), except that ddC (10 μM) and uridine (50 mg/ml) were added to the culture media. Culture media was replenished daily through half volume changes of media for up to 50 days. Cell samples were collected at Day 7, 14, 21, 25 and 50 days.

4.4.2 Recovery of mtDNA depleted HSR-GBM1 cells

HSR-GBM1 cells were allowed to recover following mtDNA depletion. After 7, 14, 21, 25 and 50 days of depletion, ddC was removed from the culture media and HSR-GBM1 cells were cultured under routine conditions for an additional 14 days in the presence of uridine. Cell samples were collected after 14 days of culture.

4.4.3 Differentiation of mtDNA depleted HSR-GBM1 cells

HSR-GBM1 cells were depleted for 7, 14 and 21 days and induced to differentiate in astrocyte induction media for 14 days. Differentiation conditions are described in *Differentiation of GBM cell lines* (Section 2.3.2) and media was supplemented with uridine. Cell samples were collected after 14 days.

4.4.4 MtDNA copy number analysis

MtDNA copy number was quantified in non-depleted, mtDNA depleted and recovering HSR-GBM1 cells using real-time PCR, as described in *MtDNA copy number analysis* (Section 2.6.4), using primer pairs specific to mtDNA and β-Globin.

4.4.5 Gene expression analysis

The expression of the NSC and lineage specific markers *NESTIN*, *MUSASHI1, CD133 and GFAP* were analyzed in mtDNA depleted and recovering HSR-GBM1 cells, as described in *Gene expression analysis* (Section 2.6.3). In addition, the pluripotency markers, *OCT4, NANOG* and *SOX2*, the proto-oncogene, *c-MYC*, and the catalytic subunit of telomerase, *hTERT*, were analyzed by real-time PCR, as described in *Gene expression analysis* (Section 2.6.3). *β-ACTIN* was selected as the housekeeping gene. Primer sequences, product lengths and annealing and secondary acquisition temperatures are listed in Table 4.I.

Gene	Forward Primer	Reverse Primer	Product Length (bp)	Annealing Temperature (°C)	Secondary Acquisition Temperature (°C)
c-MYC	ACAACACCCGAGCAAGGACGC	ACGGCTGCACCGAGTCGTAGT	180	59	83
hTERT	CACCAAGAAGTTCATCTCC	CAAGTGCTGTCTGATTCC	310	52	81
NANOG	TTAATAACCTTGGCTGCCGT	GCAGCAAATACGAGACCTCT	298	55	81
OCT4	TCACCCTGGGGGTTCTATTT	CTGGTTCGCTTTCTCTTTCG	202	55	80
SOX2	GGAGCTTTGCAGGAAGTTTG	GCAAGAAGCCTCTCCTTGAA	191	55	76

Table 4.I. Primer sequences, product sizes and annealing temperatures for conventional PCR, RT-PCR and real-time PCR. Secondary acquisition temperatures are also listed for real-time PCR reactions.

4.4.6 Growth kinetics

At the time of passage, cell counts were performed and population doubling times were calculated with the following equation:

$$1/((Log(N_1)-Log(N_0))*3.32/t)$$

Where *Log* is the logarithm of a fixed value, N_1 is the cell count at time of passage, N_0 is the cell number at time of plating and *t* is the culture duration in hours.

4.4.7 SABiosciences Real-Time PCR Array (RT^2 Profiler): Neurogenesis and neural stem cells

The expression of 80 genes associated with neurogenesis and neural stem cells were analysed in non-depleted and HSR-GBM1 cells depleted for 25 and 50 days. Samples were prepared and real-time PCR reactions performed, as described *SABiosciences Real-Time PCR Gene Expression Array* (Section 2.6.5). Relative gene expression was calculated by the $\Delta\Delta$Ct method and normalized against the average Ct values of 5 housekeeping genes (*GUSB, HPRT1, HSP90AB1*, *GAPDH and β-ACTIN*), as described in Section 2.6.5.

4.4.8 Statistical analysis

Statistical analysis was performed, as described in *Statistical analysis*, in the *General Materials and Methods* (Section 2.11).

4.5 Preliminary experiments

4.5.1 Determination of the efficacy of mtDNA depletion by 2'-3'-dideoxycytidine

Since ddC does not inhibit mtDNA gene expression (Piechota et al., 2006) whilst inducing mtDNA depletion and has a clinical history (Dagan et al., 2002), it was reasoned that ddC was an ideal mtDNA depletion agent. The HSR-GBM1 cell line was selected for mtDNA depletion experiments because this cell line is the most characterized GBM CSC and expresses multiple NSC factors. In addition, HSR-GBM1 cells were donated at a relatively high passage (p60+) but sustained their NSC factor expression and CSC properties (See Chapter 3) despite their relatively high passage number. It is therefore likely that any observed changes in HSR-GBM1 cell properties during ddC exposure are likely induced by mtDNA depletion rather than total time in culture.

ddC has previously induced mtDNA depletion *in vitro* at a concentration of 10 μM (Iyer et al., 2012). To confirm that this concentration was sufficient to induce mtDNA depletion in the HSR-GBM1 cells, a preliminary experiment was performed to determine the effect of 10 μM ddC on undifferentiated HSR-GBM1 cells. HSR-GBM1 cells were routinely cultured as neurospheres, as described in *Culture of GBM cell lines* (Section 2.2.4), with the exception that ddC was added daily into the culture medium through half volume changes of media (see *MtDNA depletion of HSR-GBM1 cells;* Section 2.3.3). HSR-GBM1 cells were cultured in the presence of ddC for up to 20 days and mtDNA copy number was quantified by real-time PCR, as described in *MtDNA copy number analysis* (Section 2.6.4), at Day 6, 9, 13, 15 and 20 of culture. In addition, after 6 days of

culture, ddC was withdrawn from the media to determine the effect of withdrawal on mtDNA copy number.

The addition of ddC led to a considerable and progressive decrease in mtDNA copy number over the 20-day culture period (Figure 4.1). MtDNA copy number was reduced by 4.5 fold by Day 6 and by 94-fold by Day 20 (Figure 4.1). In addition, withdrawal of ddC from the culture media at Day 6 allowed recovery of mtDNA copy number following an additional 7 days of routine culture, demonstrating that ddC induced mtDNA depletion is reversible (Figure 4.1). These data demonstrate that 10 μM ddC is sufficient to induce mtDNA depletion in HSR-GBM1 cells and is suitable for future depletion experiments. However, as mtDNA remained detectable in HSR-GBM1 cells depleted for 20 days, it was reasoned that an extended period of ddC culture beyond 20 days was required in order to induce near complete mtDNA depletion of HSR-GBM1 cells.

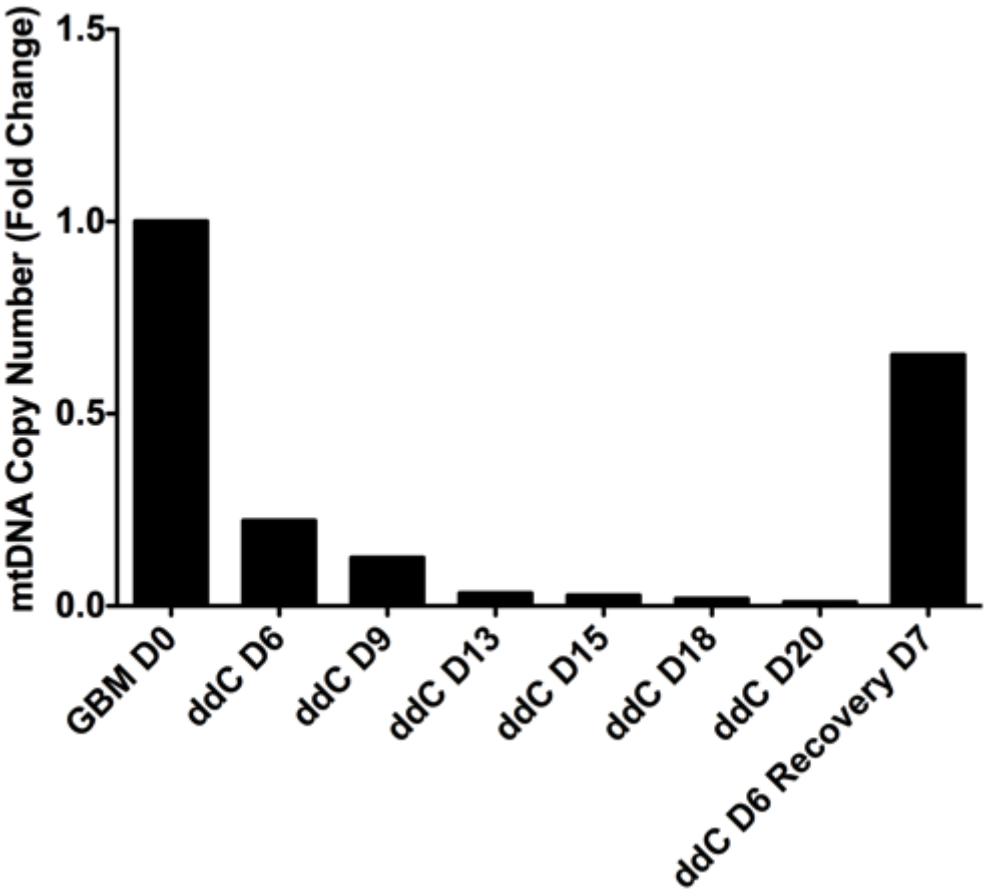

Figure 4.1. Assessment of the effect of 10 μM ddC on HSR-GBM1 cell mtDNA copy number. Fold change in copy number relative to Day 0 of HSR-GBM1 cells during 20 days of mtDNA depletion. Columns represent mean values.

4.6 Results

4.6.1 MtDNA Depletion

HSR-GBM1 cells were depleted of their mtDNA using the mtDNA specific depletion agent, ddC, for up to 50 days and mtDNA copy number was analysed at Day 7, 14, 21, 25 and 50 of depletion. HSR-GBM1 cells exhibited significant mtDNA depletion following the addition of ddC, with 9.80, 43.47, 454.54, 769.23 and 1886.79-fold reductions in copy number on Day 7, 14, 21, 25 and 50, respectively ($p<0.001$). By Day 50, the mean mtDNA copy number was < 1 (Figure 4.2).

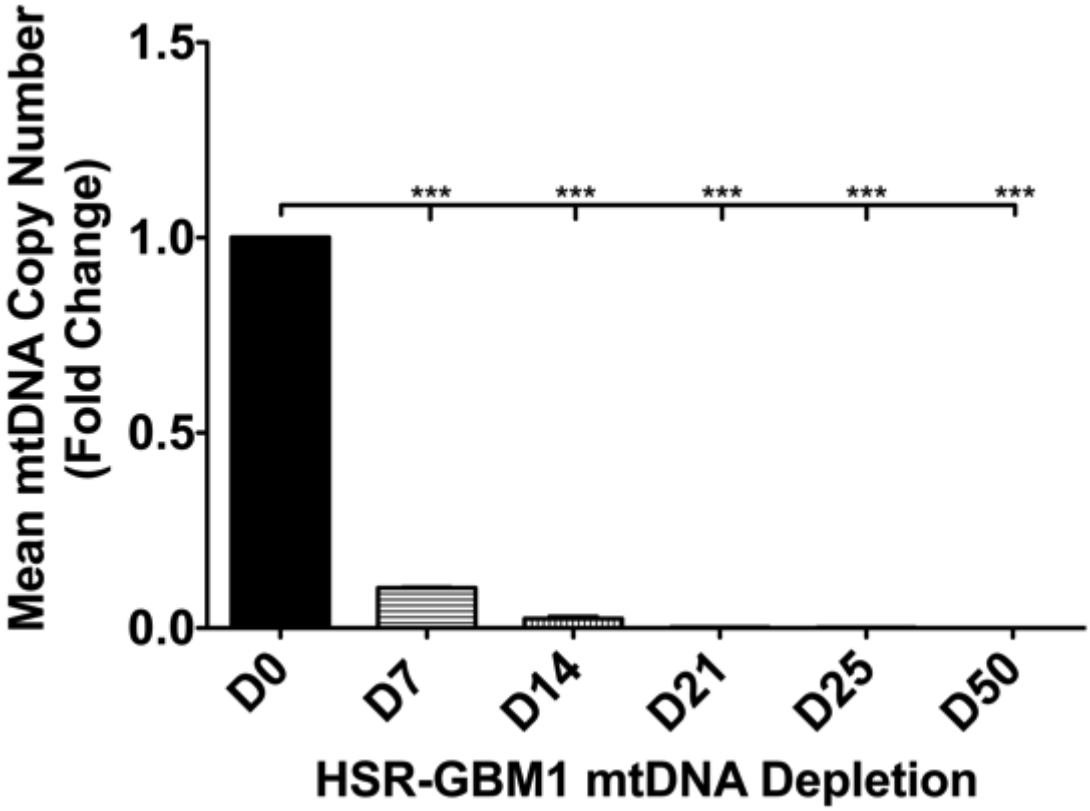

Figure 4.2. MtDNA depletion of HSR-GBM1 cells. Fold change in mtDNA copy number relative to Day 0 of HSR-GBM1 cells during 50-day mtDNA depletion. Columns represent mean values ± SEM (n=3). *** Indicates $p<0.001$.

4.6.2 Gene expression analysis

In order to determine whether mtDNA depletion led to changes in expression of the neural stem cell markers, the expression of *NESTIN*, *MUSASHI1* and *CD133* were analysed. There were differential patterns of *NESTIN* (Figure 4.3A) and *MUSASHI1* (Figure 4.3B) expression after 7 and 14 days of depletion. However, the expression of both genes was upregulated at Day 21 of depletion and down regulated by Days 25 and 50. *CD133* expression was significantly reduced after 7 ($p<0.001$; Figure 4.3C) and 14 ($p<0.001$) days of depletion, but returned to basal levels by Day 21 of depletion. The expression of *CD133* was reduced on Day 25 of depletion and was undetectable by Day 50 ($p<0.001$).

To investigate whether mtDNA depletion initiates the expression of markers of differentiation, the astrocyte marker, *GFAP*, was analysed. There were no significant changes in *GFAP* expression during the first 14 days of mtDNA depletion. However, from Day 21 of depletion onwards, the expression of *GFAP* progressively decreased (Figure 4.3D).

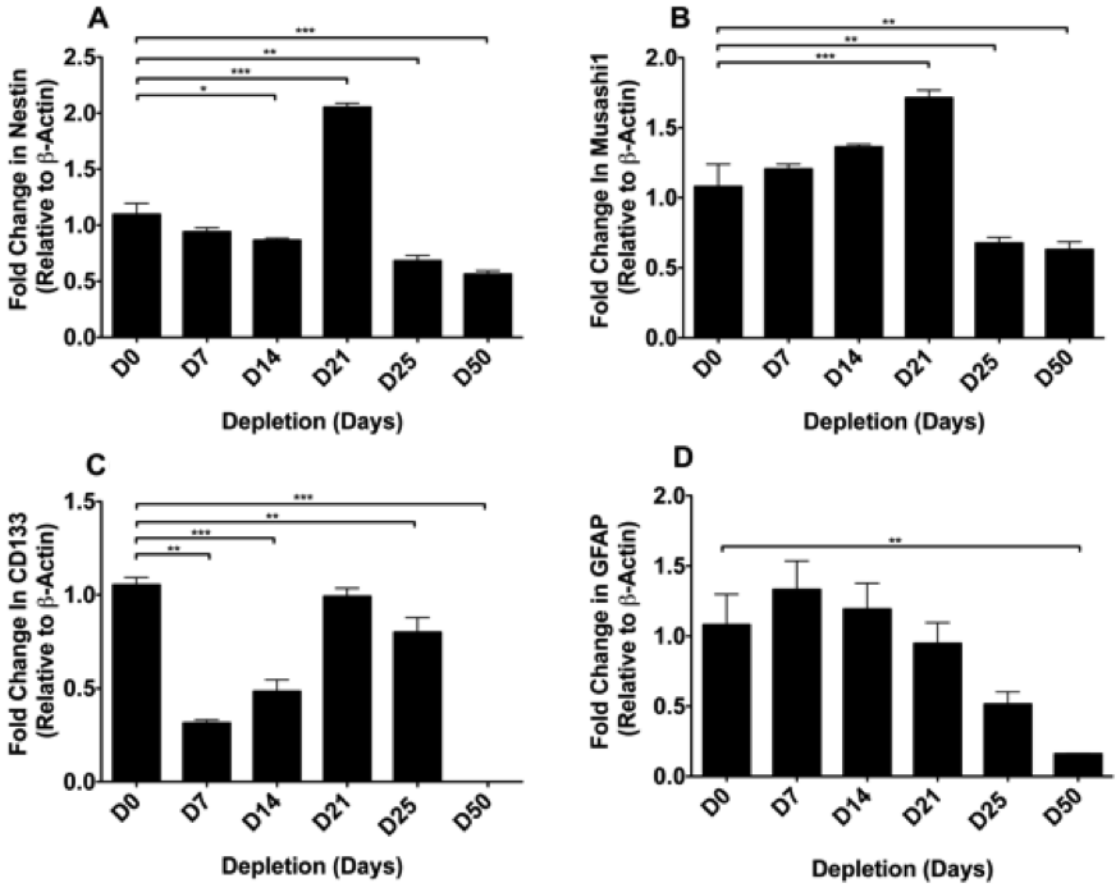

Figure 4.3 Gene expression analysis of NSC and lineage specific markers during mtDNA depletion of HSR-GBM1 cells. Fold change in expression relative to Day 0 and weighted against *β-ACTIN* of *NESTIN* (A), *MUSASHI1* (B), *CD133* (C) and *GFAP* (D) during mtDNA depletion for 50 days. Columns represent mean values ± SEM (n=3). * Indicates $p<0.05$, ** $p<0.01$ and *** $p<0.001$.

4.6.3 Neural stem cell and neurogenesis PCR array

Since there were significant decreases in the expression of the multipotent markers during mtDNA depletion, the expression profiles of non-depleted and HSR-GBM1 cells depleted for 25 and 50 days were analysed using a real-time PCR array that examined 80 genes associated with neural stem cells and neurogenesis.

Day 25 and Day 50 depleted HSR-GBM1 cells showed significant and differential expression of 26 of the 80 genes analysed with the PCR array relative to non-depleted HSR-GBM1 cells. The expression data are summarised in Table 4.II. Multiple genes were upregulated in both depleted groups that are associated with growth factor signalling, anti-apoptosis and cell proliferation (Table 4.II). Factors upregulated included fibroblast growth factor 13 (*FGF13*), glia cell line-derived neurotrohpic factor (*GDNF*), vascular endothelial growth factor A (*VEGFA*) and semaphorin-4D (*SEMA4D*) and collectively these factors are associated with anti-apoptosis, cell adhesion and proliferation (Greene et al., 1998; Leung et al., 1989; Lin et al., 1993; Zhou et al., 2012)

Sonic hedgehog (*SHH*) (Day 50 depletion only), acetylcholinesterase (*ACHE*), anaplastic lymphoma kinase (*ALK*), dopamine receptor D2 (*DRD2*), hairy/enhancer-of-split related with YRPW motif protein 1 (*HEY1*) and neuronal pentraxin 1 (*NPTX*) were upregulated in depleted HSR-GBM1 cells relative to non-depleted cells. These factors are associated with neurogenesis, synaptogenesis, cell proliferation and tumorigenesis (Grifman et al., 1998; Hulleman et al., 2009; Leimeister et al., 1999; Odent et al., 1999; Palmer et al.,

2009; Xu et al., 2008; Zhu et al., 2012) In addition, apolipoprotein E (*APOE*), achaete-scute homolog 1 (*ASCL1*), delta-like 1 (*DLL1*), which are associated with cell fate decisions and differentiation(Ball et al., 1993; Beckers et al., 1999) were significantly down-regulated in depleted HSR-GBM1 cells. Collectively, the PCR array data demonstrates that mtDNA depletion of HSR-GBM1 cells leads to broad changes in gene expression profiles.

Genes	Day 25 Depletion	Day 50 Depletion	Gene Function
ACHE	4.877	2.9752	Cell Proliferation, Cell Adhesion, Synaptogenesis
ALK	1.8307	2.2425	Negative regulator of proliferation
APOE	-1.3745	-3.1814	Synaptogenesis
ASCL1	-1.4529	-4.8572	Regulator of differentiation and transcription
CDK5RAP3	1.6607	2.0013	Cell proliferation, Neuronal differentiation
DLG4	3.0939	1.5442	Synaptogenesis
DLL1	-1.7325	-3.2369	Cell fate, Cell adhesion, Notch signalling pathway
DRD2	8.7294	3.448	Synaptogenesis
EFNB1	1.0598	-2.1937	Cell Adhesion
ERBB	3.0099	1.9495	Cell Adhesion
FGF13	2.6468	2.9754	Growth Factor
GDNF	4.9007	4.3017	Growth Factor, Anti-apoptosis
HEY1	4.1459	5.0557	Transcription Factor, Embryogenesis
HEY2	1.0118	-2.2584	Transcription Factor
NPTX	7.3376	3.7001	Synaptogenesis
NRCAM	2.4282	2.6759	Cell adhesion, Cell differentiation
NRP1	2.0396	1.2941	Cell Adhesion
NRP2	3.1056	1.569	Cell Adhesion
NTN1	2.0472	1.392	Anti-apoptosis
PARD6B	2.1265	1.4166	Cell cycle
S100A6	-1.314	2.5712	Cell proliferation, Cell Cycle, Cell differentiation
SEMA4D	5.1751	5.0328	Cell adhesion, Anti-apoptosis
SOX8	-1.2876	-2.3618	Development, Apoptosis, Oligodendrocyte differentiation
SHH	Not Detectable	3.8904	Development, Neurogenesis, Differentiation
TNR	2.0176	1.6121	Cell Adhesion

Table 4.II. Summary of gene expression analysis from the Neurogenesis and Neural Stem Cell PCR Array. Fold changes in gene expression of undifferentiated HSR-GBM1 cells and undifferentiated HSR-GBM1 cells depleted for 25 and 50 days relative to non-depleted HSR-GBM1 cells. Statistically significant ($p<0.05$) increases in expression are shown in red and decreases in expression in blue.

4.6.4 Expression of pluripotent markers

Since the Neurogenesis PCR array showed increased expression of early developmental markers, such as *SHH*, the expression of the early developmental markers and core pluripotent factors, *OCT4, NANOG* and *SOX2* were analysed. No significant changes in the expression of *NANOG* and *SOX2* were observed until Day 50 of depletion (Figure 4.4B & 4.4C), with significant decreases in expression detected ($p<0.05$). In contrast, *OCT4* expression fluctuated for the first 25 days of depletion, however, by Day 50 of depletion, *OCT4* expression was significantly increased by 3-fold ($p<0.001$; Figure 4.4A).

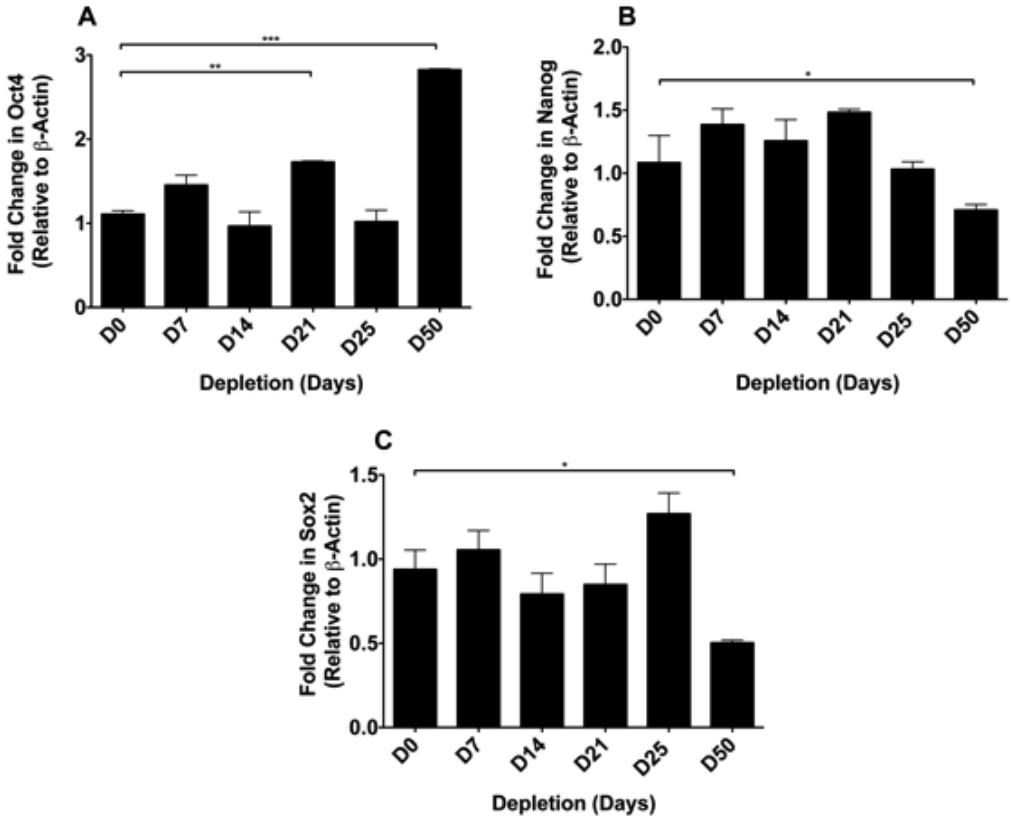

Figure 4.4. Gene expression analysis of pluripotency associated genes during mtDNA depletion of HSR-GBM1 cells. Fold change in expression relative to Day 0 and weighted against *β-ACTIN* of *OCT4* (A), *NANOG* (B),

SOX2 (C) during mtDNA depletion for 50 days. Columns represent mean values ± SEM (n=3). * Indicates $p<0.05$, ** $p<0.01$ and *** $p<0.001$.

4.6.5 HSR-GBM1 growth kinetics and expression of proliferative markers

There are contrasting reports regarding how mtDNA copy number loss influences tumor cell proliferation (Amuthan et al., 2002; Cavalli et al., 1997; Kulawiec et al., 2009b; Magda et al., 2008). In order to determine the role of mtDNA depletion in HSR-GBM1 cell proliferation, growth kinetics and population-doubling times were calculated throughout the first 25 days of mtDNA depletion. HSR-GBM1 cell proliferation was unchanged after 7 days of depletion. However, post 14 days of depletion, HSR-GBM1 cell proliferation decreased (Figure 4.5A) By day 25 of depletion, HSR-GBM1 population doubling times exceeded 450 hours, indicating very little or no proliferation (Figure 4.5A; insufficient material was available for a Day 50 calculation). The reduction in HSR-GBM1 cell proliferation correlated with a reduction in the expression of cell proliferation markers and self-renewal, *c-MYC* and *hTERT*, respectively. An initial surge in expression of both genes at Day 7 (Figure 4.5B; $p<0.001$ & 4.5C; $p<0.01$) was observed, yet by Day 50 gene expression was significantly reduced (*c-MYC* <0.01; *hTERT* $p<0.001$).

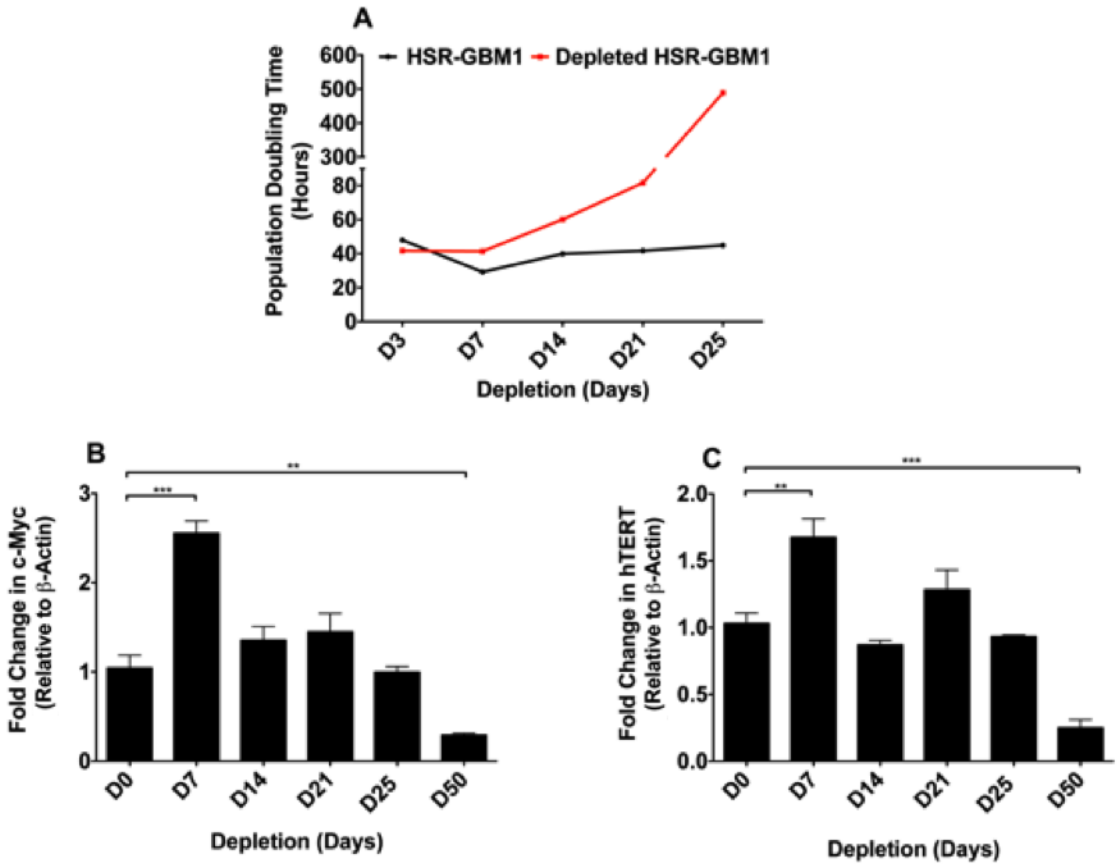

Figure 4.5. Growth kinetics and expression of cell proliferation markers. Population doubling times of non-depleted and mtDNA depleted HSR-GBM1 cells (A) and fold change in expression relative to Day 0 and weighted against *β-ACTIN* of *c-MYC* (B) and *hTERT* (C) of non-depleted and mtDNA depleted HSR-GBM1 cells. Columns represent mean values ± SEM (n=3). ** Indicates $p<0.01$ and *** $p<0.001$.

4.6.6 MtDNA copy number recovery in depleted HSR-GBM1 cells

HSR-GBM1 cells had previously exhibited only minor changes in mtDNA copy number following the induction of differentiation. To explore whether HSR-GBM1 cells could re-establish basal levels of mtDNA copy number (Day 0), HSR-GBM1 cells were depleted for 7, 14, 21, 25 and 50 days and were subsequently grown under routine conditions, without ddC, i.e. a recovery period, for 14 days as neurospheres (Figure 4.6). The mtDNA depletion for 7 days had no effect on

the ability of HSR-GBM1 cells to recover their mtDNA content and reached a mtDNA copy number 1.12-fold higher than that observed in non-depleted cells ($p<0.05$; Figure 4.6). Depletion for 14 days led to a partial recovery of mtDNA content in HSR-GBM1 cells, however, mean mtDNA copy number was 1.40-fold lower than that of non-depleted cells. MtDNA depletion in excess of 21 days resulted in mtDNA copy number recovery being compromised, with mtDNA copy number 6.60-fold ($p<0.001$) and 23.30-fold ($p<0.001$) lower in HSR-GBM1 cells depleted for 21 and 25 days, respectively, after 14 days recovery (Figure 4.6). HSR-GBM1 cells depleted for 50 days failed to replenish their mtDNA content and exhibited a mean copy number of <1 following 14 days of recovery ($p<0.001$). These data indicate that mtDNA depletion is a reversible process, providing that mtDNA copy number is not depleted beyond ~95% of basal levels. Depletion beyond this threshold appears to compromise the replenishment of mtDNA copy number in HSR-GBM1 cells.

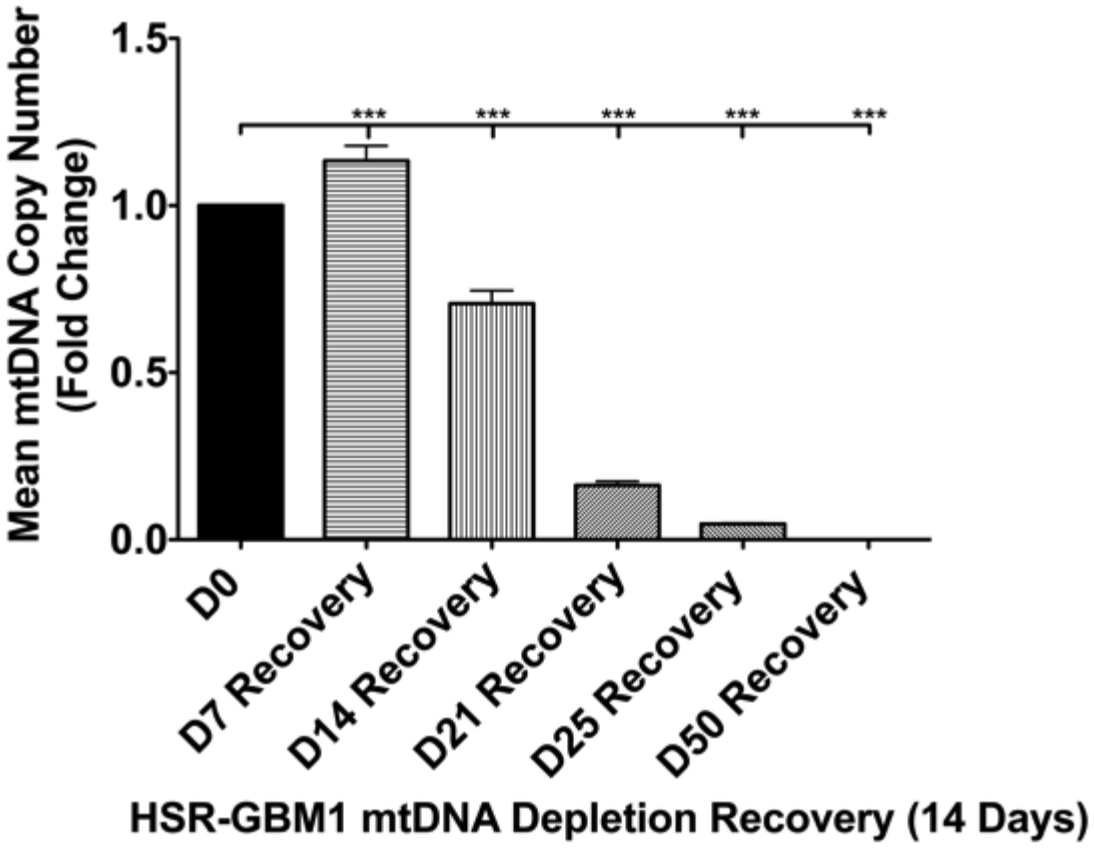

Figure 4.6. MtDNA copy number recovery of depleted HSR-GBM1 cells. Fold change in mtDNA copy number relative to Day 0 of HSR-GBM1 recovering from 7, 14, 21, 25 and 50 days of mtDNA depletion. Columns represent mean values ± SEM (n=3). ** Indicates $p<0.05$ and *** $p<0.001$.

4.6.7 Gene expression of recovering HSR-GBM1 cells

Long-term mtDNA depletion of HSR-GBM1 cells leads to reduced expression of the neural stem cell markers, *NESTIN, MUSASHI1, CD133* and the astrocyte marker, *GFAP*. To investigate whether mtDNA recovery also led to the reestablishment of gene expression patterns that were observed in non-depleted cells, expression was analyzed following the recovery from 7, 14, 21 and 25 days of mtDNA depletion (insufficient material was available for the analysis of Day 50 depleted cells). The expression of *NESTIN* was unchanged in recovering

HSR-GBM1 cells that were depleted for 7, 14 and 21 days, however expression was significantly lower ($p<0.05$; Figure 4.7A) in cells recovering after 25 days of depletion. *MUSASHI1* and *CD133* showed a similar pattern of expression, with an initial increase ($p<0.05$ *MUSASHI1* Figure 7B; $p<0.01$ *CD133* Figure 4.7C) in recovering HSR-GBM1 cells that were depleted for 7 days. This was followed by a progressive decrease in the expression of both genes that was significantly lower in recovering HSR-GBM1 cells depleted for 25 days ($p<0.001$) than non-depleted cells. In addition, the expression of *GFAP* significantly increased in recovering HSR-GBM1 cells depleted for 7 days ($p<0.001$; Figure 4.7D) and this was followed by significant decreases in expression in recovering HSR-GBM1 cells depleted for 21 ($p<0.01$) and 25 days ($p<0.001$), respectively.

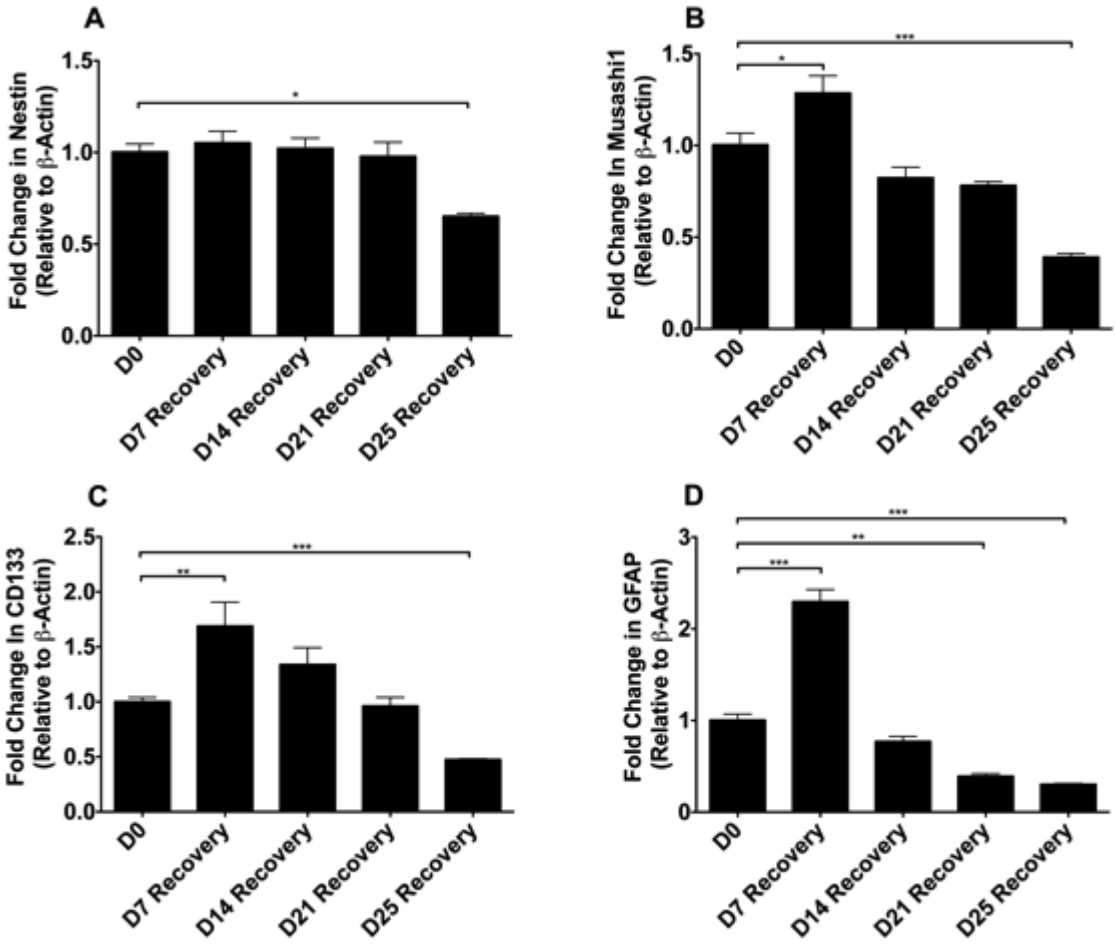

Figure 4.7. Gene expression analysis of NSC and lineage specific markers of recovering mtDNA depleted HSR-GBM1 cells. Fold change in expression relative to Day 0 and weighted against *β-ACTIN* of *NESTIN* (A), *MUSASHI1* (B), *CD133* (C) and *GFAP* (D) of HSR-GBM1 recovering from 7, 14, 21 and 25 days of mtDNA depletion. Columns represent mean values ± SEM. * Indicates $p<0.05$, ** $p<0.01$ and *** $p<0.001$.

4.6.8 MtDNA copy number in depleted and differentiating HSR-GBM1 cells

To test whether varying degrees of mtDNA depletion would promote or hinder cellular differentiation, HSR-GBM1 cells were differentiated using an astrocyte induction medium for 14 days following 7, 14 and 21 days of mtDNA depletion. HSR-GBM1 cells depleted for 7 days replenished their copy number by Day 14

of differentiation and exceeded that of non-depleted cells by 1.46-fold ($p<0.001$; Figure 4.8A). Cells depleted for 14 days replenished their mtDNA copy number and exceeded that of non-depleted cells by 1.32-fold ($p<0.001$; Figure 4.8B). However, mtDNA copy number replenishment in HSR-GBM1 cells depleted for 21 days was limited, with a copy number of >4-fold ($p<0.001$; Figure 4.8C) lower by Day 14 of differentiation than compared to non-depleted cells.

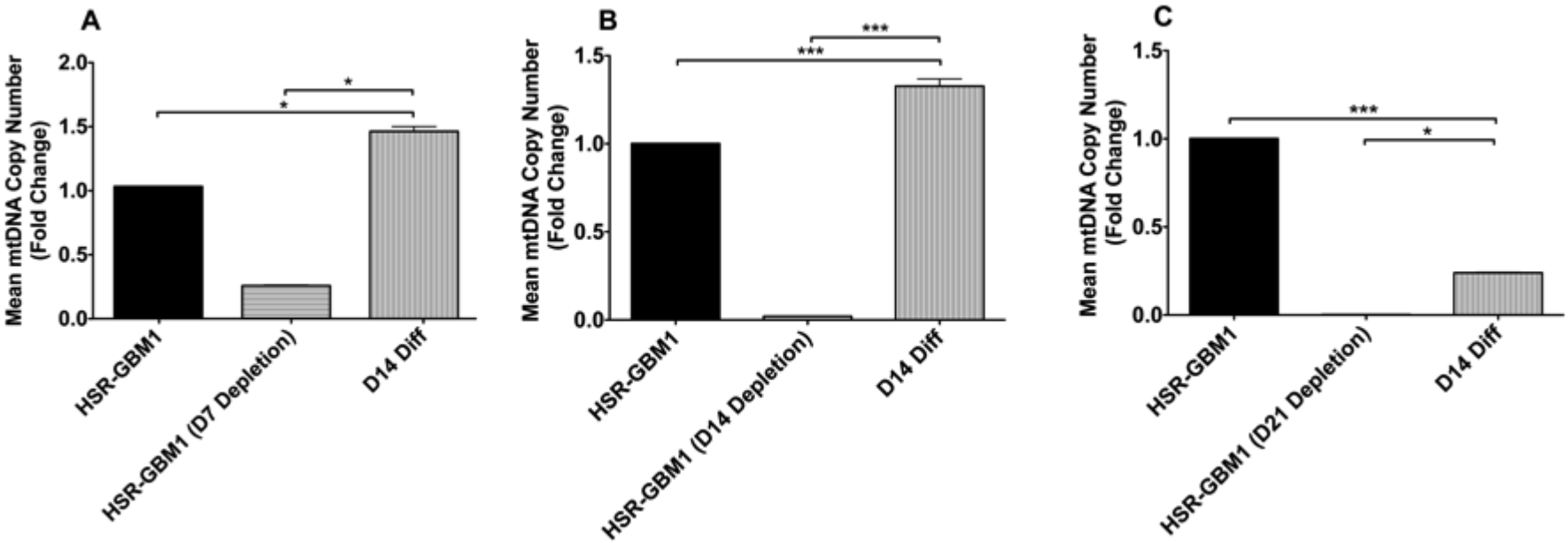

Figure 4.8. MtDNA copy number of differentiating mtDNA depleted HSR-GBM1 cells. Fold change in mtDNA copy number relative to Day 0 of HSR-GBM1 cells depleted for 7 days (A), 14 days (B) and 21 days (C) and differentiated for 14 days. Columns represent mean values ± SEM. *** Indicates $p<0.001$.

4.6.9 Gene expression of analysis of mtDNA depleted and differentiating HSR-GBM1 cells

Since Day 21 depleted HSR-GBM1 cells showed restricted mtDNA copy number recovery during differentiation, the expression of the NSC and lineage specific markers in differentiating HSR-GBM1 depleted for 7, 14 and 21 days were assessed.

After 7 days of depletion and 14 days of differentiation, the expression of *NESTIN* (Figure 4.9A) and *CD133* (Figure 4.9C) were unchanged compared to 7 day depleted HSR-GBM1 cells. *MUSASHI1* expression was elevated ($p<0.05$; Figure 4.9B) following differentiation and *GFAP* expression was also significantly increased ($p<0.001$; Figure 4.9D). The differentiation of HSR-GBM1 cells following mtDNA depletion for 14 days resulted in significant reductions in *NESTIN* ($p<0.001$; Figure 4.9E) and *CD133* ($p<0.001$; Figure 4.9G), whilst *MUSASHI1* expression was unchanged (Figure 4.9F). The expression of the astrocyte marker, *GFAP*, was significantly increased following differentiation ($p<0.001$; Figure 4.9H). HSR-GBM1 cells depleted for 21 days showed significant reductions in *NESTIN, MUASASHI1 and CD133* ($p<0.001$; Figures 4.9J-L) following differentiation. However, following mtDNA copy number reduction of >99% at the initiation of differentiation, HSR-GBM1 cells showed a significant increase in *GFAP* expression (11.79-fold; $p<0.001$; Figure 4.9M) following differentiation. Furthermore, the induction of *GFAP* expression was significantly higher than that observed for HSR-GBM1 cells depleted for 7 and 14 days.

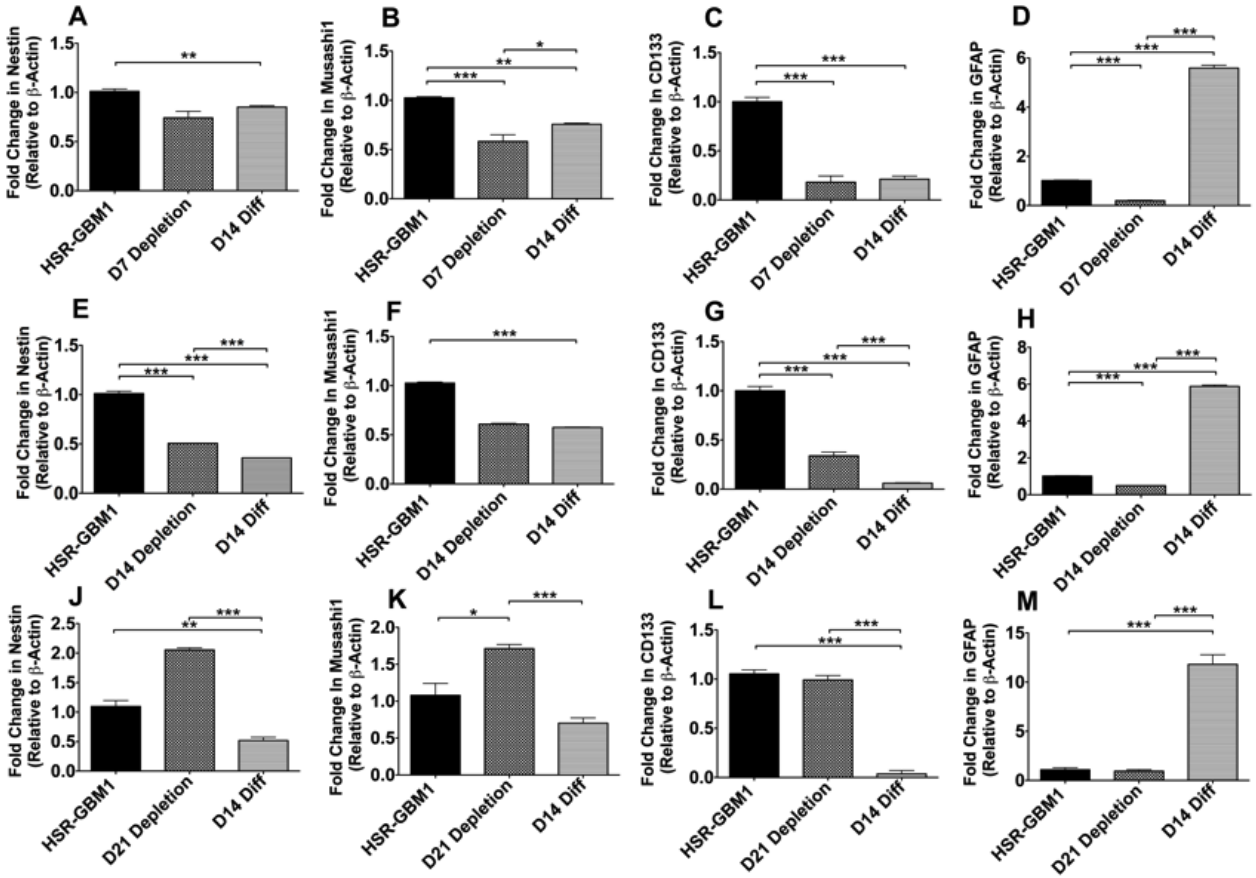

Figure 4.9. Gene expression analysis of NSC and lineage specific markers in differentiating mtDNA depleted HSR-GBM1 cells. HSR-GBM1 cells were depleted for 7 days (A-D), 14 days (E-H) and 21 days (J-M) and differentiated for 14 days. Fold change in expression relative to Day 0 and weighted against *β-ACTIN* of *NESTIN* (A, E, J), *MUSASHI1* (B, F, K), *CD133* (C, G, L) and *GFAP* (D, H, M). Columns represent mean values ± SEM. * Indicates $p<0.05$, ** $p<0.01$ and *** $p<0.001$.

4.7 Discussion

4.7.1 MtDNA depletion of HSR-GBM1 cells

Tumorigenesis is often characterized by the reestablishment of proto-oncogene activity and loss of function of tumor suppressors (Gordan et al., 2007; Matoba et al., 2006; Reya et al., 2001). However, tumor cells also exhibit abnormalities within their mitochondria (Bardella et al., 2011; Parsons et al., 2008; Pollard et al., 2007) and mitochondrial genome (Brandon et al., 2006). Loss of mtDNA integrity though mutation or deletion can have severe effects on cellular function (Brandon et al., 2006; Wallace, 2005). Furthermore, each cell type acquires a specific mtDNA copy number to ensure that appropriate quantities of ATP are available for cell specific functions and, therefore, alterations to mtDNA copy number can also have detrimental effects (Wallace, 1999; Wallace, 2005).

MtDNA copy number in tumors is highly variable, with reports of increased and decreased copy number across a broad range of tumor types (see Table 1.II; *General Introduction*). Identified mechanisms that underlie mtDNA copy number changes in tumors include accumulation of mtDNA mutations (Lee et al., 2004) and loss of function of mtDNA transcription and replication factors (Guo et al., 2011; Singh et al., 2009). Furthermore, mtDNA copy number changes appear to consistently occur in a tumor specific manner. Recent findings have demonstrated the importance of mtDNA copy number maintenance, with ρ0 cells exhibiting extensive changes in gene expression and epigenetic status (Singh et al., 2005; Smiraglia et al., 2008).

In order to address how alterations in mtDNA copy number influence GBM cells, HSR-GBM1 cells were progressively depleted of mtDNA and gene expression was analyzed. Furthermore, the ability of HSR-GBM1 cells to recover mtDNA copy number following depletion was also assessed. HSR-GBM1 cells showed rapid mtDNA depletion in the presence of the mtDNA depletion agent, ddC, and by Day 50 contained, on average, <1 copy of mtDNA per cell.

In support of a positive correlation between mtDNA depletion and cell division, mtDNA depletion occurred rapidly for the first 14 days of culture whilst HSR-GBM1 cell proliferation rates were largely unchanged. However, as mtDNA depletion progressed to Day 21 days there was a reduction in cell proliferation rates. Ultimately, 50 days of depletion was required to obtain a mean mtDNA copy number of <1 copy per cell. These observations strongly suggest that to maintain cell proliferation rates, HSR-GBM1 cells require sufficient copies of mtDNA. These contrasts with other tumor cell lines that have been reported to show either unchanged or enhanced proliferation following mtDNA depletion (Cavalli et al., 1997; Magda et al., 2008; Yen et al., 2005).

4.7.2 Gene expression analysis

The early stages of mtDNA depletion did not result in extensive changes in expression of the NSC markers *NESTIN*, *MUSASHI1* and *CD133*. However, Day 50 depleted cells showed significant reductions in *NESTIN* and *MUSASHI1* expression and a complete loss of *CD133* expression. Furthermore, the expression of the key pluripotency marker *OCT4* and multiple factors associated with neurogenesis, anti-apoptosis, cell proliferation and growth

factor signaling were also upregulated. Since the expression of the early developmental markers, *NESTIN, MUSASHI1* and *CD133* have been associated with GBM malignancy (Bao et al., 2006a; Ma et al., 2008; Rutka et al., 1999), the reduced expression of these factors may suggest that mtDNA depletion reduces the tumorigenic profile of HSR-GBM1 cells. However, the expression of *OCT4* (Ben-Porath et al., 2008), *HEY1* (Hulleman et al., 2009) and *SHH* (Xu et al., 2008) have also been associated with tumorigenicity and de-differentiation status of tumor cells and these outcomes could also suggest that mtDNA depletion results in an increased tumorigenic profile. It is also likely that expression of these factors may be functioning to maintain a stem cell-like population of GBM cells rather than promoting tumorigenicity. In support of this, knockdown of the GBM CSC marker, *SOX2*, was recently associated with the loss of de-differentiation status and increased tumorigenicity in GBM (Gangemi et al., 2009; Oppel et al., 2011). These findings demonstrate that mtDNA depletion induces extensive changes in gene expression in HSR-GBM1 cells and is in agreement with previous studies that reported that mtDNA-less cells exhibit altered gene expression (Singh et al., 2005; Smiraglia et al., 2008).

4.7.3 MtDNA copy number recovery

Since HSR-GBM1 cells exhibited an inability to expand mtDNA copy number in response to differentiation stimuli, I sought to determine whether HSR-GBM1 cells could recover their mtDNA copy number following depletion when maintained in an undifferentiated state. HSR-GBM1 cells maintained the ability to recover mtDNA copy number following 14 days of depletion, with 7 days of depletion inducing a compensatory effect, with mtDNA copy number exceeding

that of Day 0 levels. However, depletion beyond 14 days resulted in reduced mtDNA copy number recovery. The elevation in mtDNA copy number of Day 7 depleted cells also corresponded to an increase in *MUSASHI1, CD133* and *GFAP*. Since severe reductions in copy number correlated with reduced expression of GBM tumorigenic markers, a converse relationship appears to be present in HSR-GBM1 cells, with an increase in copy number correlating with increased expression of tumorigenic markers. HSR-GBM1 cells recovering from 14 and 21 days of depletion showed largely non-significant changes in gene expression, with the exception of *GFAP* in 21 day depleted cells. HSR-GBM1 cells depleted for 25 days showed minimal mtDNA copy number recovery and also showed significant reductions in *NESTIN, MUSASHI1, CD133* and *GFAP* expression. Collectively, these data suggest that the maintenance of mtDNA copy number plays a role in sustaining a tumorigenic expression profile of HSR-GBM1 cells.

4.7.4 Differentiation of mtDNA depleted HSR-GBM1 cells

In order to determine how the effects of mtDNA depletion on HSR-GBM1 cell differentiation, HSR-GBM1 cells were depleted for 7, 14 and 21 days and induced to differentiate. A similar trend was observed to that of the recovering, undifferentiated HSR-GBM1 cells, with differentiating HSR-GBM1 cells depleted for 7 and 14 days showing recovery and a small expansion of mtDNA copy number after 14 days of differentiation. Furthermore, HSR-GBM1 cells depleted for 21 days failed to fully recover mtDNA copy number. These data suggest that mtDNA copy number recovery is compromised following depletion beyond 14 days. In addition, the differentiation of HSR-GBM1 cells depleted for 21 days

resulted in down-regulation of all of the NSC markers *NESTIN, MUSASHI1, CD133* and also exhibited an increase in *GFAP* expression in excess of 10-fold, which was not observed in HSR-GBM1 cells depleted for 7 and 14 days. These results indicate that long-term (>14 days) mtDNA depletion may aid in the differentiation of HSR-GBM1 cells by assisting in the down-regulation of stem cell markers and up-regulation of lineage specific markers.

4.8 Conclusion

Alterations in mtDNA copy number appear to occur in a tumor specific manner. It is likely that the acquisition of a new mtDNA basal level, or set point hereafter, occurs during tumorigenic transformation. The maintenance of mtDNA copy number is important for normal cellular function (Wallace, 2005) and it is conceivable that the mtDNA set point of tumor cells is also of importance for tumor cell function and may play a role in the maintenance of tumorigenicity. The mtDNA copy number of the cellular origin of the HSR-GBM1 cells line is unknown, however, it likely to differ from that of the cell line, as previous studies have reported increased mtDNA copy number in brain tumors relative to non-transformed cells (Liang and Hays, 1996). In this chapter, severely depleted HSR-GBM1 cells showed altered expression of factors associated with tumorigenicity and also reduced proliferation rates. These outcomes strongly suggest that severe disruption of the mtDNA set point forces HSR-GBM1 cells towards an immature state whilst decreasing their tumorigenic profile by inducing differential expression of multiple malignant markers. Furthermore, partially depleted cells showed a drive towards reestablishing the mtDNA set point, as evidenced by recovery of copy number to comparable levels of non-

depleted cells. In addition, long-term mtDNA depletion assisted in the down-regulation of NSC markers and the up-regulation of lineage specific markers during differentiation, however, this was not accompanied by an increase in mtDNA copy number. Collectively, the data presented in this chapter illustrate that the alteration of mtDNA copy number exerts a strong influence on nuclear gene expression and that the loss of mtDNA likely induces a less tumorigenic profile in HSR-GBM1 cells.

Chapter 5: The maintenance of mitochondrial DNA copy number is an key component of HSR-GBM1 cell tumorigenicity

5.1 Introduction

The tumorigenicity of mtDNA depleted and ρ0 tumor cells remains a controversial topic due to conflicting reports that have demonstrated reduced and increased tumorigenicity in the aforementioned cell types (Amuthan et al., 2002; Cavalli et al., 1997; Kulawiec et al., 2009b; Magda et al., 2008). The majority of mtDNA depletion studies utilize ethidium bromide, which intercalates into mtDNA and induces mtDNA depletion (Amuthan et al., 2002; Cavalli et al., 1997; King and Attardi, 1989; Kulawiec et al., 2009b; Magda et al., 2008). However, ethidium bromide also intercalates into nuclear DNA (Waring, 1965), which is a property that has been exploited extensively for many decades for DNA labeling techniques, such as gel electrophoresis. The intercalation of ethidium bromide into DNA may increase the possibility of mutagenesis (Waring, 1965), which in turn could alter cellular function in an unpredictable manner. To circumvent any potential side effects of ethidium bromide, mtDNA-specific agents, such as ddC, can be utilized to determine the specific effects of mtDNA depletion on cellular function and also tumorigenicity.

In *Chapter 4*, HSR-GBM1 cells were depleted of their mtDNA content using ddC. Depletion of HSR-GBM1 cells resulted in reduced proliferation and altered gene expression profiles. However, it remains to be determined whether the

observed changes in expression of GBM tumorigenic markers correlates with reduced GBM tumorigenicity, *in vivo*. To address this issue, non-depleted HSR-GBM1 cells (100% mtDNA) and HSR-GBM1 cells depleted to 50%, 20%, 3% and 0.2% of their mtDNA content were inoculated into immunocompromised mice and tumor growth assays were performed. In addition, established tumors were harvested and their mtDNA copy number and gene expression were analyzed.

5.2 Hypothesis

Changes in the expression of factors associated with GBM tumorigenicity were observed following mtDNA depletion of HSR-GBM1 cells (See *Chapter 4*). I hypothesize that mtDNA depletion will reduce the tumorigenic potential of HSR-GBM1 cells, since GBM cells showed reduced expression of *NESTIN*, which has been shown to play a role in motility and invasiveness of GBM. Furthermore, depleted GBM cells exhibited reduced *in vitro* proliferation rates in the presence metabolic supplements (high glucose & uridine). *In vivo*, the availability of these nutrients to GBM cells will be reduced and I hypothesize that mtDNA depletion will result in restricted GBM cell proliferation, *in vivo*.

5.3 Aims

- To assess the tumorigenic potential of non-depleted and mtDNA depleted HSR-GBM1 cells through *in vivo* tumor formation assays
- To determine whether mtDNA is essential for tumor formation of HSR-GBM1 cells

- To determine the mtDNA copy number of established HSR-GBM1 cell tumors
- To analyze the gene expression profiles of HSR-GBM1 derived tumors

5.4 Materials and Methods

5.4.1 MtDNA depletion of HSR-GBM1 cells

HSR-GBM1 cells were cultured and depleted of mtDNA, as described in *MtDNA depletion of HSR-GBM1 cells* (Section 2.3.4)**.** Non-depleted and depleted HSR-GBM1 cells were used for tumor formation assays.

5.4.2 HSR-GBM1 tumor formation assay

Mouse experiments were approved by the Animal Ethics Committee, Monash University, Approval Number: MMCA/2001/76. Animal handling and tumor formation assays were performed by Dr. Jacqui Donoghue (CCR, MIMR, Australia) according to established and published protocols (Adams et al., 2009; Greenall et al., 2012). Non-depleted HSR-GBM1 cells (100% mtDNA content; control) and mtDNA depleted HSR-GBM1 cells containing variable percentages of mtDNA copy number (50%, 20%, 3% and 0.2% mtDNA content) were prepared simultaneously and cell counts performed, as described in section *Cell counting* (Section 2.2.6). 1 x 10^6 cells were resuspended in 100 µl of StemPro Complete Medium and were inoculated subcutaneously into both flanks (sides) of 4 to 6 week old, female BALB/c nude mice (Animal Research Centre, Perth, Australia). 6 mice were inoculated per experimental group generating 12 replicates for each group (100% - control, 50%, 20%, 3% and 0.2% mtDNA content). Tumors were measured every second day and tumor volumes were determined using the following formula:

$$(L \times W^2)/2$$

Where *L* is the tumor length at its longest axis and *W* is the width measured at right angles to the length. Data are expressed as mean tumor volume ± SEM in cubic millimeters (mm^3). Tumor formation assays were terminated after 200 days or when tumors volumes reached $1000mm^3$.

5.4.3 Immunohistochemistry

Tumor immunohistochemistry was performed by Dr. Jacqui Donoghue. To determine the number of proliferating cells present in HSR-GBM1 tumor xenografts, tumor sections were stained with the proliferation marker, proliferating cell nuclear antigen (PCNA). Proliferating nuclei were identified using a mouse monoclonal anti-PCNA antibody (1:1000; Cell Signaling Technology, Danvers, MA). Formalin fixed paraffin embedded tumor sections (5 µm) were dewaxed, rehydrated and microwaved in citrate buffer for antigen retrieval. Once cooled, the sections were incubated with 3% hydrogen peroxide in methanol for 15 minutes to quench endogenous peroxidase. All sections were then incubated with the DAKO protein blocking solution (Dako Australia, Kingsgrove, Australia) to prevent non-specific binding. Negative controls were performed by incubating sections without the primary antibodies. Primary antibodies were incubated for 1 hour at room temperature. The PCNA was visualized with the Link Label-HRP system by DAKO, according to manufacturer's protocol (Dako Australia), followed by the chromogen Vector Red for 15 mins (Vector Laboratories; Burlingame, CA).

Image analysis was performed using a Leica inverted bright field microscope (Leica). Sections were scanned at low magnification to identify areas of high

proliferation (hot spots). Images were then captured at X40 optical lens. Positive nuclei were counted using the cell counter plug in analysis tool from four fields of view (Image J analysis software; National Institute of Health). Positive cell counts were presented as mean values ± SEM.

5.4.4 MtDNA copy number analysis

Total DNA was extracted from HSR-GBM1 cells and tumor samples, as described in *DNA extraction from intact cells* and *DNA extraction from tumor samples* (Sections 2.4.3 & 2.4.4) and quantified by spectrometry, as described in *Quantification of nucleic acids* (Section 2.4.5). Mouse liver DNA was kindly donated by Dr. Mulyoto Pangestu (Education Program in Reproduction and Development (EPRD) Monash University). MtDNA copy number was quantified using real-time PCR, as described in *MtDNA copy number analysis* (Section 2.6.4).

5.4.5 Gene expression analysis

Total RNA was extracted from HSR-GBM1 cells and tumor samples, as described in *RNA extraction from tumor samples* (Section2.4.2) and quantified by spectrometry, as described in *Quantification of nucleic acids* (Section 2.4.5). cDNA was synthesized using the Bioline system, as described in *Reverse transcription* (Section *2.5.1*). Dr. Mulyoto Pangestu kindly donated mouse brain and mouse embryonic fibroblast (MEF) cDNA. Gene expression analysis was performed using RT-PCR and real-time PCR. PCR reaction conditions and primer pairs are described in *Polymerase Chain Reaction* (Sections 2.5.3 & 2.6.3) and are listed in Table 4.I (*Chapter 4;* Section 4.5.5), respectively.

5.4.6 D-loop sequencing

Total DNA was extracted from hNSCs, HSR-GBM1 cells and tumor samples as, described in Sections 2.4.3 & 2.4.4**.** D-loop PCR products were amplified with D-Loop-F TAATACACCAGTCTTGTAAACC and D-Loop-R TTGAGGAGGTAAGCTACATA primers by conventional PCR, electrophoretically separated, purified and sequenced, as described in Sections 2.5.3-2.5.6.

5.4.7 HRM analysis

For the detection of mtDNA variants, tumor samples were subjected to HRM analysis. HRM reactions were performed, as described in *High resolution melting curve analysis* (Section 2.6.2) using the following D-loop primers: hD-Loop F-CCACCATGAATATTGTACGGTA and hD-Loop R - TGGCTTTGGAGTTGCAGTTG. hNSCs were selected as wild type mtDNA controls and used for baseline measurements. Difference curves (calculated difference in fluorescence intensity) for tumor samples were compared to the "baseline" melting curve profiles generated by hNSC DNA.

5.4.8 Statistical analysis

Statistical analysis was performed, as described in *Statistical analysis* in the *General Materials and Methods* (Section 2.11).

5.5 Preliminary Experiments

5.5.1 Confirmation of non-PCR primer specificity to mouse DNA

To confirm that mouse DNA would not be amplified from HSR-GBM1 tumor xenografts using the primer pairs previously used to amplify mtDNA and β-Globin DNA, real-time PCR was performed, as described in *MtDNA copy number analysis* (Section 2.6.4), using HSR-GBM1 and mouse liver DNA. Real-time PCR analysis produced amplification curves for both mtDNA and β-Globin using the HSR-GBM1 DNA template. However, for mouse liver DNA, PCR amplification curves were not generated until much later in the PCR cycle profile (Ct values; >25). Furthermore, the calculated mtDNA copy number for mouse liver DNA was <1 (Figure 5.1A). These outcomes demonstrate that any mouse DNA that was co-extracted from the HSR-GBM1 tumors would not substantially influence the quantification of human mtDNA copy number in the tumor samples.

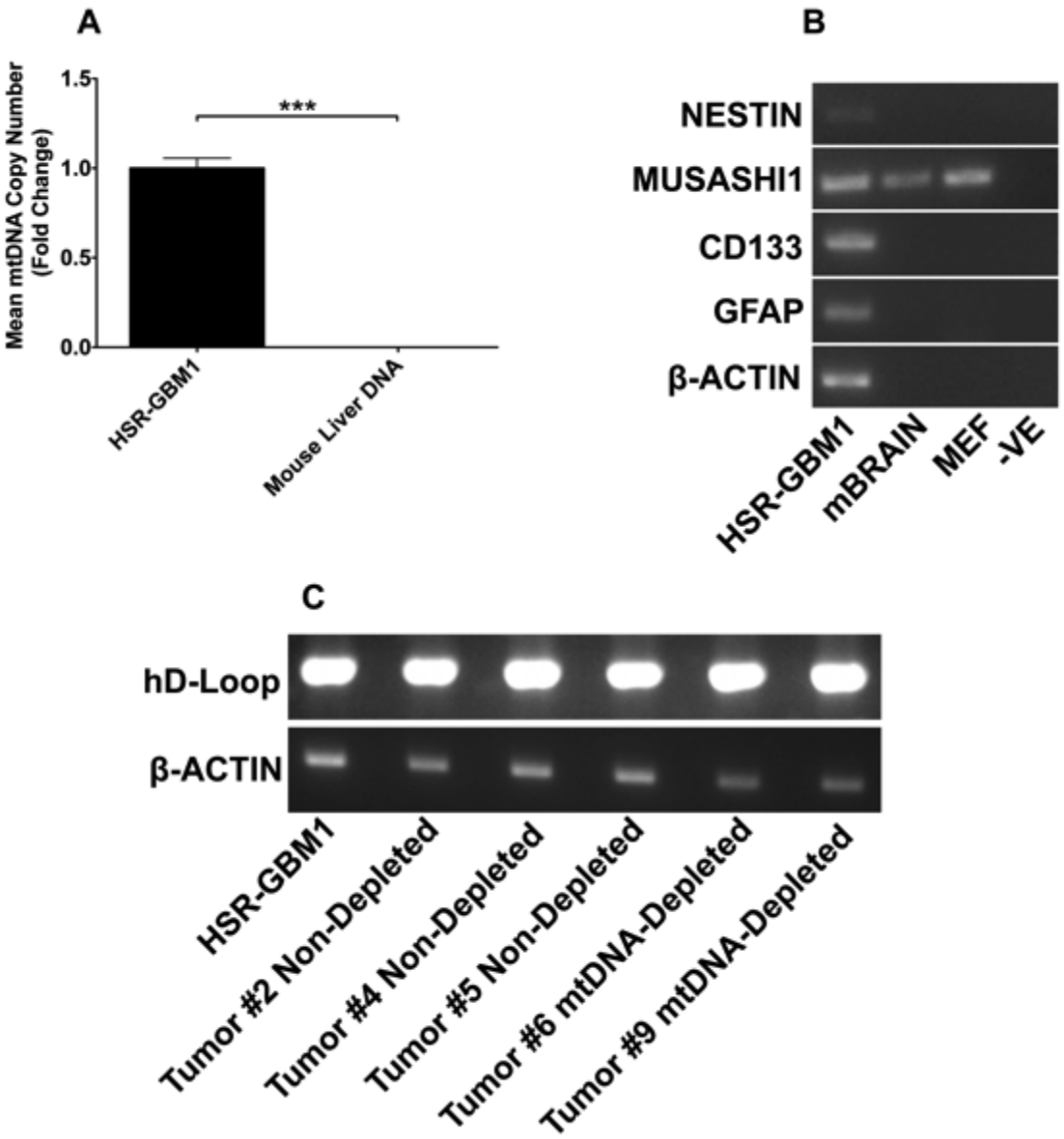

Figure 5.1. Quantification of mtDNA copy number of HSR-GBM1 and mouse liver DNA (A). RT-PCR screen of *NESTIN, MUSASHI1, CD133, GFAP* and *β-ACTIN* of HSR-GBM1, mouse brain and mouse embryonic fibroblast cDNA (B). Amplification of the D-Loop region of mtDNA and *β-ACTIN* for HSR-GBM1 cells and HSR-GBM1 cell derived tumors (C). Columns represent mean values ± SEM. *** Indicates $p<0.001$.

5.5.2 Confirmation of non-RT-PCR primer specificity to mouse cDNA

In order to confirm that mouse cDNA would not be specifically amplified from HSR-GBM1 tumor xenografts, RT-PCR reactions were performed, as described in *Polymerase Chain Reaction* (Section 2.5.3), with HSR-GBM1, mouse brain and MEF cDNA templates with the human *NESTIN, MUSASHI1, CD133, GFAP* and *β-ACTIN* primer pairs (see Table 3.I; *Chapter 3*). PCR products were generated from HSR-GBM1 cDNA with *NESTIN, MUSASHI1*, *CD133, GFAP* and *β-ACTIN* primer pairs (Figure 5.1B). PCR products were not detectable from mouse brain or fibroblasts for *NESTIN, CD133, GFAP* and *β-ACTIN* (Figure 5.1B). However, *MUSASHI1* expression was detectable in mouse brain and fibroblasts. MUSASHI1 is a transcription factor that is expressed in brain and ectodermal tissues (Sakakibara et al., 1996). Since mouse brain and MEFs are of ectodermal origin, both samples could be expected to express *MUSASHI1* following a RT-PCR screen (Figure 5.1B). Furthermore, the *MUSASHI1* cDNA sequence is highly homologous between human and mouse and may also account for the positive expression detected in these samples. However, as all the other genes of interest screened using mouse cDNA showed no expression, including the housekeeping *β-ACTIN*, I reasoned that the utilization of these primer pairs would be suitable for gene expression analysis of HSR-GBM1 tumor xenografts. Prior to gene expression analysis by real-time PCR, depleted and non-depleted HSR-GBM1 tumor xenografts were screened for *β-ACTIN* using RT-PCR to confirm that the xenograft cDNA was suitable for subsequent reactions. *β-ACTIN* PCR products were generated from each of the depleted and non-depleted tumors (Figure 5.1C).

5.5.3 Optimization of high resolution melting (HRM) curve analysis

In order to determine whether mtDNA variants were present in HSR-GBM1 cells and tumor xenografts, HRM reaction conditions required optimization. HRM primers were designed to span 147 bp region of the human D-loop that contained a previously identified D-loop variant (personal communication with Ka Yu Yueng), C16218T, which is present at low levels in the HSR-GBM1 cell line. Using HSR-GBM1 DNA as a template, a series of conventional PCR reactions were performed using an annealing temperature gradient, ranging from 52-64^{o}C, in order to determine the optimal annealing temperature. Reaction mixtures and conditions are, as described in *High resolution melting curve analysis* (Section 2.6.6). PCR products were subjected to HRM analysis, as described in *High resolution melting curve analysis* (Section 2.6.6) and subsequently loaded onto a 2% agarose gel and electrophoresis performed, as described in *Gel electrophoresis* (Section 2.5.4). With the exception of 52^{o}C, strong fluorescent signal intensity was generated by the PCR products at all annealing temperatures, with the greatest intensity observable at temperatures between 53.3-58.4^{o}C (Figure 5.2). In addition, PCR products showed overlapping melting curve profiles (Figure 5.2), which demonstrates that HRM curve analysis was successful at all of the examined annealing temperatures. For subsequent HRM analysis using the 147 bp D-loop primers, I reasoned that an annealing temperature of 55^{o}C would be appropriate, since high fluorescence signal intensity and overlapping melting curve profiles were generated for PCR products with annealing temperatures between 53.3 and 58.4^{o}C.

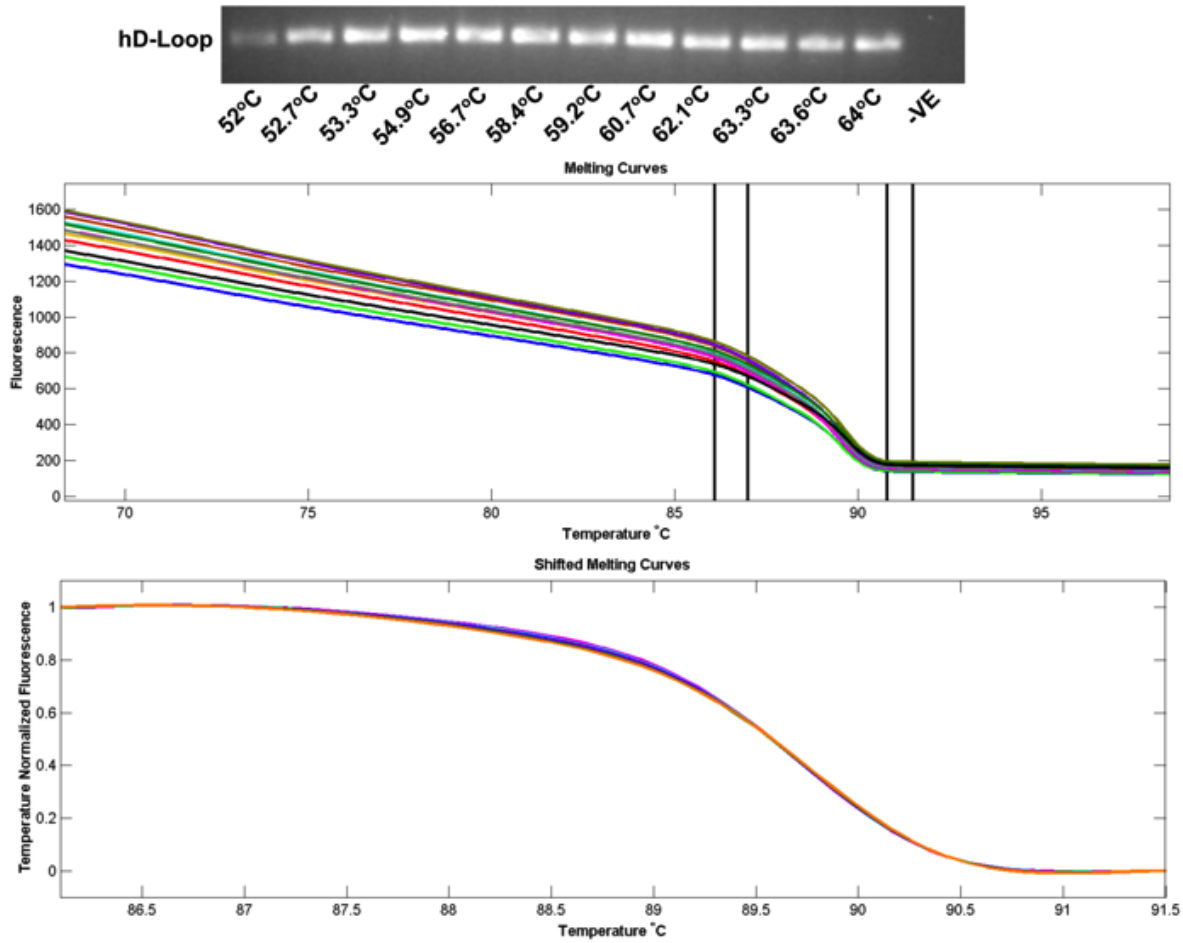

Figure 5.2. Gel electrophoresis of the D-loop temperature gradient PCR using HSR-GBM1 DNA (Top). HRM curve profiles of each of the PCR products generated from the temperature gradient (Middle) and the shifted melting curve profiles for each of PCR product generated from the temperature gradient (Bottom).

5.6 Results

5.6.1 Tumor growth analysis

In *Chapter 4*, long-term mtDNA depletion of HSR-GBM1 cells resulted in extensive changes in gene expression and a reduction in proliferation rates. Reductions in expression of the factors associated with GBM tumorigenicity were also observed. These outcomes suggested that mtDNA depletion reduces the tumorigenic potential of HSR-GBM1 cells, however, increases in expression of *OCT4, SHH, GDNF, HEY1* and *VEGFA* were also observed, which are also associated with GBM tumorigenicity (Bao et al., 2006b; Ben-Porath et al., 2008; Xu et al., 2008). In order to determine the true tumorigenic potential of mtDNA depleted HSR-GBM1 cells, non-depleted and HSR-GBM1 cells depleted to variable levels of mtDNA copy number were simultaneously transplanted into immunocompromised mice and tumor growth assays were performed.

MtDNA copy number was analyzed in non-depleted and mtDNA depleted cells and converted to a percentage loading of mtDNA, i.e. non-depleted cells would contain 100% mtDNA copy number whilst HSR-GBM1 cells with <1 mtDNA copy per cell would contain 0.2% mtDNA. Prior to inoculation into immunocompromised mice, five groups of HSR-GBM1 cells harboring varying levels of mtDNA copy number were established simultaneously and were referred to, hereafter, as non-depleted (100%- control), 50%, 20%, 3% and 0.2% (Figure 5.3). Subsequently, the tumorigenicity of these groups were analyzed using tumor formation assays.

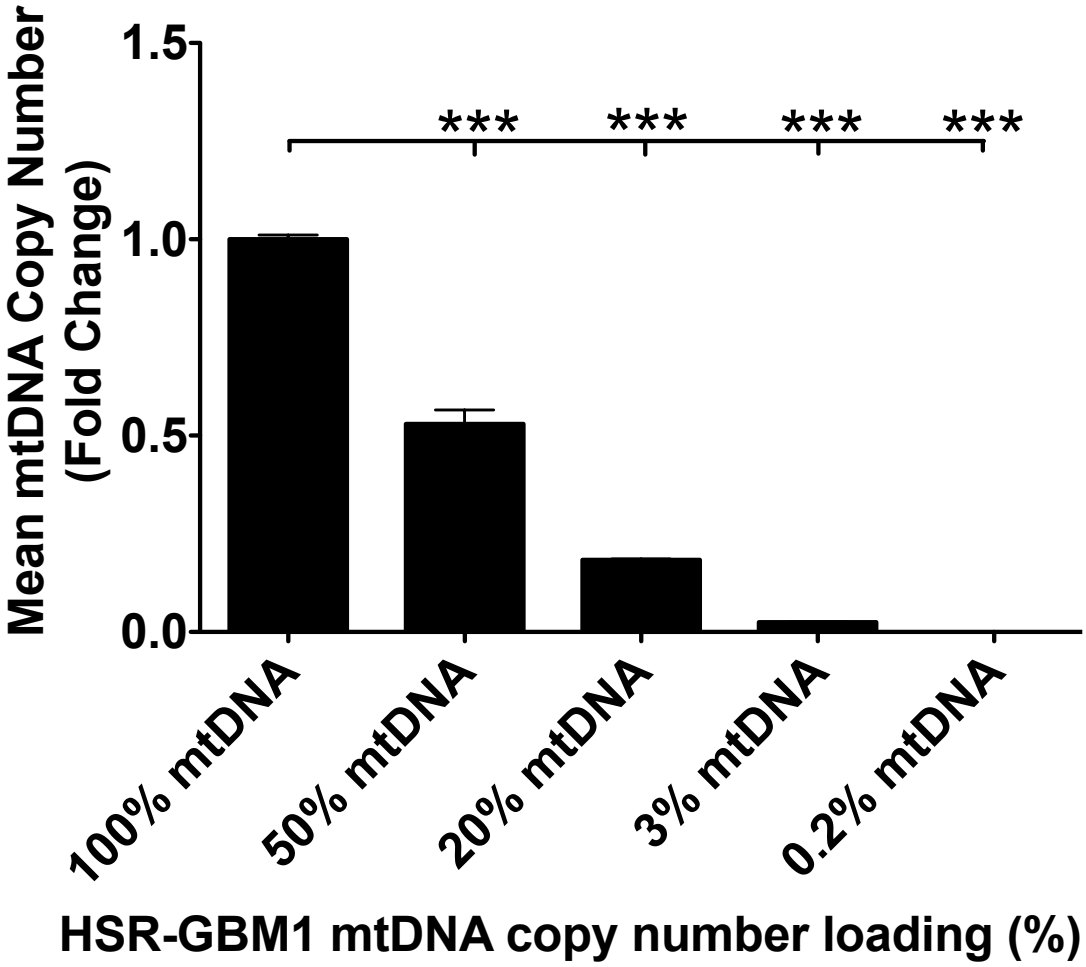

Figure 5.3. MtDNA copy number loading of non-depleted and depleted HSR-GBM1 cells. Columns represent mean values ± SEM (n=3). *** Indicates $p<0.001$.

During the first 40 days post-inoculation, 100% mtDNA and 50% mtDNA HSR-GBM1 tumors developed at a faster rate than 20% mtDNA, 3% mtDNA and 0.2% mtDNA tumors (Figure 5.4), although this was not statistically significant. Post Day 40, 50% mtDNA tumors grew at an accelerated rate compared to 100% mtDNA tumors and this trend was maintained for the remainder of the tumor formation assay. 20% mtDNA tumors continued to develop slowly until Day 55, after which tumors developed at an increasing rate and by Day 65

developed at a quicker rate than 100% mtDNA tumors (Figure 5.4; p>0.01). 3% and 0.2% mtDNA tumors showed delayed development compared to 100% mtDNA tumors (p<0.01), with tumor development only occurring from Day 65 (0.2% mtDNA) and Day 70 (3% mtDNA) onwards (Figure 5.4). The tumor formation rate was significantly lower than that of 100% mtDNA tumors (p<0.01).

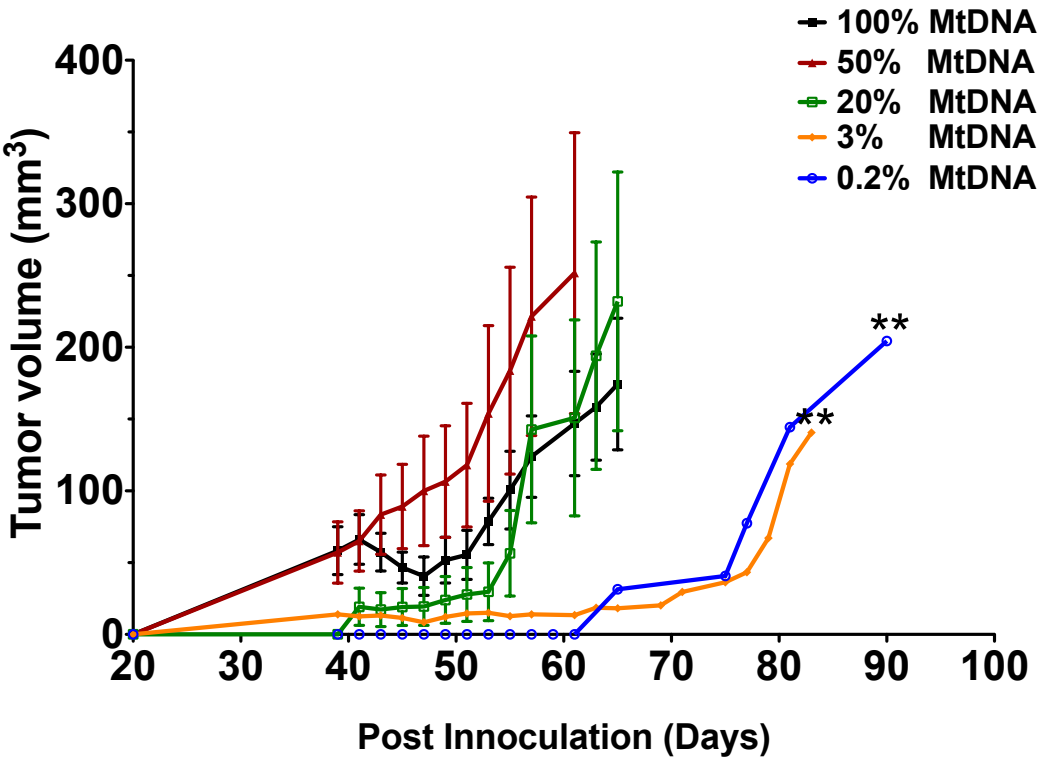

Figure 5.4. HSR-GBM1 tumor formation assay. Tumor growth curve analysis of non-depleted and depleted HSR-GBM1 cells (n=12). ** Indicates p<0.01 relative to non-depleted (100% mtDNA) HSR-GBM1 cells.

The frequency of tumor formation was inversely related to mtDNA depletion. From the 100% mtDNA cells, 11/12 tumors were generated (1 regressed); 10/12 tumors were derived from 50% mtDNA cells (2 regressed); 6/12 tumors from 20% mtDNA cells, 6/12 tumors from 3% mtDNA cells (3 regressed) and

2/12 tumors from 0.2% mtDNA cells (Table 5.I). Furthermore, the percentage of tumors that reached a volume of 500mm^3 was least in the 0.2% mtDNA cells and greatest in the 100% mtDNA cohort (Figure 5.5). There was also statistical significance between the number of tumors formed/failed and the percentage loading of mtDNA copy number (p=0.0048), as determined by a Chi squared test (Figure 5.6).

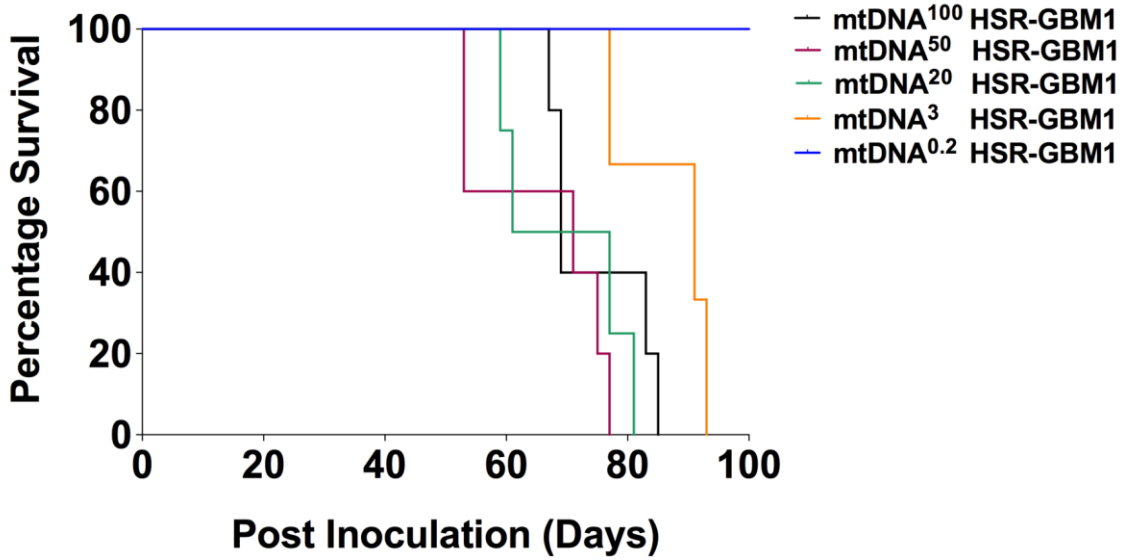

Figure 5.5. Kaplain-Meier survival plot for non-depleted and depleted HSR-GBM1 cell cohorts that reached 500mm^3.

Tumor Group	Number of Tumors Formed
100% MtDNA	**11/12** (1 regressed)
50% mtDNA	**10/12** (2 regressed)
20% mtDNA	**6/12**
3% mtDNA	**6/12** (3 regressed)
0.2% mtDNA	**2/12**

Table 5.I Summary of the number of tumors formed by non-depleted and mtDNA depleted HSR-GBM1 cells.

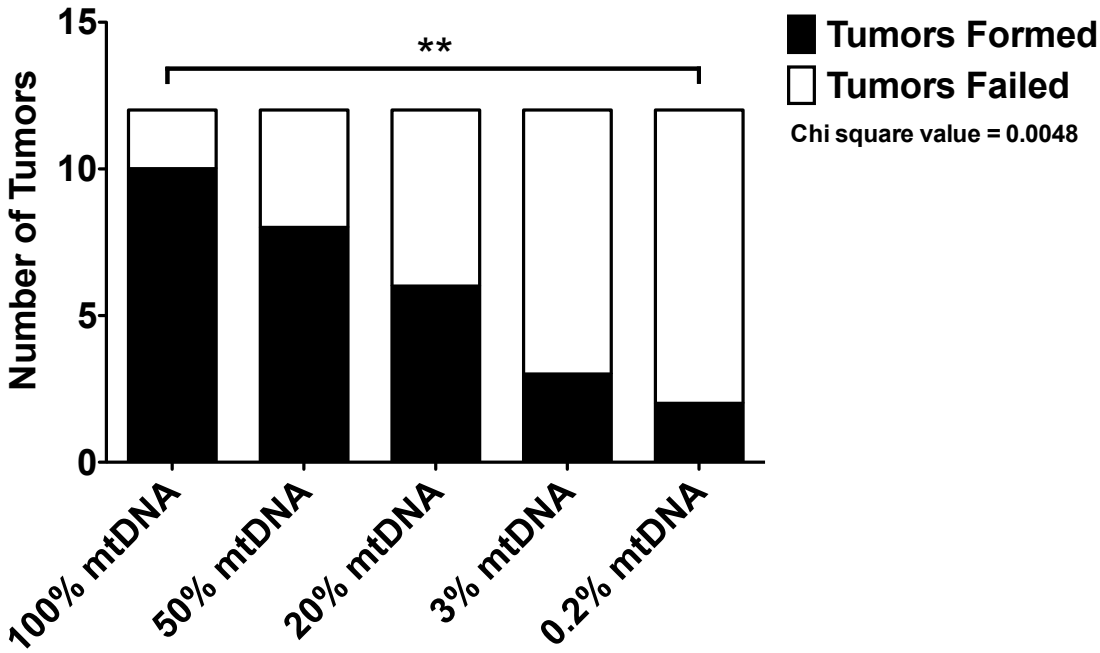

Figure 5.6. Contingency graph of the number of tumors formed and failed from HSR-GBM1 cells that were depleted to variable levels of mtDNA content. ** Indicates $p<0.01$.

5.6.2 Cell Proliferation

Since 100% mtDNA HSR-GBM1 tumors developed significantly quicker than 0.2% depleted tumors, histological analysis was performed on these two

groups. Tumor sections were stained with the cell proliferation marker, proliferating cell nuclear antigen (PCNA), to determine the proliferation status of the HSR-GBM1 cells within the established tumors. 100% mtDNA HSR-GBM1 tumors contained considerably more proliferating cells (indicated by positive stained nuclei) than 0.2% mtDNA tumors (Figure 5.7B-G). These observations support the tumor growth curve data and indicate that mtDNA depletion results in reduced proliferation rates of HSR-GBM1 cells. Statistical analysis could not be performed on these data as 0.2% mtDNA HSR-GBM1 cells only generated one full sized ($1000mm^3$) tumor. However, the graphical representation of positively stained nuclei strongly suggests that 100% mtDNA HSR-GBM1 tumors contained greater numbers of proliferating cells (Figure 5.7A).

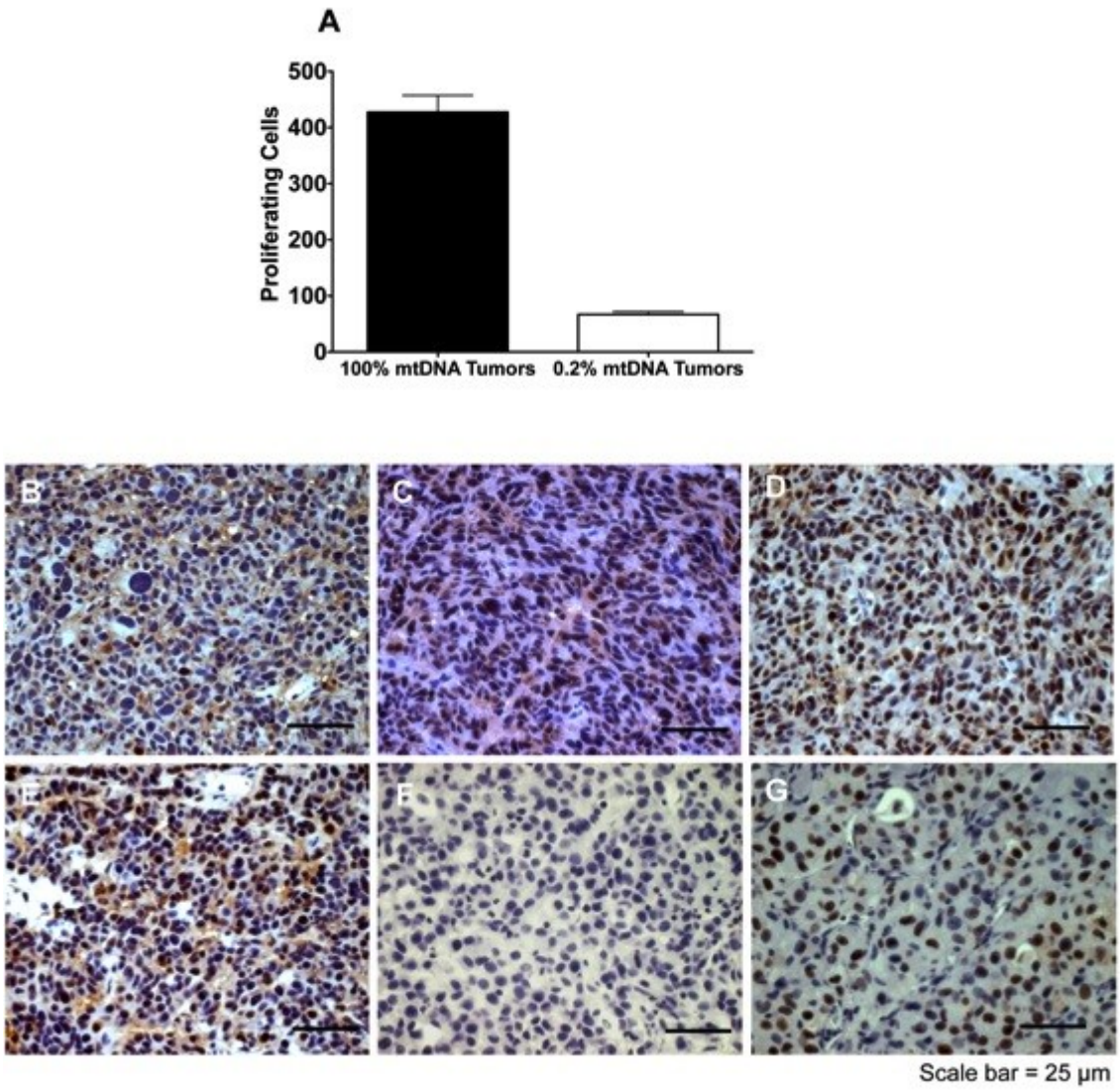

Figure 5.7. Immunohistochemical analysis of HSR-GBM1 tumors. Graphical representation of the number of PCNA positive cells in 100% mtDNA (non-depleted) and 0.2% mtDNA (depleted) HSR-GBM1 cell tumors (A). Columns represent mean values ± SEM. PCNA labeling of non-depleted (B-D) and depleted (E) HSR-GBM1 cell tumors with positive (F) and negative (G) antibody controls. Scale bar as indicated.

5.6.3 MtDNA copy number of established HSR-GBM1 tumors

Prior to inoculation, 0.2% mtDNA HSR-GBM1 cells contained, on average, <1 mtDNA copy per cell. Since the 3% and 0.2 % mtDNA HSR-GBM1 cells formed tumors at a reduced rate, I next determined the mean mtDNA copy number of the tumors that established from 100%, 50%, 20%, 3% and 0.2% mtDNA groups.

The rationale for analyzing the mean copy number of HSR-GBM1 tumors was to determine whether the *in vivo* environment affected the ability of HSR-GBM1 cells to reestablish their mtDNA copy number following varying levels of depletion. It is worthy of note that one of the 0.2% mtDNA tumors analyzed did not reach a volume of $1000mm^3$ by the termination of the tumor formation assay. $1000mm^3$ was the end point volume for tumor harvest; however, this sample was included in the analysis to provide insight into the mtDNA copy number of 0.2% mtDNA tumors. The mtDNA copy number of 100%, 50%, 3% and 0.2% mtDNA tumors were comparable to one another, however, the mtDNA copy number of 20% mtDNA tumors were significantly lower than 100% ($p<0.05$), 50% ($p<0.05$) and 0.2% ($p<0.01$) mtDNA tumors (Figure 5.8). Collectively, these outcomes demonstrate that despite HSR-GBM1 cells containing between 100% and 0.2% mtDNA of their original mtDNA content, they proceeded to reestablish and maintain comparable levels of mtDNA copy number to one another *in vivo*.

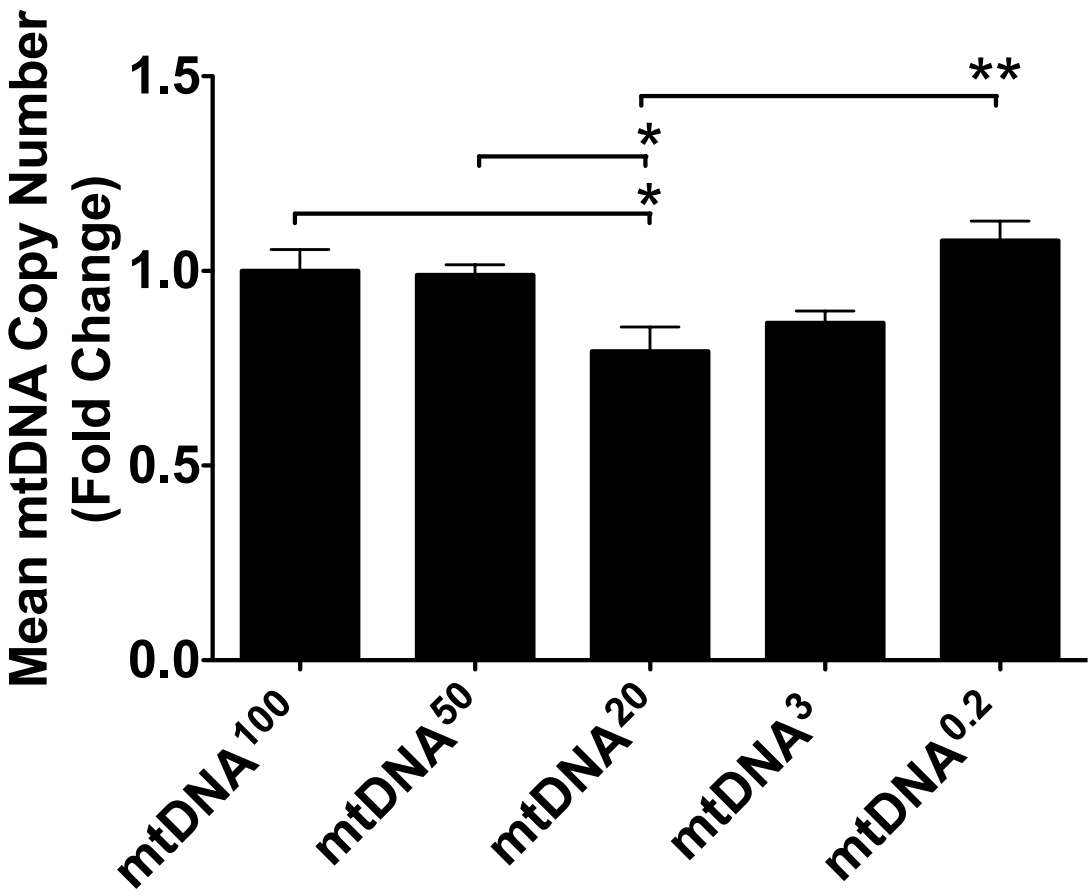

Figure 5.8. MtDNA copy number analysis of HSR-GBM1 cell tumors. Fold change in mtDNA copy number of 50%, 20% 3% and 0.2% mtDNA HSR-GBM1 cell tumors relative to 100% mtDNA tumors (A). Columns represent mean values ± SEM. * Indicates $p<0.05$ and ** indicates $p<0.01$.

5.6.4 Gene expression analysis

Since mtDNA depletion induced gene expression changes in *in vitro* cultured HSR-GBM1 cells and the tumors generated from 0.2% mtDNA HSR-GBM1 cells reestablished their mtDNA copy number *in vivo*, I determined whether recovery of mtDNA copy number *in vivo* also induced changes in gene expression of NSC, pluripotency and early developmental markers in tumors. Due to the time limitations of my PhD study, I was unable to analyze the gene expression of all the tumors that developed. Since non-depleted HSR-GBM1

cells formed the greatest number of tumors and 0.2% mtDNA HSR-GBM1 cells formed the fewest tumors, I selected these two experimental groups for gene expression analysis.

The expression of the NSC marker, *NESTIN*, was comparable in 100% mtDNA tumor #2 to *in vitro* grown HSR-GBM1 cells, whilst the expression was significantly increased in 100% mtDNA tumors #4 and #5 ($p<0.001$; Figure 5.9A). The expression of *NESTIN* was comparable in 0.2% mtDNA tumor #6 compared to *in vitro* grown HSR-GBM1 cells, however the expression was significantly higher than in 0.2% mtDNA tumor #9 ($p<0.001$). *NESTIN* expression in 0.2% mtDNA tumor #9 was significantly greater than that of all other tumors ($p<0.001$; Figure 5.9A).

The expression of NSC transcription factor, *MUSASHI1*, was significantly lower in all tumors samples compared to *in vitro* cultured HSR-GBM1 cells ($p<0.001$; Figure 5.9B). Gene expression was significantly lower in 100% mtDNA tumor #2 and 0.2% mtDNA tumor #6 compared to 100% mtDNA tumors #4 and #5 ($p<0.001$). The expression of *MUSASHI1* was significantly higher in 0.2% mtDNA tumor #9 compared to 0.2% mtDNA tumor #6 and 100% mtDNA tumors #2 and #5 ($p<0.001$; Figure 5.9B).

The expression of the cell surface proteoglycan, *CD133*, was significantly reduced in 100% mtDNA tumor 2 ($p<0.01$) and 0.2% mtDNA tumor #9 ($p<0.01$) compared to *in vitro* cultured cells (Figure 5.9C). *CD133* expression was comparable to *in vitro* cultured cells in 100% mtDNA tumors #4 and #5. 0.2%

mtDNA tumor #6 showed the highest level of expression and was significantly greater than *in vitro* cultured cells and all other tumor samples ($p<0.001$; Figure 5.9C).

The expression of *GFAP* showed a similar trend to *MUSASHI1*, with all tumor samples exhibiting significantly lower expression than *in vitro* cultured HSR-GBM1 cells. However, between tumor groups, 0.2% mtDNA tumors expressed significantly higher levels of *GFAP* compared to 100% mtDNA tumors ($p<0.001$; Figure 5.9D), with 0.2% mtDNA tumor #6 exhibiting the highest level of *GFAP* expression across all tumor samples ($p<0.001$; Figure 5.9D).

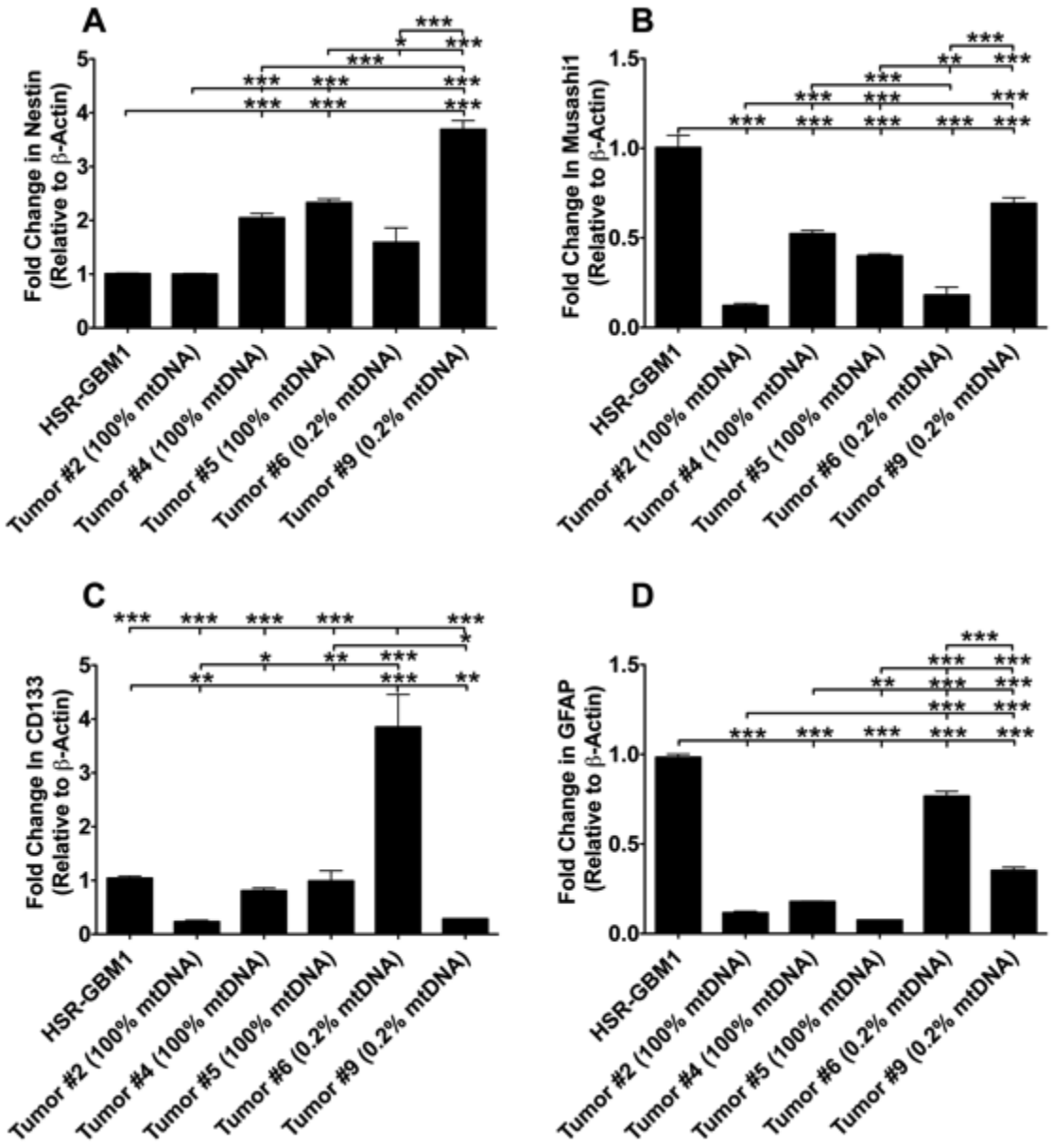

Figure 5.9. Gene expression analysis NSC and lineage specific markers in HSR-GBM1 cell tumors. Fold change in expression relative to *in vitro* cultured HSR-GBM1 cells and weighted against *β-ACTIN* of *NESTIN* (A), *MUSASHI1* (B), *CD133* (C) and *GFAP* (D). Columns represent mean values ± SEM. * Indicates $p<0.05$, ** $p<0.01$ and *** $p<0.001$.

The expression of the core pluripotency markers, *SOX2, OCT4* and *NANOG* was also assessed in tumor samples. The expression of *SOX2* was comparable across all tumor samples and expression levels were also comparable to *in vitro* cultured HSR-GBM1 cells (Figure 5.10A). *OCT4* expression was elevated in all tumor samples compared to *in vitro* cultured HSR-GBM1 cells. In addition, 0.2% mtDNA tumors #6 and #9 showed significantly higher levels of *OCT4* expression than 100% mtDNA tumors ($p<0.001$; Figure 5.10B). 0.2% mtDNA tumor #6 showed a 34.16-fold greater level of *OCT4* expression compared to *in vitro* grown HSR-GBM1 cells ($p<0.001$). The expression of *NANOG* was lower in all tumor samples compared to *in vitro* cultured HSR-GBM1 cells (Figure 5.10C). *NANOG* expression was similar across tumor samples except for 0.2% mtDNA tumor #6, which exhibited significantly higher levels of expression compared to tumors #2 ($p<0.05$) and #9 ($p<0.05$; Figure 5.10C).

Since mtDNA depletion resulted in reduced expression of the proto-oncogene, *c-MYC* and the self-renewal factor, *hTERT*, in HSR-GBM1 cells *in vitro*, the expression of these factors was also assessed in HSR-GBM1 tumors. The expression of *c-MYC* was reduced in all tumor samples compared to *in vitro* cultured HSR-GBM1 cells (Figure 5.10D). *c-MYC* expression levels were comparable between 100% mtDNA tumor samples. Differential expression was observed between 0.2% mtDNA tumor samples with tumor #9 exhibiting the lowest expression level, whilst tumor #6 exhibited the highest level of *c-MYC* expression and was significantly greater than all other tumor samples ($p<0.001$; Figure 5.10D). However, *c-MYC* expression was highly variable in 0.2% mtDNA tumor #6 as indicated by a large SEM (Figure 5.10D). The expression of the

self-renewal factor *hTERT*, was comparable between 100% mtDNA tumor samples (Figure 5.10E). 0.2% mtDNA tumor samples showed reduced gene expression compared to *in vitro* cultured HSR-GBM1 cells, however, these differences were not significant (Figure 5.10E). Furthermore, *hTERT* expression was significantly higher in 0.2% mtDNA tumors compared to 100% mtDNA tumors.

The expression of *SHH*, a morphogen that plays a key role in development and neurogenesis, was elevated in depleted HSR-GBM1 cells *in vitro* (See *Chapter 4*) and the expression level of *SHH* in HSR-GBM1 tumor samples was therefore determined. *SHH* expression was significantly reduced in 100% mtDNA tumors #2 and #4 compared to *in vitro* cultured HSR-GBM1 cells ($p<0.001$; Figure 5.10F), whilst tumor #5 exhibited comparable gene expression levels to *in vitro* cultured HSR-GBM1 cells (Figure 5.10F). 0.2% mtDNA tumor #6 demonstrated the highest level of *SHH* gene expression.

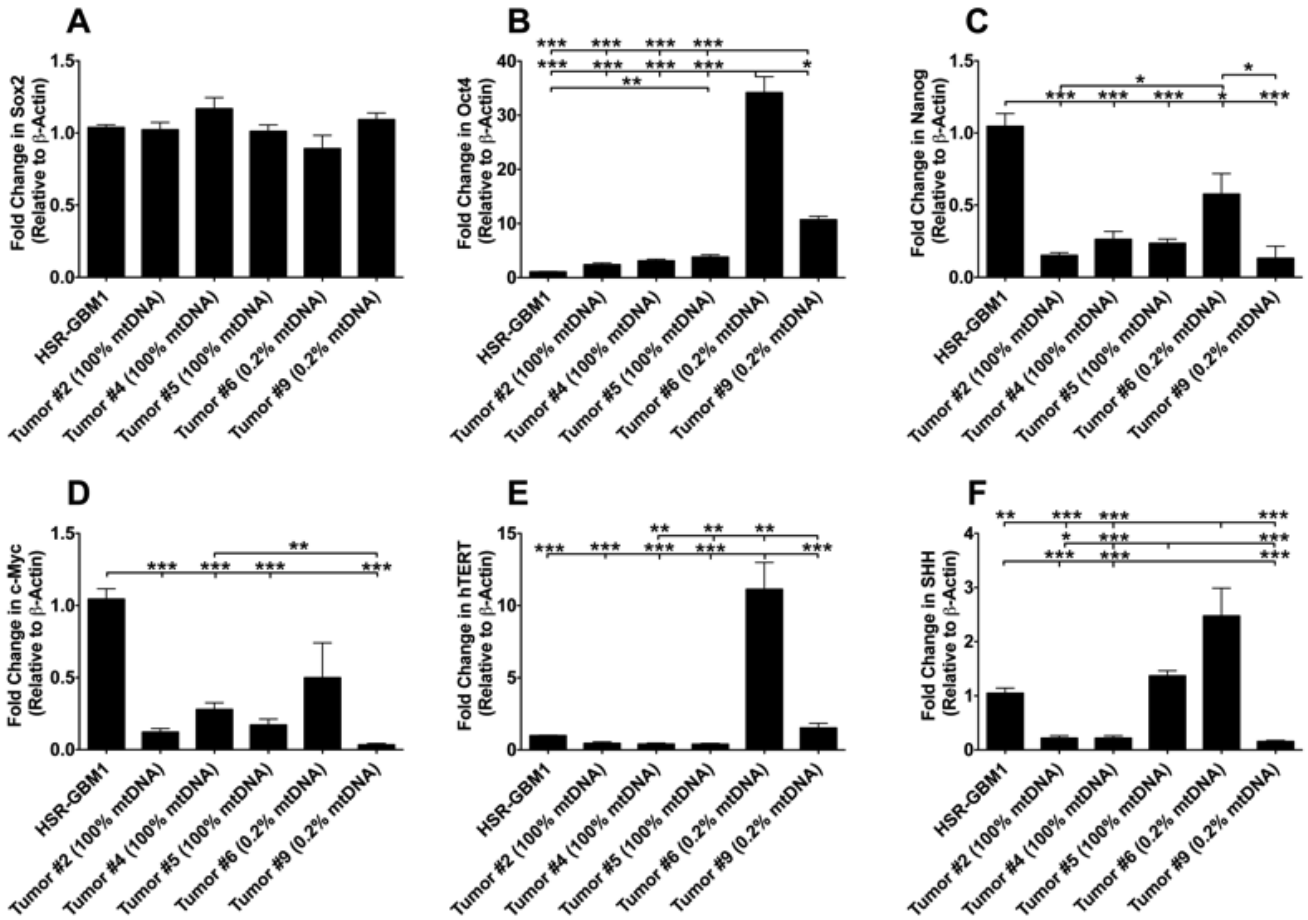

Figure 5.10. Gene expression analysis of pluripotent and early developmental markers in HSR-GBM1 cell tumors. Fold change in expression relative to *in vitro* cultured HSR-GBM1 cells and weighted against *β-ACTIN* of *SOX2* (A), *OCT4* (B), *NANOG* (C), *c-MYC* (D), *hTERT* (E) and *SHH* (F). Columns represent mean values ± SEM. * Indicates $p<0.05$, ** $p<0.01$ and *** $p<0.001$.

5.6.5 D-loop sequencing

Previous work within our laboratory has identified multiple variants within the mitochondrial genome of HSR-GBM1 cells (personal communication with Ka Yu Yeung). I sought to address whether *in vivo* growth of HSR-GBM1 cells alters the level of mtDNA variants and if mtDNA depletion leads to an elimination of mtDNA variants. I selected one of the identified variants, C16218T, found within the D-loop region, and performed Sanger sequencing of a 1000bp D-loop PCR product with *in vitro* cultured HSR-GBM1 DNA. Sanger sequencing readouts showed evidence of the previously identified D-loop variant, which was detected as two fluorescent peaks (Figure 5.11; boxed region). I proceeded to amplify and sequence the D-loop regions for each of the HSR-GBM1 tumor samples. Sequencing readouts showed evidence of heteroplasmy (C→T) at position 16218 in each of the non-depleted tumors (Figure 5.11; boxed regions). Furthermore, the fluorescence peaks generated for the variants were higher in each of the 100% mtDNA tumor samples compared to *in vitro* cultured HSR-GBM1 cells (Figure 5.11). In contrast, no conclusive evidence of the D-loop variant in the 0.2% mtDNA tumor samples was observed. Sequencing readouts from the 0.2% mtDNA tumor samples were comparable to that of hNSCs, which were selected to represent a wild-type population of mtDNA.

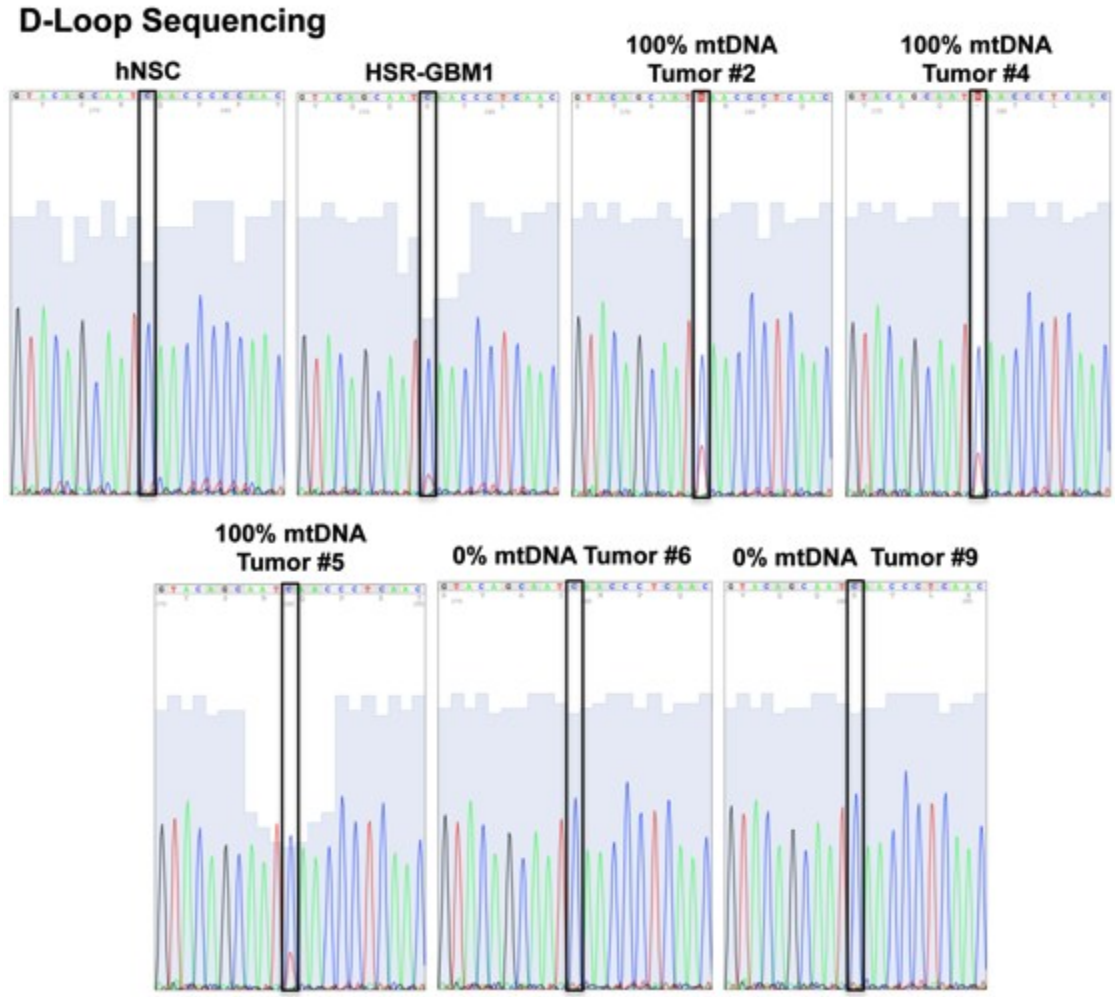

Figure 5.11. Sanger sequencing analysis of a 1000 base pairs of the D-loop region of mtDNA. D-loop sequencing readouts of hNSCs and HSR-GBM1 cells and derived tumors. Boxed regions indicate the position of the C16218T variant.

5.6.6 HRM analysis

To confirm that the frequency or load of the D-loop variant was variable in non-depleted (100% mtDNA) and depleted tumor samples (0.2% mtDNA), HRM analysis was performed. HRM is a powerful and sensitive tool that can detect single or multiple base mutations or variants in 150-300 bp regions of DNA. A single variant in the DNA sequence (e.g. A→C) results in a change in the G/C content of the PCR product, which in turn influences the melting temperature profile of a given PCR product. HRM is capable of detecting minute changes in temperature, which are detected as “shifts” in the melting curve profile of PCR products.

A 147 bp region encompassing the D-loop variant was amplified by conventional PCR. In agreement with the sequencing outcomes, HRM analysis indicated that the D-loop variant was present at higher levels in 100% mtDNA tumor samples than *in vitro* cultured HSR-GBM1 cells, as evidenced by greater shifts in the melting curve profiles (Figure 5.12A-B). The D-loop variant was also confirmed in the *in vitro* cultured HSR-GBM1 cells, which was demonstrated by a shift in the melting curve compared to the baseline control, hNSCs (Figure 5.12A-B). In agreement with the Sanger sequencing results, 0.2% mtDNA tumor samples showed small changes in melting curve profiles in relation to the baseline control, which suggests that the frequency of the D-loop variant was reduced in 0.2% mtDNA tumor samples (Figure 5.12A-B). However, as there were small shifts in the melting curve profiles of these samples, the complete elimination of the variant could not be confirmed.

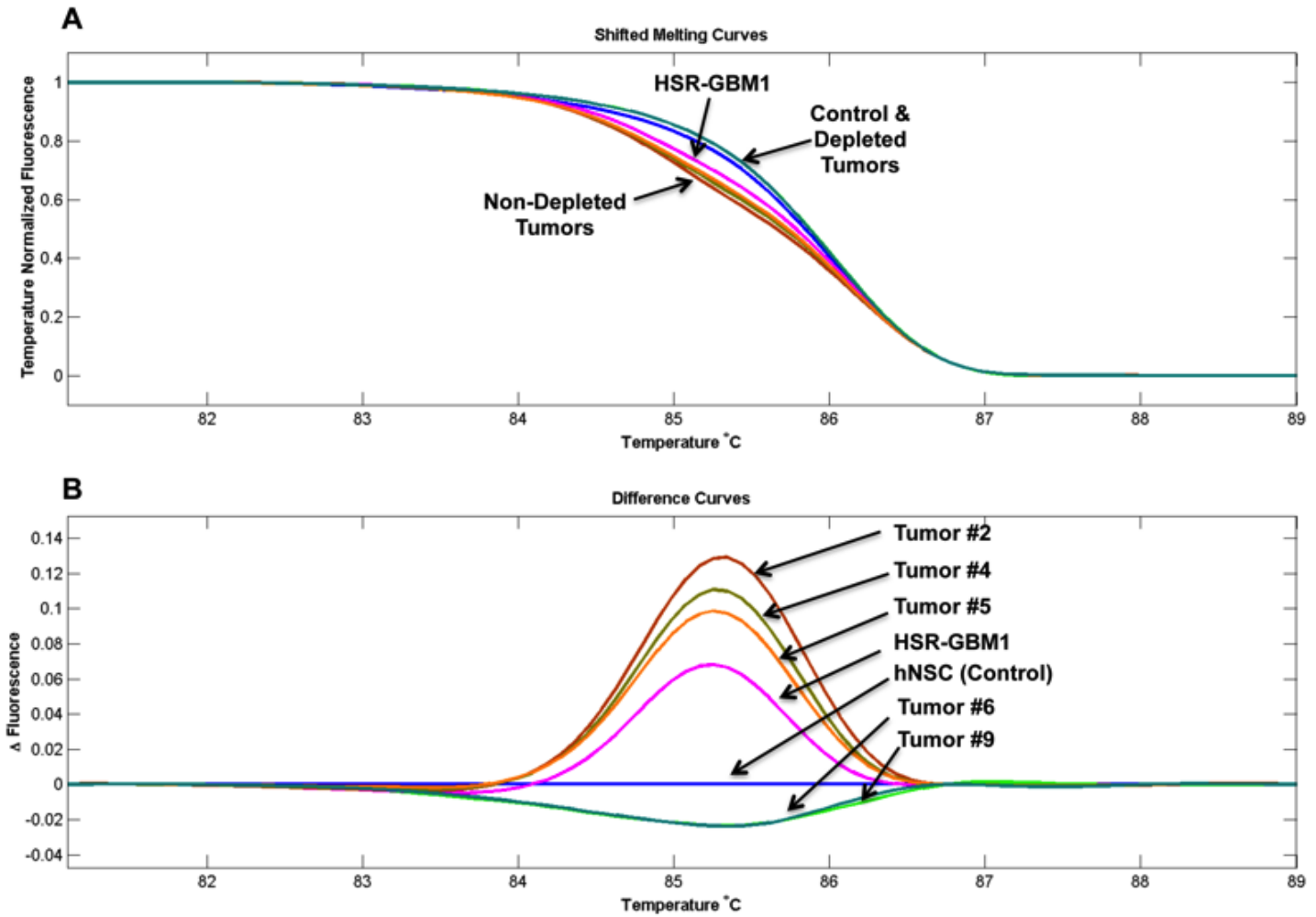

Figure 5.12. HRM analysis of the C16218T D-Loop variant. Melting curve profiles of hNSCs and HSR-GBM1 cells and derived tumors (A). Difference curve analysis of hNSCs and HSR-GBM1 cells and derived tumors (B).

5.7 Discussion

5.7.1 MtDNA depletion and tumorigenicity of HSR-GBM1 cells

Previous studies investigating the effects of mtDNA depletion on tumorigenicity have provided contrasting results (Amuthan et al., 2002; Cavalli et al., 1997; Kulawiec et al., 2009b; Magda et al., 2008). *In vivo* tumor formation assays are a robust test of tumorigenicity. However, not all of the mtDNA depletion studies cited above utilized these assays and instead employed *in vitro* techniques such as colony formation and matrigel migration assays. This may have contributed to the conflicting reports regarding the tumorigenicity of mtDNA depleted tumor cells. In order to appropriately address how mtDNA depletion influences HSR-GBM1 cell tumorigenicity, GBM cells were depleted of mtDNA using the mtDNA specific depletion agent, ddC, and *in vivo* tumor formation assays were performed.

The depletion of mtDNA to very low levels (0.2%) in HSR-GBM1 cells resulted in a considerable reduction in tumor formation rate. The reduction in tumor growth rate correlated with the number of proliferating cells present in 0.2% mtDNA tumors, which was considerably lower than that of tumors containing 100% mtDNA. These outcomes strongly suggest that mtDNA plays a role in the maintenance of tumorigenicity of HSR-GBM1 cells. Indeed, HSR-GBM1 cells containing 50% mtDNA formed tumors at a slightly quicker rate than 100% mtDNA cells. This is in agreement with the pre-inoculation data presented in *Chapter 4*, which showed that HSR-GBM1 cells depleted for a short period (7 days) contained elevated mtDNA copy number (See Section 4.6.6) and

expressed higher levels of NSC markers (See Section 4.6.7) once ddC was removed from the culture media. Furthermore, higher expression levels of NSC markers are associated with greater GBM tumorigenicity and malignancy (Ma et al., 2008). Collectively, these results suggest that partial mtDNA depletion may enhance HSR-GBM1 cell tumorigenicity. However, as the extent of mtDNA depletion increases beyond 20% of basal levels the tumor formation rates of HSR-GBM1 cells decreases, with 3% and 0.2% mtDNA HSR-GBM1 cells forming tumors at a significantly reduced rate compared to 100% mtDNA cells. In addition, copy number analysis revealed that tumors generated from 50%, 20%, 3% and 0.2% mtDNA HSR-GBM1 cells recovered their mtDNA copy number to levels that were comparable to 100% mtDNA tumors. In summary, these outcomes strongly suggest that the maintenance of mtDNA copy number is important for HSR-GBM tumor formation and it is likely that the reestablishment of the mtDNA set point is required for HSR-GBM1 cells to establish tumors. Further evidence that mitochondria are an important aspect of tumorigenicity was reported by Skrtic et al, who demonstrated that inhibition of mitochondrial translation restricted tumor formation in acute myeloid leukemic cells (Skrtic et al., 2011). Collectively, these outcomes suggest that mtDNA content and mitochondrial function is essential for the maintenance of tumorigenicity.

5.7.2 Gene expression analysis

Gene expression patterns between the 100% and 0.2% mtDNA depleted HSR-GBM1 cell tumors was highly variable. No clear trends were identifiable regarding changes in expression of factors associated with tumorigenicity.

NESTIN, OCT4 and *hTERT* expression was elevated in HSR-GBM1 tumors whilst expression in *MUSASHI1*, *NANOG* and *c-MYC* was reduced. It is possible to draw comparisons to a previous study by Holmberg *et al.* who reported differential expression of NSC and pluripotency factors between *in vivo* and *in vitro* glioma cells (Holmberg et al., 2011). Furthermore, the variability in the gene expression profiles observed between 100% mtDNA and 0.2% mtDNA tumors shows that despite inoculating immunocompromised mice with what is assumed to be a homogenous population of cells, variable gene expression was observed. It is likely that the observed differences in gene expression are associated with the extent of mtDNA depletion prior to inoculation into immunocompromised mice.

Tumor #6 showed considerable increases in *CD133, OCT4, hTERT* and *SHH*. However, tumor #6 failed to reach the 1000mm^3 end point for tumor harvest and thus was never fully established. Since all of the other tumors that fully formed showed differential gene expression profiles relative to tumor #6, it is likely that the irregular gene expression shown in this tumor, such as the up-regulation of both pluripotency (*OCT4*) and differentiation (*GFAP*) markers, may have disrupted tumor formation. Indeed, the coordinated expression of stem cell factors may be required for HSR-GBM1 cells to form tumors. Indeed, ESCs, which also express the stem cell factors *OCT4, NANOG, SOX2* are able to form teratomas (tumors containing normal cell types of the primary germ layers). However, it is also possible that tumor #6 is an experimental anomaly and the outcomes observed may be unreliable in comparison to tumors that fully established. Unfortunately, due to time limitations of my study, further

experimental replicates could not be performed to resolve the observed outcomes and requires further investigation.

5.7.3 Analysis of mtDNA variants

Previous work in the laboratory identified multiple mtDNA variants in HSR-GBM1 cells (Ka Yu Yeung, personal communication). One variant found within the D-loop, C16218T, which was identifiable by Sanger sequencing, was analyzed in both *in vitro* cultured HSR-GBM1 cells and tumors formed from 0.2% and 100% mtDNA HSR-GBM1 cells. HRM analysis suggested that the D-loop variant was present at variable levels within 100% mtDNA tumors. These results provide some evidence that the accumulation or loss of mtDNA variants may occur randomly and is thus, tumor specific. It is also likely that following therapeutic intervention, specific mtDNA variants may be selected for during the reestablishment of mtDNA copy number and may promote chemo-resistance and the reestablishment of tumors. However, evidence linking mtDNA variants to chemo-resistance is currently lacking.

The HRM curve analysis of 0.2% tumors showed similar profiles to wild type mtDNA (hNSCs), which suggests that during the depletion process *in vitro*, the D-loop variant was reduced and not reestablished during mtDNA copy number recovery *in vivo*. It is reasonable to speculate that tumor cells containing altered mtDNA genotypes may possess different growth and chemo-resistant properties, which may influence the tumorigenicity of HSR-GBM1 cells and requires further investigation.

5.8 Conclusion

The outcomes of this chapter identify a clear relationship between mtDNA copy number and tumor formation rate in HSR-GBM1 cells. Extensive depletion (>20%) of mtDNA results in reduced tumor formation rate. The analysis of tumors formed from mtDNA depleted HSR-GBM1 cells also shows a recovery of mtDNA copy number, to a level that is similar to non-depleted HSR-GBM1 cell tumors. I hypothesize that HSR-GBM1 cells are required to reestablish their mtDNA set point in order to maintain their tumorigenic potential. It is likely that this process occurs during the tumor development lag phase that was observed for 3% and 0.2% mtDNA tumors. In conclusion, the maintenance of mtDNA copy number is essential for HSR-GBM1 cells to maintain their tumorigenic potential.

Chapter 6: The derivation of 143BTK- and HSR-GBM1 trans-mitochondrial cybrids

6.1 Introduction

The data presented in Chapters 4 and 5 strongly suggest that changes in mtDNA copy number can elicit strong influences on the gene expression profiles and tumorigenicity of HSR-GBM1 cells. These outcomes also provide strong evidence that mtDNA copy number plays a role in nuclear-mtDNA crosstalk.

Germline mtDNA mutations are associated with mitochondrial diseases and diabetes, amongst others (Wallace, 1999; Wallace, 2005), whilst the accumulation of somatic mtDNA mutations has been more recently linked to cancer. MtDNA mutations are deleterious when mutant load is high and this is evidenced in the neuropathic and myopathic mtDNA disorders, NARP (Holt et al., 1990), MELAS (Schon et al., 1992) and LOHN (Holt et al., 1989), which are caused by single point mutations. In contrast, tumor cells have been shown to posses multiple mtDNA variants (Kirches et al., 2001; Liu et al., 2001; Polyak et al., 1998; Wong et al., 2003) at a frequency of ~70% and these are likely to cause cellular dysfunction in a similar manner to single point mutations, providing the mutant loading is sufficient. Since changes in mtDNA copy number alone are capable of inducing changes in gene expression and tumorigenicity HSR-GBM1 cells, it is likely that single or multiple mtDNA variants can also alter cellular function and the regulation of mtDNA copy number, which may in turn influence tumorigenic potential. Indeed, there is

evidence to suggest that the accumulation of mtDNA variants is associated with mitochondrial dysfunction and elevated ROS production (Lee and Wei, 1997). Furthermore, ROS have been implicated in the regulation of cell proliferation and apoptosis, which may act as a stimulus for tumorigenic transformation (Levine and Puzio-Kuter, 2010).

In order to study how the mtDNA of tumor cells affect cellular function, metabolism and tumorigenesis, researchers have utilized trans-mitochondrial cybrid technology. Trans-mitochondrial cybrids are hybrid cells, generated by the fusion of ρ0 cells (devoid of mtDNA) with enucleated cytoplasts containing donor mitochondria and mtDNA (King and Attardi, 1989). Cells lines have been depleted of mtDNA by long-term treatment with ethidium bromide or short-term exposure to Rhodamine 6G (R6G), a mitochondrial poison (Trounce and Wallace, 1996), and subsequently repopulated with the desired mtDNA genotype. Cybrids generated by this method commonly utilize an identical nuclear background, which allows the investigation of how different mtDNA populations interact with the nuclear genome.

The majority of trans-mitochondrial cybrids have been derived using cancer cells containing a common nuclear background such as the osteosarcoma cell line, 143BTK- (Bonora et al., 2006; Ma et al., 2010). The 143BTK- cell line is deficient in thymidine kinase (TK) and was derived using a similar technique to that described by Kit et al. which involved long-term culture in media containing high concentrations (25-50 μg/ml) of bromo-deoxyuridine (BrdU) (Kit et al., 1963). 143BTK- cells are resistant to BrdU and can be successfully propagated

in media containing BrdU (25-50 µg/ml). This contrasts with TK+ cells, which are sensitive to similar concentrations of BrdU (McKenzie and Trounce, 2000). BrdU sensitivity provides an excellent selection marker during the trans-mitochondrial cybrid derivation by which non-enucleated mitochondrial donor cells are selectively killed in BrdU supplemented media (McKenzie and Trounce, 2000). TK activity also provides an additional selection marker when culture media is supplemented with hypoxanthine-aminopterin-thymidine (HAT). Aminopterin blocks *de novo* DNA synthesis (Kennett 1979), which is required for cell division, however, hypoxanthine and thymidine provide the necessary substrates for DNA synthesis to continue through functional TK (Harlow and Lane, 1988; Freshney, 1994). Cells containing functional TK enzyme are therefore able to perform DNA synthesis and survive. Since 143BTK- cells are TK deficient, they are unable to perform DNA synthesis in HAT +VE media and subsequently perish over time (McKenzie et al., 2004).

An advantage of generating trans-mitochondrial cybrids using transformed cells is that, unlike primary cell lines, which enter senescence following multiple passages, transformed cell lines are essentially immortal. Thus, the generated cybrids provide an abundant cellular source for experimentation. The repopulation of cancer cells with mtDNA harboring the point mutations T8993G, G13997A and G15557A, amongst others, were shown to increase ROS production, promote xenograft tumor growth and metastasis and reduce ETC activity (Bonora et al., 2006; Ishikawa et al., 2008; Petros et al., 2005; Shidara et al., 2005). These outcomes demonstrate that mtDNA mutations are capable of inducing diverse changes in tumor cells. However, the effect of mtDNA

mutations on copy number in a common nuclear background has yet to be determined.

To date, very little is known regarding how mtDNA mutations impact on cellular differentiation. The majority of cybrid cells lines are derived from tumor cells that do not undergo differentiation and is one possible shortcoming of cell lines such as 143BTK-. However, there are some reports of multipotent cybrid cell lines. In 2004, McKenzie et al. derived cybrids from murine ESCs (McKenzie et al., 2004). In this study, murine ESCs were depleted of mtDNA with R6G, and repopulated with mtDNA from the domestic mouse (*Mus Musculus Domesticus*), which is referred to hereafter as wild type, and mtDNA two divergent species, *Mus spretus* and *Mus dunni* (otherwise known as *Mus terricolor)*. ESCs containing *Mus spretus* and Mus *dunni* exhibited characteristics of mitochondrial dysfunction with increases in lactate production when compared to ESCs containing wild type mtDNA. This study demonstrated that pluripotent cells could be utilized to generate cybrids models of mitochondrial dysfunction and provided a rationale to investigate the role of mtDNA mutations in cellular differentiation. Recently, a study by Kelly et al. utilized the afore mentioned ESC cybrids and examined how divergent populations of mtDNA impacted the maintenance of pluripotency and differentiation (Kelly et al., 2013). Compared to wild type ESCs, ESCs containing divergent mtDNA were shown to differentially express pluripotency factors and lineage specific markers during differentiation (Kelly et al., 2013). This study provided evidence that divergent populations of mtDNA are able to

influence the maintenance of stemness and also cellular differentiation of stem cells.

HSR-GBM1 cells are a transformed cell line that exhibits multipotent properties. HSR-GBM1 cells therefore provide an excellent cell source to generate a multipotent cybrid cell lines harboring altered mtDNA backgrounds or genotypes. HSR-GBM1 cybrids would also provide an opportunity to investigate how modifying the mtDNA background of a cell alters gene expression profiles and differentiation potential. In addition, it remains to be determined how changes to mtDNA genotype impact on the maintenance of a cancer stem cell-like phenotype and cellular differentiation.

6.2 Hypothesis

I hypothesize that the introduction of different mtDNA genotypes into a common nuclear background (143BTK-) will result in variable mtDNA copy number levels by inducing differential interactions between nuclear and mitochondrial genomes. Using the same rationale, I hypothesize that changes to the mtDNA genotype of HSR-GBM1 cells will induce changes in gene expression and alter the differentiation profile of HSR-GBM1 cell cybrids.

6.3 Aims

- To derive mtDNA donor cell lines through the fusion of 143BTK- ρ0 cells with enucleated hNSCs, HSR-GBM1, GBM-L1 and GBM-L2 cells
- Assess the mtDNA copy number of 143BTK- cybrids

- To derive of HSR-GBM1 cybrids containing HSR-GBM1 and hNSC mtDNA
- To assess the differentiation potential of HSR-GBM1 cybrids

6.4 Materials and methods

6.4.1 Cell lines

Osteosarcoma cells (143BTK-), hNSCs, HSR-GBM1, GBM-L1 and GBM-L2 cells were routinely cultured, as described *Cell culture* (Sections 2.2.3-2.2.5) until sufficient numbers were available for experiments.

6.4.2 Enucleation of mtDNA donor cells

3 x 10^6 hNSCs, HSR-GBM1, GBM-L1 and GBM-L2 cells were collected and each resuspended in 10 ml of SD-DMEM (see Section 2.2.5) and gently mixed with 10 ml pre-warmed (37^{o}C) Percoll solution (Sigma), 200 μl Penicillin/Streptomycin, 2 mg/ml cytochalasin B (2 mg/ml; Sigma) and transferred to 50 ml Nalgene high-speed centrifuge tubes (Nalgene, Waltham, MA, USA). Cells were enucleated by centrifugation at 20,000 rpm using a SS-34 fixed angle rotor (Thermo) for 70 minutes at 27^{o}C. Following centrifugation, the interface (7.5 ml) containing both enucleated cytoplasts and non-enucleated cells was transferred to 15 ml tubes. 7.5 ml of fresh SD-DMEM was added and gently mixed to the cell suspension to dilute the remaining Percoll and centrifuged for 5 minutes at 4,400 rpm. The supernatant was removed and the cell pellets were resuspended in 10 ml SD-DMEM prior to cell fusion.

1 x 10^6 143BTK-$^{\rho 0}$ cells were used per fusion. 143BTK-$^{\rho 0}$ cells were resuspended in 10 ml SD-DMEM and mixed with the 10 ml cell suspensions of hNSCs, HSR-GBM1, GBM-L1 and GBM-L2 cells and transferred to clean 50 ml Nalgene high-speed centrifuge tubes. The cell suspension was centrifuged at 10,000 rpm using a SS-34 fixed angel rotor for 10 minutes at 27^{o}C. The

supernatant was carefully removed from the cell pellet. To initiate cell fusion, cell pellets were covered with 500 μl of cell culture grade polyethylene glycol (PEG; Sigma) for exactly 1 minute. PEG was removed immediately and the cell pellet was gently resuspended in 10 ml of SD-DMEM.

6.4.3 Trans-mitochondrial cybrid selection

Intact cells (143BTK-$^{\rho 0}$) were plated at a density of 2.5 x 10^5, 1 x 10^5 and 5 x 10^4 cells per 100mm culture dish in SD-DMEM for 24 hours at 37^{o}C with 5% CO_2/95% humidity. After 24 hours, the media was substituted for CSM, which consisted of RPMI medium (Gibco), 2 mM Glutamax, 5% dFBS, 1% Penicillin/Streptomycin and BrdU (50 mg/ml). In this selection medium, free of uridine and sodium pyruvate, only 143BTK-$^{\rho 0}$ cells that have received functional mitochondria and mtDNA from cytoplast donors (hNSC and GBM cell lines) were able to survive by reestablishing a functional respiratory chain. Non-fused 143BTK-$^{\rho 0}$ cells are auxotrophic for uridine and sodium pyruvate and do not propagate under these conditions. Non-enucleated hNSCs and GBM cells are thymidine kinase positive (TK+) and are sensitive to the high concentrations of BrdU (50 mg/ml). At this concentration, TK+ cells do not survive and propagate under these conditions. In contrast, 143BTK-$^{\rho 0}$ cells are deficient in thymidine kinase (TK-) and are resistant to BrdU exposure. After 7 to 14 days, cell colonies began to emerge and propagate in the CSM. The colonies were expanded and passed using standard protocols, as described in *Culture of osteosarcoma cells* (Section 2.2.5) and were continued to be cultured in CSM to ensure that there was no carry over of hNSCs and GBM cells. Cell samples were collected after each passage for analysis.

6.4.4 MtDNA genotyping

In order to confirm that the desired mtDNA population had been successfully transferred into the recipient 143BTK-$^{\rho 0}$ cells, total DNA was extracted from both the mtDNA donor cells and the putative 143BTK- cybrids. Extracted DNA was used to amplify a 1200 bp fragment of the D-loop region of mtDNA using conventional PCR. PCR reactions were performed, as described in *PCR* (Section 2.5.3) with D-loop primers, as described in Section 5.5.6. PCR products were resolved on 2% agarose gels, excised and purified as described in *Gel electrophoresis* and *PCR product purification* (Sections 2.5.4 & 2.5.5). Purified PCR products were quantified by spectrophotometry, as described in *Quantification of nucleic acids* (Section 2.4.5) prior to capillary sequencing.

Samples were processed through the Gandel Charitable Trust Sequencing Centre service. Sequencing reactions consisted of 100 ng of purified PCR product (1-6 μl), 1 μl hD-Loop Primers (312 nM) and dH_2O to a volume of 16 μl. Reactions were performed using the automated Applied Biosystems 3130xl Genetic Analyzer and the Applied Biosystems BigDye Terminator 3.1 reaction kit, as described in *DNA Sequencing* (Section 2.5.6). Sequencing output files were analyzed for sequence read quality using the sequence viewer software, 4 Peaks (v1.7.1) (mekentosj.com). hNSC, HSR-GBM1, GBM-L1 and GBM-L2 D-loop sequences were used as references for the generation 143BTK- cybrids and were aligned using the ClustalW2 alignment software tool (EMBL, Germany). For example, the D-loop sequence of hNSC cells was aligned against the D-loop sequence of 143BTK-^{NSC} cells. The generation of the

143BTK-^{NSC} cybrid was deemed to be successful if 100% homology between the D-loop sequences (hNSC & 143BTK-^{NSC}) was observed. This D-loop sequence comparison was performed for each of the 143BTK- cybrids. 143BTK- cybrid cell lines are referred to hereafter as 143B-TK-^{NSC}, 143BTK-^{GBM}, 143BTK-^{GBML1} and 143BTK-^{GBML2}.

6.4.5 Generation of trans-mitochondrial cybrid (HSR-GBM1) cell lines

143BTK-^{NSC} and 143BTK-^{GBM} were routinely cultured, as described in *Culture of osteosarcoma cells* (Section 2.2.5). 3 x 10^6 cells of each cell line were enucleated, as described above (Section 6.5.2) with the exception that the pelleted cytoplasts were resuspended in 10 ml of StemPro Complete Medium prior to cell fusion.

HSR-GBM1 cells were routinely cultured, as described in *Culture of GBM cell lines* (Section 2.2.5) with exception that R6G (2 µg/ml) and uridine (50 mg/ml) were added daily for 72 hours prior to cell fusion. R6G is a mitochondrial poison and was utilized to disrupt mitochondrial function and deplete HSR-GBM1 cells of mtDNA. After 72 hours HSR-GBM1 cells were harvested and cell counts performed. 1 x 10^6 HSR-GBM1 cells were used per cell fusion. HSR-GBM1 cells were resuspended in 10ml of StemPro Complete Medium and gently mixed with the cell suspension of either 143BTK-^{NSC} or 143BTK-^{GBM} cells (fusion control). The cell fusion process was performed, as described above in (Section 6.5.2).

Intact HSR-GBM1 cells were plated at a density of 1 x 10^6 cells per 100mm dish. The 100mm dishes were pretreated with laminin (Section 2.2.2) to promote attachment of HSR-GBM1 cells. Cells were incubated for 24 hours.

After 24 hours, the media was substituted for neural cybrid selection medium (NCSM), which consisted of DMEM (2g/litre) medium, 2 mM Glutamax, 2% (v/v) StemPro neural supplement, 1x HAT supplement (Invitrogen), bFGF (20 ng/ml), EGF (20 ng/ml). NSCM media contained no sodium pyruvate or uridine in order to promote the survival of only HSR-GBM1 cells that received cytoplast donors. The rationale of pretreating the culture plates was to improve the monitoring of cell viability following the fusion process, which proved difficult when culturing in suspension. After 72 hours of monolayer culture, HSR-GBM1 cells were detached using Accutase and re-plated in low attachment plates to promote neurosphere formation.

HSR-GBM1 cells that do not receive cytoplast donors containing functional mitochondria and mtDNA do not survive and propagate in NCSM in the absence of sodium pyruvate and uridine, due to R6G induced mitochondrial dysfunction (See Figure 6.4). The addition of HAT supplement blocks *de novo* DNA synthesis (Kennett 1979) and selects against 143BTK- cells (McKenzie et al., 2004) (Figure 6.6 and see *Trans-mitochondrial cybrid selection;* Section 6.5.4 and *Culture of osteosarcoma cells;* Section 2.2.5) whilst HSR-GBM1 cells that receive cytoplast donors are able to propagate through the successful transfer of functional mitochondria.

Putative HSR-GBM1 neurospheres were cultured for a further 7 days in NSCM before re-plating onto laminin treated 100mm culture dishes. The rationale for re-plating HSR-GBM1 cells was to assist in the removal of dead cells, since viable cells would adhere to the cell culture plastic whilst dead cells float and

could be removed by the changing of media. Very few neurospheres attached to the cell culture plastic, however, small colonies propagated over time (See Figure 6.5) and were referred to as HSR-GBM1 cybrids. HSR-GBM1 cells that were fused with 143BTK-^{GBM} cells are referred to hereafter as HSR-HSR cells and HSR-GBM1 cells fused with 143BTK-^{NSC} cells as HSR-NSC cells.

HSR-HSR and HSR-NSC cells were cultured in monolayer for an additional 72 hours in NSCM to increase cell numbers. After 72 hours the cells were detached using Accutase and then routinely cultured. Once sufficient cell numbers were available, the mtDNA genotypes of HSR-HSR and HSR-NSC cells were determined using the protocols described above in *MtDNA genotyping* (Section 6.5.5). The mtDNA genotypes of HSR-HSR and HSR-NSC cells were compared to that of hNSCs and HSR-GBM1 cells (See Figure 7) to determine if hNSC mtDNA had been successfully transferred into HSR-GBM1 cells. HSR-GBM1 cells and HSR-GBM1 cybrids were differentiated for up to 28 days, as described in *Differentiation of GBM cell lines* (Section 2.3.2).

6.4.6 MtDNA Copy Number Analysis

MtDNA copy number of 143BTK- cybrids, HSR-GBM1 cybrids and mtDNA donor cell lines was determined by real-time PCR, as described in *MtDNA copy number analysis* in the *General Materials and Methods* (Section 2.6.4).

6.4.7 Gene expression Analysis

Gene expression was determined by real-time PCR, as described in *Gene expression analysis* in the *General Materials and Methods* (Section 2.6.3).

Primer pairs, annealing and secondary acquisition temperatures are listed in Table 4.I (*Chapter 3;* Section 3.5)

6.4.8 Cellular respiration

Cellular respiration analyses of 143BTK- trans-mitochondria cybrids, HSR-GBM1 cybrids (undifferentiated and differentiated for 14 & 21 days) and mtDNA donor cell lines was performed using the Oxygraph-2K system, as described in *Cellular respiration* in the *General Materials and Methods* (Section 2.7.1).

6.4.9 Total ATP content and lactate production

Total ATP content and lactate production were determined using luminescence and fluorescence based assays, as described in *Measurement of total cellular ATP content* and *Measurement of cellular lactate production* in the *General Materials and Methods* (Section 2.8).

6.4.10 Statistical analysis

Statistical analysis was performed, as described in *Statistical analysis* in the *General Materials and Methods* (Section 2.11).

6.5 Preliminary experiments

6.5.1 Confirmation of the sensitivity of 143BTK-$^{\rho 0}$ cells to uridine and pyruvate –VE media

143BTK-$^{\rho 0}$ cells are devoid of mtDNA and thus lack a respiratory chain. 143BTK-$^{\rho 0}$ cells require uridine and pyruvate supplementation in order survive. This characteristic of 143BTK-$^{\rho 0}$ cells is an excellent selection marker during the generation of trans-mitochondrial cybrids. The removal of uridine and pyruvate from the culture media selects for cells that have accepted donor mtDNA from cytoplasts, which will survive by generating uridine and replenishing NADH stocks through the reestablishment of a functional respiratory chain. To test whether the 143BTK-$^{\rho 0}$ cells utilized in this chapter were sensitive to uridine and pyruvate withdrawal, 143BTK-$^{\rho 0}$ cells were cultured in a low glucose selection media cybrid selection media (CSM; see Materials and Methods above) without uridine and pyruvate and monitored for 12 days. 143BTK-$^{\rho 0}$ cells appeared normal after the first day of culture and showing signs of proliferation (rounded and glowing cell bodies) with no gross changes in morphology observed (Figure 6.1A). On Day 3 of culture, 143BTK-$^{\rho 0}$ cells began to exhibit a broadened morphology (Figure 6.1B). By Day 6, there was some cell death (Figure 6.1C) and a lack of cell proliferation and this continued through to Day 12 (Figure 6.1D), with few cells of abnormal morphology remaining. These outcomes demonstrate that 143BTK-$^{\rho 0}$ cells do not thrive and proliferate when cultured in CSM.

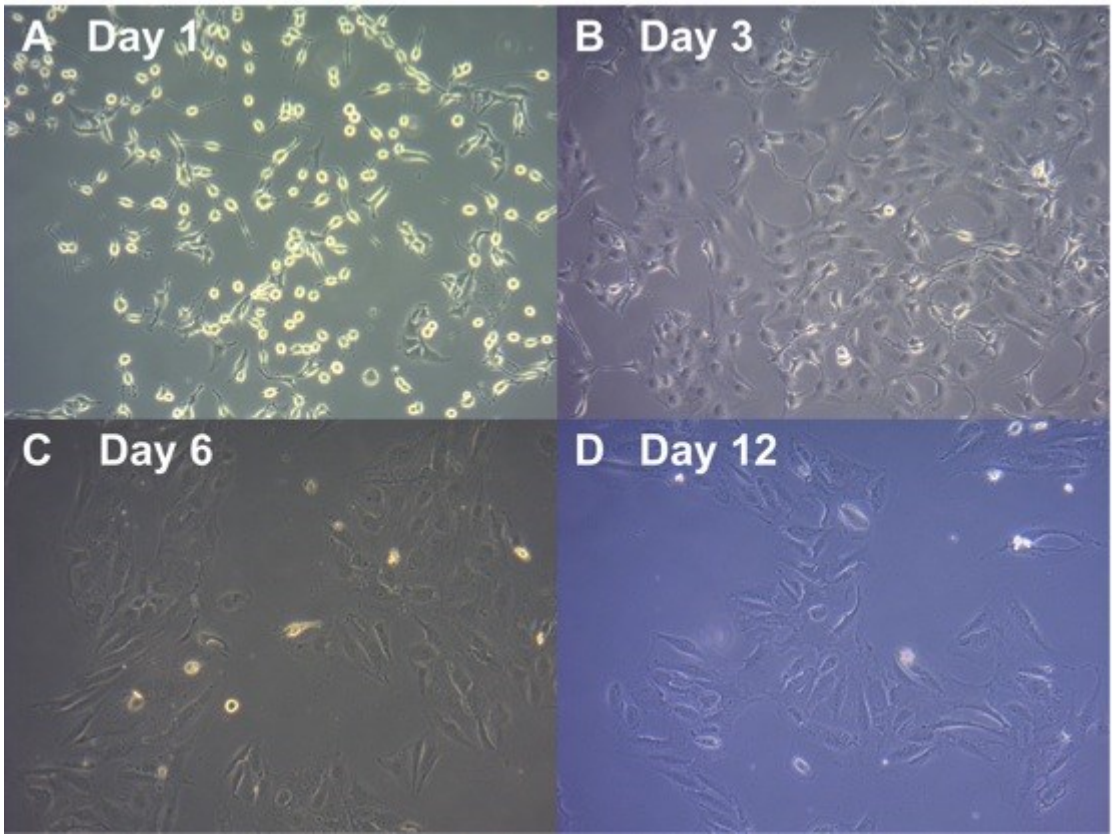

Figure 6.1. Phase-microscopy analysis of 143BTK-$^{\rho 0}$ cells cultured in uridine and pyruvate free media for 12 days at X10 magnification. Day 1 (A), Day 3 (B), Day 6 (C) and Day 12 (D).

6.5.2 Survival of trans-mitochondrial cybrids in selection media

To confirm that cybrids generated from the fusion 143BTK-$^{\rho 0}$ cells with donor cytoplasts could survive in CSM (see Materials and Methods above), a cell fusion was performed and the culture was monitored for 10 days. 10 days after the fusion process cell colonies began to emerge (Figure 6.2A) and demonstrated that trans-mitochondrial cybrids could survive and thrive under selection conditions. Continued expansion of the identified colony was observed after a further 24 hours of culture (Figure 6.2B).

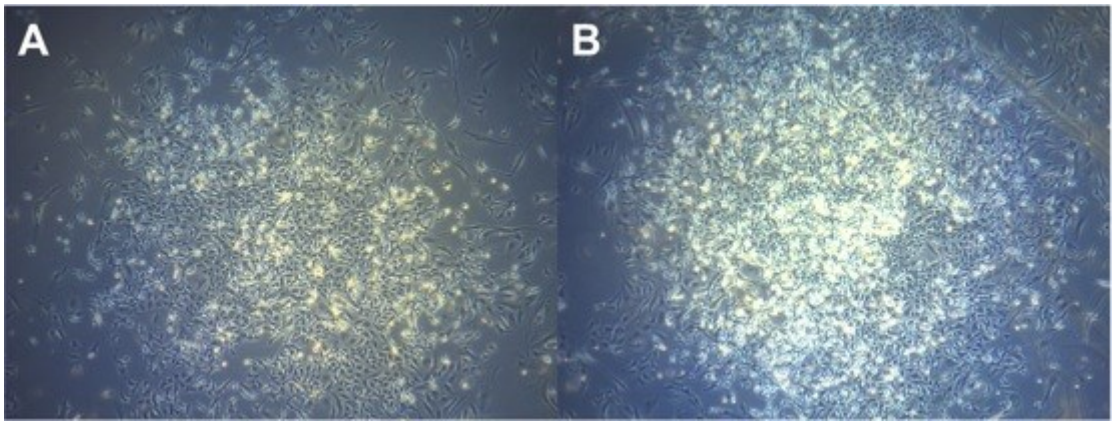

Figure 6.2. Emergence of a trans-mitochondrial cybrid colony cultured in CSM after 10 days (A) and 11 (B) days at X10 magnification.

6.5.3 Repopulation of 143BTK-$^{\rho 0}$ cells with donor mtDNA

To confirm that trans-mitochondrial cybrids had been generated following the fusion of 143BTK-$^{\rho 0}$ cells with donor cytoplasts, the D-loop region of 143BTK-^{NSC} & 143BTK-^{GBM} cells was amplified by conventional PCR. No PCR product was generated using the DNA template of 143BTK-$^{\rho 0}$ cells, confirming the absence of mtDNA in this cell line (Figure 6.3A). The PCR reactions of 143BTK-$^{\rho 0}$ cells fused with hNSC and HSR-GBM1 cytoplasts (143BTK-^{NSC} & 143BTK-^{GBM}) yielded D-loop PCR products (Figure 6.3A). D-loop PCR was also performed on a donated cybrid cell line, 143BTK-^{3243}, to confirm the presence of mtDNA. To confirm that the 143BTK-$^{\rho 0}$ cells had been repopulated with the desired mtDNA, sequencing was performed on the D-loop PCR products. Sequencing readouts confirmed that the D-loop sequences of the 143BTK-^{NSC} & 143BTK-^{GBM} cells were identical to that of their mtDNA donors, hNSCs and HSR-GBM1 cells, respectively (Figure 6.3B-E). Collectively, these outcomes show that 143BTK-$^{\rho 0}$ cells were successfully repopulated with the desired mtDNA genotype.

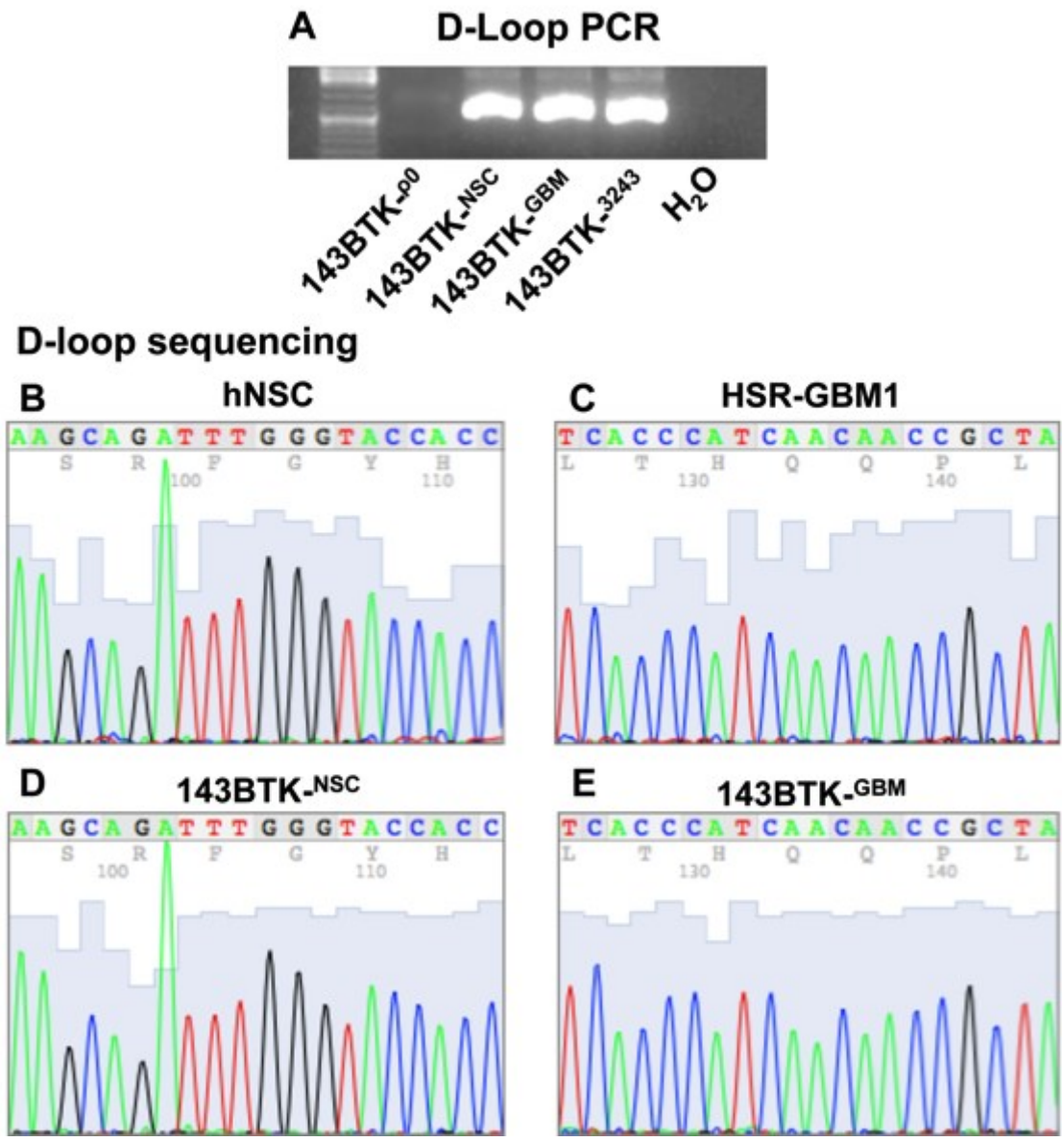

Figure 6.3. D-loop PCR of 143BTK-ρ0 cells and trans-mitochondrial cybrids (A). Sequencing of the D-loop regions of hNSC (B), HSR-GBM1 (C), 143BTK-^{NSC} (D) & 143BTK-^{GBM} cells (E).

6.5.4 R6G titration assay

To determine the optimal concentration of R6G to eliminate mitochondria in HSR-GBM1 cells, a titration assay was performed. R6G is a mitochondrial poison and was utilized to disrupt mitochondrial function and deplete HSR-GBM1 cells of mtDNA. HSR-GBM1 cells were plated as a monolayer and treated with 1 and 2 µg/ml R6G for 72 hours and monitored (Figure 6.4). 1 µg/ml R6G had very little effect on cell viability after 72 hours of culture, however, considerable cell death was observed once the culture media was changed to NCSM (Figure 6.4 C). 2 µg/ml R6G induced some cell death in HSR-GBM1 cells and the cells were at approximately 50% confluence after 72 hours of culture (Figure 6.4 B). Once more, the transfer of HSR-GBM1 cells to NCSM for 5 days resulted in very few cells surviving (Figure 6.4 C and D). As a control, HSR-GBM1 cells were cultured in NCSM without R6G for up to 72 hours. HSR-GBM1 showed no adverse effects during culture in NCSM and showed signs of proliferation (Figure 6.4 E & F). It was reasoned that using the highest possible concentration of R6G, which did not induce considerable cell death after 72 hours, would limit the likelihood of non-mtDNA depleted and non-fused HSR-GBM1 cells contaminating the cybrid selection process. Consequently, 2 µg/ml of R6G was selected for future experiments.

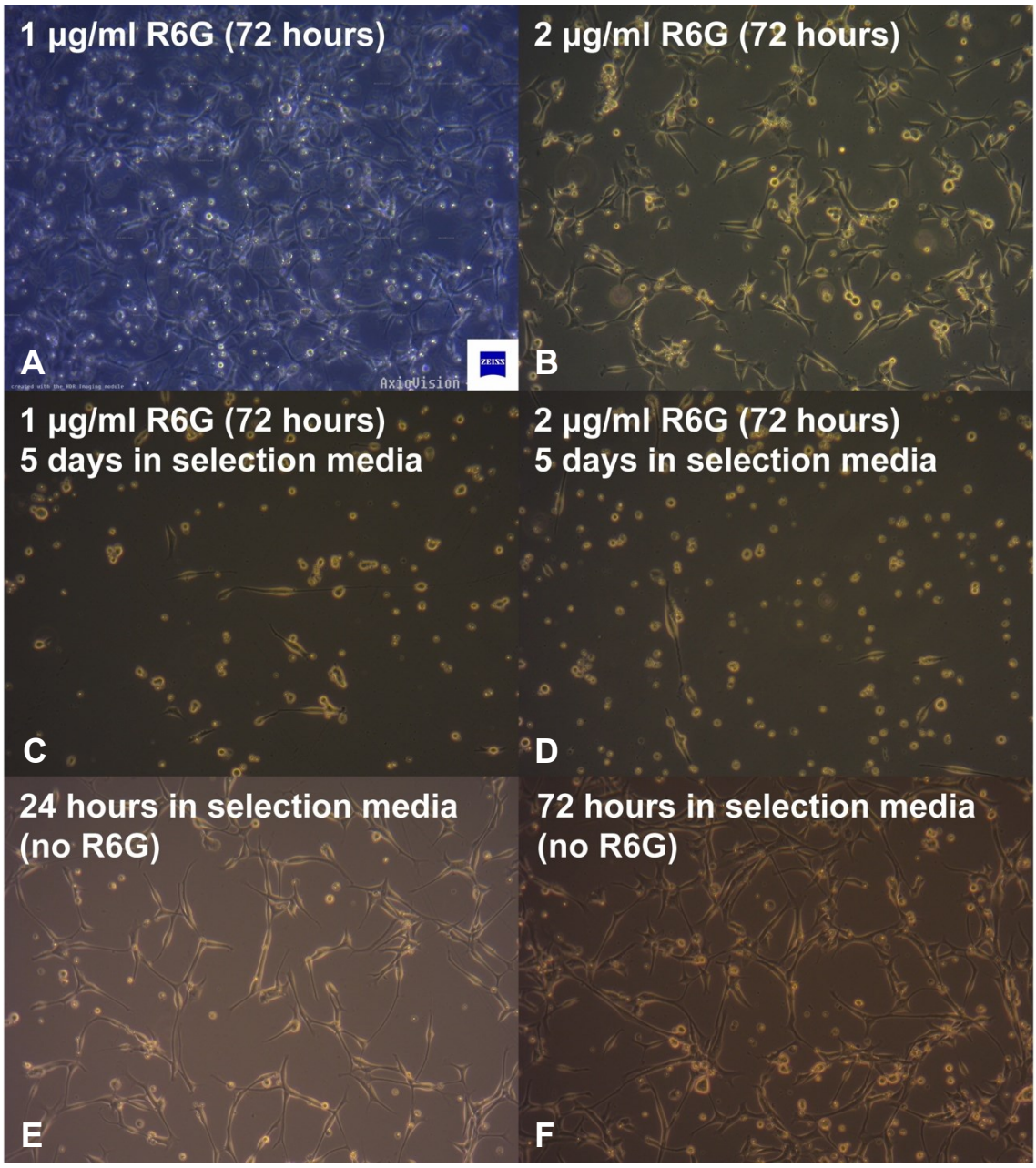

Figure 6.4. R6G titration. HSR-GBM1 cells were treated with 1 µg (A) and 2 µg (B) R6G for 72 hours. After 72 hours HSR-GBM1 cells were transferred into CSM and growth was monitored (C & D). To confirm that HSR-GBM1 cells could propagate in CSM, HSR-GBM1 cells were cultured in CSM for 24-72 hours (E & F).

6.5.5 Generation of HSR-GBM1 trans-mitochondrial cybrids

R6G treated HSR-GBM1 cells were fused with cytoplasts of 143BTK-^{NSC} and 143BTK-^{GBM} cells, as described in the Materials and Methods above. Putative HSR-GBM1 cybrids were plated onto laminin treated culture plates and were monitored. The majority of plated cells did not adhere and whilst some cells attached and established colonies (Figure 6.5 represents 17 days post fusion). These colonies propagated in CSM and were detached once sufficient cell numbers were available.

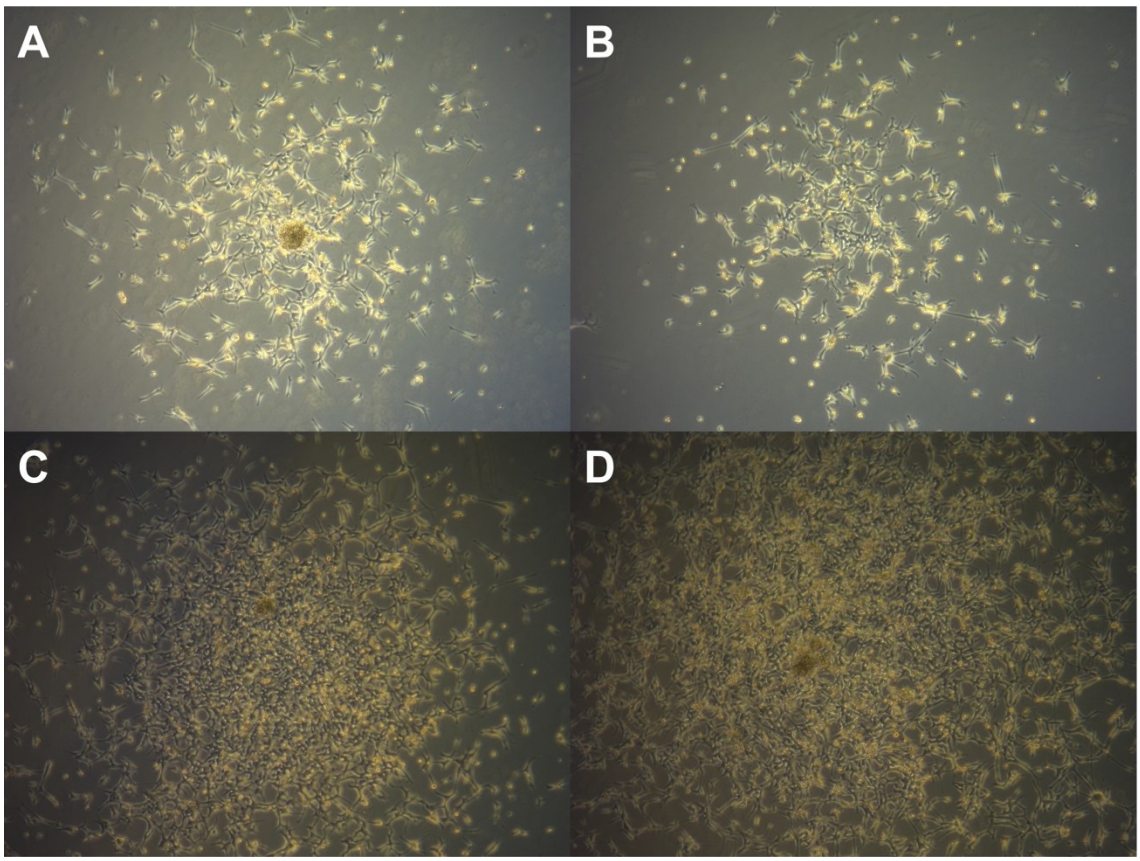

Figure 6.5. Identification of HSR-GBM1 cybrids. Monitoring of putative HSR-GBM1 cybrids using phase microscopy at X10 magnification 17 days post fusion (A & B) and 25 days post fusion (C & D).

6.5.6 Confirmation of 143BTK- sensitivity to HAT supplementation

To confirm that 143BTK- cells were sensitive to HAT supplementation, 143BTK-^{NSC} cells were cultured in SD-DMEM with 1X HAT for up to 7 days. Initially 143BTK-^{NSC} cells maintained a normal morphology at Day 0 (Figure 6.6A) and Day 3 (Figure 6.6B). However, by Day 5 143BTK-^{NSC} cells started to die (i.e. floating cells) and exhibited a broadened morphology (Figure 6.6C). By Day 7 of culture very few 143BTK-^{NSC} cells remained (Figure 6.6D). These outcomes demonstrated the sensitivity of 143BTK- cells to HAT supplementation.

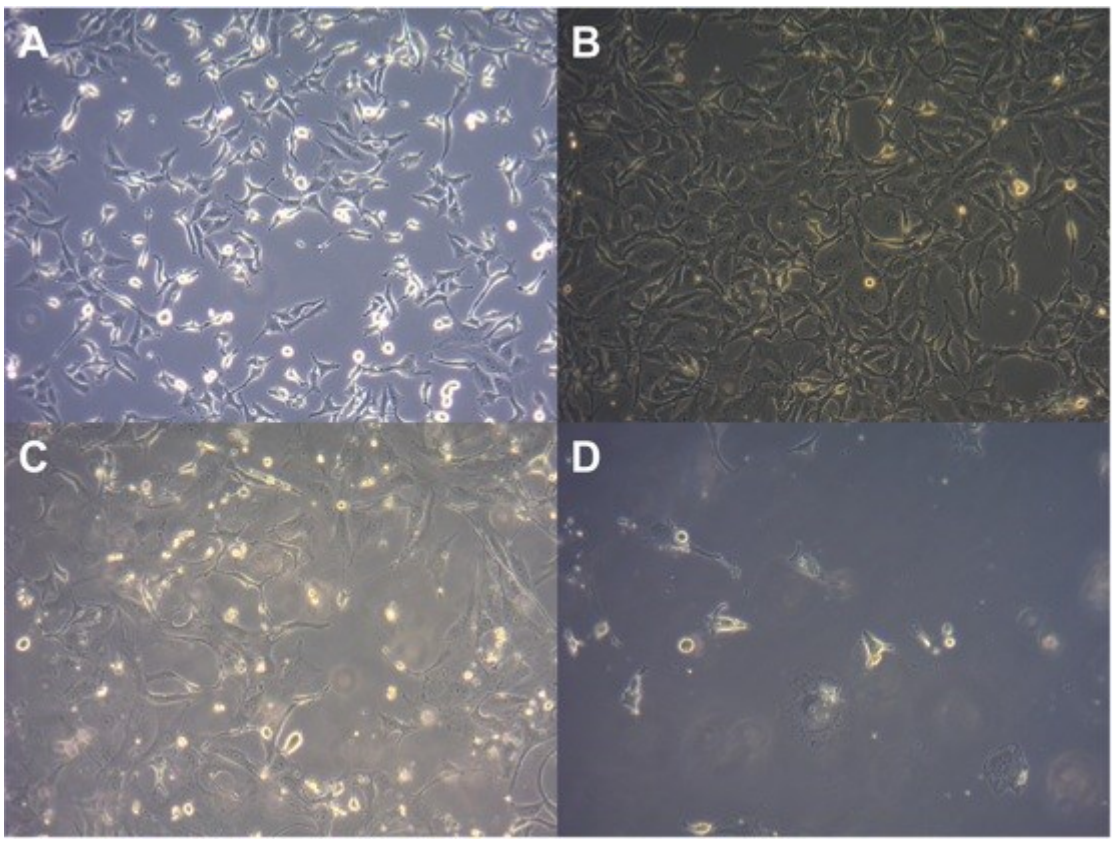

Figure 6.6 Culture of 143BTK-^{NSC} cells in HAT supplemented media for up to 7 days. Day 0 (A), Day 3 (B), Day 5 (C) and Day 7 (D). Magnification at X10.

6.5.7 MtDNA genotyping of HSR-GBM1 cybrids

HSR-GBM1 cybrids generated from the fusion of R6G treated HSR-GBM1 cells with 143BTK-^{NSC} (HSR-NSC) and 143BTK-^{GBM} (HSR-HSR) cells were subjected to mtDNA genotyping, as described in the Materials and Methods below. The D-loop sequence of HSR-HSR cells was identical to that of HSR-GBM1 cells (Figure 6.7). Interestingly, the D-loop of HSR-NSC cells contained two populations of mtDNA, or heteroplasmy. HSR-NSC mtDNA was found to be primarily of HSR-GBM1 origin, however there were low but identifiable levels of hNSC mtDNA present, as indicated by the dual fluorescent peaks in the boxed regions of the sequencing readouts (Figure 6.7).

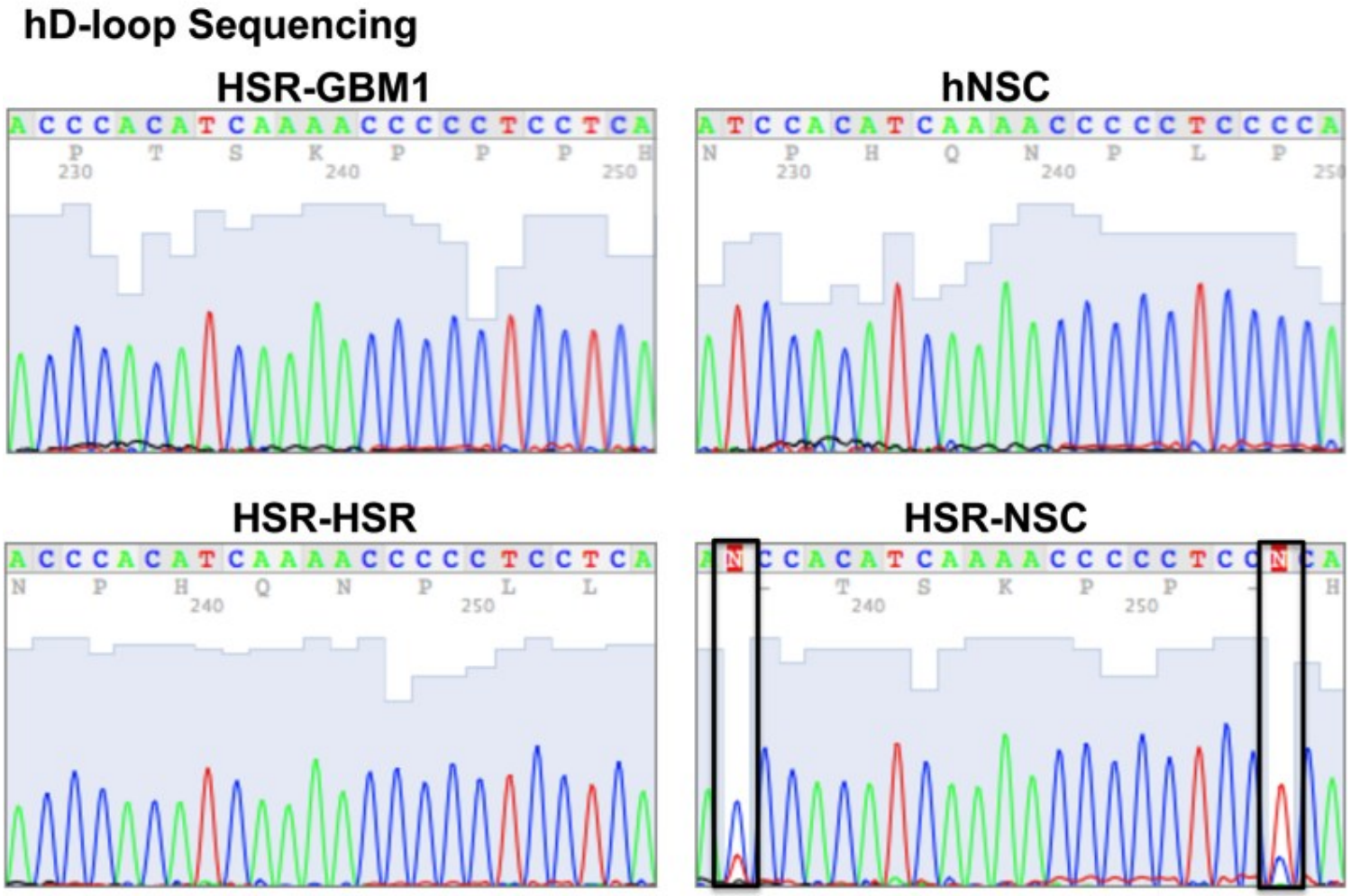

Figure 6.7. D-loop sequencing of the HSR-GBM1 cybrids, HSR-HSR and HSR-NSC. The D-loop sequences of HSR-HSR and HSR-NSC cells were compared to that of HSR-GBM1 cells and hNSCs.

6.6 Results

6.6.1 MtDNA copy number analysis of 143BTK-ρ^0 cells repopulated with donor mtDNA

To investigate how different mtDNA genotypes can influence mtDNA copy number, 143BTK-ρ^0 cells were fused with cytoplasts from hNSCs, HSR-GBM1, GBM-L1 and GBM-L2 cells to generate trans-mitochondrial cybrids. Since 143BTK-ρ^0 cells contain no mtDNA, mtDNA copy number of the trans-mitochondrial cybrids was compared to non-depleted, non-fused, 143BTK-ρ^+ cells and these values were used as an indicator of the mtDNA copy number set point of 143BTK- cells.

The mtDNA copy number of 143BTK-^{NSC} cells was comparable to that of 143BTK-ρ^+ cells whilst 143BTK-^{GBM} cells showed a 1.25-fold increase ($p<0.01$) in copy number relative to 143BTK-ρ^+ cells (Figure 6.8). 143BTK-^{GBML1} and 143BTK-^{GBML2} established a similar mtDNA copy number to one another; however, these values were significantly lower ($p<0.01$) than for the parental 143BTK-ρ^+ cells (Figure 6.8). I also analyzed the mtDNA copy number of 143BTK- cybrid cells harboring single mtDNA point mutations that are the underlying cause of the mitochondrial diseases MELAS (143BTK-^{3243}), NARP (143BTK-^{8993}) and LOHN (143BTK-^{11778}). The mtDNA copy number of 143BTK-^{8993} and 143BTK-^{11778} cells were not significantly different to the parental 143BTK-ρ^+ cells whilst 143BTK-^{3243} cells showed a significant elevation in copy number (1.65-fold; $p<0.001$; Figure 6.8).

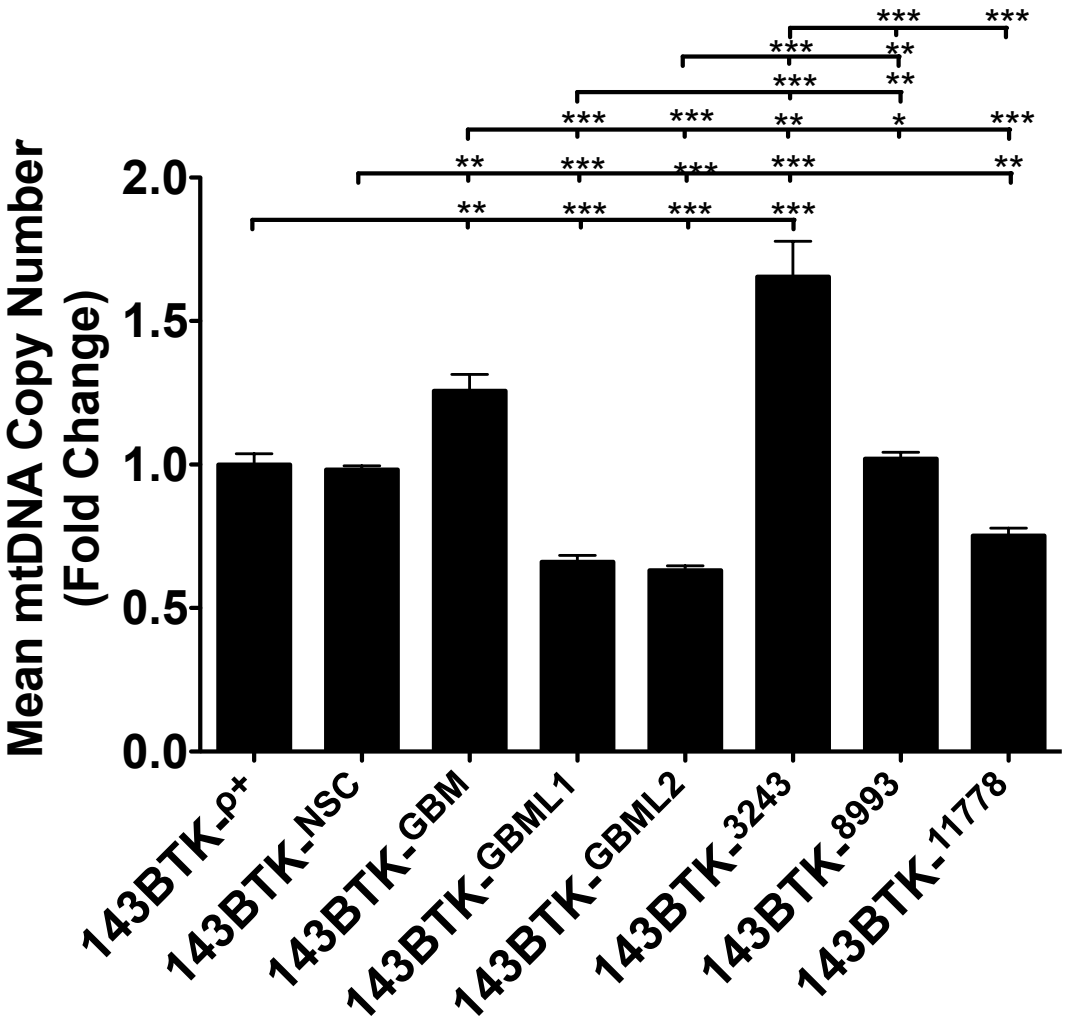

Figure 6.8. MtDNA copy number analysis of 143BTK- cells. Fold change in mtDNA copy number relative to 143BTK-$^{\rho+}$ cells of trans-mitochondrial cybrids. Columns represent mean values ± SEM (n=3). * Indicates $p<0.05$, ** $p<0.01$ and *** $p<0.001$.

Prior to the cell fusion process, the mtDNA copy number of the mtDNA donor cells (hNSC, HSR-GBM1, GBM-L1 and GBM-L2) was calculated and compared to the mtDNA copy number of the trans-mitochondrial cybrid cell lines (143BTK-^{NSC}, 143BTK-^{GBM}, 143BTK-^{GBML1} and 143BTK-^{GBML2}). By comparing these values, I was able to determine whether the initial number of mtDNA copies donated during the fusion process affected the final copy number in the trans-mitochondrial cybrids. Each of the trans-mitochondrial cell lines showed significant differences ($p<0.001$; Figure 6.9) in mtDNA copy number relative to of their mtDNA donor cells. 143BTK-^{NSC} cells showed a 2.73-fold increase ($p<0.01$) in copy number relative to their mtDNA donor, hNSCs. 143BTK-^{GBM} and 143BTK-^{GBML1} showed a 1.50 and 1.51-fold increase in copy number compared to their respective mtDNA donor cells. Finally, 143BTK-^{GBML2} cells showed a 2-fold ($p<0.001$) reduction in copy number relative to their mtDNA donor cells (Figure 6.9).

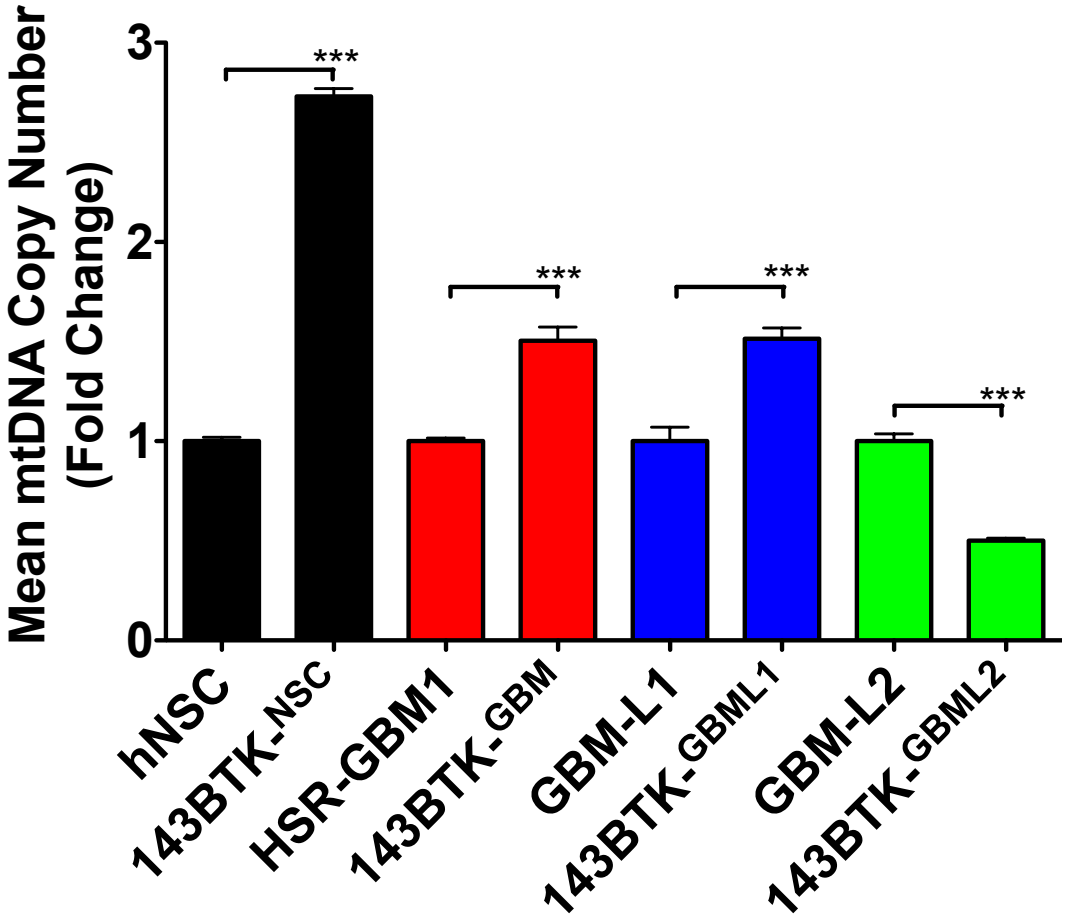

Figure 6.9. MtDNA copy number analysis of mtDNA donor cell lines and trans-mitochondrial cybrids. Fold change in mtDNA copy number relative to mtDNA donor cell lines of trans-mitochondrial cybrids. Columns represent mean values ± SEM (n=3). *** Indicates $p<0.001$.

6.6.2 O_2 consumption analysis

Since 143BTK- cybrids showed variable levels of mtDNA copy number, I sought to determine whether mtDNA copy number influenced their O_2 consumption rates. Once more, O_2 consumption rates of the trans-mitochondrial cybrids was compared the non-depleted parental 143BTK-$^{\rho+}$ cells. The values generated from the 143BTK-$^{\rho+}$ cells were used as an indicator of basal O_2 consumption rates of non-depleted and non-fused 143BTK- cells.

Each of the trans-mitochondrial cybrids showed significantly lower resting O_2 consumption rates than the parental 143BTK-$^{\rho+}$ cells ($p<0.001$; Figure 6.10A), whilst there were no significant differences between the trans-mitochondrial cybrid lines. ETC coupling efficiency was significantly reduced ($p<0.05$-0.001; Figure 6.10B) in all of the trans-mitochondrial cybrids relative to the parental 143BTK-$^{\rho+}$ cells with the exception of the 143BTK-^{GBM} cells. Between the cybrids cell lines, ETC coupling efficiency was greatest in the 143BTK-^{GBM} and 143BTK-^{3243} cells whilst the remaining cybrids exhibited similar ETC coupling efficiencies to each other (Figure 6.10B). The ETC reserve capacity was significantly greater ($p<0.001$) in the 143BTK-^{NSC}, 143BTK-^{GBML1}, 143BTK-^{GBML2} and 143BTK-^{8993} cells relative to the parental 143BTK-$^{\rho+}$ cells whilst the remaining cybrids showed similar ETC reserve capacities to one another (Figure 6.10C).

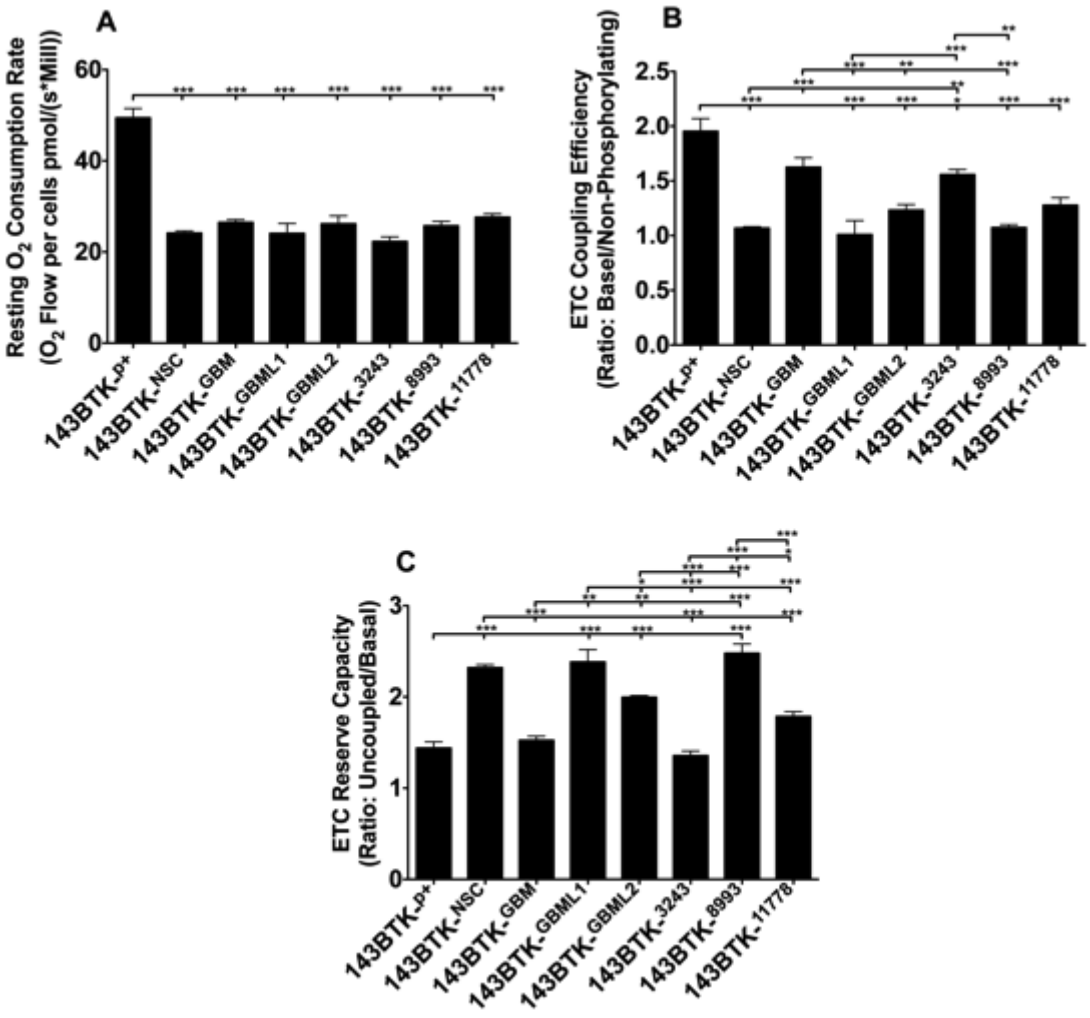

Figure 6.10. Resting O_2 consumption rates (A), ETC coupling efficiency (B) and ETC reserve capacity (C) of 143BTK- $^{\rho+}$ cells and trans-mitochondrial cybrids. Columns represent mean values ± SEM (n=3). * Indicates $p<0.05$, ** $p<0.01$ and *** $p<0.001$.

The amount of O_2 consumption dedicated to ATP production (Basal respiration – Non-phosphorylating respiration) was significantly lower ($p<0.001$) in all of the trans-mitochondrial cybrids relative to the parental 143BTK-$^{\rho+}$ cells (Figure 6.11). Between the trans-mitochondrial cybrid cell lines, ATP dedicated O_2 consumption was greatest in the 143BTK-^{GBM} and 143BTK-^{3243} and was significantly greater ($p<0.05$-0.001) than that of 143BTK-^{NSC}, 143BTK-^{GBML1} and

143BTK-^{8993} cells but not significantly different to 143BTK-^{GBML2} and 143BTK-^{11778} cells (Figure 6.11).

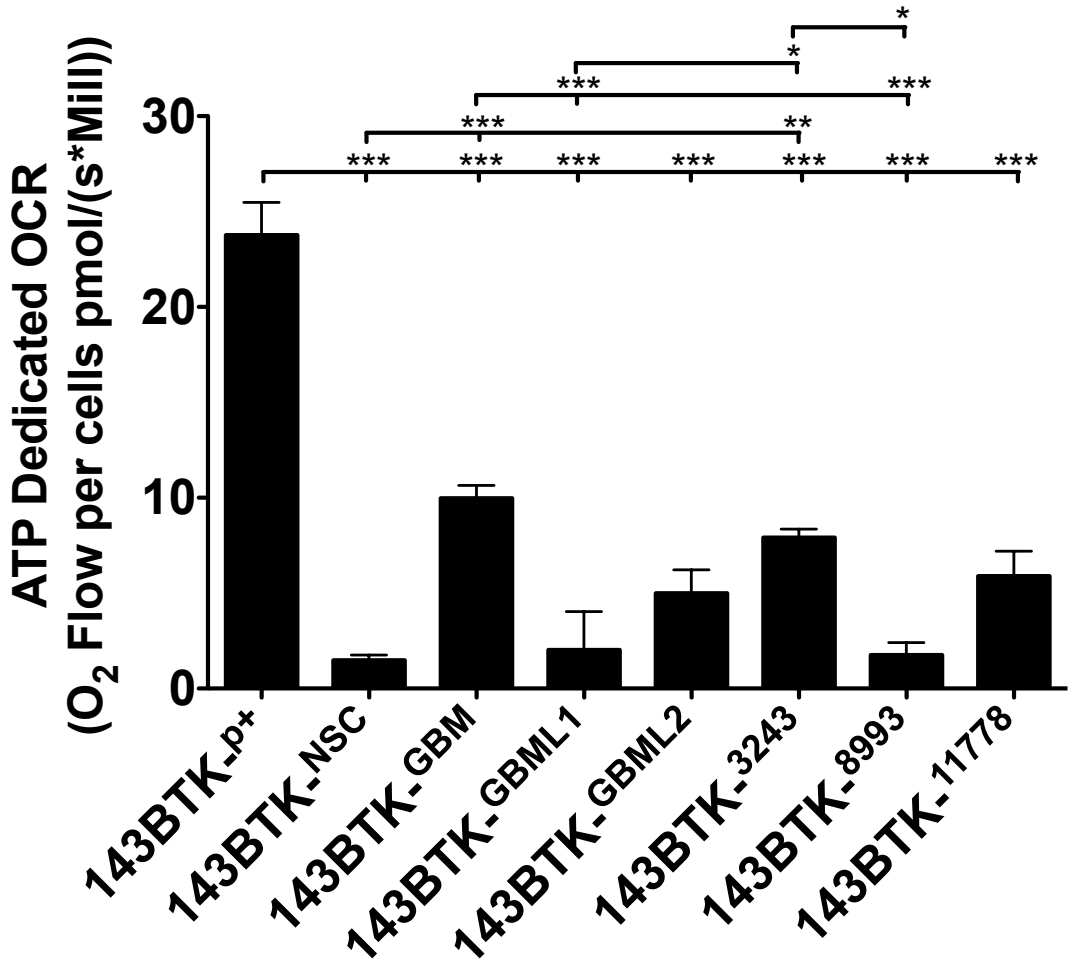

Figure 6.11. O_2 consumption rate dedicated to ATP production of 143BTK-$^{\rho+}$ cells and trans-mitochondrial cybrids. Columns represent mean values ± SEM (n=3). * Indicates p<0.05, ** p<0.01 and *** p<0.001.

The maximal O_2 consumption rate (ETC uncoupling by FCCP) was highest in the parental 143BTK-$^{\rho+}$ cells and was significantly greater (p<0.01-0.001) than all of the trans-mitochondrial cybrids with the exception of 143BTK-^{GBML1} and 143BTK-^{8993} cells (Figure 6.12). Maximal O_2 consumption rate was similar between 143BTK-^{NSC}, 143BTK-^{GBML1}, 143BTK-^{GBML2} and 143BTK-^{8993} cells,

whilst the lowest maximal O_2 consumption rate was observed in the 143BTK-^{3243} cells (Figure 6.12).

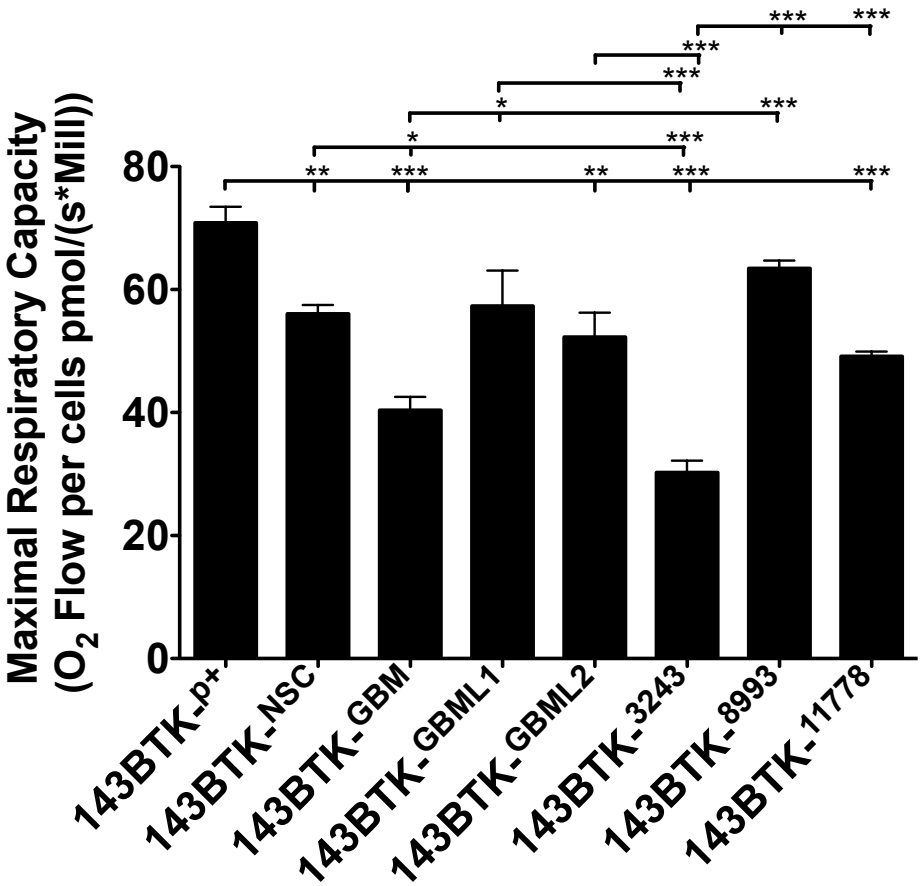

Figure 6.12. Maximal O_2 consumption rates of 143BTK-$^{\rho+}$ cells and trans-mitochondrial cybrids. Columns represent mean values ± SEM (n=3). * Indicates $p<0.05$ and *** $p<0.001$.

6.6.3 Cellular ATP content

Since all of the trans-mitochondrial cybrids exhibited significantly lower resting and ATP dedicated O_2 consumption rates than the parental 143BTK-$^{\rho+}$ cells, I compared the cellular ATP content in 143BTK-$^{\rho+}$ cells and the three cybrids cell lines, 143BTK-^{NSC}, 143BTK-^{GBM} and 143BTK-^{3243}. In addition, I analyzed the

ATP content in the mtDNA depleted 143BTK-$^{\rho 0}$ cell line to provide a reference value for the cellular ATP content of a fully mtDNA depleted cell line. In agreement with the reduced resting and ATP dedicated O_2 consumption rates observed in the trans-mitochondrial cybrids, the cellular ATP content was significantly lower ($p<0.001$) in the cybrids and the 143BTK-$^{\rho 0}$ cells compared to the parental 143BTK-$^{\rho +}$ cells (Figure 6.13). 143BTK-^{GBM} and 143BTK-^{3243} showed similar ATP content to the depleted 143BTK-$^{\rho 0}$ cell line, whilst 143BTK-^{NSC} cells showed slightly higher and significant ATP content than the 143BTK-^{3243} cells ($p<0.01$; Figure 6.13).

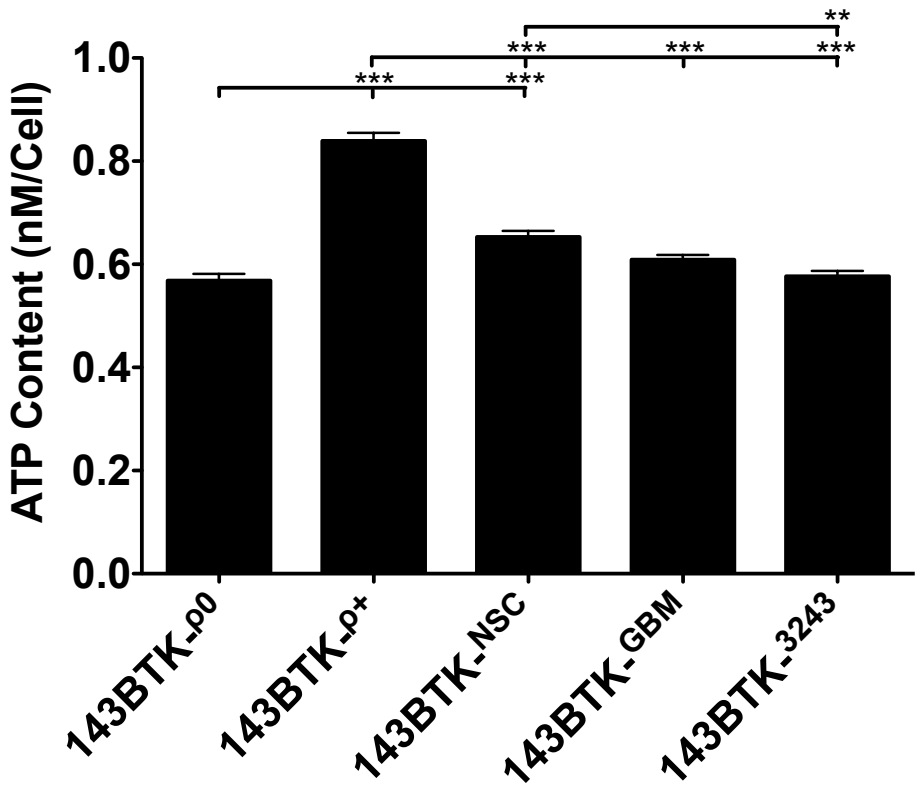

Figure 6.13. Cellular ATP content of 143BTK-$^{\rho 0}$, 143BTK-$^{\rho +}$ and trans-mitochondrial cybrids. Columns represent mean values ± SEM (n=3). ** Indicates $p<0.01$ and *** $p<0.001$.

6.6.4 Lactate production

Prior to the repopulation of 143BTK- $^{\rho 0}$ cells with mtDNA from donor cells, 143BTK- $^{\rho 0}$ cells are reliant on glycolysis for ATP production and would be expected to secrete a large amount of lactate since glycolysis derived pyruvate cannot be fully metabolized in the mitochondria due to a lack of a functional respiratory chain. I, therefore, determined the cellular lactate production of 143BTK- $^{\rho 0}$ cells and compared these values to the parental 143BTK-$^{\rho +}$ cells and the three selected trans-mitochondrial cybrids. 143BTK- $^{\rho 0}$ cells secreted the highest amount of lactate out of the cell lines analyzed and this value was significantly greater than that of 143BTK-$^{\rho +}$ and 143BTK-^{NSC} cells ($p<0.05$; Figure 6.14). 143BTK-^{GBM} and 143BTK-^{3243} secreted comparable amounts of lactate to 143BTK- $^{\rho 0}$ cells (Figure 6.14).

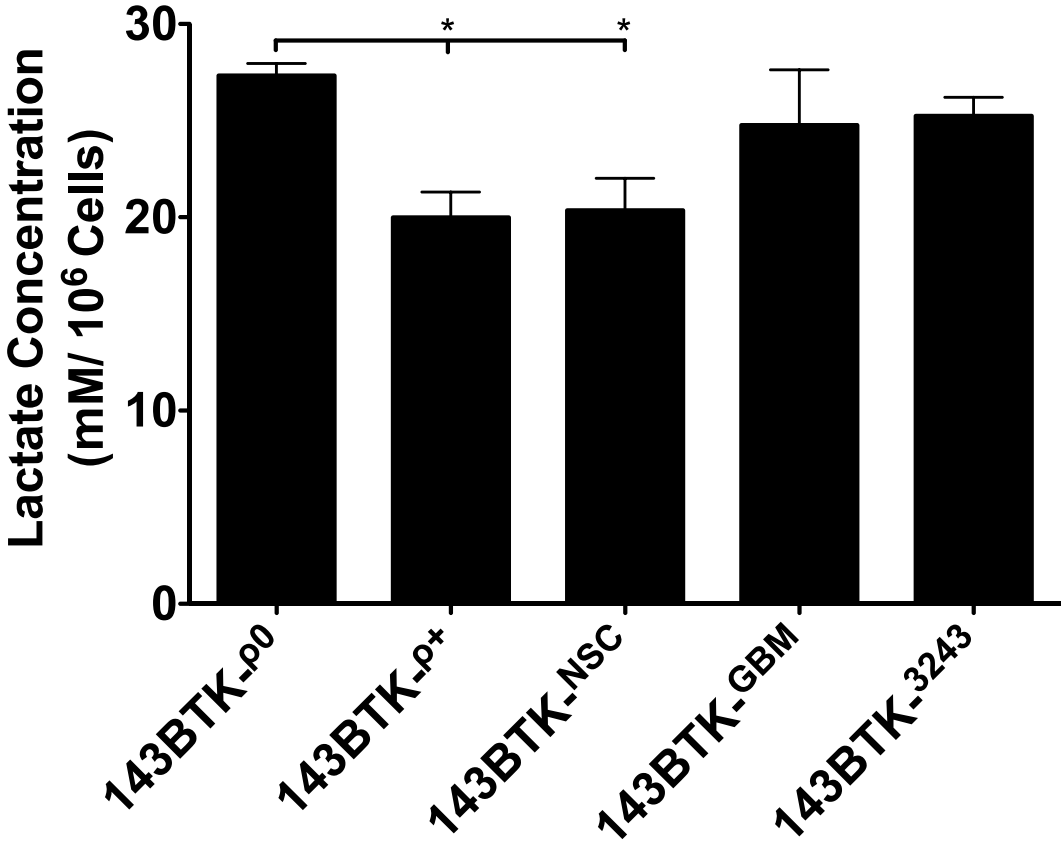

Figure 6.14. Cellular lactate production of 143BTK-$^{\rho 0}$, 143BTK-$^{\rho +}$ and trans-mitochondrial cybrids. Columns represent mean values ± SEM (n=3). * Indicates $p<0.05$.

6.6.5 MtDNA copy number analysis of HSR-GBM1 trans-mitochondrial cybrids

Since HSR-GBM1 cells had been treated with R6G and subsequently repopulated with HSR-GBM1 and hNSC mtDNA, I determined whether the re-population process elicited an effect on mtDNA copy number regulation during differentiation and compared these outcomes to non-cybrid HSR-GBM1 cells and hNSCs.

HSR-HSR cells showed a 2.34 ($p<0.001$) and 2.00-fold ($p<0.001$) increase in mtDNA copy number on Day 7 and 14 of differentiation, respectively, compared to Day 0 and by Day 28 where an increase of 4.23 fold ($p<0.001$) was observed. Throughout differentiation, the changes in HSR-HSR mtDNA copy number were significantly different ($p<0.001$) to that observed for HSR-GBM1 cells and hNSC (Figure 6.15). HSR-NSC cells showed significant increases in mtDNA copy number during differentiation ($p<0.01$-0.001), although these were not at as profound as HSR-HSR cells on Day 7 (1.45-fold) and 14 (1.78-fold) (Figure 6.15). However, by Day 28 of differentiation, HSR-NSC had increased their mtDNA number by 4.58-fold, which was significantly greater than that of HSR-GBM1 cells and hNSCs (Figure 6.15). Collectively, the patterns of copy number regulation in HSR-HSR and HSR-NSC cells more closely correlated with that of hNSCs rather than HSR-GBM1 cells, in that they exhibited increased copy number during differentiation.

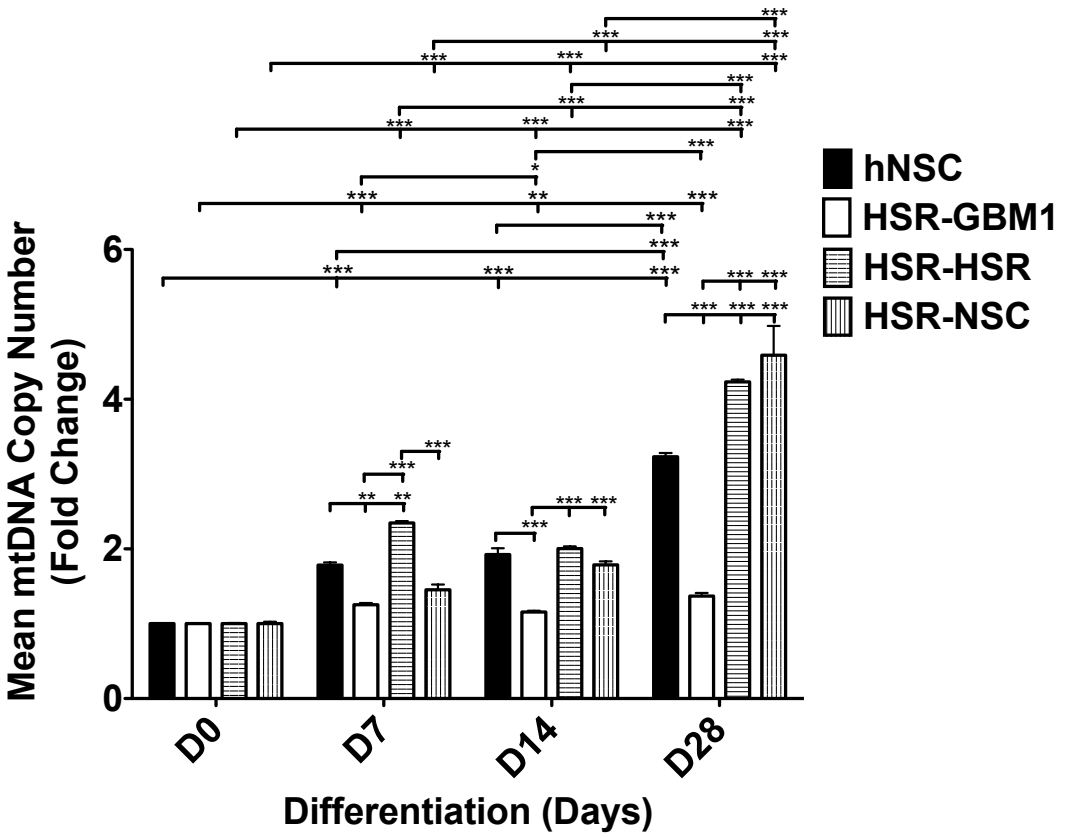

Figure 6.15. Analysis of mtDNA copy number of differentiating hNSC, HSR-GBM1, HSR-HSR and HSR-NSC cells. Fold change in mtDNA copy number relative to Day 0 of differentiation. Columns represent mean values ± SEM (n=3). * Indicates $p<0.05$, ** $p<0.01$ and *** $p<0.001$.

6.6.6 Gene expression analysis of HSR-GBM1 cybrids

I hypothesized that altering the mtDNA genotype of HSR-GBM1 cells would modify their differentiation profiles. To test this hypothesis, I examined the expression of the neural stem cell markers NESTIN, MUSASHI1 and CD133 and the astrocyte marker, GFAP, during a 28-day differentiation period and once more, compared these outcomes to non-cybrid HSR-GBM1 cells and hNSCs.

HSR-HSR cells showed an increase of 1.56–fold ($p<0.01$) and 1.40–fold ($p>0.05$) in *NESTIN* expression on Day 7 and 14 of differentiation, respectively (Figure 6.16). By Day 28 of differentiation, *NESTIN* expression was comparable to that of Day 0. HSR-NSC cells showed a significant reduction in *NESTIN* expression on Day 7 of differentiation (2-fold; $p<0.05$) relative to Day 0, which was followed by an increase of 1.39-fold on Day 14, although this was not significantly different to Day 0 (Figure 6.16). By Day 28 of differentiation, *NESTIN* expression returned to similar levels to Day 0. Both HSR-HSR and HSR-NSC cells showed different patterns of *NESTIN* expression compared to HSR-GBM1 cells and more closely mirrored the expression profiles of hNSCs. In HSR-GBM1 cells, *NESTIN* expression was significantly reduced on Day 28 of differentiation whilst *NESTIN* expression was unchanged in HSR-HSR, HSR-NSC cells and hNSCs (Figure 6.16).

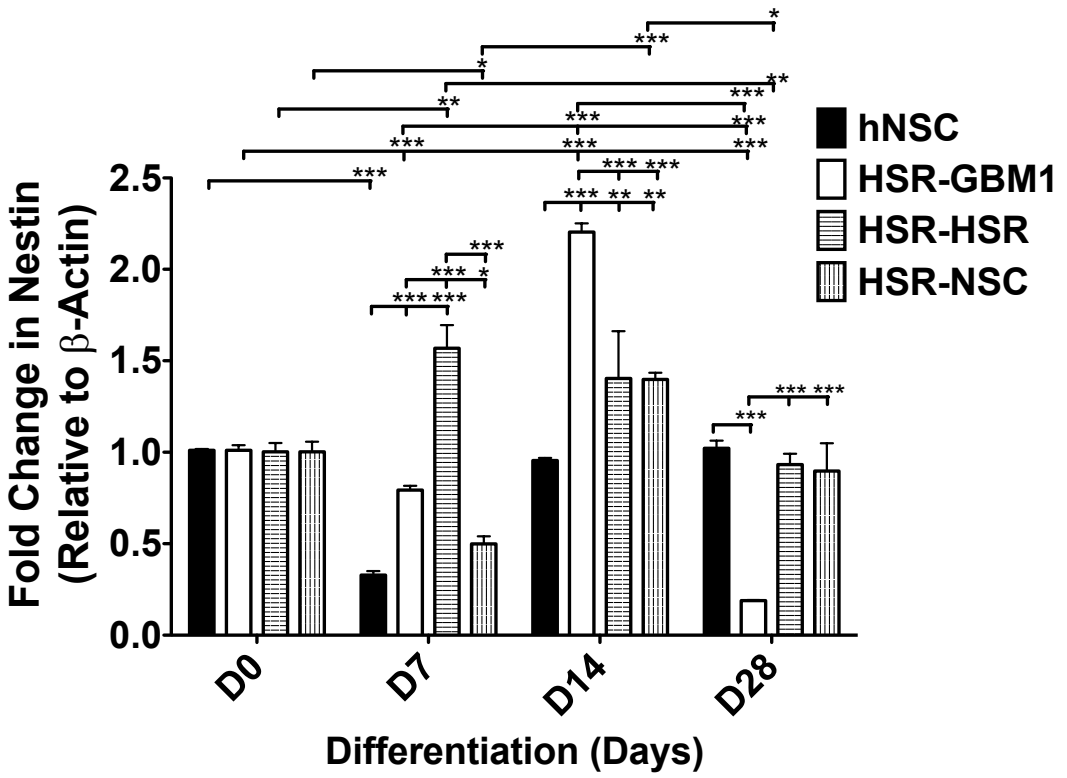

Figure 6.16. Fold change in expression relative to Day 0 and weighted against *β-ACTIN* of *NESTIN* in differentiating hNSC, HSR-GBM1, HSR-HSR and HSR-NSC cells. Columns represent mean values ± SEM (n=3). * Indicates $p<0.05$, ** $p<0.01$ and *** $p<0.001$.

Differential patterns of *MUSASHI1* expression were observed between HSR-HSR and HSR-NSC cells. HSR-HSR cells showed an initial increase in expression on Day 7 (1.62-fold; $p<0.01$) and 14 (1.45-fold; $p>0.05$) of differentiation before expression returned to comparable levels to Day 0 on Day 28 of differentiation (Figure 6.17). HSR-NSC cells showed an initial decrease in *MUSASHI1* expression on Day 7 (3.44-fold; $p<0.05$) and this was followed by a 1.72-fold increase in expression relative to Day 0 on Day 14 of differentiation ($p<0.05$). By Day 28 of differentiation *MUSASHI1* expression was increased by 1.88-fold ($p<0.05$) relative to Day 0 (Figure 6.17). HSR-GBM1 cells showed a similar pattern of *MUSASHI1* expression to HSR-HSR cells for the first 14 days

of differentiation, however, *MUSASHI1* expression was significantly higher in HSR-HSR cells on Day 28 differentiation compared to HSR-GBM1 cells ($p<0.05$; Figure 6.17). Collectively, HSR-HSR and HSR-NSC cells showed different patterns of expression compared to hNSCs.

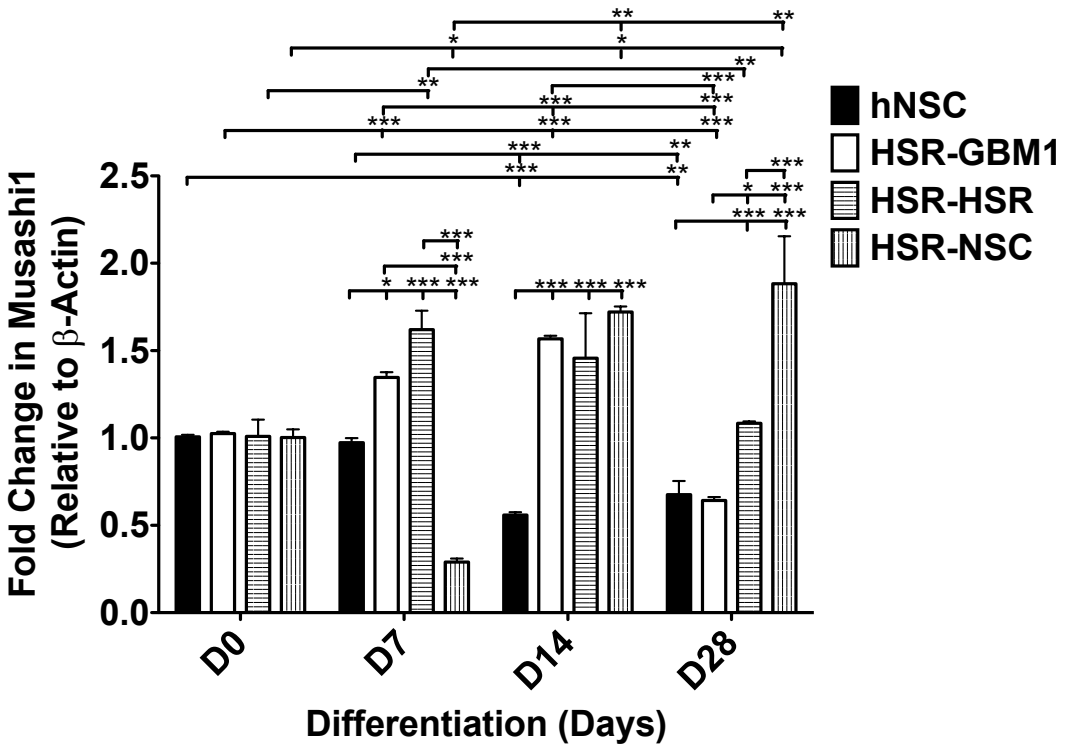

Figure 6.17. Fold change in expression relative to Day 0 and weighted against *β-ACTIN* of *MUSASHI1* in differentiating hNSC, HSR-GBM1, HSR-HSR and HSR-NSC cells. Columns represent mean values ± SEM (n=3). * Indicates $p<0.05$, ** $p<0.01$ and *** $p<0.001$.

HSR-HSR cells showed progressive and significant ($p<0.01$-0.001) reductions in *CD133* expression during the differentiation process, which cumulated with a 7.14-fold reduction in expression on Day 28 of differentiation, relative to Day 0 (Figure 6.18). A similar trend for *CD133* expression was observed in HSR-GBM1 cells. HSR-NSC cells showed fluctuations in *CD133* expression and by

Day 28 of differentiation, *CD133* was not significantly different to that of Day 0 and was also significantly greater ($p<0.01$) than that of HSR-HSR cells. Although HSR-NSC cells showed similar *CD133* expression patterns to HSR-GBM1 cells for the first 14 days of differentiation, by Day 28, CD133 was elevated in HSR-NSCs cells (Figure 6.18). hNSCs showed a differential pattern of *CD133* expression to the other cell lines, and exhibited a steady increase in expression throughout differentiation.

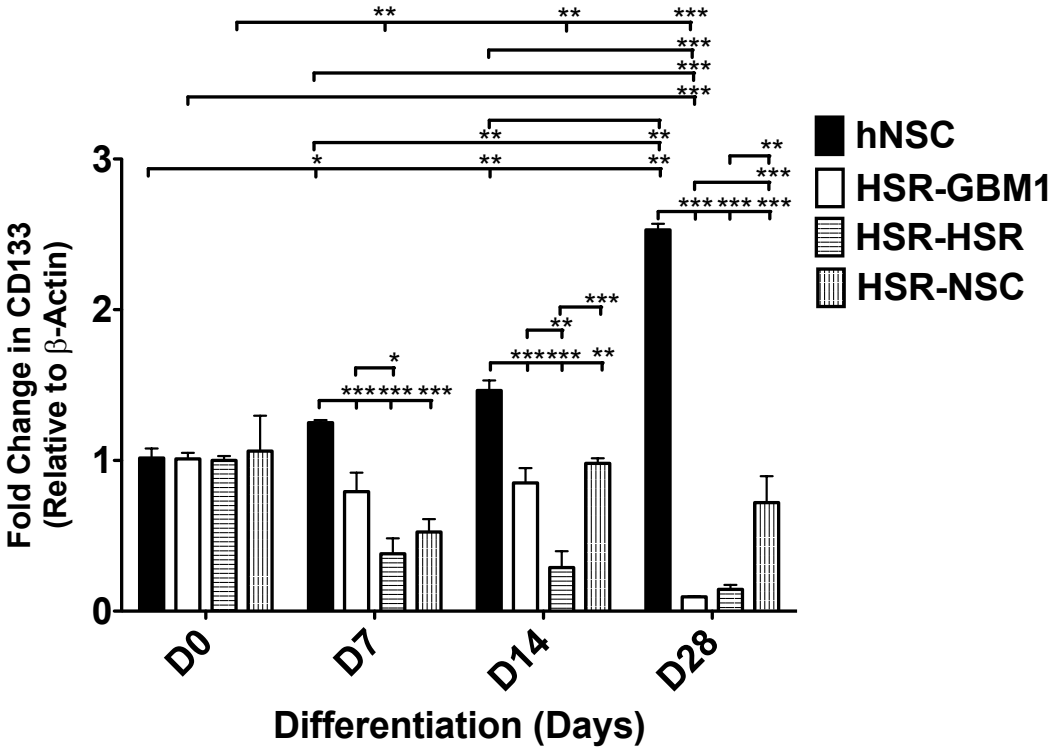

Figure 6.18. Fold change in expression relative to Day 0 and weighted against *β-ACTIN* of *CD133* in differentiating hNSC, HSR-GBM1, HSR-HSR and HSR-NSC cells. Columns represent mean values ± SEM (n=3). * Indicates $p<0.05$, ** $p<0.01$ and *** $p<0.001$.

Each of the cell lines analyzed showed increases in *GFAP* expression during differentiation relative to Day 0, however, the patterns of expression varied between cell lines (Figure 6.19). HSR-HSR cells showed a similar trend to HSR-GBM1 cells with a 16.15-fold ($p<0.001$) increase in *GFAP* expression on Day 7 of differentiation relative to Day 0, however, *GFAP* expression levels were reduced to 6.93 ($p<0.001$) and 5.41-fold ($p<0.001$) on Day 14 and 28 of differentiation, respectively (Figure 6.19). In contrast, HSR-NSC cells exhibited a 8.60-fold ($p<0.001$) increase on Day 7 of differentiation, which was followed by a 42.24-fold increase ($p<0.001$) on Day 14 of differentiation. *GFAP* expression was reduced on Day 28 of differentiation; however, expression levels remained 35.43-fold ($p<0.001$) higher than that of Day 0 (Figure 6.19). hNSCs showed a steady increase in GFAP expression during differentiation, however, the increases in GFAP expression were more prominent in HSR-NSC cells.

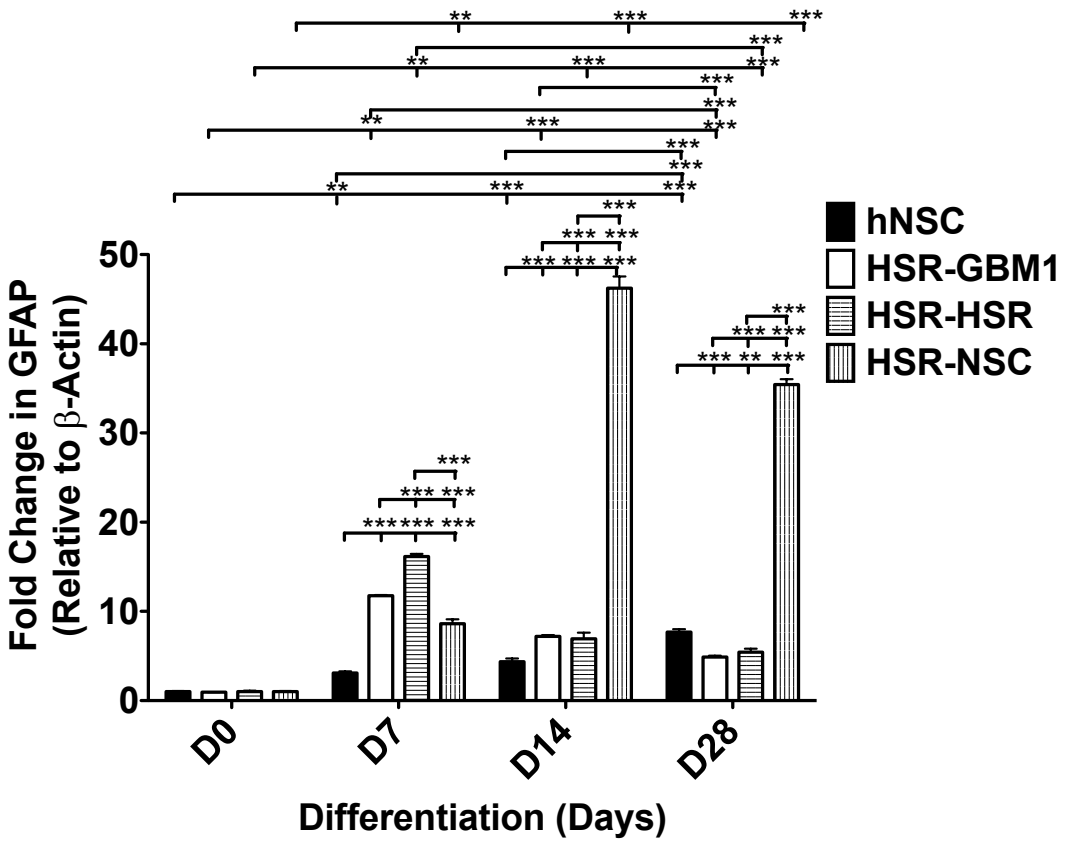

Figure 6.19. Fold change in expression relative to Day 0 and weighted against *β-ACTIN* of *GFAP* in differentiating hNSC, HSR-GBM1, HSR-HSR and HSR-NSC cells. Columns represent mean values ± SEM (n=3). * Indicates $p<0.05$, ** $p<0.01$ and *** $p<0.001$.

6.6.7 Cellular respiration of HSR-GBM1 trans-mitochondrial cybrids

Since HSR-GBM1 cybrids exhibited altered copy number regulation and gene expression profiles during differentiation, I sought to assess their cellular respiration on Day 14 and 21 of differentiation. Each of the cell lines analyzed exhibited increases in O_2 consumption following the onset of differentiation. HSR-HSR cells showed the greatest change in O_2 consumption rate, which was increased by 1.87-fold increase ($p<0.001$; Figure 6.20) compared to a 1.35-fold increase in HSR-NSC cells. Although HSR-HSR cells showed the greatest fold

change in O_2 consumption rate relative to undifferentiated cells, the final O_2 consumption rates were similar between HSR-HSR and HSR-NSCs.

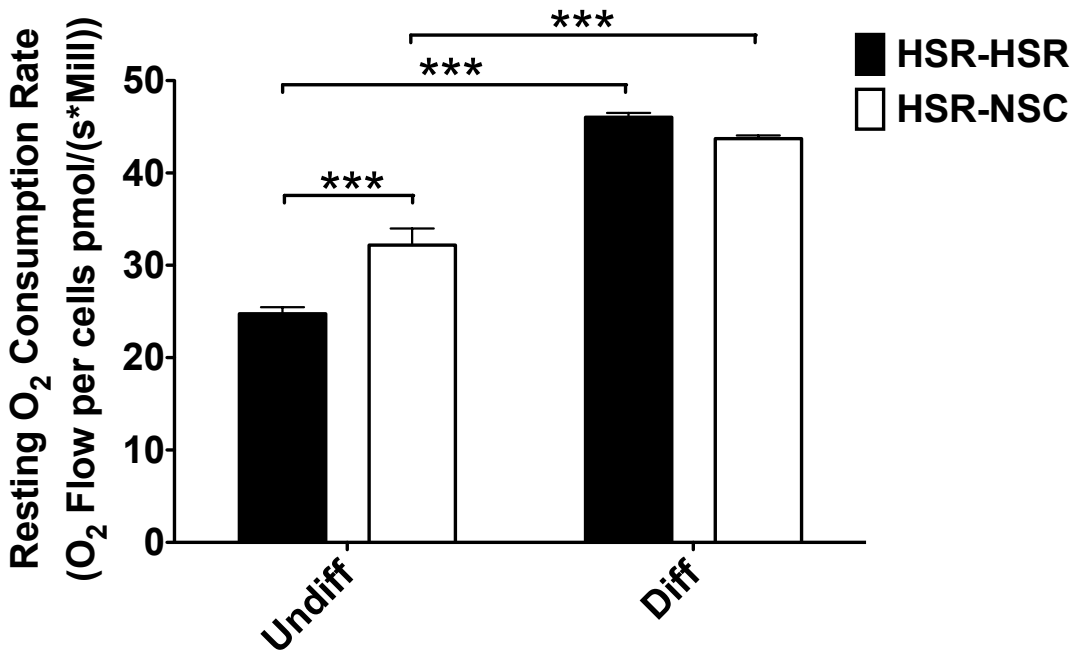

Figure 6.20. Fold change in O_2 consumption rates, relative to undifferentiated cells of HSR-HSR and HSR-NSC cells. Columns represent mean values ± SEM (n=3). *** Indicates $p<0.001$.

ETC coupling efficiency was high in each of the cell lines analyzed, as indicated by ratios close to a value of 2. Both HSR-HSR and HSR-NSC cells showed reductions in coupling efficiency following differentiation and this was statically significant in HSR-NSC cells ($p<0.05$). Nevertheless, each cell line showed evidence of a tightly coupled ETC (Figure 6.21).

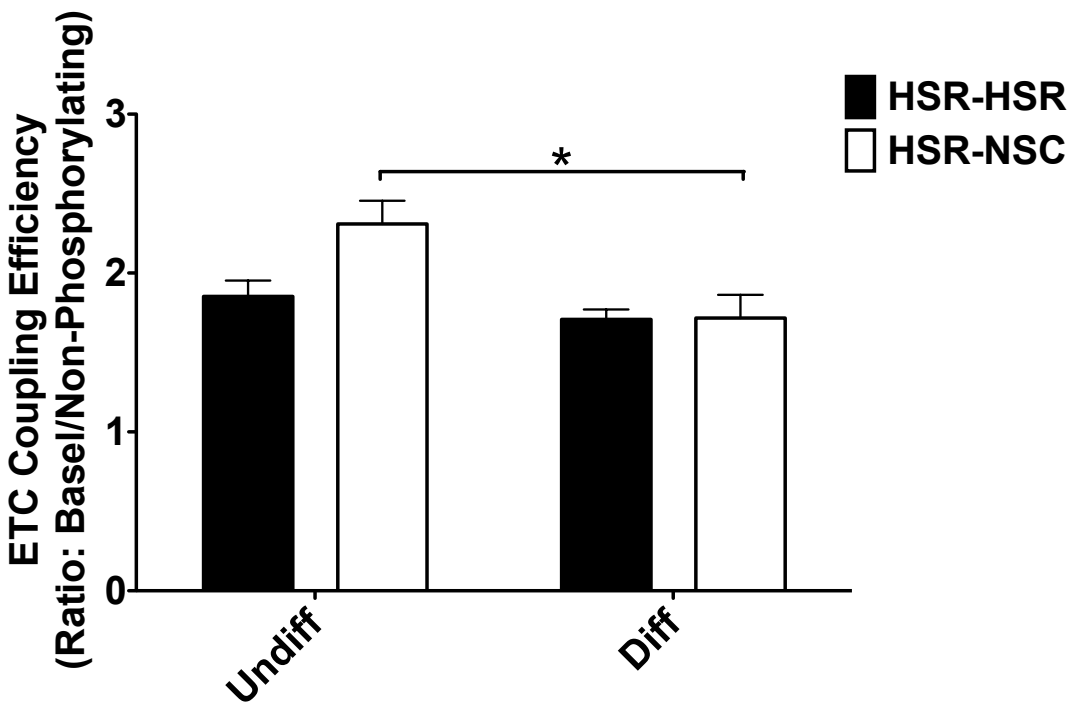

Figure 6.21. ETC coupling efficiencies of undifferentiated and differentiated HSR-HSR and HSR-NSC cells. Columns represent mean values ± SEM (n=3). * Indicates $p<0.05$.

HSR-NSC cells exhibited the lowest ETC reserve capacity in the undifferentiated state; however, they also showed the greatest increase in reserve capacity following the onset of differentiation (1.47-fold; $p<0.001$; Figure 6.22). HSR-HSR cells exhibited a similar ETC reserve capacity in the undifferentiated state, whilst the reserve capacity was slightly lower than HSR-NSC cells in the differentiated state. Collectively, both cell lines exhibiting significant increases in ETC reserve capacity following differentiation ($p<0.05$).

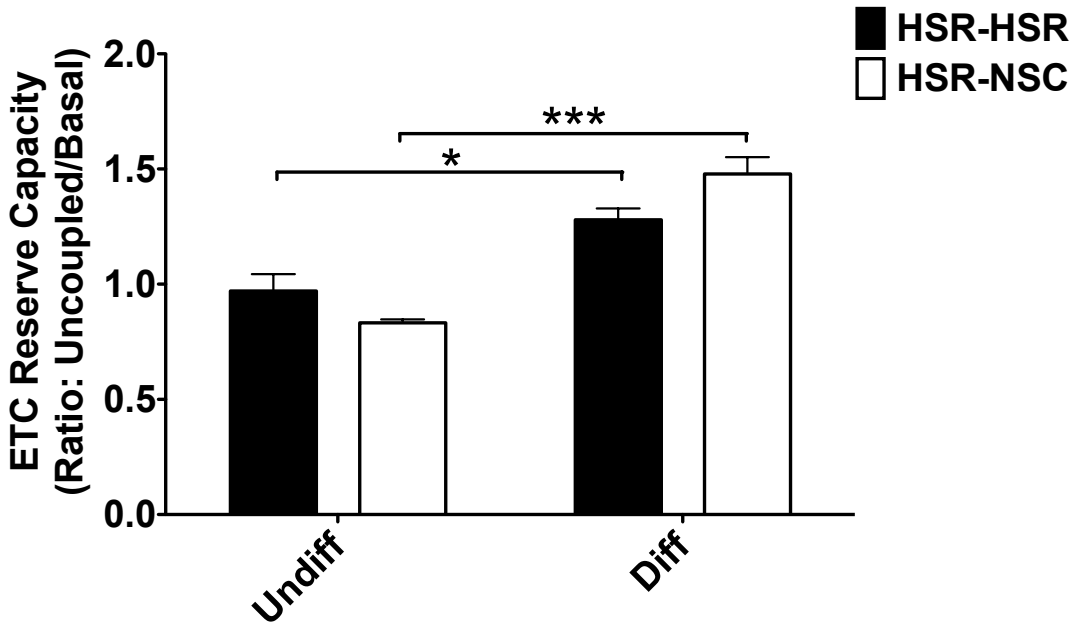

Figure 6.22. ETC reserve capacities of undifferentiated and differentiated HSR-HSR and HSR-NSC cells. Columns represent mean values ± SEM (n=3). * Indicates $p<0.05$ and *** indicates $p<0.001$.

6.6.8 Cellular ATP content

I next sought to determine the cellular ATP and lactate production of the HSR-GBM1 cybrids. HSR-HSR cells exhibited the greatest increase in cellular ATP content following the onset of differentiation, with a 2.50-fold increase ($p<0.001$; Figure 6.23). HSR-NSC cells did not significantly increase their cellular ATP content during differentiation, however, their ATP content at the undifferentiated state was greater than that of HSR-HSR cells and differentiated HSR-HSR and HSR-NSC cells had similar ATP contents (Figure 6.23).

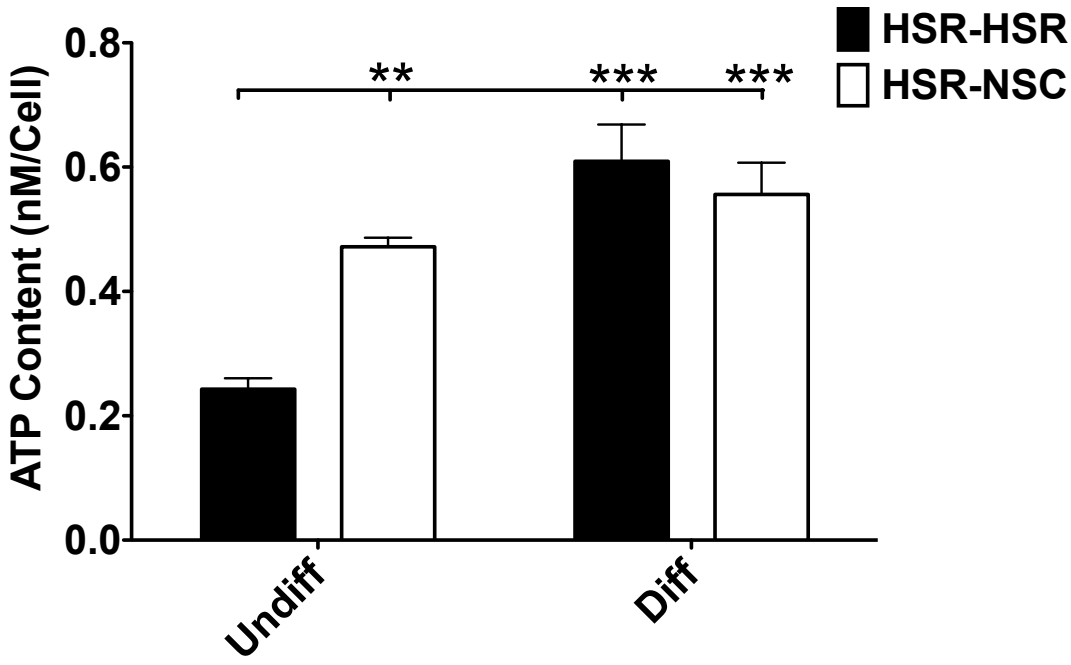

Figure 6.23. Cellular ATP content of undifferentiated and differentiated HSR-HSR and HSR-NSC cells. Columns represent mean values ± SEM (n=3). ** Indicates $p<0.01$ and *** indicates $p<0.001$.

6.6.9 Cellular lactate production

Lactate production was analyzed as an index of glycolytic rate. Each cell line showed a reduction in lactate production following the onset of differentiation (Figure 6.24). 1.63 ($p<0.01$) and 2.63-fold ($p<0.001$) reductions in lactate production were observed in HSR-HSR and HSR-NSC cells, respectively.

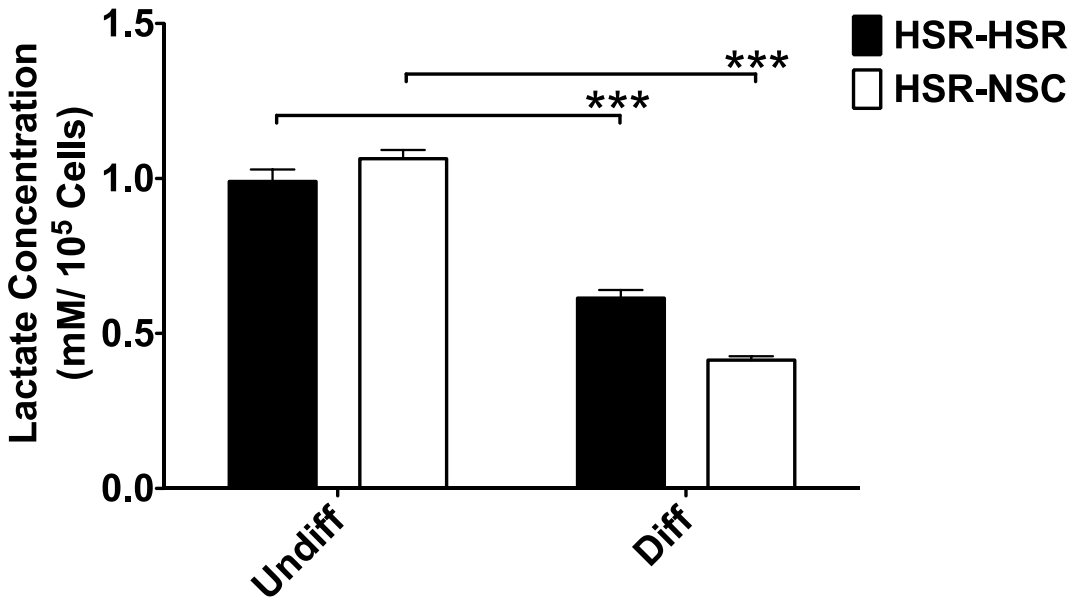

Figure 6.24. Cellular lactate production of undifferentiated and differentiated HSR-HSR and HSR-NSC cells. Columns represent mean values ± SEM (n=3). *** Indicates $p<0.001$.

6.7 Discussion

Over the last two decades trans-mitochondrial cybrids have been utilized to investigate how mtDNA mutations impact upon cellular function (Bonora et al., 2006; Ishikawa et al., 2008; Kelly et al., 2013; Ma et al., 2010; McKenzie and Trounce, 2000; McKenzie et al., 2004; Petros et al., 2005; Shidara et al., 2005). These studies have provided the foundation for our current understanding of how single point mutations, responsible for mitochondrial diseases, can cause metabolic defects. Indeed, cybrid cells harboring T8993G, G13997A and G15557A mtDNA variants were shown to exhibit increased ROS production and reduced ETC function (Bonora et al., 2006; Ishikawa et al., 2008; Petros et al., 2005; Shidara et al., 2005) and highlight the deleterious effects of mtDNA mutations. Currently, there is limited evidence linking mtDNA mutations outside that of the D-loop region, with changes in mtDNA copy number. To address this issue, the mtDNA copy number of trans-mitochondrial cybrids harboring wild-type mtDNA, single mtDNA variants and multiple mtDNA variants were analyzed.

6.7.1 MtDNA copy number analysis of 143BTK- trans-mitochondrial cybrids

The mtDNA copy number of the trans-mitochondrial cybrid lines was variable and distinct differences were observed between the newly established mtDNA set points of the cybrid cells. It is difficult to correlate the changes in copy number with the presence of single mtDNA point mutations, since 143BTK-^{3243} cells exhibited the highest mtDNA copy number whilst 143BTK-^{8993} and 143BTK-^{11778} cells exhibited comparable copy numbers to the parental 143BTK-

ρ^+ cells. However, it is likely that the elevation in copy number in 143BTK-^{3243} cells may be functioning as a compensatory mechanism for the severe OXPHOS defect that the A3243G mutation induces (Lee et al., 1998). Similarly, variable mtDNA copy number was observed between cybrids harboring GBM mtDNA. 143BTK-^{GBM} cells exhibited higher mtDNA copy number than the parental 143BTK- $^{\rho+}$ cells, whilst 143BTK- ^{GBML1} and 143BTK- ^{GBML2} cells contained fewer copies of mtDNA. Multiple mtDNA variants have been detected in HSR-GBM1, GBM-L1 and GBM-L2 cells and are currently under investigation in our laboratory (personal communication with Ka Yu Yeung). It is likely that each cell line possess different mtDNA variants of variable mutant load and this may account for the differences in copy number observed. Indeed, there is some evidence to suggest that mtDNA copy number is increased to compensate for reduced ETC function (Lee et al., 2000). Interestingly, 143BTK-^{NSC} cells, which contain wild type mtDNA, exhibited a similar copy number to that of 143BTK- $^{\rho+}$ cells. It is likely that the wild type mtDNA more closely mirrored the mtDNA genotype of the 143BTK- $^{\rho+}$ cells and allowed for a reestablishment of a comparable mtDNA copy number. Since each of the cybrids were generated using a common nuclear background, these outcomes indicate that the mtDNA set point established by the nucleus is strongly influenced by the mtDNA genotype and provides direct evidence that mtDNA variants influence mtDNA copy number regulation.

6.7.2 O_2 consumption analysis of 143BTK- trans-mitochondrial cybrids

The O_2 consumption rates of the 143BTK- trans-mitochondrial cybrids were analyzed to determine the effects of the newly established mtDNA copy

numbers. Each cybrid cell line demonstrated similar resting O_2 consumption rates to one another; however, these were considerably lower than that of the parental 143BTK- $^{\rho+}$ cell line. Furthermore, each of the cybrids possessed an ETC reserve capacity, which demonstrates that each cell line was not respiring at a maximal rate.

The treatment of cells with Oligomycin inhibits Complex V (ATP Synthase) function and allows for the measurement of ETC coupling or how much O_2 consumption was dedicated to ATP production through the ETC. Each of the cybrids lines showed considerably less ATP dedicated O_2 consumption rates than the parental 143BTK-$^{\rho+}$cell line. In support of these observations the cellular ATP content of 143BTK- ^{NSC}, 143BTK- ^{GBM} and 143BTK- ^{3243} mimicked that of 143BTK-$^{\rho0}$ cells, whilst 143BTK-$^{\rho+}$ cells, which showed high ATP dedicated O_2 consumption, contained significantly higher ATP content. Furthermore, 143BTK- ^{GBM} and 143BTK- ^{3243} cells secreted comparable amounts of lactate to 143BTK-$^{\rho0}$ cells. Collectively, these data suggest that despite the repopulation of 143BTK-$^{\rho0}$ cells with donor mtDNA, 143BTK- cybrids do not reestablish a similar O_2 consumption profile to the original and parental 143BTK-$^{\rho+}$cell line. 143BTK- cybrids more closely mimic 143BTK-$^{\rho0}$ cells in ATP and lactate production and it is likely that the generation of 143BTK-$^{\rho0}$ cells through long-term ethidium bromide treatment has induced lasting changes to the metabolic profile of 143BTK- cell line, rendering them highly glycolytic due to the chronic absence of mtDNA.

The repopulation of 143BTK-$^{\rho 0}$ cells with mtDNA reestablishes a respiratory chain, which is evidenced by their resting O_2 consumption rates and ETC reserve capacities. However, the low ETC coupling efficiencies observed in the 143BTK- cybrids suggests that a large proportion of the O_2 consumed by 143BTK- cybrids is being utilized by non-ATP generating processes. The ETC and OXPHOS are chiefly under the regulation of nuclear encoded factors and the introduction of mtDNA into 143BTK-$^{\rho 0}$ cells does no fully reverse the glycolytic profile that is adopted during the establishment and maintenance of 143BTK-$^{\rho 0}$ cells. Indeed, data from other studies showed reduced O_2 consumption rates and ATP content in 143BTK- cybrids relative to 143BTK-$^{\rho +}$ cells (Cho et al., 2012).

6.7.3 HSR-GBM1 trans-mitochondrial cybrids

To determine the effect that different mtDNA genotypes have on gene expression and differentiation potential, HSR-GBM1 cells were treated with R6G to disrupt mitochondrial function and fused with 143BTK- cybrids containing hNSC (wild type) and HSR-GBM1 cells (Controls). D-loop sequencing analysis showed that the mtDNA genotype of HSR-NSC was heteroplasmic and contained both wild type and HSR-GBM1 mtDNA. The ultimate aim of this study was to repopulate HSR-GBM1 cells with 100% wild type mtDNA, however, time restrictions limited the number of opportunities to achieve this outcome. However, it was reasoned that the analysis of HSR-GBM1 cells containing a heteroplasmic mtDNA population would be a worthy investigation.

6.7.4 MtDNA copy number analysis of HSR-GBM1 trans-mitochondrial cybrids

HSR-GBM1 trans-mitochondrial cybrids were subjected to a 28-day differentiation assay to determine the effect of the mtDNA repopulation process on mtDNA copy number regulation. Both trans-mitochondrial cybrids lines (HSR-HSR & HSR-NSC) showed very different copy number patterns to non-cybrid HSR-GBM1 cells during differentiation. HSR-HSR and HSR-HSR cells showed copy number increases in excess of 3-fold on Day 28 differentiation, which was considerably greater than that previously observed for non-cybrid HSR-GBM1 cells. Since HSR-HSR cells contained the same mtDNA population as non-cybrid HSR-GBM1 cells, it is likely that the observed changes in mtDNA copy number regulation in the HSR-GBM1 cybrids are due to the R6G treatment prior to the fusion process. A possible explanation is that the disruption of mitochondrial function with R6G and subsequent repopulation with donor mitochondria and mtDNA may have functioned as a “reset switch” and allowed for improved interaction between the nuclear and mitochondrial genomes of HSR-GBM1 cells. Since mtDNA copy number regulation during differentiation has not been investigated following R6G treatment, it cannot be confirmed whether the observed differences in copy number regulation between HSR-GBM1 cells and HSR-GBM1 cybrids is due to the application of R6G alone or the interaction between R6G and the transformed nature of HSR-GBM1 cells.

6.7.5 Gene expression analysis of HSR-GBM1 trans-mitochondrial cybrids

The HSR-GBM1 cybrids exhibited differential expression of the neural stem cell markers *NESTIN*, *MUSASHI1* and *CD133* compared to non-cybrid HSR-GBM1 cells. Whilst non-cybrid HSR-GBM1 cells down-regulated the expression *NESTIN, MUSASHI1* and *CD133* by Day 28 of differentiation, HSR-HSR and HSR-NSC cells did not match this pattern of expression. Furthermore, HSR-NSC cells showed profound differences in *GFAP* expression relative to HSR-HSR and non-cybrid HSR-GBM1 cells. HSR-HSR and non-cybrid HSR-GBM1 cells showed similar patterns of *GFAP* expression, with peak levels of expression observable on Day 7 of differentiation that were further reduced on Day 14 and 28. In contrast, HSR-NSC cells showed a large surge in *GFAP* expression on Day 14, which remained high on Day 28 of differentiation. Although HSR-HSR and HSR-NSC cells showed similar patterns of mtDNA copy number regulation during differentiation, they exhibited very different patterns of gene expression. The partial repopulation of HSR-GBM1 cells with wild type mtDNA appears to have enhanced or altered the differentiation potential of HSR-NSC cells relative to HSR-HSR cells that harbor 100% GBM mtDNA. These outcomes could be compared to those of by Kelly et al. who observed differential patterns of pluripotency and differentiation marker expression in ESCs containing divergent and homoplasmic populations of mtDNA (Kelly et al., 2013).

6.7.6 O_2 consumption analysis of HSR-GBM1 trans-mitochondrial cybrids

HSR-HSR cells exhibited differences in O_2 consumption rates, ETC coupling efficiencies and ETC reserve capacities. However, the final O_2 consumption rates of each cell line were ultimately similar following differentiation. A similar trend was observed regarding ATP production, with both cell lines containing comparable ATP content after 14-21 days of differentiation. Furthermore, both cell lines exhibited significant reductions in lactate production following differentiation, which is indicative of the transition between glycolytic and OXPHOS metabolism that occurs during differentiation (Cho et al., 2006; Facucho-Oliveira et al., 2007; Prigione et al., 2010; Varum et al., 2011). Collectively these results suggest that HSR-NSC cells, which demonstrated higher O_2 consumption rates and ATP content in the undifferentiated state, exhibit a more OXPHOS-like profile than HSR-HSR cells when undifferentiated.

6.8 Conclusion

In summary, single and multiple mtDNA variants are capable of influencing the reestablishment of the mtDNA set point in 143BTK- cells. Changes in mtDNA copy number have been associated with tumorigenesis and these data presented here show direct evidence that mtDNA variants influence mtDNA copy number regulation, which is also likely to play a role in tumorigenesis. Furthermore, the partial repopulation of multipotent HSR-GBM1 cells with wild type mtDNA enhances their ability to upregulate and maintain the expression of differentiation markers. These outcomes suggest that mtDNA variants present in HSR-GBM1 cells may hinder the ability of these cells to undergo complete differentiation and maintain these cells in a naïve and tumorigenic state.

Chapter 7: General Discussion

7.1 GBM CSCs show differential regulation of mtDNA copy number compared to hNSCs

Tumor cell metabolism has been chiefly characterized by aerobic glycolysis (the Warburg Effect), which is defined as an enhanced glycolytic state under aerobic conditions that are otherwise sufficient to support OXPHOS (Warburg, 1956). Elevated glycolytic rates generate sufficient quantities of ATP for cellular function whilst providing an abundant source of biosynthetic intermediates to support growth and proliferation (Moreno-Sanchez et al., 2007). The majority of metabolomic studies on tumor cells have not discriminated between CSCs and differentiated cell types (Griguer et al., 2005; Yang et al., 2009) and there is currently no existing data examining how GBM CSCs regulate their mtDNA copy number in undifferentiated and differentiated states.

Normal stem cell populations, which include ESCs and NSCs, contain few copies of mtDNA and generate ATP primarily via glycolysis (Facucho-Oliveira et al., 2007; Moreno-Sanchez et al., 2007; Prigione et al., 2010; Wang et al., 2010). The differentiation of ESCs and NSCs is associated with an expansion of mtDNA copy number and a concurrent up-regulation of markers of differentiation (Facucho-Oliveira et al., 2007; Moreno-Sanchez et al., 2007; Prigione et al., 2010; Wang et al., 2010) (Figure 7.1). Indeed, I observed a similar outcome in differentiating hNSCs, which progressively increased their mtDNA copy number and the expression of the astrocyte marker, GFAP. In a novel observation, differentiating GBM cells failed to mimic this expansion of mtDNA copy number and the concurrent increase in GFAP expression (Figure

7.1). Since mtDNA transcription and replication are entirely mediated by nuclear encoded factors, these outcomes strongly suggest that abnormal regulation of these factors may be inhibiting copy number expansion in GBM cells during differentiation. Furthermore, from other observations, differentiating HSR-GBM1 cells expressed lower levels of the mtDNA transcription and replication factors TFAM, POLGA, TWINKLE than differentiated hNSCs (personal communication with Ka Yu Yeung) (Figure 7.1), which strongly suggests that there is an asynchronous relationship between the nuclear and mitochondrial genomes of GBM cells.

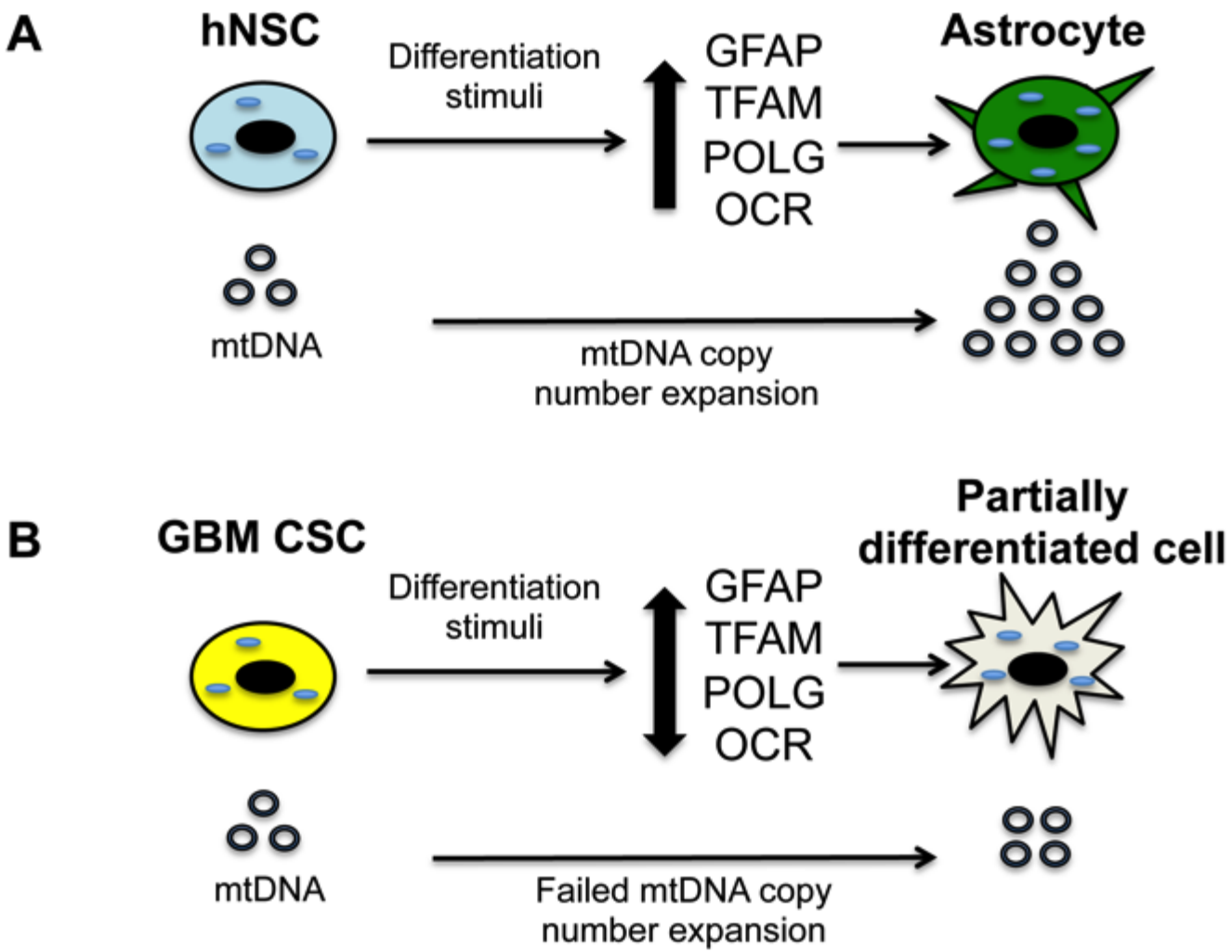
A
hNSC
Differentiation stimuli
GFAP
TFAM
POLG
OCR
Astrocyte
mtDNA
mtDNA copy number expansion
B
GBM CSC
Differentiation stimuli
GFAP
TFAM
POLG
OCR
Partially differentiated cell
mtDNA
Failed mtDNA copy number expansion

Figure 7.1. Diagrammatic representation of differentiating hNSCs and GBM cells. (A) Undifferentiated hNSCs contain very few copies of mtDNA and following the onset of differentiation, there is a concurrent increase in the expression of mtDNA transcription and replication factors (TFAM & POLG) and lineage specific markers (GFAP). Subsequently, hNSCs expand their mtDNA copy number and increase their OXPHOS potential and O_2 consumption rates (OCR). (B) In contrast, differentiating GBM cells show an aberrant regulation of the mtDNA transcription and replication factors and also the expression of lineage specific markers, which leads to a failed expansion in mtDNA copy number and inhibition of differentiation.

Further evidence of the asynchronous relationship in GBM cells was observed in the expression profiles of GFAP. GBM cells have previously been shown to differentiate into astrocyte and neuronal-like cells, with the expression of glial (GFAP) and neuronal (β-III-tubulin) markers observed (Chen et al., 2010; Galli et al., 2004; Singh et al., 2003). In these studies, differentiation was induced for a short duration (~7-14 days) (Chen et al., 2010; Galli et al., 2004; Singh et al., 2003), which renders the long-term differentiation of GBM cells an unknown entity. Through a long-term differentiation assay (28 days), I observed that GBM cells either failed to sustain GFAP expression during differentiation (HSR-GBM1 & GBM-L2 cells) or increased GFAP expression without an accompanying expansion in mtDNA copy number (GBM-L1 cells). These outcomes suggest that GBM cells fail to fully commit to differentiation and the patterns GFAP expression in GBM cells may represent a transient state by which GBM cells become partially differentiated but ultimately fail to fully commit to differentiation (Figure 7.1).

This hypothesis is also supported by the contrasting energy metabolism profiles of differentiated HSR-GBM1 and hNSCs. In agreement with previous studies of differentiating ESCs and NSCs (Cho et al., 2006; Varum et al., 2011; Wang et al., 2010; Zhu et al., 2012), differentiating hNSCs increased their O_2 consumption rates, which was accompanied by an increase in ETC capacity, increased cellular ATP content and reduced lactate production. In contrast, HSR-GBM1 cells exhibited only modest increases in O_2 consumption rate, ETC capacity and ATP content. These outcomes suggest that hNSCs undergo glycolysis to OXPHOS transition during differentiation, to meet the ATP requirements of differentiated cell types whilst HSR-GBM1 cells appear incapable of completing this transition. Despite GBM cells demonstrating some OXPHOS potential through my own observations and those of others (Griguer et al., 2005), HSR-GBM1 cells fail to fully adopt a true OXPHOS profile. Collectively, the failed expansion of mtDNA, abnormal GFAP expression and limited OXPHOS profile of GBM cells suggests that GBM cells are unable to fully alter their naïve/stem-cell like state and are likely to continue to exhibit aerobic glycolysis and consume elevated amounts of glucose and glutamine (DeBerardinis et al., 2008; Vander Heiden et al., 2009).

GBM cells not only express a number of NSC factors but also a number of factors associated with ESCs that include OCT4, NANOG, SOX2 and c-MYC (Ben-Porath et al., 2008; Ma et al., 2008; Xu et al., 2008). c-MYC is a potent regulator of cellular metabolism and enhances glycolytic rate (Gordan et al., 2007) and since c-MYC is overexpressed in ~70% of tumors (Nilsson et al., 2005), the reestablishment of c-MYC expression in GBM cells may inhibit a

glycolysis to OXPHOS transition that occurs during differentiation of normal stem cell populations. Furthermore, the aberrant activation of OCT4, NANOG and SOX2 could potentially interfere with the ability of GBM cells to upregulate and sustain the expression of differentiation markers such as GFAP. Indeed, it is possible to draw comparisons between GBM cells and induced pluripotent stem cells, which are somatic cells that have been reprogrammed to a stem-like state by the forced expression of OCT4, SOX2 and c-MYC, amongst others (Takahashi et al., 2007; Takahashi and Yamanaka, 2006). Like GBM cells, iPS cells have also been shown to abnormally regulate their mtDNA copy number (Kelly et al., 2011) and it is likely that GBM cells behave in a similar manner to poorly reprogrammed cells. Nevertheless, I hypothesize that the aberrant expression of stem cell factors may be a contributing factor that inhibits GBM cells from completing differentiation and maintains GBM cells in a stem-cell like state, which in turn supports their glycolytic, proliferative and tumorigenic nature.

7.2 Maintenance of the mtDNA set point in HSR-GBM1 cells is an essential component of tumorigenicity

Previous studies have investigated the effect of the complete removal of mtDNA (ρ0 cells) on the tumorigenicity of various tumor types, such as bone (Singh et al., 2005), cervical (Shidara et al., 2005) and lung (Amuthan et al., 2002). However, it remained to be determined how mtDNA depletion influences brain tumor cells. Using the mtDNA-specific depletion agent, ddC, I progressively depleted HSR-GBM1 cells of their mtDNA content until the average mtDNA copy number per cell was <1 and subsequently analysed gene expression

changes. I also depleted HSR-GBM1 cells to variable levels of mtDNA content (50%, 20%, 3% and 0.2%) and assessed their tumorigenic potential in immunocompromised mice.

Short-term depletion (7 days) of HSR-GBM1 cells was associated with an increase in the expression of NSC markers NESTIN, MUSASHI1 and CD133 whilst long-term depletion was associated with reduced expression of these factors along with the ESC factors SOX2, NANOG, c-MYC and hTERT. The expression of stem cell factors in GBM is associated with increased tumorigenicity (Ma et al., 2008) and it is therefore reasonable to speculate that short-term depletion of HSR-GBM1 cells enhances their tumorigenicity whilst long-term depletion reduces tumorigenicity. Indeed, HSR-GBM1 cells depleted to 50%, of their original mtDNA content, which were representative of short-term depletion, formed tumors at a faster rate than non-depleted cells. Furthermore, HSR-GBM1 cells depleted to 3% and 0.2%, which were equivalent to long-term depletion, generated fewer tumors that developed at a significantly reduced rate than that of non-depleted cells (Figure 7.2). The gene expression outcomes during mtDNA depletion of HSR-GBM1 cells is in agreement with multiple gene knockdown studies which have demonstrated reduced tumorigenicity of GBM cells following the silencing of MUSASHI1 (Sureban et al., 2008) and SOX2 (Gangemi et al., 2009). This further strengthens the link between GBM tumorigenicity and the expression of stem cell factors. In addition, these outcomes provide evidence that deviations in mtDNA copy number exert powerful influences on the nuclear genome of GBM cells and that mtDNA depletion can reduce GBM tumorigenicity in a similar manner to gene silencing.

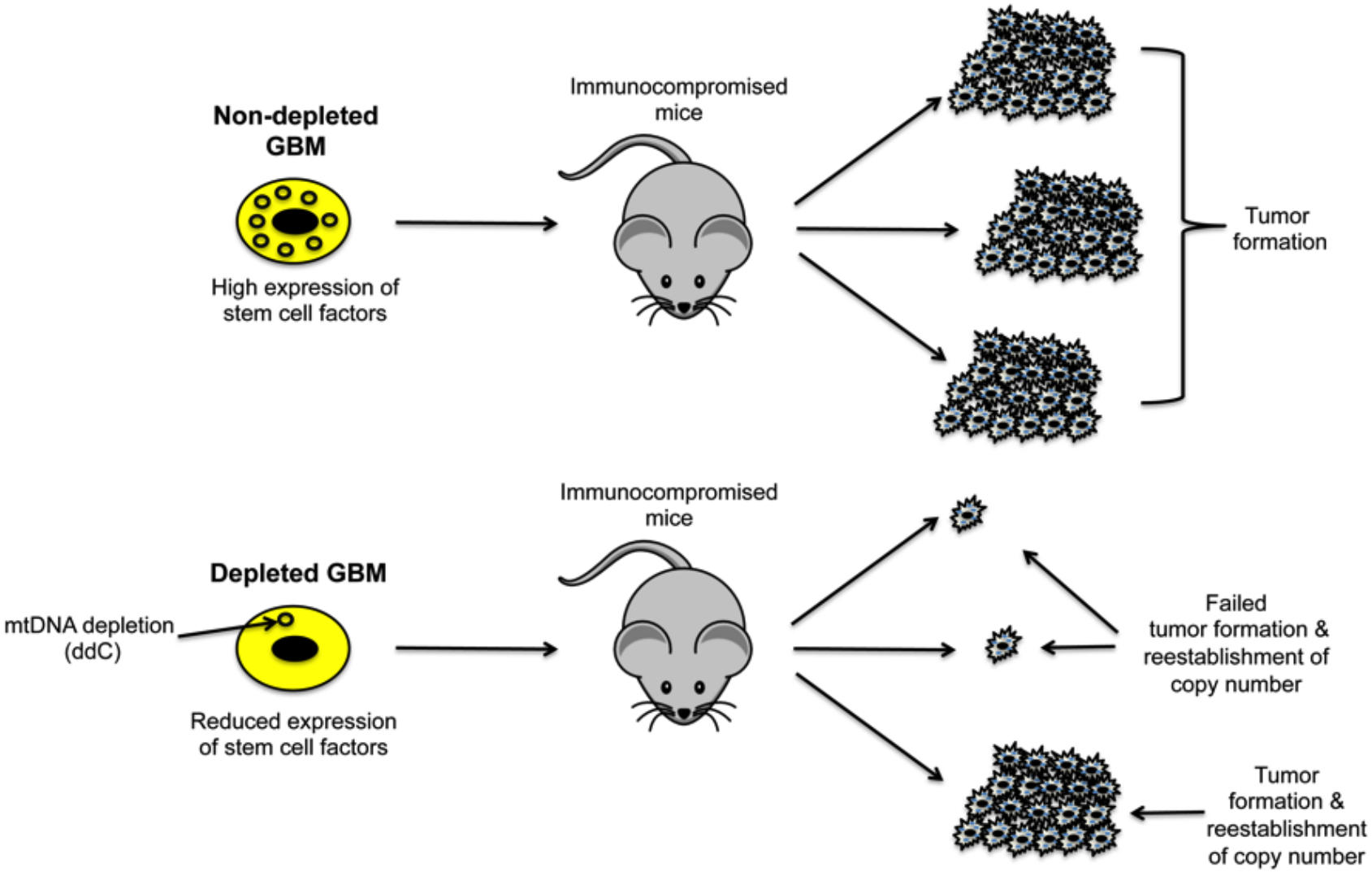
Non-depleted GBM
High expression of stem cell factors
Immunocompromised mice
Tumor formation
Depleted GBM
mtDNA depletion (ddC)
Reduced expression of stem cell factors
Immunocompromised mice
Failed tumor formation & reestablishment of copy number
Tumor formation & reestablishment of copy number

Figure 7.2. Schematic representation of tumor formation assays using non-depleted and mtDNA depleted HSR-GBM1 cells. (Top) Non-depleted HSR-GBM1 cells express stem cell associated factors and generate tumors at a high frequency. (Bottom) mtDNA depleted HSR-GBM1 cells expressed lower levels of stem cell factors and generated tumors at a reduced rate and frequency in immunocompromised mice. Tumors developed from mtDNA depleted HSR-GBM1 cells possessed comparable levels of mtDNA content to non-depleted tumors, which suggests that the reestablishment of mtDNA copy number or mtDNA set point, is a prerequisite to tumor formation. It is likely that the failed development of tumors by depleted HSR-GBM1 cells is due to their inability to reestablish their mtDNA set point.

The observed changes in gene expression in depleted HSR-GBM1 cells are in agreement with previous studies reporting altered gene expression and epigenetic status of ρ0 tumor cells (Singh et al., 2005; Smiraglia et al., 2008). Despite the down regulation of a number of stem cell factors in depleted GBM cells, I also observed elevated expression of multiple factors associated with early developmental processes and GBM tumorigenicity, which included OCT4, SHH and HEY1 (Ben-Porath et al., 2008; Hulleman et al., 2009; Xu et al., 2008). Since mtDNA depletion was inhibitory to GBM tumorigenicity, it is likely that that these factors are playing a role in the maintenance of a stem cell-like population of GBM cells that are resistant to mtDNA depletion. MtDNA copy number analysis of the tumors formed from 3% and 0.2% mtDNA HSR-GBM1 cells revealed that their copy number had recovered to a comparable level to 100% mtDNA tumors. It is likely that in order for HSR-GBM1 cells to establish a tumor, they must first reestablish their mtDNA set point. It is also highly probable that the observed lag phase in tumor development by 3% and 0.2% mtDNA cells is associated with the time required to reestablish the mtDNA set

point. In addition, the reduced frequency of tumors formed by 3% and 0.2% mtDNA cells may be a consequence of HSR-GBM1 cells failing to reestablish their mtDNA set point (Figure 7.2).

MtDNA depleted and ρ0 cells are commonly supplemented with the pyrimidine, uridine. Uridine and other pyrimidines are essential for the generation of nucleotides and require a functional ETC in order to be continuously replenished. Depletion of mtDNA disrupts ETC function and will therefore negatively impact on pyrimidine and nucleotide synthesis. A reduction in nucleotide stores will limit the ability of a cell to perform DNA synthesis and ultimately proliferate. MtDNA depleted HSR-GBM1 cells are supported *in vitro* with uridine, however, following their transfer into immunocompromised mice this substrate support is lost. It is likely that mtDNA depleted HSR-GBM1 cells are unable to sustain their normal rates of DNA synthesis and maintain their nucleotide stores until they successfully reestablish their mtDNA copy number and ETC function. Once this process is complete, HSR-GBM1 cells are able to successfully perform DNA synthesis, proliferate and establish tumors.

Another possible mechanism for mtDNA depletion inhibiting HSR-GBM1 proliferation and tumorigenicity is cross-talk between the nucleus and mtDNA that results in changes in the expression of genes that regulate cell cycle progression. Indeed, Mineri et al. reported altered expression of cell cycle associated genes in ρ0 cells of bone (143BTK-) and lung (A459) tumor cells relative to their ρ+ counterparts (Mineri et al., 2009). The authors hypothesized that a loss of mitochondrial function may signal to the nucleus in a retrograde

manner to slow cell cycle progression. A similar signaling mechanism may be active in depleted HSR-GBM1 cells and may account for their slowed growth and tumor formation rates. Comparative studies of ρ0 and ρ+ cells of lung, breast and bone tumors have been performed and have reported broad changes in gene expression, however, recent studies have lacked consistency regarding the observed changes in gene expression (Behan et al., 2005; Delsite et al., 2002; Magda et al., 2008). Mineri et al. performed a comparative analysis of ρ0 lung and bone tumor cells and identified a cohort of 88 genes that were altered in ρ0 cells of both tumor types, however, there were also a large number of genes that were differentially regulated (Mineri et al., 2009). It is likely that tumor cells of differing origin each respond uniquely to mtDNA depletion. Nevertheless, HSR-GBM1 cells responded negatively to mtDNA by reducing their proliferation rates and tumorigenic potential. These outcomes strongly suggest that maintenance of mtDNA copy number is an essential component of the tumorigenicity of HSR-GBM1 and may also be of importance to other GBM types (Figure 7.2). Indeed, disruption to mitochondrial translation in acute myeloid leukemic cells was recently shown to inhibit tumorigenicity (Skrtic et al., 2011) and further highlights the importance mitochondria and mtDNA in tumor cell function.

7.3 MtDNA genotype influences the establishment of mtDNA copy number in trans-mitochondrial cybrids

As discussed above, changes in mtDNA content directly influence the nucleus. Since the nucleus is receptive to changes in mtDNA copy number, it is highly

likely that discrete changes in the mtDNA genotype of a cell, such as base changes, mutations and/or variants, can also be detected by the nucleus.

Trans-mitochondrial cybrid technology has been extensively utilized to determine the effects of single and multiple point mutations on cellular function (Chomyn et al., 1992; Ghelli et al., 2003; Trounce et al., 1994). These experiments demonstrated that point mutations are extremely deleterious to mitochondrial function that underlies the mitochondrial diseases MELAS, NARP and LOHN (Chomyn et al., 1992; Ghelli et al., 2003; Trounce et al., 1994). Despite the great value of these outcomes, these studies shed little light on how mtDNA mutations can impact on mtDNA copy number regulation and cellular differentiation.

The outcomes described in this thesis reveal that tumor (143BTK-) cells harbouring differing mtDNA genotypes, which contained wild type mtDNA or single and multiple mtDNA mutations, established variable mtDNA copy numbers. Despite no clear trend emerging regarding the established mtDNA copy number of 143BTK- cells containing single or multiple mtDNA mutations, the large increase in copy number of 143BTK-^{3243} may be a compensatory effect due to the severity of the A3243G mutation. It is possible that this mutation, which causes MELAS (Schon et al., 1992), may induce the nucleus to expand mtDNA copy number to compensate for the mitochondrial defects that this mutation causes. This outcome may be similar to that observed in primary lung cells exposed high levels of oxidative stress, which exhibited an increase in mtDNA copy number relative to control cells (Lee et al., 2000). It is unclear

why a similar increase in copy number was not observed in 143BTK-^{8993} and 143BTK-^{11778} cells, which also harbor deleterious mtDNA mutations. However, 143BTK-^{8993} and 143BTK-^{11778} cells possessed greater ETC reserve capacities than 143BTK-^{3243} cells and this may suggest that the increase in copy number is a mechanism to improve the ETC capacity of 143BTK-^{3243} cells, which was not required by 143BTK-^{8993} and 143BTK-^{11778} cells.

The mtDNA of GBM-L1 and GBM-L2 cells contain multiple mtDNA mutations/variants (personal communication with Ka Yu Yueng) and 143BTK- cells containing the donor mtDNA from these cell types contained fewer copies of mtDNA relative to controls. It is possible that these mutations could be present in the regulatory regions of mtDNA, such as the D-loop. Mutations in the D-loop region have been frequently reported in multiple tumor types and are also associated with reductions in mtDNA copy number (Lee et al., 2004; Yu et al., 2010; Yu et al., 2007). It has been postulated that mutations within the D-loop region may reduce the binding efficiency of TFAM and disrupt mtDNA transcription and replication efficiency (Lee et al., 2004; Yu et al., 2010; Yu et al., 2007). The presence of D-loop mutations in 143BTK-^{GBML1} and 143BTK-^{GBML2} cells could potentially disrupt mtDNA copy number regulation in these cells, resulting in reduced copy number. In summary, differences in mtDNA genotype are able to elicit changes in mtDNA copy number by either stimulating the nucleus to increase copy number in response to cellular stress or by disrupting the action of the nuclear encoded mtDNA transcription and replication factors.

7.4 MtDNA genotype influences the differentiation of HSR-GBM1 cells

Single and multiple mtDNA mutations are deleterious to cellular function, however, what remains to be fully determined is how changes in mtDNA affect cellular differentiation. To address this area, mitochondrial dysfunction was induced in HSR-GBM1 cells by R6G exposure before recuse with mitochondria and mtDNA from HSR-GBM1 cells (HSR-HSR) or hNSCs (HSR-NSC) (Figure 7.3). HSR-HSR and HSR-NSC cells exhibited similar expression profiles of NSC associated factors, however, there were differences in GFAP expression and ETC reserve capacity following differentiation. Differentiated HSR-NSC cells showed greater elevation and sustained expression of GFAP and also a greater ETC reserve capacity than HSR-HSR cells (Figure 7.3). These outcomes suggest that the presence of wild type mtDNA (~20%) enhances the differentiation and OXPHOS potential of HSR-NSCs compared to HSR-HSR cells. Once more, discrete changes in mtDNA are capable of inducing profound effects on gene expression and provide some evidence to suggest that alterations to mtDNA, such as mutations, can affect cellular differentiation. These observations are in agreement with previous work by Kelly et al who observed altered gene expression profiles between undifferentiated and differentiated murine ESC cybrids containing divergent populations of mtDNA (Kelly et al., 2013). The mechanism(s) by which the nucleus responds to changes in mtDNA status by altering gene expression requires further investigation. In summary, the partial repopulation of HSR-GBM1 cells with wild type mtDNA enhances their differentiation and OXPHOS potential and further suggests that the mtDNA genotype of HSR-GBM1s restricts their ability to differentiate and maintains their tumorigenic phenotype.

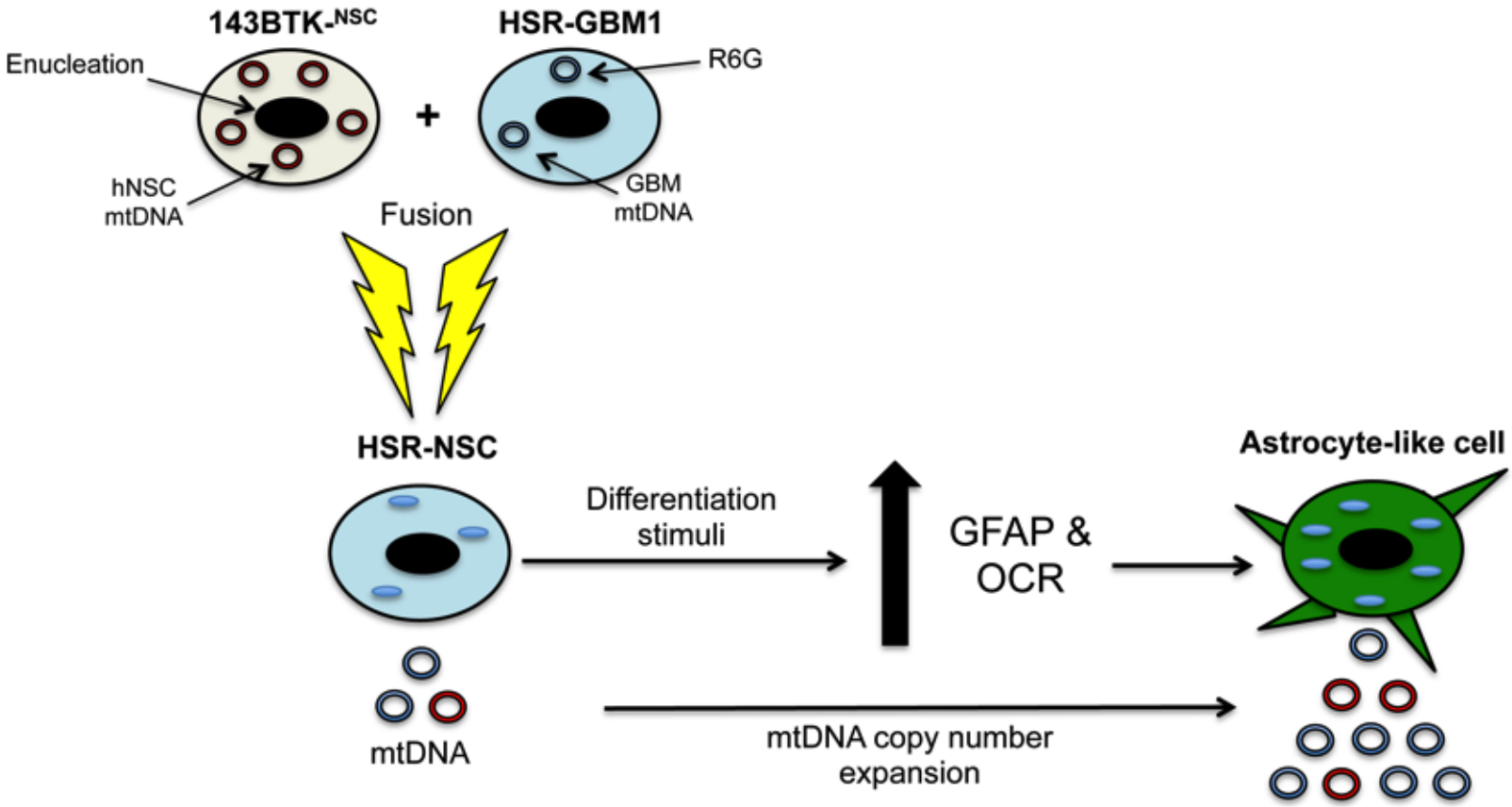
143BTK-NSC
HSR-GBM1
Enucleation
R6G
hNSC
mtDNA
GBM
mtDNA
Fusion
HSR-NSC
Differentiation
stimuli
GFAP &
OCR
Astrocyte-like cell
mtDNA
mtDNA copy number
expansion

Figure 7.3. Schematic representation of the derivation of HSR-NSC cells. HSR-GBM1 cells treated with rhomadine 6G (R6G) for 72 hours were recused by the transferred of hNSC derived mitochondria and mtDNA (red circles). HSR-NSC cells contained ~20% wild type mtDNA and exhibited enhanced properties of differentiation relative to HSR-GBM1 cells, which included sustained elevation of GFAP expression, increased mtDNA copy number and increased O_2 consumption rates (OCR).

7.5 Conclusion

GBM are a highly malignant subgroup of brain tumors that consistently exhibit resistance to therapeutic intervention (Buckner et al., 2007; Hess et al., 2004). GBM contain sub-populations of cells with stem cell-like characteristics called cancer stem cells (CSCs) (Galli et al., 2004; Singh et al., 2003). HSR-GBM1 cells are an established GBM CSC line (Galli et al., 2004), which shares numerous properties with hNSCs. Despite their similarities, I observed that HSR-GBM1 cells do not regulate their mtDNA copy number in a similar manner to hNSCs, which was evidenced by a failed expansion in copy number in response to differentiation stimuli. Consequently, HSR-GBM1 cells do not fully differentiate and acquire an OXPHOS metabolism profile that is exhibited by differentiated hNSCs. I hypothesize that the failed expansion of mtDNA copy number supports the glycolytic, proliferative and tumorigenic properties of HSR-GBM1 cells. Partial repopulation of HSR-GBM1 cells with wild type mtDNA enhanced their differentiation potential and suggests a direct role for mtDNA in the regulation of gene expression and differentiation of HSR-GBM1 cells that is likely to be underpinned by nucleo-mitochondrial DNA cross-talk. Further evidence of the influential power of mtDNA on nuclear gene expression was observed following mtDNA depletion of HSR-GBM1 cells. Depleted HSR-GBM1

cells exhibited changes in the expression of stem cell factors associated with tumorigenicity. In addition, mtDNA depleted HSR-GBM1 cells generated fewer tumors that formed at a slower rate than non-depleted cells in immunocompromised mice. The tumorigenicity of HSR-GBM1 cells was inversely related to mtDNA depletion and strongly suggests that HSR-GBM1 cells require a defined number of mtDNA copies, or set point, to maintain their tumorigenic potential. Collectively, these outcomes highlight that mtDNA is an essential aspect of HSR-GBM1 cellular function and tumorigenicity.

7.6 Future Perspectives

7.6.1 MtDNA copy number regulation in CSCs

The outcomes of this thesis demonstrate that GBM CSCs regulate their copy number in a differential manner to hNSCs. Future work will focus on elucidating the mechanisms that govern the abnormal copy number regulation in GBM CSCs. Recent work in the laboratory has provided evidence to suggest that the mtDNA transcription and replication factors are down regulated in GBM CSCs relative to hNSCs (personal communication with Ka Yu Yueng). Thus, examining the factors that control mtDNA transcription and regulation in GBM CSCs may provide further insight in to how copy number is regulated in these cell types.

Other tumor types have been shown to contain populations of CSCs and it would be interesting to determine whether these cells also show abnormal patterns of mtDNA copy number regulation. Furthermore, analyzing how mtDNA copy umber is regulated in other CSCs is important for two reasons, 1) to build a collection of data outlining how CSCs regulate their copy number and 2) potentially identify pathways/mechanisms that, if targeted, could potentially attenuate abnormal copy number regulation that may in turn reduce tumorigenicity.

7.6.2 MtDNA copy number and tumorigenicity

The data presented in Chapter 5 provides strong evidence to suggest that GBM CSCs require sufficient copies of mtDNA to maintain their tumorigenic potential.

To build upon the association between sufficient mtDNA content and tumorigenicity, future experiments will aim to determine whether other GBM CSCs and indeed other tumor cell types, require sufficient copies of mtDNA to successfully form tumors. If it is determined that other tumor cells types require sufficient copies of mtDNA to maintain their tumorigenicity, this may confirm mtDNA as a potential therapeutic target for tumors

In vitro, ddC effectively depletes cells of mtDNA, however, the systemic application of ddC is associated with cellular toxicity and mitochondrial dysfunction, which renders ddC unsuitable for the targeting of mtDNA in tumors, *in vivo*. Future work will focus on identifying the mechanisms by which mtDNA depletion reduces the tumorigenicity of tumor cells, which at present remains to be fully determined. A greater understanding of how mtDNA depletion reduces tumorigenicity may reveal other approaches that could be utilized to mimic the effects of mtDNA depletion in tumors cells. Such approaches may circumvent the systemic toxicity of ddC and provide new, safer therapeutic strategies.

Another intriguing outcome was that GBM CSCs depleted, on average, to 0.2% mtDNA content were able to reestablish their mtDNA copy number over time and also generate tumors in mice. It is unclear how GBM CSCs are able to initially survive *in vivo* with very little or no mtDNA before generating tumors. Recent studies have shown that healthy cells can transfer mitochondria to neighboring injured or diseased cells in order restore their normal cellular function (Islam et al., 2012). It is likely that a similar interaction between mtDNA depleted GBM CSCs and healthy neighboring cells may occur *in vivo*, however,

this hypothesis requires further investigation. Finally a greater understanding of the role of mtDNA in tumor cells will provide a greater understanding of tumor biology and also the mechanisms that underlie therapeutic resistance.

References

Achanta, G., Sasaki, R., Feng, L., Carew, J. S., Lu, W., Pelicano, H., Keating, M. J., and Huang, P. (2005). Novel role of p53 in maintaining mitochondrial genetic stability through interaction with DNA Pol gamma. The EMBO journal *24*, 3482-3492.

Adam-Vizi, V., and Chinopoulos, C. (2006). Bioenergetics and the formation of mitochondrial reactive oxygen species. Trends in pharmacological sciences *27*, 639-645.

Adams, T. E., Koziolek, E. J., Hoyne, P. H., Bentley, J. D., Lu, L., Lovrecz, G., Ward, C. W., Lee, F. T., Scott, A. M., Nash, A. D.*, et al.* (2009). A truncated soluble epidermal growth factor receptor-Fc fusion ligand trap displays anti-tumour activity in vivo. Growth Factors *27*, 141-154.

Al-Hajj, M., Wicha, M. S., Benito-Hernandez, A., Morrison, S. J., and Clarke, M. F. (2003). Prospective identification of tumorigenic breast cancer cells. Proc Natl Acad Sci U S A *100*, 3983-3988.

Amuthan, G., Biswas, G., Ananadatheerthavarada, H. K., Vijayasarathy, C., Shephard, H. M., and Avadhani, N. G. (2002). Mitochondrial stress-induced calcium signaling, phenotypic changes and invasive behavior in human lung carcinoma A549 cells. Oncogene *21*, 7839-7849.

Anderson, S., Bankier, A. T., Barrell, B. G., de Bruijn, M. H., Coulson, A. R., Drouin, J., Eperon, I. C., Nierlich, D. P., Roe, B. A., Sanger, F.*, et al.* (1981). Sequence and organization of the human mitochondrial genome. Nature *290*, 457-465.

Attardi, G., and Schatz, G. (1988). Biogenesis of mitochondria. Annual review of cell biology *4*, 289-333.

Ball, D. W., Azzoli, C. G., Baylin, S. B., Chi, D., Dou, S., Donis-Keller, H., Cumaraswamy, A., Borges, M., and Nelkin, B. D. (1993). Identification of a human achaete-scute homolog highly expressed in neuroendocrine tumors. Proc Natl Acad Sci U S A *90*, 5648-5652.

Ballot, C., Kluza, J., Lancel, S., Martoriati, A., Hassoun, S. M., Mortier, L., Vienne, J. C., Briand, G., Formstecher, P., Bailly, C.*, et al.* (2010). Inhibition of mitochondrial respiration mediates apoptosis induced by the anti-tumoral alkaloid lamellarin D. Apoptosis : an international journal on programmed cell death *15*, 769-781.

Baltzer, C., Tiefenbock, S. K., and Frei, C. (2010). Mitochondria in response to nutrients and nutrient-sensitive pathways. Mitochondrion *10*, 589-597.

Bao, S., Wu, Q., McLendon, R. E., Hao, Y., Shi, Q., Hjelmeland, A. B., Dewhirst, M. W., Bigner, D. D., and Rich, J. N. (2006a). Glioma stem cells promote radioresistance by preferential activation of the DNA damage response. Nature *444*, 756-760.

Bao, S., Wu, Q., Sathornsumetee, S., Hao, Y., Li, Z., Hjelmeland, A. B., Shi, Q., McLendon, R. E., Bigner, D. D., and Rich, J. N. (2006b). Stem cell-like glioma cells promote tumor angiogenesis through vascular endothelial growth factor. Cancer Res *66*, 7843-7848.

Barazzoni, R., Short, K. R., and Nair, K. S. (2000). Effects of aging on mitochondrial DNA copy number and cytochrome c oxidase gene expression in rat skeletal muscle, liver, and heart. The Journal of biological chemistry *275*, 3343-3347.

Bardella, C., Pollard, P. J., and Tomlinson, I. (2011). SDH mutations in cancer. Biochimica et biophysica acta *1807*, 1432-1443.

Beckers, J., Clark, A., Wunsch, K., Hrabe De Angelis, M., and Gossler, A. (1999). Expression of the mouse Delta1 gene during organogenesis and fetal development. Mechanisms of development *84*, 165-168.

Behan, A., Doyle, S., and Farrell, M. (2005). Adaptive responses to mitochondrial dysfunction in the rho degrees Namalwa cell. Mitochondrion *5*, 173-193.

Beier, D., Hau, P., Proescholdt, M., Lohmeier, A., Wischhusen, J., Oefner, P. J., Aigner, L., Brawanski, A., Bogdahn, U., and Beier, C. P. (2007). CD133(+) and CD133(-) glioblastoma-derived cancer stem cells show differential growth characteristics and molecular profiles. Cancer Res *67*, 4010-4015.

Ben-Porath, I., Thomson, M. W., Carey, V. J., Ge, R., Bell, G. W., Regev, A., and Weinberg, R. A. (2008). An embryonic stem cell-like gene expression signature in poorly differentiated aggressive human tumors. Nature genetics *40*, 499-507.

Bogenhagen, D. F., and Clayton, D. A. (2003). The mitochondrial DNA replication bubble has not burst. Trends Biochem Sci *28*, 357-360.

Bonora, E., Porcelli, A. M., Gasparre, G., Biondi, A., Ghelli, A., Carelli, V., Baracca, A., Tallini, G., Martinuzzi, A., Lenaz, G*., et al.* (2006). Defective oxidative phosphorylation in thyroid oncocytic carcinoma is associated with pathogenic mitochondrial DNA mutations affecting complexes I and III. Cancer Res *66*, 6087-6096.

Bose, H. S., Lingappa, V. R., and Miller, W. L. (2002). Rapid regulation of steroidogenesis by mitochondrial protein import. Nature *417*, 87-91.

Bradley, A., Evans, M., Kaufman, M. H., and Robertson, E. (1984). Formation of germ-line chimaeras from embryo-derived teratocarcinoma cell lines. Nature *309*, 255-256.

Brandon, M., Baldi, P., and Wallace, D. C. (2006). Mitochondrial mutations in cancer. Oncogene *25*, 4647-4662.

Brini, M. (2003). Ca(2+) signalling in mitochondria: mechanism and role in physiology and pathology. Cell calcium *34*, 399-405.

Brown, G. C. (1992). Control of respiration and ATP synthesis in mammalian mitochondria and cells. The Biochemical journal *284 (Pt 1)*, 1-13.

Brustle, O., Jones, K. N., Learish, R. D., Karram, K., Choudhary, K., Wiestler, O. D., Duncan, I. D., and McKay, R. D. (1999). Embryonic stem cell-derived glial precursors: a source of myelinating transplants. Science *285*, 754-756.

Buckner, J. C., Brown, P. D., O'Neill, B. P., Meyer, F. B., Wetmore, C. J., and Uhm, J. H. (2007). Central nervous system tumors. Mayo Clinic proceedings Mayo Clinic *82*, 1271-1286.

Bustin, S. A. (2000). Absolute quantification of mRNA using real-time reverse transcription polymerase chain reaction assays. Journal of molecular endocrinology *25*, 169-193.

Cai, J., Chen, J., Liu, Y., Miura, T., Luo, Y., Loring, J. F., Freed, W. J., Rao, M. S., and Zeng, X. (2006). Assessing self-renewal and differentiation in human embryonic stem cell lines. Stem cells *24*, 516-530.

Carling, P. J., Cree, L. M., and Chinnery, P. F. (2011). The implications of mitochondrial DNA copy number regulation during embryogenesis. Mitochondrion *11*, 686-692.

Carrodeguas, J. A., Theis, K., Bogenhagen, D. F., and Kisker, C. (2001). Crystal structure and deletion analysis show that the accessory subunit of mammalian DNA polymerase gamma, Pol gamma B, functions as a homodimer. Molecular cell *7*, 43-54.

Cavalli, L. R., Varella-Garcia, M., and Liang, B. C. (1997). Diminished tumorigenic phenotype after depletion of mitochondrial DNA. Cell growth & differentiation : the molecular biology journal of the American Association for Cancer Research *8*, 1189-1198.

Chan, S. S., and Copeland, W. C. (2009). DNA polymerase gamma and mitochondrial disease: understanding the consequence of POLG mutations. Biochimica et biophysica acta *1787*, 312-319.

Chandra, D., and Singh, K. K. (2011). Genetic insights into OXPHOS defect and its role in cancer. Biochimica et biophysica acta *1807*, 620-625.

Chen, R., Nishimura, M. C., Bumbaca, S. M., Kharbanda, S., Forrest, W. F., Kasman, I. M., Greve, J. M., Soriano, R. H., Gilmour, L. L., Rivers, C. S.*, et al.* (2010). A hierarchy of self-renewing tumor-initiating cell types in glioblastoma. Cancer cell *17*, 362-375.

Chen, T., He, J., Shen, L., Fang, H., Nie, H., Jin, T., Wei, X., Xin, Y., Jiang, Y., Li, H.*, et al.* (2011). The mitochondrial DNA 4,977-bp deletion and its implication in copy number alteration in colorectal cancer. BMC medical genetics *12*, 8.

Chinnery, P. F., Howell, N., Lightowlers, R. N., and Turnbull, D. M. (1997). Molecular pathology of MELAS and MERRF. The relationship between mutation load and clinical phenotypes. Brain : a journal of neurology *120 (Pt 10)*, 1713-1721.

Cho, Y. M., Kim, J. H., Kim, M., Park, S. J., Koh, S. H., Ahn, H. S., Kang, G. H., Lee, J. B., Park, K. S., and Lee, H. K. (2012). Mesenchymal stem cells transfer mitochondria to the cells with virtually no mitochondrial function but not with pathogenic mtDNA mutations. PLoS One *7*, e32778.

Cho, Y. M., Kwon, S., Pak, Y. K., Seol, H. W., Choi, Y. M., Park do, J., Park, K. S., and Lee, H. K. (2006). Dynamic changes in mitochondrial biogenesis and antioxidant enzymes during the spontaneous differentiation of human embryonic stem cells. Biochemical and biophysical research communications *348*, 1472-1478.

Chomyn, A., Martinuzzi, A., Yoneda, M., Daga, A., Hurko, O., Johns, D., Lai, S. T., Nonaka, I., Angelini, C., and Attardi, G. (1992). MELAS mutation in mtDNA binding site for transcription termination factor causes defects in protein synthesis and in respiration but no change in levels of upstream and downstream mature transcripts. Proc Natl Acad Sci U S A *89*, 4221-4225.

Christofk, H. R., Vander Heiden, M. G., Harris, M. H., Ramanathan, A., Gerszten, R. E., Wei, R., Fleming, M. D., Schreiber, S. L., and Cantley, L. C. (2008). The M2 splice isoform of pyruvate kinase is important for cancer metabolism and tumour growth. Nature *452*, 230-233.

Chung, S., Dzeja, P. P., Faustino, R. S., Perez-Terzic, C., Behfar, A., and Terzic, A. (2007). Mitochondrial oxidative metabolism is required for the cardiac differentiation of stem cells. Nature clinical practice Cardiovascular medicine *4 Suppl 1*, S60-67.

Clarke, M. F., Dick, J. E., Dirks, P. B., Eaves, C. J., Jamieson, C. H., Jones, D. L., Visvader, J., Weissman, I. L., and Wahl, G. M. (2006). Cancer stem cells--perspectives on current status and future directions: AACR Workshop on cancer stem cells. Cancer Res *66*, 9339-9344.

Clayton, D. A. (1998). Nuclear-mitochondrial intergenomic communication. BioFactors *7*, 203-205.

Clement, V., Sanchez, P., de Tribolet, N., Radovanovic, I., and Ruiz i Altaba, A. (2007). HEDGEHOG-GLI1 signaling regulates human glioma growth, cancer stem cell self-renewal, and tumorigenicity. Curr Biol *17*, 165-172.

Collins, A. T., Berry, P. A., Hyde, C., Stower, M. J., and Maitland, N. J. (2005). Prospective identification of tumorigenic prostate cancer stem cells. Cancer Res *65*, 10946-10951.

Dagan, T., Sable, C., Bray, J., and Gerschenson, M. (2002). Mitochondrial dysfunction and antiretroviral nucleoside analog toxicities: what is the evidence? Mitochondrion *1*, 397-412.

DeBerardinis, R. J., Lum, J. J., Hatzivassiliou, G., and Thompson, C. B. (2008). The biology of cancer: metabolic reprogramming fuels cell growth and proliferation. Cell metabolism *7*, 11-20.

DeBerardinis, R. J., Mancuso, A., Daikhin, E., Nissim, I., Yudkoff, M., Wehrli, S., and Thompson, C. B. (2007). Beyond aerobic glycolysis: transformed cells can engage in glutamine metabolism that exceeds the requirement for protein and nucleotide synthesis. Proc Natl Acad Sci U S A *104*, 19345-19350.

Dell'Albani, P. (2008). Stem cell markers in gliomas. Neurochemical research *33*, 2407-2415.

Delsite, R., Kachhap, S., Anbazhagan, R., Gabrielson, E., and Singh, K. K. (2002). Nuclear genes involved in mitochondria-to-nucleus communication in breast cancer cells. Molecular cancer *1*, 6.

Egan, K., Kusao, I., Troelstrup, D., Agsalda, M., and Shiramizu, B. (2010). Mitochondrial DNA in residual leukemia cells in cerebrospinal fluid in children with acute lymphoblastic leukemia. Journal of clinical medicine research *2*, 225-229.

Ekstrand, M. I., Falkenberg, M., Rantanen, A., Park, C. B., Gaspari, M., Hultenby, K., Rustin, P., Gustafsson, C. M., and Larsson, N. G. (2004). Mitochondrial transcription factor A regulates mtDNA copy number in mammals. Human molecular genetics *13*, 935-944.

Ertel, A., Tsirigos, A., Whitaker-Menezes, D., Birbe, R. C., Pavlides, S., Martinez-Outschoorn, U. E., Pestell, R. G., Howell, A., Sotgia, F., and Lisanti, M. P. (2012). Is cancer a metabolic rebellion against host aging? In the quest for immortality, tumor cells try to save themselves by boosting mitochondrial metabolism. Cell cycle *11*, 253-263.

Evan, G. I., and Vousden, K. H. (2001). Proliferation, cell cycle and apoptosis in cancer. Nature *411*, 342-348.

Evans, M. J., and Kaufman, M. H. (1981). Establishment in culture of pluripotential cells from mouse embryos. Nature *292*, 154-156.

Facucho-Oliveira, J. M., Alderson, J., Spikings, E. C., Egginton, S., and St John, J. C. (2007). Mitochondrial DNA replication during differentiation of murine embryonic stem cells. Journal of cell science *120*, 4025-4034.

Falkenberg, M., Larsson, N. G., and Gustafsson, C. M. (2007). DNA replication and transcription in mammalian mitochondria. Annual review of biochemistry *76*, 679-699.

Fan, A. X., Radpour, R., Haghighi, M. M., Kohler, C., Xia, P., Hahn, S., Holzgreve, W., and Zhong, X. Y. (2009). Mitochondrial DNA content in paired normal and cancerous breast tissue samples from patients with breast cancer. Journal of cancer research and clinical oncology *135*, 983-989.

Fernandez-Silva, P., Enriquez, J. A., and Montoya, J. (2003). Replication and transcription of mammalian mitochondrial DNA. Experimental physiology *88*, 41-56.

Finkel, T., Serrano, M., and Blasco, M. A. (2007). The common biology of cancer and ageing. Nature *448*, 767-774.

Fong, H., Hohenstein, K. A., and Donovan, P. J. (2008). Regulation of self-renewal and pluripotency by Sox2 in human embryonic stem cells. Stem cells *26*, 1931-1938.

Fraichard, A., Chassande, O., Bilbaut, G., Dehay, C., Savatier, P., and Samarut, J. (1995). In vitro differentiation of embryonic stem cells into glial cells and functional neurons. Journal of cell science *108 (Pt 10)*, 3181-3188.

Frey, T. G., and Mannella, C. A. (2000). The internal structure of mitochondria. Trends Biochem Sci *25*, 319-324.

Frosina, G. (2009). DNA repair and resistance of gliomas to chemotherapy and radiotherapy. Molecular cancer research : MCR *7*, 989-999.

Furnari, F. B., Fenton, T., Bachoo, R. M., Mukasa, A., Stommel, J. M., Stegh, A., Hahn, W. C., Ligon, K. L., Louis, D. N., Brennan, C.*, et al.* (2007). Malignant astrocytic glioma: genetics, biology, and paths to treatment. Genes & development *21*, 2683-2710.

Gage, F. H. (2000). Mammalian neural stem cells. Science *287*, 1433-1438.

Galli, R., Binda, E., Orfanelli, U., Cipelletti, B., Gritti, A., De Vitis, S., Fiocco, R., Foroni, C., Dimeco, F., and Vescovi, A. (2004). Isolation and characterization of tumorigenic, stem-like neural precursors from human glioblastoma. Cancer Res *64*, 7011-7021.

Gangemi, R. M., Griffero, F., Marubbi, D., Perera, M., Capra, M. C., Malatesta, P., Ravetti, G. L., Zona, G. L., Daga, A., and Corte, G. (2009). SOX2 silencing in glioblastoma tumor-initiating cells causes stop of proliferation and loss of tumorigenicity. Stem cells *27*, 40-48.

Ghelli, A., Zanna, C., Porcelli, A. M., Schapira, A. H., Martinuzzi, A., Carelli, V., and Rugolo, M. (2003). Leber's hereditary optic neuropathy (LHON) pathogenic mutations induce mitochondrial-dependent apoptotic death in transmitochondrial cells incubated with galactose medium. The Journal of biological chemistry *278*, 4145-4150.

Ginis, I., Luo, Y., Miura, T., Thies, S., Brandenberger, R., Gerecht-Nir, S., Amit, M., Hoke, A., Carpenter, M. K., Itskovitz-Eldor, J., and Rao, M. S. (2004). Differences between human and mouse embryonic stem cells. Developmental biology *269*, 360-380.

Gleyzer, N., Vercauteren, K., and Scarpulla, R. C. (2005). Control of mitochondrial transcription specificity factors (TFB1M and TFB2M) by nuclear respiratory factors (NRF-1 and NRF-2) and PGC-1 family coactivators. Molecular and cellular biology *25*, 1354-1366.

Gordan, J. D., Thompson, C. B., and Simon, M. C. (2007). HIF and c-Myc: sibling rivals for control of cancer cell metabolism and proliferation. Cancer cell *12*, 108-113.

Greenall, S. A., Gherardi, E., Liu, Z., Donoghue, J. F., Vitali, A. A., Li, Q., Murphy, R., Iamele, L., Scott, A. M., and Johns, T. G. (2012). Non-agonistic bivalent antibodies that promote c-MET degradation and inhibit tumor growth and others specific for tumor related c-MET. PLoS One *7*, e34658.

Greene, J. M., Li, Y. L., Yourey, P. A., Gruber, J., Carter, K. C., Shell, B. K., Dillon, P. A., Florence, C., Duan, D. R., Blunt, A.*, et al.* (1998). Identification and characterization of a novel member of the fibroblast growth factor family. The European journal of neuroscience *10*, 1911-1925.

Grifman, M., Galyam, N., Seidman, S., and Soreq, H. (1998). Functional redundancy of acetylcholinesterase and neuroligin in mammalian neuritogenesis. Proc Natl Acad Sci U S A *95*, 13935-13940.

Griguer, C. E., and Oliva, C. R. (2011). Bioenergetics pathways and therapeutic resistance in gliomas: emerging role of mitochondria. Current pharmaceutical design *17*, 2421-2427.

Griguer, C. E., Oliva, C. R., and Gillespie, G. Y. (2005). Glucose metabolism heterogeneity in human and mouse malignant glioma cell lines. Journal of neuro-oncology *74*, 123-133.

Guo, J., Zheng, L., Liu, W., Wang, X., Wang, Z., French, A. J., Kang, D., Chen, L., and Thibodeau, S. N. (2011). Frequent truncating mutation of TFAM induces mitochondrial DNA depletion and apoptotic resistance in microsatellite-unstable colorectal cancer. Cancer Res *71*, 2978-2987.

Hance, N., Ekstrand, M. I., and Trifunovic, A. (2005). Mitochondrial DNA polymerase gamma is essential for mammalian embryogenesis. Human molecular genetics *14*, 1775-1783.

Hansson, A., Hance, N., Dufour, E., Rantanen, A., Hultenby, K., Clayton, D. A., Wibom, R., and Larsson, N. G. (2004). A switch in metabolism precedes increased mitochondrial biogenesis in respiratory chain-deficient mouse hearts. Proc Natl Acad Sci U S A *101*, 3136-3141.

Heddi, A., Faure-Vigny, H., Wallace, D. C., and Stepien, G. (1996). Coordinate expression of nuclear and mitochondrial genes involved in energy production in carcinoma and oncocytoma. Biochimica et biophysica acta *1316*, 203-209.

Hess, K. R., Broglio, K. R., and Bondy, M. L. (2004). Adult glioma incidence trends in the United States, 1977-2000. Cancer *101*, 2293-2299.

Hildenbeutel, M., Habib, S. J., Herrmann, J. M., and Rapaport, D. (2008). New insights into the mechanism of precursor protein insertion into the mitochondrial membranes. International review of cell and molecular biology *268*, 147-190.

Hirschey, M. D., Shimazu, T., Goetzman, E., Jing, E., Schwer, B., Lombard, D. B., Grueter, C. A., Harris, C., Biddinger, S., Ilkayeva, O. R.*, et al.* (2010). SIRT3 regulates mitochondrial fatty-acid oxidation by reversible enzyme deacetylation. Nature *464*, 121-125.

Holmberg, J., He, X., Peredo, I., Orrego, A., Hesselager, G., Ericsson, C., Hovatta, O., Oba-Shinjo, S. M., Marie, S. K., Nister, M., and Muhr, J. (2011). Activation of neural and pluripotent

stem cell signatures correlates with increased malignancy in human glioma. PLoS One *6*, e18454.

Holt, I. J., Harding, A. E., Petty, R. K., and Morgan-Hughes, J. A. (1990). A new mitochondrial disease associated with mitochondrial DNA heteroplasmy. American journal of human genetics *46*, 428-433.

Holt, I. J., and Jacobs, H. T. (2003). Response: The mitochondrial DNA replication bubble has not burst. Trends Biochem Sci *28*, 355-356.

Holt, I. J., Miller, D. H., and Harding, A. E. (1989). Genetic heterogeneity and mitochondrial DNA heteroplasmy in Leber's hereditary optic neuropathy. Journal of medical genetics *26*, 739-743.

Hubner, K., Fuhrmann, G., Christenson, L. K., Kehler, J., Reinbold, R., De La Fuente, R., Wood, J., Strauss, J. F., 3rd, Boiani, M., and Scholer, H. R. (2003). Derivation of oocytes from mouse embryonic stem cells. Science *300*, 1251-1256.

Hulleman, E., Quarto, M., Vernell, R., Masserdotti, G., Colli, E., Kros, J. M., Levi, D., Gaetani, P., Tunici, P., Finocchiaro, G.*, et al.* (2009). A role for the transcription factor HEY1 in glioblastoma. Journal of cellular and molecular medicine *13*, 136-146.

Ishikawa, K., Takenaga, K., Akimoto, M., Koshikawa, N., Yamaguchi, A., Imanishi, H., Nakada, K., Honma, Y., and Hayashi, J. (2008). ROS-generating mitochondrial DNA mutations can regulate tumor cell metastasis. Science *320*, 661-664.

Islam, M. N., Das, S. R., Emin, M. T., Wei, M., Sun, L., Westphalen, K., Rowlands, D. J., Quadri, S. K., Bhattacharya, S., and Bhattacharya, J. (2012). Mitochondrial transfer from bone-marrow-derived stromal cells to pulmonary alveoli protects against acute lung injury. Nat Med *18*, 759-765.

Iyer, S., Xiao, E., Alsayegh, K., Eroshenko, N., Riggs, M. J., Bennett, J. P., Jr., and Rao, R. R. (2012). Mitochondrial gene replacement in human pluripotent stem cell-derived neural progenitors. Gene therapy *19*, 469-475.

Jiang, W. W., Masayesva, B., Zahurak, M., Carvalho, A. L., Rosenbaum, E., Mambo, E., Zhou, S., Minhas, K., Benoit, N., Westra, W. H.*, et al.* (2005). Increased mitochondrial DNA content in saliva associated with head and neck cancer. Clinical cancer research : an official journal of the American Association for Cancer Research *11*, 2486-2491.

Joza, N., Susin, S. A., Daugas, E., Stanford, W. L., Cho, S. K., Li, C. Y., Sasaki, T., Elia, A. J., Cheng, H. Y., Ravagnan, L.*, et al.* (2001). Essential role of the mitochondrial apoptosis-inducing factor in programmed cell death. Nature *410*, 549-554.

Kaneko, Y., Sakakibara, S., Imai, T., Suzuki, A., Nakamura, Y., Sawamoto, K., Ogawa, Y., Toyama, Y., Miyata, T., and Okano, H. (2000). Musashi1: an evolutionally conserved marker for CNS progenitor cells including neural stem cells. Dev Neurosci *22*, 139-153.

Kehat, I., Kenyagin-Karsenti, D., Snir, M., Segev, H., Amit, M., Gepstein, A., Livne, E., Binah, O., Itskovitz-Eldor, J., and Gepstein, L. (2001). Human embryonic stem cells can differentiate into myocytes with structural and functional properties of cardiomyocytes. J Clin Invest *108*, 407-414.

Kelly, R. D., Rodda, A. E., Dickinson, A., Mahmud, A., Nefzger, C. M., Lee, W., Forsythe, J., Polo, J. M., Trounce, I. A., McKenzie, M.*, et al.* (2013). Mitochondrial DNA haplotypes define gene expression patterns in pluripotent and differentiating embryonic stem cells. Stem cells.

Kelly, R. D., Sumer, H., McKenzie, M., Facucho-Oliveira, J., Trounce, I. A., Verma, P. J., and St John, J. C. (2011). The Effects of Nuclear Reprogramming on Mitochondrial DNA Replication. Stem cell reviews.

Kim, J., Chu, J., Shen, X., Wang, J., and Orkin, S. H. (2008). An extended transcriptional network for pluripotency of embryonic stem cells. Cell *132*, 1049-1061.

Kim, M. M., Clinger, J. D., Masayesva, B. G., Ha, P. K., Zahurak, M. L., Westra, W. H., and Califano, J. A. (2004). Mitochondrial DNA quantity increases with histopathologic grade in premalignant and malignant head and neck lesions. Clinical cancer research : an official journal of the American Association for Cancer Research *10*, 8512-8515.

King, M. P., and Attardi, G. (1989). Human cells lacking mtDNA: repopulation with exogenous mitochondria by complementation. Science *246*, 500-503.

Kirches, E., Krause, G., Warich-Kirches, M., Weis, S., Schneider, T., Meyer-Puttlitz, B., Mawrin, C., and Dietzmann, K. (2001). High frequency of mitochondrial DNA mutations in glioblastoma multiforme identified by direct sequence comparison to blood samples. International journal of cancer Journal international du cancer *93*, 534-538.

Kit, S., Dubbs, D. R., Piekarski, L. J., and Hsu, T. C. (1963). Deletion of Thymidine Kinase Activity from L Cells Resistant to Bromodeoxyuridine. Experimental cell research *31*, 297-312.

Kobayashi, K., Takahashi, H., Inoue, A., Harada, H., Toshimori, S., Kobayashi, Y., Goto, K., Sugimoto, K., Yano, H., Ohnishi, T., and Tanaka, J. (2012). Oct-3/4 promotes migration and invasion of glioblastoma cells. Journal of cellular biochemistry *113*, 508-517.

Krebs, H. A., and Johnson, W. A. (1937). Metabolism of ketonic acids in animal tissues. The Biochemical journal *31*, 645-660.

Kulawiec, M., Ayyasamy, V., and Singh, K. K. (2009a). p53 regulates mtDNA copy number and mitocheckpoint pathway. Journal of carcinogenesis *8*, 8.

Kulawiec, M., Owens, K. M., and Singh, K. K. (2009b). mtDNA G10398A variant in African-American women with breast cancer provides resistance to apoptosis and promotes metastasis in mice. Journal of human genetics *54*, 647-654.

Kurland, C. G., and Andersson, S. G. (2000). Origin and evolution of the mitochondrial proteome. Microbiology and molecular biology reviews : MMBR *64*, 786-820.

Kusao, I., Agsalda, M., Troelstrup, D., Villanueva, N., and Shiramizu, B. (2008). Chemotoxicity recovery of mitochondria in non-Hodgkin lymphoma resulting in minimal residual disease. Pediatric blood & cancer *51*, 193-197.

Lapidot, T., Sirard, C., Vormoor, J., Murdoch, B., Hoang, T., Caceres-Cortes, J., Minden, M., Paterson, B., Caligiuri, M. A., and Dick, J. E. (1994). A cell initiating human acute myeloid leukaemia after transplantation into SCID mice. Nature *367*, 645-648.

Lee, H. C., Li, S. H., Lin, J. C., Wu, C. C., Yeh, D. C., and Wei, Y. H. (2004). Somatic mutations in the D-loop and decrease in the copy number of mitochondrial DNA in human hepatocellular carcinoma. Mutation research *547*, 71-78.

Lee, H. C., Lu, C. Y., Fahn, H. J., and Wei, Y. H. (1998). Aging- and smoking-associated alteration in the relative content of mitochondrial DNA in human lung. FEBS letters *441*, 292-296.

Lee, H. C., and Wei, Y. H. (1997). Mutation and oxidative damage of mitochondrial DNA and defective turnover of mitochondria in human aging. Journal of the Formosan Medical Association = Taiwan yi zhi *96*, 770-778.

Lee, H. C., Yin, P. H., Lu, C. Y., Chi, C. W., and Wei, Y. H. (2000). Increase of mitochondria and mitochondrial DNA in response to oxidative stress in human cells. The Biochemical journal *348 Pt 2*, 425-432.

Lee, J., Kotliarova, S., Kotliarov, Y., Li, A., Su, Q., Donin, N. M., Pastorino, S., Purow, B. W., Christopher, N., Zhang, W.*, et al.* (2006). Tumor stem cells derived from glioblastomas cultured in bFGF and EGF more closely mirror the phenotype and genotype of primary tumors than do serum-cultured cell lines. Cancer cell *9*, 391-403.

Legros, F., Malka, F., Frachon, P., Lombes, A., and Rojo, M. (2004). Organization and dynamics of human mitochondrial DNA. Journal of cell science *117*, 2653-2662.

Leimeister, C., Externbrink, A., Klamt, B., and Gessler, M. (1999). Hey genes: a novel subfamily of hairy- and Enhancer of split related genes specifically expressed during mouse embryogenesis. Mechanisms of development *85*, 173-177.

Lendahl, U., Zimmerman, L. B., and McKay, R. D. (1990). CNS stem cells express a new class of intermediate filament protein. Cell *60*, 585-595.

Leung, D. W., Cachianes, G., Kuang, W. J., Goeddel, D. V., and Ferrara, N. (1989). Vascular endothelial growth factor is a secreted angiogenic mitogen. Science *246*, 1306-1309.

Levine, A. J., and Puzio-Kuter, A. M. (2010). The control of the metabolic switch in cancers by oncogenes and tumor suppressor genes. Science *330*, 1340-1344.

Li, J., Tang, H., Mullen, T. M., Westberg, C., Reddy, T. R., Rose, D. W., and Wong-Staal, F. (1999). A role for RNA helicase A in post-transcriptional regulation of HIV type 1. Proc Natl Acad Sci U S A *96*, 709-714.

Li, M., Pevny, L., Lovell-Badge, R., and Smith, A. (1998). Generation of purified neural precursors from embryonic stem cells by lineage selection. Curr Biol *8*, 971-974.

Li, X. J., Du, Z. W., Zarnowska, E. D., Pankratz, M., Hansen, L. O., Pearce, R. A., and Zhang, S. C. (2005). Specification of motoneurons from human embryonic stem cells. Nature biotechnology *23*, 215-221.

Liang, B. C., and Hays, L. (1996). Mitochondrial DNA copy number changes in human gliomas. Cancer letters *105*, 167-173.

Lin, C. S., Wang, L. S., Tsai, C. M., and Wei, Y. H. (2008). Low copy number and low oxidative damage of mitochondrial DNA are associated with tumor progression in lung cancer tissues after neoadjuvant chemotherapy. Interactive cardiovascular and thoracic surgery *7*, 954-958.

Lin, L. F., Doherty, D. H., Lile, J. D., Bektesh, S., and Collins, F. (1993). GDNF: a glial cell line-derived neurotrophic factor for midbrain dopaminergic neurons. Science *260*, 1130-1132.

Lisanti, M. P., Martinez-Outschoorn, U. E., Lin, Z., Pavlides, S., Whitaker-Menezes, D., Pestell, R. G., Howell, A., and Sotgia, F. (2011a). Hydrogen peroxide fuels aging, inflammation, cancer metabolism and metastasis: the seed and soil also needs "fertilizer". Cell cycle *10*, 2440-2449.

Lisanti, M. P., Martinez-Outschoorn, U. E., Pavlides, S., Whitaker-Menezes, D., Pestell, R. G., Howell, A., and Sotgia, F. (2011b). Accelerated aging in the tumor microenvironment: connecting aging, inflammation and cancer metabolism with personalized medicine. Cell cycle *10*, 2059-2063.

Litonin, D., Sologub, M., Shi, Y., Savkina, M., Anikin, M., Falkenberg, M., Gustafsson, C. M., and Temiakov, D. (2010). Human mitochondrial transcription revisited: only TFAM and TFB2M are required for transcription of the mitochondrial genes in vitro. The Journal of biological chemistry *285*, 18129-18133.

Liu, V. W., Shi, H. H., Cheung, A. N., Chiu, P. M., Leung, T. W., Nagley, P., Wong, L. C., and Ngan, H. Y. (2001). High incidence of somatic mitochondrial DNA mutations in human ovarian carcinomas. Cancer Res *61*, 5998-6001.

Livak, K. J., and Schmittgen, T. D. (2001). Analysis of relative gene expression data using real-time quantitative PCR and the 2(-Delta Delta C(T)) Method. Methods *25*, 402-408.

Lumelsky, N., Blondel, O., Laeng, P., Velasco, I., Ravin, R., and McKay, R. (2001). Differentiation of embryonic stem cells to insulin-secreting structures similar to pancreatic islets. Science *292*, 1389-1394.

Ma, Y., Bai, R. K., Trieu, R., and Wong, L. J. (2010). Mitochondrial dysfunction in human breast cancer cells and their transmitochondrial cybrids. Biochimica et biophysica acta *1797*, 29-37.

Ma, Y. H., Mentlein, R., Knerlich, F., Kruse, M. L., Mehdorn, H. M., and Held-Feindt, J. (2008). Expression of stem cell markers in human astrocytomas of different WHO grades. Journal of neuro-oncology *86*, 31-45.

Magda, D., Lecane, P., Prescott, J., Thiemann, P., Ma, X., Dranchak, P. K., Toleno, D. M., Ramaswamy, K., Siegmund, K. D., and Hacia, J. G. (2008). mtDNA depletion confers specific gene expression profiles in human cells grown in culture and in xenograft. BMC genomics *9*, 521.

Mambo, E., Chatterjee, A., Xing, M., Tallini, G., Haugen, B. R., Yeung, S. C., Sukumar, S., and Sidransky, D. (2005). Tumor-specific changes in mtDNA content in human cancer. International journal of cancer Journal international du cancer *116*, 920-924.

Mao, P., Gallagher, P., Nedungadi, S., Manczak, M., Shirendeb, U. P., Kohama, S. G., Ferguson, B., Park, B. S., and Reddy, P. H. (2012). Mitochondrial DNA deletions and differential mitochondrial DNA content in Rhesus monkeys: implications for aging. Biochimica et biophysica acta *1822*, 111-119.

Matoba, S., Kang, J. G., Patino, W. D., Wragg, A., Boehm, M., Gavrilova, O., Hurley, P. J., Bunz, F., and Hwang, P. M. (2006). p53 regulates mitochondrial respiration. Science *312*, 1650-1653.

McKay, R. (1997). Stem cells in the central nervous system. Science *276*, 66-71.

McKenzie, M., and Trounce, I. (2000). Expression of Rattus norvegicus mtDNA in Mus musculus cells results in multiple respiratory chain defects. The Journal of biological chemistry *275*, 31514-31519.

McKenzie, M., Trounce, I. A., Cassar, C. A., and Pinkert, C. A. (2004). Production of homoplasmic xenomitochondrial mice. Proc Natl Acad Sci U S A *101*, 1685-1690.

Meierhofer, D., Mayr, J. A., Foetschl, U., Berger, A., Fink, K., Schmeller, N., Hacker, G. W., Hauser-Kronberger, C., Kofler, B., and Sperl, W. (2004). Decrease of mitochondrial DNA content and energy metabolism in renal cell carcinoma. Carcinogenesis *25*, 1005-1010.

Meyerhof, O. (1951). Mechanisms of glycolysis and fermentation. Canadian journal of medical sciences *29*, 63-77.

Miller, F. J., Rosenfeldt, F. L., Zhang, C., Linnane, A. W., and Nagley, P. (2003). Precise determination of mitochondrial DNA copy number in human skeletal and cardiac muscle by a PCR-based assay: lack of change of copy number with age. Nucleic acids research *31*, e61.

Mineri, R., Pavelka, N., Fernandez-Vizarra, E., Ricciardi-Castagnoli, P., Zeviani, M., and Tiranti, V. (2009). How do human cells react to the absence of mitochondrial DNA? PLoS One *4*, e5713.

Mitchell, P. (1961). Coupling of phosphorylation to electron and hydrogen transfer by a chemi-osmotic type of mechanism. Nature *191*, 144-148.

Mizumachi, T., Muskhelishvili, L., Naito, A., Furusawa, J., Fan, C. Y., Siegel, E. R., Kadlubar, F. F., Kumar, U., and Higuchi, M. (2008). Increased distributional variance of mitochondrial DNA content associated with prostate cancer cells as compared with normal prostate cells. The Prostate *68*, 408-417.

Moreno-Sanchez, R., Rodriguez-Enriquez, S., Marin-Hernandez, A., and Saavedra, E. (2007). Energy metabolism in tumor cells. The FEBS journal *274*, 1393-1418.

Moyes, C. D., Battersby, B. J., and Leary, S. C. (1998). Regulation of muscle mitochondrial design. The Journal of experimental biology *201*, 299-307.

Nat, R., Nilbratt, M., Narkilahti, S., Winblad, B., Hovatta, O., and Nordberg, A. (2007). Neurogenic neuroepithelial and radial glial cells generated from six human embryonic stem cell lines in serum-free suspension and adherent cultures. Glia *55*, 385-399.

Nilsson, J. A., Keller, U. B., Baudino, T. A., Yang, C., Norton, S., Old, J. A., Nilsson, L. M., Neale, G., Kramer, D. L., Porter, C. W., and Cleveland, J. L. (2005). Targeting ornithine decarboxylase in Myc-induced lymphomagenesis prevents tumor formation. Cancer cell *7*, 433-444.

Odent, S., Atti-Bitach, T., Blayau, M., Mathieu, M., Aug, J., Delezo de, A. L., Gall, J. Y., Le Marec, B., Munnich, A., David, V., and Vekemans, M. (1999). Expression of the Sonic hedgehog (SHH) gene during early human development and phenotypic expression of new mutations causing holoprosencephaly. Human molecular genetics *8*, 1683-1689.

Ogden, A. T., Waziri, A. E., Lochhead, R. A., Fusco, D., Lopez, K., Ellis, J. A., Kang, J., Assanah, M., McKhann, G. M., Sisti, M. B.*, et al.* (2008). Identification of A2B5+CD133- tumor-initiating cells in adult human gliomas. Neurosurgery *62*, 505-514; discussion 514-505.

Oppel, F., Muller, N., Schackert, G., Hendruschk, S., Martin, D., Geiger, K. D., and Temme, A. (2011). SOX2-RNAi attenuates S-phase entry and induces RhoA-dependent switch to protease-independent amoeboid migration in human glioma cells. Molecular cancer *10*, 137.

Palmer, R. H., Vernersson, E., Grabbe, C., and Hallberg, B. (2009). Anaplastic lymphoma kinase: signalling in development and disease. The Biochemical journal *420*, 345-361.

Park, D. M., and Rich, J. N. (2009). Biology of glioma cancer stem cells. Molecules and cells *28*, 7-12.

Parsons, D. W., Jones, S., Zhang, X., Lin, J. C., Leary, R. J., Angenendt, P., Mankoo, P., Carter, H., Siu, I. M., Gallia, G. L.*, et al.* (2008). An integrated genomic analysis of human glioblastoma multiforme. Science *321*, 1807-1812.

Pavlides, S., Whitaker-Menezes, D., Castello-Cros, R., Flomenberg, N., Witkiewicz, A. K., Frank, P. G., Casimiro, M. C., Wang, C., Fortina, P., Addya, S.*, et al.* (2009). The reverse Warburg effect: aerobic glycolysis in cancer associated fibroblasts and the tumor stroma. Cell cycle *8*, 3984-4001.

Pesta, D., and Gnaiger, E. (2012). High-resolution respirometry: OXPHOS protocols for human cells and permeabilized fibers from small biopsies of human muscle. Methods in molecular biology *810*, 25-58.

Petros, J. A., Baumann, A. K., Ruiz-Pesini, E., Amin, M. B., Sun, C. Q., Hall, J., Lim, S., Issa, M. M., Flanders, W. D., Hosseini, S. H.*, et al.* (2005). mtDNA mutations increase tumorigenicity in prostate cancer. Proc Natl Acad Sci U S A *102*, 719-724.

Pfaffl, M. W. (2001). A new mathematical model for relative quantification in real-time RT-PCR. Nucleic acids research *29*, e45.

Pfeiffer, T., Schuster, S., and Bonhoeffer, S. (2001). Cooperation and competition in the evolution of ATP-producing pathways. Science *292*, 504-507.

Piechota, J., Szczesny, R., Wolanin, K., Chlebowski, A., and Bartnik, E. (2006). Nuclear and mitochondrial genome responses in HeLa cells treated with inhibitors of mitochondrial DNA expression. Acta biochimica Polonica *53*, 485-495.

Pollard, P. J., Spencer-Dene, B., Shukla, D., Howarth, K., Nye, E., El-Bahrawy, M., Deheragoda, M., Joannou, M., McDonald, S., Martin, A.*, et al.* (2007). Targeted inactivation of fh1 causes proliferative renal cyst development and activation of the hypoxia pathway. Cancer cell *11*, 311-319.

Polyak, K., Li, Y., Zhu, H., Lengauer, C., Willson, J. K., Markowitz, S. D., Trush, M. A., Kinzler, K. W., and Vogelstein, B. (1998). Somatic mutations of the mitochondrial genome in human colorectal tumours. Nature genetics *20*, 291-293.

Prigione, A., Fauler, B., Lurz, R., Lehrach, H., and Adjaye, J. (2010). The senescence-related mitochondrial/oxidative stress pathway is repressed in human induced pluripotent stem cells. Stem cells *28*, 721-733.

Puigserver, P., Wu, Z., Park, C. W., Graves, R., Wright, M., and Spiegelman, B. M. (1998). A cold-inducible coactivator of nuclear receptors linked to adaptive thermogenesis. Cell *92*, 829-839.

Reya, T., Morrison, S. J., Clarke, M. F., and Weissman, I. L. (2001). Stem cells, cancer, and cancer stem cells. Nature *414*, 105-111.

Ricci-Vitiani, L., Lombardi, D. G., Pilozzi, E., Biffoni, M., Todaro, M., Peschle, C., and De Maria, R. (2007). Identification and expansion of human colon-cancer-initiating cells. Nature *445*, 111-115.

Richter, C., Gogvadze, V., Laffranchi, R., Schlapbach, R., Schweizer, M., Suter, M., Walter, P., and Yaffee, M. (1995). Oxidants in mitochondria: from physiology to diseases. Biochimica et biophysica acta *1271*, 67-74.

Ropp, P. A., and Copeland, W. C. (1996). Cloning and characterization of the human mitochondrial DNA polymerase, DNA polymerase gamma. Genomics *36*, 449-458.

Rutka, J. T., Ivanchuk, S., Mondal, S., Taylor, M., Sakai, K., Dirks, P., Jun, P., Jung, S., Becker, L. E., and Ackerley, C. (1999). Co-expression of nestin and vimentin intermediate filaments in invasive human astrocytoma cells. International journal of developmental neuroscience : the official journal of the International Society for Developmental Neuroscience *17*, 503-515.

Sakakibara, S., Imai, T., Hamaguchi, K., Okabe, M., Aruga, J., Nakajima, K., Yasutomi, D., Nagata, T., Kurihara, Y., Uesugi, S.*, et al.* (1996). Mouse-Musashi-1, a neural RNA-binding protein highly enriched in the mammalian CNS stem cell. Developmental biology *176*, 230-242.

Satoh, M., and Kuroiwa, T. (1991). Organization of multiple nucleoids and DNA molecules in mitochondria of a human cell. Experimental cell research *196*, 137-140.

Schon, E. A., Koga, Y., Davidson, M., Moraes, C. T., and King, M. P. (1992). The mitochondrial tRNA(Leu)(UUR)) mutation in MELAS: a model for pathogenesis. Biochimica et biophysica acta *1101*, 206-209.

Schwartz, M., and Vissing, J. (2002). Paternal inheritance of mitochondrial DNA. The New England journal of medicine *347*, 576-580.

Selvanayagam, P., and Rajaraman, S. (1996). Detection of mitochondrial genome depletion by a novel cDNA in renal cell carcinoma. Laboratory investigation; a journal of technical methods and pathology *74*, 592-599.

Shadel, G. S., and Clayton, D. A. (1997). Mitochondrial DNA maintenance in vertebrates. Annual review of biochemistry *66*, 409-435.

Shidara, Y., Yamagata, K., Kanamori, T., Nakano, K., Kwong, J. Q., Manfredi, G., Oda, H., and Ohta, S. (2005). Positive contribution of pathogenic mutations in the mitochondrial genome to the promotion of cancer by prevention from apoptosis. Cancer Res *65*, 1655-1663.

Shieh, D. B., Chou, W. P., Wei, Y. H., Wong, T. Y., and Jin, Y. T. (2004). Mitochondrial DNA 4,977-bp deletion in paired oral cancer and precancerous lesions revealed by laser microdissection and real-time quantitative PCR. Annals of the New York Academy of Sciences *1011*, 154-167.

Singh, K. K., Ayyasamy, V., Owens, K. M., Koul, M. S., and Vujcic, M. (2009). Mutations in mitochondrial DNA polymerase-gamma promote breast tumorigenesis. Journal of human genetics *54*, 516-524.

Singh, K. K., Kulawiec, M., Still, I., Desouki, M. M., Geradts, J., and Matsui, S. (2005). Inter-genomic cross talk between mitochondria and the nucleus plays an important role in tumorigenesis. Gene *354*, 140-146.

Singh, S. K., Clarke, I. D., Terasaki, M., Bonn, V. E., Hawkins, C., Squire, J., and Dirks, P. B. (2003). Identification of a cancer stem cell in human brain tumors. Cancer Res *63*, 5821-5828.

Skrtic, M., Sriskanthadevan, S., Jhas, B., Gebbia, M., Wang, X., Wang, Z., Hurren, R., Jitkova, Y., Gronda, M., Maclean, N.*, et al.* (2011). Inhibition of mitochondrial translation as a therapeutic strategy for human acute myeloid leukemia. Cancer cell *20*, 674-688.

Smiraglia, D. J., Kulawiec, M., Bistulfi, G. L., Gupta, S. G., and Singh, K. K. (2008). A novel role for mitochondria in regulating epigenetic modification in the nucleus. Cancer biology & therapy *7*, 1182-1190.

Smoly, J. M., Kuylenstierna, B., and Ernster, L. (1970). Topological and functional organization of the mitochondrion. Proc Natl Acad Sci U S A *66*, 125-131.

Spangrude, G. J., Heimfeld, S., and Weissman, I. L. (1988). Purification and characterization of mouse hematopoietic stem cells. Science *241*, 58-62.

St John, J. C., Ramalho-Santos, J., Gray, H. L., Petrosko, P., Rawe, V. Y., Navara, C. S., Simerly, C. R., and Schatten, G. P. (2005). The expression of mitochondrial DNA transcription factors during early cardiomyocyte in vitro differentiation from human embryonic stem cells. Cloning and stem cells *7*, 141-153.

Stoll, E. A., Cheung, W., Mikheev, A. M., Sweet, I. R., Bielas, J. H., Zhang, J., Rostomily, R. C., and Horner, P. J. (2011). Aging neural progenitor cells have decreased mitochondrial content and lower oxidative metabolism. The Journal of biological chemistry *286*, 38592-38601.

Suh, H., Consiglio, A., Ray, J., Sawai, T., D'Amour, K. A., and Gage, F. H. (2007). In vivo fate analysis reveals the multipotent and self-renewal capacities of Sox2+ neural stem cells in the adult hippocampus. Cell stem cell *1*, 515-528.

Sureban, S. M., May, R., George, R. J., Dieckgraefe, B. K., McLeod, H. L., Ramalingam, S., Bishnupuri, K. S., Natarajan, G., Anant, S., and Houchen, C. W. (2008). Knockdown of RNA binding protein musashi-1 leads to tumor regression in vivo. Gastroenterology *134*, 1448-1458.

Svendsen, C. N., ter Borg, M. G., Armstrong, R. J., Rosser, A. E., Chandran, S., Ostenfeld, T., and Caldwell, M. A. (1998). A new method for the rapid and long term growth of human neural precursor cells. Journal of neuroscience methods *85*, 141-152.

Takahashi, K., Tanabe, K., Ohnuki, M., Narita, M., Ichisaka, T., Tomoda, K., and Yamanaka, S. (2007). Induction of pluripotent stem cells from adult human fibroblasts by defined factors. Cell *131*, 861-872.

Takahashi, K., and Yamanaka, S. (2006). Induction of pluripotent stem cells from mouse embryonic and adult fibroblast cultures by defined factors. Cell *126*, 663-676.

Takamatsu, C., Umeda, S., Ohsato, T., Ohno, T., Abe, Y., Fukuoh, A., Shinagawa, H., Hamasaki, N., and Kang, D. (2002). Regulation of mitochondrial D-loops by transcription factor A and single-stranded DNA-binding protein. EMBO reports *3*, 451-456.

Tan, D. J., Chang, J., Liu, L. L., Bai, R. K., Wang, Y. F., Yeh, K. T., and Wong, L. J. (2006). Significance of somatic mutations and content alteration of mitochondrial DNA in esophageal cancer. BMC cancer *6*, 93.

Thomson, J. A., Itskovitz-Eldor, J., Shapiro, S. S., Waknitz, M. A., Swiergiel, J. J., Marshall, V. S., and Jones, J. M. (1998). Embryonic stem cell lines derived from human blastocysts. Science *282*, 1145-1147.

Trounce, I., Neill, S., and Wallace, D. C. (1994). Cytoplasmic transfer of the mtDNA nt 8993 T--->G (ATP6) point mutation associated with Leigh syndrome into mtDNA-less cells demonstrates cosegregation with a decrease in state III respiration and ADP/O ratio. Proc Natl Acad Sci U S A *91*, 8334-8338.

Trounce, I., and Wallace, D. C. (1996). Production of transmitochondrial mouse cell lines by cybrid rescue of rhodamine-6G pre-treated L-cells. Somatic cell and molecular genetics *22*, 81-85.

Tseng, L. M., Yin, P. H., Chi, C. W., Hsu, C. Y., Wu, C. W., Lee, L. M., Wei, Y. H., and Lee, H. C. (2006). Mitochondrial DNA mutations and mitochondrial DNA depletion in breast cancer. Genes, chromosomes & cancer *45*, 629-638.

Uchida, N., Buck, D. W., He, D., Reitsma, M. J., Masek, M., Phan, T. V., Tsukamoto, A. S., Gage, F. H., and Weissman, I. L. (2000). Direct isolation of human central nervous system stem cells. Proc Natl Acad Sci U S A *97*, 14720-14725.

van Inzen, W. G., Peppelenbosch, M. P., van den Brand, M. W., Tertoolen, L. G., and de Laat, S. W. (1996). Neuronal differentiation of embryonic stem cells. Biochimica et biophysica acta *1312*, 21-26.

Vander Heiden, M. G., Cantley, L. C., and Thompson, C. B. (2009). Understanding the Warburg effect: the metabolic requirements of cell proliferation. Science *324*, 1029-1033.

Varum, S., Rodrigues, A. S., Moura, M. B., Momcilovic, O., Easley, C. A. t., Ramalho-Santos, J., Van Houten, B., and Schatten, G. (2011). Energy metabolism in human pluripotent stem cells and their differentiated counterparts. PLoS One *6*, e20914.

Vivekanandan, P., Daniel, H., Yeh, M. M., and Torbenson, M. (2010). Mitochondrial mutations in hepatocellular carcinomas and fibrolamellar carcinomas. Modern pathology : an official journal of the United States and Canadian Academy of Pathology, Inc *23*, 790-798.

Vogelstein, B., Lane, D., and Levine, A. J. (2000). Surfing the p53 network. Nature *408*, 307-310.

Wallace, D. C. (1999). Mitochondrial diseases in man and mouse. Science *283*, 1482-1488.

Wallace, D. C. (2005). A mitochondrial paradigm of metabolic and degenerative diseases, aging, and cancer: a dawn for evolutionary medicine. Annual review of genetics *39*, 359-407.

Wang, J., Sakariassen, P. O., Tsinkalovsky, O., Immervoll, H., Boe, S. O., Svendsen, A., Prestegarden, L., Rosland, G., Thorsen, F., Stuhr, L.*, et al.* (2008a). CD133 negative glioma

cells form tumors in nude rats and give rise to CD133 positive cells. International journal of cancer Journal international du cancer *122*, 761-768.

Wang, J., Wang, H., Li, Z., Wu, Q., Lathia, J. D., McLendon, R. E., Hjelmeland, A. B., and Rich, J. N. (2008b). c-Myc is required for maintenance of glioma cancer stem cells. PLoS One *3*, e3769.

Wang, W., Esbensen, Y., Kunke, D., Suganthan, R., Rachek, L., Bjoras, M., and Eide, L. (2011). Mitochondrial DNA damage level determines neural stem cell differentiation fate. The Journal of neuroscience : the official journal of the Society for Neuroscience *31*, 9746-9751.

Wang, W., Osenbroch, P., Skinnes, R., Esbensen, Y., Bjoras, M., and Eide, L. (2010). Mitochondrial DNA integrity is essential for mitochondrial maturation during differentiation of neural stem cells. Stem cells *28*, 2195-2204.

Wang, Y., Liu, V. W., Xue, W. C., Cheung, A. N., and Ngan, H. Y. (2006). Association of decreased mitochondrial DNA content with ovarian cancer progression. British journal of cancer *95*, 1087-1091.

Wang, Y., Liu, V. W., Xue, W. C., Tsang, P. C., Cheung, A. N., and Ngan, H. Y. (2005). The increase of mitochondrial DNA content in endometrial adenocarcinoma cells: a quantitative study using laser-captured microdissected tissues. Gynecologic oncology *98*, 104-110.

Warburg, O. (1956). On respiratory impairment in cancer cells. Science *124*, 269-270.

Waring, M. J. (1965). Complex formation between ethidium bromide and nucleic acids. Journal of molecular biology *13*, 269-282.

Wei, Y. H. (1998). Oxidative stress and mitochondrial DNA mutations in human aging. Proceedings of the Society for Experimental Biology and Medicine Society for Experimental Biology and Medicine *217*, 53-63.

Whitaker-Menezes, D., Martinez-Outschoorn, U. E., Flomenberg, N., Birbe, R. C., Witkiewicz, A. K., Howell, A., Pavlides, S., Tsirigos, A., Ertel, A., Pestell, R. G.*, et al.* (2011). Hyperactivation of oxidative mitochondrial metabolism in epithelial cancer cells in situ: visualizing the therapeutic effects of metformin in tumor tissue. Cell cycle *10*, 4047-4064.

Wichterle, H., Lieberam, I., Porter, J. A., and Jessell, T. M. (2002). Directed differentiation of embryonic stem cells into motor neurons. Cell *110*, 385-397.

Wolf, A., Agnihotri, S., Micallef, J., Mukherjee, J., Sabha, N., Cairns, R., Hawkins, C., and Guha, A. (2011). Hexokinase 2 is a key mediator of aerobic glycolysis and promotes tumor growth in human glioblastoma multiforme. J Exp Med *208*, 313-326.

Wong, L. J., Lueth, M., Li, X. N., Lau, C. C., and Vogel, H. (2003). Detection of mitochondrial DNA mutations in the tumor and cerebrospinal fluid of medulloblastoma patients. Cancer Res *63*, 3866-3871.

Woodson, J. D., and Chory, J. (2008). Coordination of gene expression between organellar and nuclear genomes. Nature reviews Genetics *9*, 383-395.

Wu, C. W., Yin, P. H., Hung, W. Y., Li, A. F., Li, S. H., Chi, C. W., Wei, Y. H., and Lee, H. C. (2005). Mitochondrial DNA mutations and mitochondrial DNA depletion in gastric cancer. Genes, chromosomes & cancer *44*, 19-28.

Wu, Z., Puigserver, P., Andersson, U., Zhang, C., Adelmant, G., Mootha, V., Troy, A., Cinti, S., Lowell, B., Scarpulla, R. C., and Spiegelman, B. M. (1999). Mechanisms controlling mitochondrial biogenesis and respiration through the thermogenic coactivator PGC-1. Cell *98*, 115-124.

Xing, J., Chen, M., Wood, C. G., Lin, J., Spitz, M. R., Ma, J., Amos, C. I., Shields, P. G., Benowitz, N. L., Gu, J., *et al.* (2008). Mitochondrial DNA content: its genetic heritability and association with renal cell carcinoma. Journal of the National Cancer Institute *100*, 1104-1112.

Xu, Q., Yuan, X., Liu, G., Black, K. L., and Yu, J. S. (2008). Hedgehog signaling regulates brain tumor-initiating cell proliferation and portends shorter survival for patients with PTEN-coexpressing glioblastomas. Stem cells *26*, 3018-3026.

Yamada, S., Nomoto, S., Fujii, T., Kaneko, T., Takeda, S., Inoue, S., Kanazumi, N., and Nakao, A. (2006). Correlation between copy number of mitochondrial DNA and clinico-pathologic parameters of hepatocellular carcinoma. European journal of surgical oncology : the journal of the European Society of Surgical Oncology and the British Association of Surgical Oncology *32*, 303-307.

Yang, C., Sudderth, J., Dang, T., Bachoo, R. M., McDonald, J. G., and DeBerardinis, R. J. (2009). Glioblastoma cells require glutamate dehydrogenase to survive impairments of glucose metabolism or Akt signaling. Cancer Res *69*, 7986-7993.

Yasukawa, T., Reyes, A., Cluett, T. J., Yang, M. Y., Bowmaker, M., Jacobs, H. T., and Holt, I. J. (2006). Replication of vertebrate mitochondrial DNA entails transient ribonucleotide incorporation throughout the lagging strand. The EMBO journal *25*, 5358-5371.

Yen, H. C., Tang, Y. C., Chen, F. Y., Chen, S. W., and Majima, H. J. (2005). Enhancement of cisplatin-induced apoptosis and caspase 3 activation by depletion of mitochondrial DNA in a human osteosarcoma cell line. Annals of the New York Academy of Sciences *1042*, 516-522.

Yin, A. H., Miraglia, S., Zanjani, E. D., Almeida-Porada, G., Ogawa, M., Leary, A. G., Olweus, J., Kearney, J., and Buck, D. W. (1997). AC133, a novel marker for human hematopoietic stem and progenitor cells. Blood *90*, 5002-5012.

Yin, P. H., Lee, H. C., Chau, G. Y., Wu, Y. T., Li, S. H., Lui, W. Y., Wei, Y. H., Liu, T. Y., and Chi, C. W. (2004). Alteration of the copy number and deletion of mitochondrial DNA in human hepatocellular carcinoma. British journal of cancer *90*, 2390-2396.

Ying, Q. L., Stavridis, M., Griffiths, D., Li, M., and Smith, A. (2003). Conversion of embryonic stem cells into neuroectodermal precursors in adherent monoculture. Nature biotechnology *21*, 183-186.

Yu, M., Wan, Y., and Zou, Q. (2010). Decreased copy number of mitochondrial DNA in Ewing's sarcoma. Clinica chimica acta; international journal of clinical chemistry *411*, 679-683.

Yu, M., Zhou, Y., Shi, Y., Ning, L., Yang, Y., Wei, X., Zhang, N., Hao, X., and Niu, R. (2007). Reduced mitochondrial DNA copy number is correlated with tumor progression and prognosis in Chinese breast cancer patients. IUBMB life *59*, 450-457.

Zaehres, H., Lensch, M. W., Daheron, L., Stewart, S. A., Itskovitz-Eldor, J., and Daley, G. Q. (2005). High-efficiency RNA interference in human embryonic stem cells. Stem cells *23*, 299-305.

Zbinden, M., Duquet, A., Lorente-Trigos, A., Ngwabyt, S. N., Borges, I., and Ruiz i Altaba, A. (2010). NANOG regulates glioma stem cells and is essential in vivo acting in a cross-functional network with GLI1 and p53. The EMBO journal *29*, 2659-2674.

Zhou, H., Binmadi, N. O., Yang, Y. H., Proia, P., and Basile, J. R. (2012). Semaphorin 4D cooperates with VEGF to promote angiogenesis and tumor progression. Angiogenesis *15*, 391-407.

Zhu, L., Wang, Q., Zhang, L., Fang, Z., Zhao, F., Lv, Z., Gu, Z., Zhang, J., Wang, J., Zen, K.*, et al.* (2010). Hypoxia induces PGC-1alpha expression and mitochondrial biogenesis in the myocardium of TOF patients. Cell research *20*, 676-687.

Zhu, S., Lee, J. S., Guo, F., Shin, J., Perez-Atayde, A. R., Kutok, J. L., Rodig, S. J., Neuberg, D. S., Helman, D., Feng, H.*, et al.* (2012). Activated ALK collaborates with MYCN in neuroblastoma pathogenesis. Cancer cell *21*, 362-373.

Zimmerman, L., Parr, B., Lendahl, U., Cunningham, M., McKay, R., Gavin, B., Mann, J., Vassileva, G., and McMahon, A. (1994). Independent regulatory elements in the nestin gene direct transgene expression to neural stem cells or muscle precursors. Neuron *12*, 11-24.